National Library of Canada
Canadian Theses Service
Ottawa, Canada
K1A 0N4

Bibliothèque nationale du Canada
Services des thèses canadiennes

CANADIAN THESES

THÈSES CANADIENNES

NOTICE

The quality of this microfiche is heavily dependent upon the quality of the original thesis submitted for microfilming. Every effort has been made to ensure the highest quality of reproduction possible.

If pages are missing, contact the university which granted the degree.

Some pages may have indistinct print especially if the original pages were typed with a poor typewriter ribbon or if the university sent us an inferior photocopy.

Previously copyrighted materials (journal articles, published tests, etc.) are not filmed.

Reproduction in full or in part of this film is governed by the Canadian Copyright Act, R.S.C. 1970, c. C-30.

AVIS

La qualité de cette microfiche dépend grandement de la qualité de la thèse soumise au microfilmage. Nous avons tout fait pour assurer une qualité supérieure de reproduction.

S'il manque des pages, veuillez communiquer avec l'université qui a conféré le grade.

La qualité d'impression de certaines pages peut laisser à désirer, surtout si les pages originales ont été dactylographiées à l'aide d'un ruban usé ou si l'université nous a fait parvenir une photocopie de qualité inférieure.

Les documents qui font déjà l'objet d'un droit d'auteur (articles de revue, examens publiés, etc.) ne sont pas microfilmés.

La reproduction, même partielle, de ce microfilm est soumise à la Loi canadienne sur le droit d'auteur, SRC 1970, c. C-30.

THIS DISSERTATION
HAS BEEN MICROFILMED
EXACTLY AS RECEIVED

LA THÈSE A ÉTÉ
MICROFILMÉE TELLE QUE
NOUS L'AVONS REÇUE

NL-339 (r.86/06)

Canada

THE UNIVERSITY OF ALBERTA

GEOCHEMISTRY OF THE NELSON-ROSSLAND AREA, SOUTHEASTERN BRITISH COLUMBIA

by

(C) DIPAK KUMAR GHOSH

A THESIS

SUBMITTED TO THE FACULTY OF GRADUATE STUDIES AND RESEARCH

IN PARTIAL FULFILMENT OF THE REQUIREMENTS FOR THE DEGREE

OF DOCTOR OF PHILOSOPHY

DEPARTMENT OF GEOLOGY

EDMONTON, ALBERTA

SPRING, 1986

Permission has been granted to the National Library of Canada to microfilm this thesis and to lend or sell copies of the film.

The author (copyright owner) has reserved other publication rights, and neither the thesis nor extensive extracts from it may be printed or otherwise reproduced without his/her written permission.

L'autorisation a été accordée à la Bibliothèque nationale du Canada de microfilmer cette thèse et de prêter ou de vendre des exemplaires du film.

L'auteur (titulaire du droit d'auteur) se réserve les autres droits de publication; ni la thèse ni de longs extraits de celle-ci ne doivent être imprimés ou autrement reproduits sans son autorisation écrite.

ISBN 0-315-30321-2

THE UNIVERSITY OF ALBERTA

RELEASE FORM

NAME OF AUTHOR DIPAK KUMAR GHOSH

TITLE OF THESIS GEOCHEMISTRY OF THE NELSON-ROSSLAND AREA, SOUTHEASTERN BRITISH COLUMBIA

DEGREE FOR WHICH THESIS WAS PRESENTED DOCTOR OF PHILOSOPHY

YEAR THIS DEGREE GRANTED SPRING, 1986

Permission is hereby granted to THE UNIVERSITY OF ALBERTA LIBRARY to reproduce single copies of this thesis and to lend or sell such copies for private, scholarly or scientific research purposes only.

The author reserves other publication rights, and neither the thesis nor extensive extracts from it may be printed or otherwise reproduced without the author's written permission.

(SIGNED) Ghosh

PERMANENT ADDRESS:

Vill- Vennapara
P.O.- Chandpara Bazar
Dist.- 24 pgs. (W.B.) INDIA

DATED Apr. 26 1986.

THE UNIVERSITY OF ALBERTA

FACULTY OF GRADUATE STUDIES AND RESEARCH

The undersigned certify that they have read, and recommend to the Faculty of Graduate Studies and Research, for acceptance, a thesis entitled GEOCHEMISTRY OF THE NELSON-ROSSLAND AREA, SOUTHEASTERN BRITISH COLUMBIA submitted by Dipak Kumar Ghosh in partial fulfilment of the requirements for the degree of DOCTOR OF PHILOSOPHY.

R. St J Lambert

Supervisor

H. Baadsgaard

R A Burwash

G L Cumming

Richard Lee Armstrong

External Examiner

Date 21 Apr 1986

Dedication

To

My Parents

ABSTRACT

Detailed isotopic and geochemical investigations of all rock-types (sedimentary, volcanic, gneissic and granitoids) in the Nelson-Rossland area of southeastern British Columbia are reported and discussed. Major and trace element data and modelling with extensive use of three isotopic systems (Sr, Pb and Nd), have made it possible to determine the nature and relative degree of contributions of mantle and crustal components to the granitic(s.l.) bodies.

A metamorphic event has been dated by the whole rock Rb-Sr method at 971 Ma for the middle Aldridge Group of argillitic sediments. A Rb-Sr date (557 Ma) for the Nelway Formation is interpreted as the age of sedimentation, while 160 Ma for the Active Formation is thought to represent an isotopic resetting event. The two similar dates (≈248 Ma) obtained for the Slocan and Ymir Groups suggest that these two Groups were deposited in the same sedimentary basin during the same time interval.

U-Pb dating of zircons has established the ages of crystallization for the Nelson Batholith and Bonnington Pluton at 164 Ma and for the Castlegar Gneiss and Unit A at 54 Ma.

The Nd isotopic study of sedimentary rocks shows that, irrespective of their stratigraphic ages, crustal residence ages do not vary much (average 1.7 Ga), except for the Laib and a part of the Milford (2.32 to 2.26 Ga). The average crustal residence age of most of the sediments in southeastern British Columbia is similar to that of modern river sediments and therefore, negates the presence of a large mantle input during crustal growth for the last 2 Ga of Earth's history.

Major and trace elements establish a calc-alkaline nature for the granitic bodies (typical of an island arc regime). LIL element (Rb, Sr, and Ba) modelling shows the dominant effects of progressive **in-situ** fractional crystallization during the final stages of solidification.

The presence of ≈ 1.8 Ga old lower crust underlying the study area has been established on the basis of (i) Nd isotopic compositions of granitic samples and (ii) evidence for the incorporation of an old Pb component in the zircons in the batholiths.

Because of inadequacies of Simple Binary Mixing Models as an explanation of the complex isotopic and trace element variations in the granitic bodies, a more realistic model

(Assimilation and Fractional Crystallization) has been tested using mantle and crustal end-members with fixed composition: mantle magma ($\epsilon_{Nd} = +8.0$, $\epsilon_{Sr} = -20.0$, $^{206}Pb/^{204}Pb = 18.88$, $^{207}Pb/^{204}Pb = 15.60$, $^{208}Pb/^{204}Pb = 38.00$, $Nd = 10.0$, $Sr = 500.0$ and $Pb = 2.0$) and lower crust (-13.2, 60.0, 18.20, 15.55, 38.88, 26.0, 430.0 and 15.0).

Such modelling shows that all the batholithic magma originated in the mantle and rose to lower to mid-crustal levels, where it interacted with the crust and underwent concomitant fractional crystallization mainly of clinopyroxene, amphibole and plagioclase. Different batholiths and different phases of the same batholith have undergone variable degrees of mixing with the lower crust (20 to 50%) with r (ratio of mass-rate of assimilation to crystallization) values in the range 0.5 to 0.7. Consistent results obtained from different isotopes and elements reinforce the validity of the AFC modelling.

A detailed Pb isotopic study of both the granitic and sedimentary rocks supports the above mixing process, but necessitates the incorporation of a Pb component of upper crustal composition in the granitic samples lying to the east of a *Pb line*. This line defines the pre-Mesozoic western edge of the miogeoclinal package and is approximately coincident with the Slocan Lake and Champion Lake Faults.

A simple tectonic model has been developed suggesting that the miogeoclinal sedimentary mass and the underlying craton (called Craton(A), source of above sedimentary mass), bounded by Kootenay Lake and the Southern Rocky Mountain Trench are allochthonous. Lower Jurassic eastward-dipping and Lower Cretaceous westward-dipping subduction episodes, in conjunction with accretion of terrane Quesnellia to the western edge of the miogeocline, provide a realistic tectonic framework for southeastern British Columbia.

Acknowledgement

I wish to thank Dr. R. St J. Lambert for his continued interest and enthusiasm in this work. The project was financed under the terms of NSERC grant A-7489 to Dr. Lambert.

I am grateful to Dr. H. Baadsgaard for teaching me many aspects of chemical separation techniques and explaining many analytical problems with great patience.

I wish to thank Dr. G. L. Cumming for letting me use his chemistry laboratory and specially Dragan Krstic for putting up with my work and also for many suggestions regarding ion exchange chromatography.

I wish to thank Dr. K. Muehlenbachs for carrying out oxygen isotopic analysis.

Special thanks go to Dr. J. G. Holland for carrying out all XRF analyses without which this work would have remained partly incomplete.

Lastly I wish to thank John Duke for helping me carrying out Uranium analysis by INAA.

Table of Contents

Chapter Page

Dedication iv

ABSTRACT v

Acknowledgement vii

List of Tables xiii

List of Figures xv

Abbreviations xviii

1. INTRODUCTION 1

    1.1 Purposes of Investigation 1

    1.2 Previous work 2

    1.3 Field area: Location and Sampling 3

    1.4 Data Representation 3

2. GEOLOGIC BACKGROUND 14

    2.1 Regional Geology and Tectonic Setting 14

    2.2 Local Geology 16

        2.2.1 Introduction 17

        2.2.2 Stratigraphy 19

    2.3 Structure and Metamorphism 25

3. GEOCHRONOLOGY OF SEDIMENTS AND GRANITES 31

    3.1 Rb-Sr dating of Sediments 31

    3.2 Proterozoic Sediments 33

        3.2.1 Geology 33

        3.2.2 Structure and Metamorphism 33

        3.2.3 Earlier Work 35

        3.2.4 Results 36

        3.2.5 Discussion 36

    3.3 Lower Paleozoic Sediments 40

3.3.1 Geology 40
3.3.2 Structure and Metamorphism 41
3.3.3 Results 42
3.3.4 Discussion 42
3.4 Upper Paleozoic and Lower Mesozoic Sediments 47
3.4.1 Geology 47
3.4.2 Structure and Metamorphism 49
3.4.3 Results 50
3.4.4 Discussion 55
3.5 Geochronology of Granitic Rocks 57
3.5.1 Age Determination 57
3.5.2 Results 60
3.5.3 Discussion 65
4. Nd-ISOTOPIC STUDY OF SEDIMENTS AND CRUSTAL EVOLUTION 67
4.1 Introduction 67
4.2 Crustal Residence Age 70
4.3 Sample Selection 71
4.4 Results 72
4.4.1 Precambrian sediments 72
4.4.2 Phanerozoic sediments 72
4.5 Nd Isotopic Evidence for Crustal Growth 74
4.6 Nd Isotope Evolution in Sediments 75
4.7 Nd evolution in sediments in southeastern British Columbia 81
5. PETROGENESIS OF THE NELSON BATHOLITH 89
5.1 Classification 89
5.2 Nelson Batholith (NB) 90
5.3 Results 94

5.3.1 Major Elements 94
5.3.2 Trace Elements 94
5.4 Petrogenesis 99
5.4.1 Introduction 99
5.4.2 Major Elements 104
5.4.3 Trace Elements: 105
6. PETROGENESIS OF THE BONNINGTON PLUTON 122
6.1 Introduction 122
6.2 Results 125
6.2.1 Major Elements 125
6.2.2 Trace Elements: 125
6.3 Petrogenesis 131
6.3.1 Introduction 131
6.3.2 Major Elements: 134
6.3.3 Trace Elements: 134
7. Nd-Sr ISOTOPE GEOCHEMISTRY OF GRANITIC ROCKS 143
7.1 Introduction 143
7.2 Previous Work 145
7.3 Isotopic Models 146
7.4 Results 148
7.4.1 Volcanic Rocks 148
7.4.2 Nelson Batholith(NB) 148
7.4.3 Bonnington Pluton(BP) 153
7.4.4 Kuskanax Batholith(KB) 153
7.4.5 Bayonne Batholith(BB) 153
7.4.6 Trail Pluton(TP) and Trail(TN) and Castlegar Gneiss(CGN) 154
7.4.7 Summit Stock(SS) and Shoreline Creek Stock(SLCS) 154

7.5 Identification of the End-Members 154
- 7.5.1 Mantle End-Member 154
- 7.5.2 Crustal End-Members 157
- 7.5.3 Subducted Materials 159
- 7.5.4 Mixture of Volcanic and Sedimentary Rocks 160

7.6 Nature of Crystalline Basement 160

7.7 Petrogenetic Modelling 165
- 7.7.1 Modelling Parameters and Assumptions 167
- 7.7.2 Mathematical Background 168

7.8 Simple Binary mixing 173

7.9 Assimilation Fractional Crystallization(AFC) Models 184
- 7.9.1 ϵ_{Nd} vs. ϵ_{Sr} correlation 184
- 7.9.2 ϵ_{Sr} vs. Sr correlation. 194
- 7.9.3 $\epsilon_{Nd}(T)$ vs. Nd correlation. 200
- 7.9.4 ϵ_{Sr} vs. Rb/Sr relationship 202
- 7.9.5 Oxygen Isotopes 205
- 7.9.6 ϵ_{Nd} vs. Sm/Nd relationship 207

7.10 Nd-Sr isotopic relationships of Phanerozoic granitoids and crustal growth 214

8. PB ISOTOPE GEOCHEMISTRY OF GRANITIC ROCKS 218

8.1 Introduction 218

8.2 Analytical Data or Results 220
- 8.2.1 Bonnington Pluton(BP) 225
- 8.2.2 Nelson Batholith(NB) 225
- 8.2.3 Bayonne Batholith(BB) 226
- 8.2.4 Summit Stock(SS) 226
- 8.2.5 Kuskanax Batholitth(KB) 226
- 8.2.6 Shore Line Creek Stock(SLCS) 226

8.2.7 Trail Pluton(TP) and Gneiss(TN) 226
8.2.8 Unclassified Granite UNIT A(8064E) and 8021D 231
8.2.9 Rossland Volcanics(RV) 231
8.3 Mantle Pb 231
8.4 Discussion 232
9. TECTONICS OF SOUTHEASTERN BRITISH COLUMBIA 244
9.1 Introduction 244
9.2 Lower Crust 245
9.3 Times of Collision 247
9.4 Evidence of Allochthoneity 249
9.5 Structural Setting of the Nelson-Rossland Arc 251
9.6 Relationship among Metamorphism, Deformation and Plutonism 253
9.7 Tectonic Model 255
REFERENCES 261
APPENDIX 1 284
APPENDIX 2 291

List of Tables

1.1 Sample Location 9

3.1 Rb-Sr data from the middle Aldridge Formation. 37

3.2 Rb-Sr data from the Nelway and Active Formations. 43

3.3 Rb-Sr data from the Milford Group 51

3.4 Rb-Sr data from the Slocan and Ymir Groups. 51

3.5 Common Pb isotopic compositions. 61

3.6 U-Pb isotopic data for zircon analyses. 62

3.7 Isotopic data for Concordia plot and Model ages. 62

4.1 Trace element and isotopic data and model ages for sedimentary rocks. 73

5.1 Chemical character of the Nelson Batholith samples. 91

5.2 Table of distribution coefficients for large ion lithophile elements. 111

5.3a Table of distribution coefficients for REE for major minerals. 121

5.3b Table of distribution coefficients of REE for accessory minerals. 121

6.1 Chemical character of the Bonnington Pluton. 125

7.1 Trace element concentrations and their ratios for granitic samples. 149

7.1 Trace element concentrations and their ratios for sedimentary samples 150

7.3 Isotopic data and model ages for granitic samples. 151

7.4 Isotopic data and model ages for sedimentary samples 152

7.5 End-member compositions. 175

7.6 Summary of results of Simple Binary Mixing. 183

7.7 List of distribution coefficients for clinopyroxene, hornblende and plagioclage. 193

7.8 Oxygen isotopic data. 206

8.1 Initial Pb isotopic composition for granitic samples. 221

8.2 Initial Pb isotopic composition for granitic rocks. 222

8.3 Initial Pb isotopic composition for sedimentary rocks 223-224

A1.2 Sample Location and Description of Granitic samples 285-287

A1.3 Sample Location and Description of sedimentary samples. 288-290

A2.2.1 Major and Trace element data for the NB 292-297

A2.2.2 Major and Trace element data for the BP 298-303

A2.4.1 Results of SRM 984 and 987. 308

A2.4.2 Results of 607 K-Feldspar. 309

A2.4.3 Summary of results of 607 K-Feldspar and NBS values. 309

List of Figures

1.1a-b Geological Maps of Moyie Lake Area and Nakusp Area 5

1.1c Geological Map of Nelson East Half. 7

1.1d Geolical Map of Nelson West Half 8

2.1 Regional tectonic divisions of the Canadian Cordillera 15

2.2 Generalised stratigraphic succession for the Nelson-Rossland area. 20

3.1 Rb-Sr isochron diagram for the middle Aldridge Formation. 38

3.2 Rb-Sr isochron diagram for the Nelway Formation. 44

3.3 Rb-Sr isochron diagram for the Active Formation. 45

3.4 Rb-Sr isochron diagram for the Milford Group. 52

3.5 Rb-Sr isochron diagram for the Slocan Group. 53

3.6 Rb-Sr isochron diagram for the Ymir Group. 54

3.7 Concordia plot (theoretical explanation) 58

3.8 Concordia plot for the granitic samples. 63

4.1 Continental crust growth models 68

4.2 Theoretical models of continental growth. 76

4.3 Theoretical evolutionary models of sediments (Michard et al., 1985). 78

4.4 Plot of stratigraphic and crustal residence ages. 82

4.5 Model of sedimentary evolution in southeastern British Columbia. 83

5.1 Plot of total alkalis (K_2O+Na_2O) vs. SiO_2. for the Nelson Batholith. 92

5.2 AFM plot. 93

5.3 Major elements vs. SiO_2 (Harker's plot). 95-97

5.4 K/Rb vs. K_2O 98

5.5 Zr, Nb vs. SiO_2 100

5.6 Zr vs. Nb. 101

5.7 La, Y vs. SiO_2. 102

5.8 Zr, Nb vs. Y. 103

5.9 Crystallization behaviour in the system Qz-Or-Ab-An. 106

5.10 Large Ion Lithophile (LIL) element modelling for crystallization in a granitic magma. 109-110

5.11 LIL element modelling, effects of trapped intercumulus melts with the cumulate. 112-113

5.12 LIL element applied to the Nelson Batholith samples. 115-116

6.1 Total alkalis vs. SiO_2 for the Bonnington Pluton. 123

6.2 AFM plot. 124

6.3 Major elements vs SiO_2. 126-128

6.4 K_2O, Na_2O vs. SiO_2. 129

6.5 Rb, Sr vs. SiO_2 130

6.6 Nb, Zr Vs. SiO_2. 132

6.7 La, Y Vs. SiO_2. 133

6.8 LIL element modelling for the Bonnington Pluton. 136-137

6.9 LIL element modelling applied to the Bonnington Pluton. 139-140

7.1 Present day ϵ_{Sr} and ϵ_{Nd} values for mantle-derived rocks and the crusts of different ages. 147

7.2 $\epsilon_{Sr}(T)$ vs. $\epsilon_{Nd}(T)$ plot of all the granitic and sedimentary rocks. 156

7.3 Geographic variations in Pb, Sr and Nd isotopic composition in southeastern B. C. 163-164

7.4 Theory of Simple Binary Mixing(SMB). 171

7.5 SMB, ϵ_{Sr} vs. ϵ_{Nd}. 176

7.6 SMB, Pb vs Nd. 177-179

7.7 SMB, Pb vs Sr. 180-182

7.8 SMB, ϵ_{Nd} vs Nd. 185

7.9 SMB, Pb6/4 vs Pb. 186

7.10 SMB, ϵ_{Sr} vs Sr. 187

7.11 Assimilation and Fractional Crystallization Model: $\epsilon_{Sr}(T)$ vs. $\epsilon_{Nd}(T)$. 189

7.12 Sample identification with respective Sr and Nd concentrations. 191

7.13 AFC models, ϵ_{Sr} vs Sr (r=0.1, 0.3, 0.5, 0.7, 0.9) 195-197

7.14 AFC model, ϵ_{Nd} vs Nd 214

7.15 AFC model, ϵ_{Sr} vs Rb/Sr. 203
7.16 AFC model, ϵ_{Nd} vs Sm/Nd. 208-209
7.17 ϵ_{Nd} vs Sm/Nd. 211
7.18 ϵ_{Sr} vs ϵ_{Nd} plot of Phanerozoic Granitoids. 216
7.19 ϵ_{Nd} vs T for the Phanerozoic Granitoids. 216
8.1 Pb6/4 vs Pb7/4: Sample Identification. 228
8.2 Pb6/4 vs Pb8/4: Sample Identification. 230
8.3 Pb6/4 vs Pb7/4: Plot of all sedimentary and granitic samples. 234
8.4 Pb6/4 vs Pb8/4: Plot of all sedimentary and granitic samples. 236
8.5 Pb6/4 vs Pb7/4: Shows Pb-isotopic provinces. 240
8.6 Pb6/4 vs Pb8/4: Shows Pb-isotopic provinces. 242
9.1 Schematic representation of a tectonic model in southeastern B.C. 257

Abbreviations.

Gr	Granite	Grdi	Granodiorite
Dir	Diorite	Syen	Syenite
Monz	Monzonite	Gn	Gneiss
Ands	Andesite	Perth	Perthite
CA	Calc-alkaline	RV	Rossland Volcanics
Alk	Alkaline	Ald	Aldridge Formation
Met	Metaluminous	HORS	Horsethief Group
Per	Peraluminous	HAM	Hamill Group
NB	Nelson Bath.	LARD	Lardeau Group
BP	Bonnington Pluton	LAIB	Laib Formation
BB	Bayonne Batholith	NEL	Nelway Formation
KB	Kuskanax Batholith	ACT	Active Formation
TP	Trail Pluton	MIL-3	Milford Group-3
TN	Trail Gneiss	MIL-27	Milford Group-27
CGN	Castlegar Gneiss	YMR	Ymir Group
UA	Unit A	SLCN	Slocan Group
SLCS	Shore Line Cr Stock	KS	Kaslo Group
MP	Mackie Pluton	BH	Bunker Hill Stock
WS	Wall Stock	MS	Mine Stock
SO	Salmo Stock	SS	Summit Stock
PC	Porcupine Stock	LC	Lost Creek Stock
CP	Coryell Pluton	WCB	White Creek Batholith
FCB	Fry Creek Batholith	GCS	Grey Creek Stock
HRS	Hellroaring Cr Stock	AF	Argillite Fault
BBF	Black Bluff Fault	WF	Waneta Fault
PF	Porcupine Fault	SLF	Slocan Lake Fault
CLF	Champion Lake Fault	CRF	Columbia River Fault
Qz	Quartz	Xen	Xenotime
Kf	K-Feldspar	All	Allanite
Plag	Plagioclase	Mt	Magnetite
Bi	Biotite	Ep	Epidote
Musc	Muscovite	Gt	Garnet
Hb	Hornblende	Cc	Carbonate
Cpx	Clinopyroxene	Trem	Tremolite
Zr	Zircon	Ilm	Ilmenite
Ap	Apatite	Staur	Staurolite
Sph	Sphene	tr	Trace

1. INTRODUCTION

1.1 Purposes of Investigation

Broadly stated, the aims of this investigation are to study the petrogenesis (using both the major and minor elements) of the granitic rocks(s.l.) and the isotope geochemistry (Sr, Pb and Nd) of the granitic rocks and associated sediments, and to revise existing tectonic models for southeastern British Columbia.

Isotopic dating of the sedimentary and/or metamorphic ages of the thick sequences of sedimentary rocks constituting the miogeocline and part of the terrane Quesnellia and identification of their provenances are needed to understand their origin and the role they played in the tectonic evolution of the western Cordillera. The whole rock Rb-Sr dating method has been used to establish the sedimentary and/or metamorphic ages. Sm-Nd isotopic compositions have been determined to calculate the original times of Sm/Nd fractionation of crustal segments from which the sediments were derived and thereby their importance in understanding the crustal growth and sedimentary recycling processes. Whole rock Sr and Nd coupled with Pb isotopic compositions of the sediments have been used in deciphering the degree of involvement of the sediments in the genesis of the associated granitic rocks.

Though K-Ar mineral dates are available from the Nelson Batholith, they show wide variations. Accurate determination of the ages of crystallization is required to understand their tectonic relationships. Therefore granitic rocks from the Nelson Batholith, Bonnington Pluton, Castlegar Gneiss and Unit A have been dated by the U-Pb zircon dating method.

Generation of granitic batholiths involves a complex sequence of physicochemical events ranging from initial magma production either from the mantle or crust to interaction of the magma with wall rocks of variable compositions during ascent and concomitant crystallization. Petrogenesis of the granitic batholiths has been divided into two stages: a lower or mid-crustal stage when both isotopic and chemical evolutions were dominant and an upper crustal stage when chemical evolution predominated over the isotopic evolution. The above processes are best understood by isotopic and trace element modelling.

The present study represents the first successful combined application of Sr, Pb and Nd isotopes and trace elements to investigate the problems mentioned above and uses the significant amount of geochemical information which is now available to revise the present tectonic models.

1.2 Previous work

No systematic isotopic and trace element study has been carried out for either the sediments or the granitic batholiths except detailed geochronological studies by the K-Ar method and more limited work by the Rb-Sr method. Archibald et al. (1983, 1984) used a large data bank of K-Ar mineral dates and limited Rb-Sr and U-Pb dates, mostly from the granitic rocks, to reconstruct the tectonothermal history of southeastern British Columbia. They compiled the earlier geochronological data from Baadsgaard et al. (1961), Lowden (1961), Lowden et al. (1963), Leech et al. (1963), Wanless et al. (1968a,b) and Miller and Engels (1975). Besides these, other isotopic data published earlier include 1) K-Ar studies of Mathews (1983) from the Kootenay Arc, 2) Rb-Sr studies of Duncan and Parrish (1979) and Duncan et al. (1979) for the Nelson Batholith, and 3) Pb isotopic studies of Reylonds and Synclair (1971), Ghosh and Lambert (1983) and Andrew et al. (1984) for Pb-Zn ore deposits.

The only detailed geochemical study that has been carried out for the Rossland Volcanic Group is that of Beddoe-Stephens and Lambert (1981) and Beddoe-Stephens (1982). But only a limited Sr and O isotopic study has been carried out for this Group.

Limited U-Pb zircon dates that are available now include those of Parrish and Wheeler (1983) for the Kuskanax Batholith, Archibald et al. (1983) for the Mine Stock and Archibald et al. (1984) for the Corn Creek and Western Gneisses and Parrish and Ryan (1983), Parrish (1984) for the Valhalla Complex, Corbett and Simony (1984) for the Trail Pluton. Limited major and trace element studies for the Nelson Batholith and Slocan Group sediments have been carried out by Cox (1979) and Brame (1979).

1.3 Field area: Location and Sampling

The area of study is located in southeastern British Columbia, bounded by Longitudes of 116°00' and 118°00' and Latitudes of 49°N and 50°N. This area includes two geological maps: Nelson East Half (603A) and Nelson West Half (1090A) on a scale of 1 cm to 2.5 kms (Fig. 1.1). In addition to this area, samples have also been collected from Lardeau West Half map area (82k W1/2) which lies north of the maps 603A and 1090A and Moyie Lake area that lies east of the Nelson East Half map. The general geology of the map areas (603A and 1090A) has been described in Geological Survey of Canada Memoirs 228 (East Half) by Rice (1941) and 308 (West Half) by H. W. Little (1960)

75 samples have been collected from the well-preserved sedimentary sequences ranging in age from mid-Proterozoic to Triassic (Fig. 1.1 and Table 1.1). These sedimentary samples weigh in the range of 2 to 5 kg. 90 samples have been collected from most of the granitic batholiths/plutons/gneissic bodies from the area (Fig. 1.1 and Table 1.1) and they weigh around 10 to 15 kg.

1.4 Data Representation

Isotopic compositions obtained from mass spectrometry are expressed in the form of isotopic ratios:

$^{87}Sr/^{86}Sr$ and $^{87}Rb/^{86}Sr$ for Rb-Sr isotopic system,

$^{143}Nd/^{144}Nd$ and $^{147}Sm/^{144}Nd$ for the Sm-Nd isotopic systems, and

$^{206,207,208}Pb/^{204}Pb$ and $^{238,235}U/^{204}Pb$, $^{232}Th/^{204}Pb$ for the U-Th-Pb isotopic systems

Nd and Sr Systematics:

DePaolo and Wasserburg (1976, 1977) introduced a new notation of presenting isotopic data for Nd and Sr in terms of the parameters ϵ_{Nd} and ϵ_{Sr}. For Nd, $^{143}Nd/^{144}Nd$ ratios are always given as deviations from $^{143}Nd/^{144}Nd$ in a Chondritic Uniform Reservoir (CHUR), whose Nd isotopic evolution is tentatively assumed to be identical to that in the Juvinas achondrite. Lugmair et. al. (1976) determined a crystallization age of 4.56 Ga for the Juvinas achondrite whose present-day Sm/Nd (0.307 atomic) is almost identical to the average value of

LEGEND (Nakusp Area)

Cretaceous	12	Plutonic rocks	Granite, granodiorite
Mesozoic	11	Plutonic rocks	Granite, granodiorite and quartz diorite.
	10	Slocan Group	Slate, argillite, quartzite, limestone, schists
	9	Kaslo Group	Lavas, tuffs, breccias, allied intrusives, schists
Paleozoic	8	Milford Group	Slate, argillite, chert, limestone, schists, some greenstone
	7	Lardeau Group	Micaceous and chloritic schists; quartzite and limestone; paragneiss
	5	Hamill Group	Grey, green and white, siliceous quartzite
Upper Proterozoic	4	Horsethief Creek Group	Green argillaceous quartzite; blue-grey limestone, arkose, pebble conglomerate

LEGEND (Moyie Lake Area)

Pleistocene and Recent	7	Alluvial sand and gravel	
Upper Proterozoic	6	Sills and Dykes	Intrusive Gabbro and Diorite
	5	Nicol Creek Formation	Amygdaloidal Basic Volcanics
	4	Van Creek Formation	Argillite, siltite
	3	Kitchener Formation	Dolomite, argillitaceous limestone
	2	Creston Formation	Argillite, siltite, quartzite
	1c	Upper Aldridge Formation	Argillite, siltite
	1b	Middle Aldridge Formation	Quartzite, argillite, siltite
	1a	Lower Aldridge Formation	Quartzite, quartz-wacke

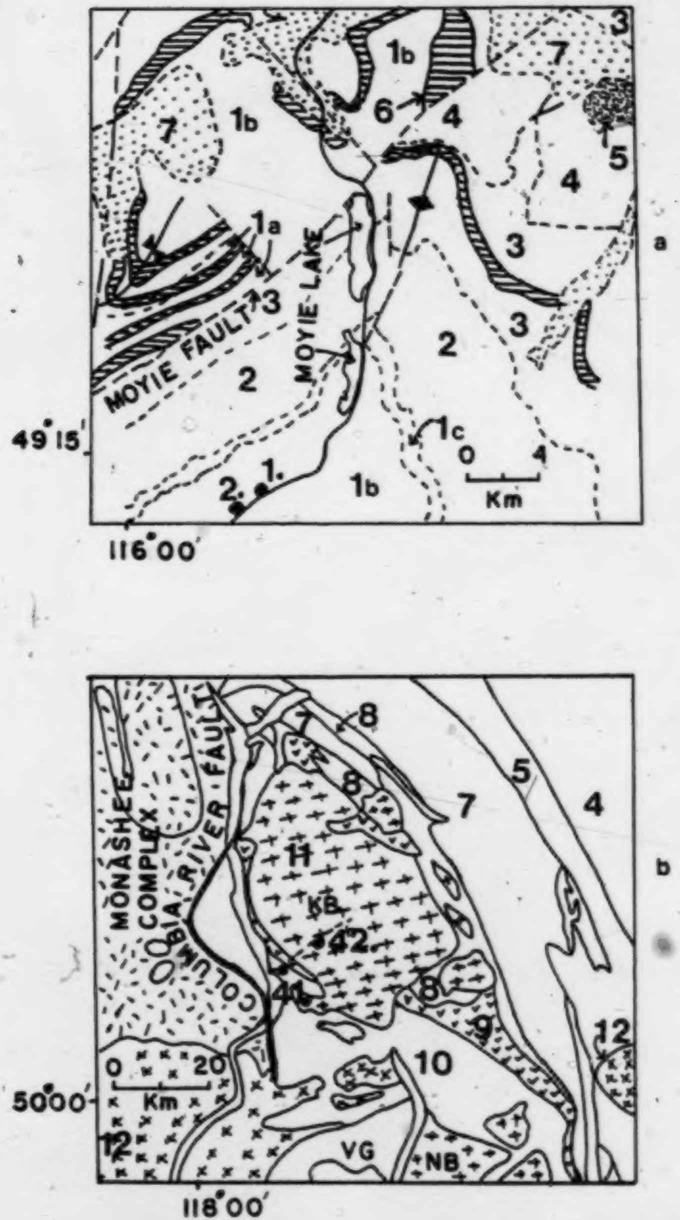
1b
7
1b
6
4
3
7
5
4
1a
3
MOYIE FAULT
MOYIE LAKE
3
2
3
2
1c
0
4
Km
49°15'
2.
1.
1b
116°00'
a
8
8
7
5
4
MONASHEE COMPLEX
COLUMBIA RIVER FAULT
11
KB
42
41
8
9
12
0
20
Km
10
5000'
12
VG
NB
118°00'
b

Fig. 1.1. Geological Maps of the Moyie Lake area (a) after Hoy and Diakow (1981), Nakusp area (b) after Parrish Wheeler (1983), Nelson East half (c) after Rice (1941), and Nelson West half (d) after Little (1960) and Simony (1979). Lithological units are indentified by numbers (see Legend). Solid circles with accompanying numbers refer to the sample locations.

LEGEND (Nelson, East Half)

Cretaceous	12	Plutonic rocks	Granite, granodiorite
Mesozoic	11	Plutonic rocks	Granite, granodiorite and quartz diorite.
	10	Slocan Group	Slate, argillite, quartzite, limestone, schists
	9	Kaslo Group	Lavas, tuffs, breccias, allied intrusives, schists
Paleozoic	8	Milford Group	Slate, argillite, chert, limestone, schists, some greenstone
	7	Lardeau Group	Micaceous and chloritic schists, quartzite and limestone; paragneiss
	6	Badshot Formation	Magnesian limestone
	5	Hamill Group	Grey, green and white, siliceous quartzite
Upper Proterozoic	4	Horsethief Creek Group	Green argillaceous quartzite, blue-grey limestone, arkose, pebble conglomerate
	3	Irene Volcanic Formation	Sheared, andesitic volcanic rocks
	2	Toby Conglomerate	Conglomerate
	1	Purcell Supergroup	Argillite, siltite, dolomite, quartzite, basalt.

LEGEND (Nelson West Half)

Tertiary	21	Coryell Plutons	Syenite, minor granite, monzonite and shonkinite
	20	Valhalla Plutonic Rocks	Granite, minor pegmatite, granodiorite
	19	Unit A	Granitic Gneiss
	19	Castlegar Gneiss	Granitic gneiss, some diorite
Cretaceous	18	Plutonic Rocks	Granitic Batholiths
Mesozoic	17	Trail Gneiss	Granitic gneiss, amphibolite
	16	Plutonic Rocks	Granite, granodiorite, diorite, gabbro
	15	Rossland Group	Andesite, latite, basalt, flow breccia, augite porphyry, agglomerate, tuff,
	14	Ymir Group	Argillite, slate, argillaceous quartzite
	13	Slocan Group	Slate, argillite, quartzite, limestone, carbonate
	12	Kaslo Group	Greenstone, minor slate
Paleozoic	11	Mt. Roberts Formn.	Argillaceous quartzite, slate, limestone, greenstone
	10	Unnamed	White quartzite, schist, limestone, paragneiss
	9	Active Formation	Slate, argillite, argillaceous quartzite, limestone
	8	Nelway Formation	Dolomite, limestone, phyllite, slate
	7	Liab Formation	Argillite, argillaceous quartzite, limestone, dolomite, phyllite, schist
	6	Reno Formation	Argillaceous quartzite, schist, argillite
	5	Quartzite Range Formation	Quartzite, argillaceous quartzite, conglomerate
Upper Proterozoic	4	Three Sisiters Formation	Grit, quartzite, conglomerate
	3	Monk Formation	Argillite, phyllite, argillaceous phyllite
	2	Irene Volcanic Formation	Greenstone, minor interbedded argillite and limestone
	1	Toby Conglomerate	Conglomerate

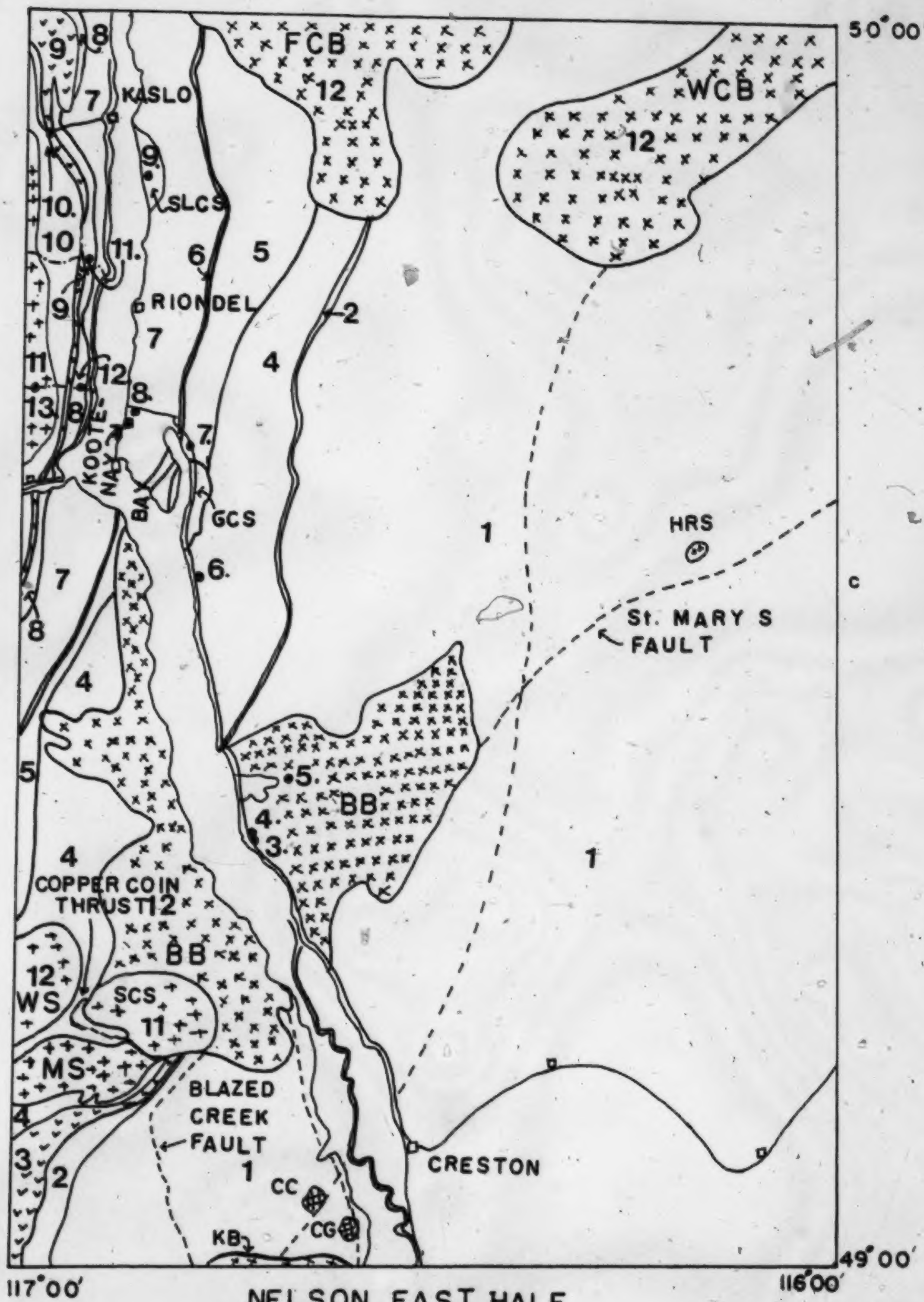
50°00'
49°00'
117°00'
116°00'
FCB
WCB
12
KASLO
9
8
7
10
11
SLCS
6
5
4
2
RIONDEL
13
KOOTENAY BAY
GCS
1
HRS
ST. MARY S FAULT
BB
3
COPPER COIN THRUST
WS
SCS
MS
BLAZED CREEK FAULT
CRESTON
CC
CG
KB
c

NELSON EAST HALF

L

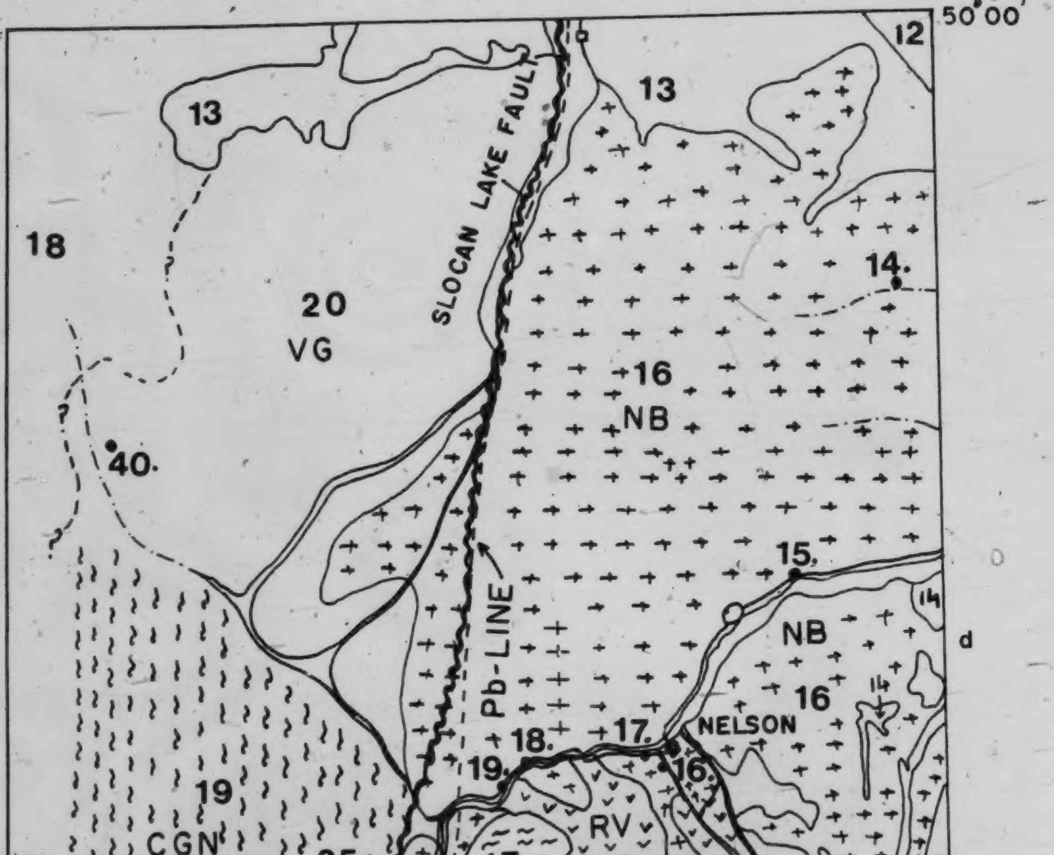
50°00'
12
13
13
SLOCAN LAKE FAULT
18
20
VG
14.
16
NB
40.
?
15.
Pb-LINE
NB
16
14
14
d
18.
17.
NELSON
19.
16.
19
CGN
RV
17
15
35.
36.
BP
14
39.
38.
37.
33
CGN
UA
B
34.
16
BP
HALL F.
15
21
16
10
32.
MP
24.
24
22
PC
20.
CHAMPION LAKE FAULT
SO
HC
11
30.
31.
SALMO
RV
15
BBF
AF
9
7
8
7
4
21
29.
23.
28.
16
BH
CP
TRAIL
25
LC
ROSSLAND
21
WF
27.
15
RV
26.
7
9
8
3
SS
5, 6
49°00'
118°00'
117 00

NELSON WEST HALF

Table 1.1 Sample Location (Refer to Fig.1.1)

Location #	Formn./Bath.	Sample ID
	Moyie Lake	**Area (Fig. 1.1a)**
1	Mid-Aldridge	8001B,C,E,F,G,H,I
2	,,	8002A,D,E,F,G,H,I
	Nelson (East Half)	**(Fig. 1.1b)**
3	BB	8038A,B,C,D
4	,,	8038E
5	,,	8096E,G,I,J
6	Horsethief	8094A,B,D
7	Hamill	8090A,C
8	Lardeau	8037B,C,D,M
9	SLCS	8088A,B, 8089D,F
10	Kaslo	8106B
11	Milford-27	8027B,C,D,F,H,I,P,S
12	Milford-3	8003A,B,C,D,E,F
13	NB	8057A,B,C,D,E,F,G
	Nelson (West HAlf)	**(Fig.1.1c)**
14	NB	SB29.7
15	,,	8004, 8059A,B,C,D,E
16a	,,	8011
16	,,	8012A,B
17	,,	8013A,B,C
18	,,	8053A,B,D,E
19	,,	8052A,B,C,D
20	,,	8061A,B
21	Ymir	8006A,B,C,E,F,G,H,I,J,K,L
22	,,	8006M,N,P
23	SS	8007A,B
24	BP	8075A,B,C,F,G,H,J,K
24a	RV	74/054, 75/5116
25	Active	8009A,D,J,L,R,T,U
26	Nelway	8010Q,R,S,T,U,V,W
27	Laib	8084A,B
28	TP	8073A,C,D
29	,,	8072A,B,C
30	TN	8071H
31	,,	8070B,C,E,F,
32	CGN	8069B
33	BP	8021A,B,D
34	,,	8022A,B,C
35	,,	8067A,B,C,E,F,G,H
36	,,	8068A,B,C1,D1,E,F
37	CGN	8065A
38	UA	8064E
39	CGN	8063A
40	VG	8049A,C,D,E
	Nakusp Area	**(Fig. 1.1d)**
41	Slocan	8035A,B,C,D,E,F,G,H
42	KB	8033A,C,D,G,H,M,P

Sm/Nd measured in chondritic meteorites (0.309 ± 0.005, 1σ) (Masuda et al., 1973; Nakamura, 1974).

The present-day isotopic composition of Nd measured in any sample is expressed as:

$$\epsilon_{Nd}(0) = \left[\frac{(^{143}Nd/^{144}Nd)_{Rock}(0)}{(^{143}Nd/^{144}Nd)_{CHUR}(0)} - 1\right].10^4 \quad \ldots\ldots\ldots\ldots\ldots\ldots\ldots\ldots\ldots\ldots\ldots\ldots\ 1.1$$

However for determining ϵ_{Nd} values at any time in the past (T), eqn. 1.1 is rewritten as:

$$\epsilon_{Nd}(T) = \left[\frac{(^{143}Nd/^{144}Nd)_{Rock}(T)}{(^{143}Nd/^{144}Nd)_{CHUR}(T)} - 1\right].10^4 \quad \ldots\ldots\ldots\ldots\ldots\ldots\ldots\ldots\ldots\ldots\ldots\ldots\ 1.2$$

where

$$(^{143}Nd/^{144}Nd)_{Rock}(T) =$$

$$(^{143}Nd/^{144}Nd)_{Rock}(0) - (^{147}Sm/^{144}Nd)_{Rock}(0).(e^{\lambda_{Sm}T} - 1) \quad \ldots\ldots\ldots\ldots\ldots\ldots\ldots\ldots\ 1.3$$

and

$$(^{143}Nd/^{144}Nd)_{CHUR}(T) =$$

$$(^{143}Nd/^{144}Nd)_{CHUR}(0) - (^{147}Sm/^{144}Nd)_{CHUR}(0).(e^{\lambda_{Sm}T} - 1) \quad \ldots\ldots\ldots\ldots\ldots\ldots\ldots\ldots\ 1.4$$

and $\lambda_{Sm} = 0.00654 AE^{-1}$ (DePaolo, 1981a).

Therefore $\epsilon_{Nd}(T)$ (generally equated to Rock's initial ϵ-value) is the deviation in parts in 10^4 of a Rock's initial $^{143}Nd/^{144}Nd$ ratio from that ratio in CHUR at T.

In an analogous way following equations could be written for Rb-Sr isotopic systems, with respect to a model reservoir (UR) thought to be representative of the total Earth.

$$\epsilon_{Sr}(0) = \left[\frac{(^{87}Sr/^{86}Sr)_{Rock(0)}}{(^{87}Sr/^{86}Sr)_{UR}(0)} - 1\right].10^4 \quad \ldots\ldots\ldots\ldots\ldots\ldots\ldots\ldots\ldots\ldots\ldots\ldots\ 1.5$$

or at T

$$\epsilon_{Sr}(T) = \left[\frac{(^{87}Sr/^{86}Sr)_{Rock}(T)}{(^{87}Sr/^{86}Sr)_{UR}(T)} - 1\right].10^4 \quad \ldots\ldots\ldots\ldots\ldots\ldots\ldots\ldots\ldots\ldots\ldots\ldots\ 1.6$$

where

$$(^{87}Sr/^{86}Sr)_{Rock}(T) =$$

$$(^{87}Sr/^{86}Sr)_{Rock}(0) - (^{87}Rb/^{86}Sr)_{Rock}(0)(e^{\lambda_{Rb}T} - 1) \quad \ldots\ldots\ldots\ldots\ldots\ldots\ldots\ldots\ldots\ldots\ 1.7$$

and

$(^{87}87Sr/^{86}Sr)_{UR}(T)=$

$$(^{87}Sr/^{86}Sr)_{UR}(0)-(^{87}Rb/^{86}Sr)_{UR}(0)(e^{\lambda}Rb^{T}-1) \qquad 1.8$$

and $\lambda_{Rb}=1.42x10^{-11}yr^{-1}$ (Steiger and Jager, 1977)

Enrichment factors for $^{147}Sm/^{144}Nd$ and $^{87}Rb/^{86}Sr$ ratios of a Rock are defined as (DePaolo, 1979):

$$f_{Sm/Nd}=[\frac{(^{147}Sm/^{144}Nd)_{Rock}}{(^{147}Sm/^{144}Nd)_{CHUR}}-1] \qquad 1.9$$

and

$$f_{Rb/Sr}=[\frac{(^{87}Sr/^{86}Sr)_{Rock}}{(^{87}Sr/^{86}Sr)_{UR}}-1] \qquad 1.10$$

DePaolo (1981) derived a simplified expression relating $\epsilon_{Nd}(T)$, $\epsilon_{Nd}(0)$ and Sm/Nd:

$$\epsilon_{Nd}(T)=\epsilon_{Nd}(0)-f_{Sm/Nd}Q_{Nd}T \qquad 1.11$$

where

$$Q_{Nd}=[\frac{\lambda_{Sm}(^{147}Sm/^{144}Nd)_{CHUR}(0)}{(^{143}Nd/^{144}Nd)_{CHUR}(0)}].10^{4} \qquad 1.12$$

and for Sr

$$\epsilon_{Sr}(T)=\epsilon Sr(0)-f_{Rb/Sr}Q_{Sr}T \qquad 1.13$$

where

$$Q_{Sr}=[\frac{\lambda_{Rb}(^{87}Rb/^{86}Sr)_{UR}(0)}{(^{87}Sr/^{86}Sr)_{UR}(0)}].10^{4} \qquad 1.14$$

T_{DM} model ages have been calculated relative to a depleting mantle evolution of DePaolo (1981b) by solving for T in the following equations:

$$\epsilon_{Nd}(T)=0.25T^{2}-3T+8.5 \qquad 1.15$$

$$\epsilon_{Sr}(T)=0.65T^{2}+8T-23 \qquad 1.16$$

Table 1.2

Constants	Values	References
$(^{143}Nd/^{144}Nd)_{CHUR}(0)$	0.51262	Allègre and Rousseau, 1984.
$(^{147}Sm/^{144}Nd)_{CHUR}(0)$	0.1967	Jacobsen and Wasserburg, 1980.
$(^{87}Sr/^{86}Sr)_{UR}(0)$	0.70478	Allègre et al., 1979.
$(^{87}Rb/^{86}Sr)_{UR}(0)$	0.087	,,
Q_{Nd}	25.09	Present calculation
Q_{Sr}	17.52	,,

The following table (Table 1.2) contains the constants used in solving the above equations:

U-Th-Pb Systematics

Unlike Sr and Nd isotopes, Pb isotopes, the measured data are not normalised to any standard or reference reservoir. Parent-daughter isotopic ratios are related according to the following equations:

$$(^{206}Pb/^{204}Pb)_m = (^{206}Pb/^{204}Pb)_i + (^{238}U/^{204}Pb)(e^{\lambda_1 T} - 1) \quad \text{1.17}$$

$$(^{207}Pb/^{204}Pb)_m = (^{207}Pb/^{204}Pb)_i + (^{235}U/^{204}Pb)(e^{\lambda_2 T} - 1) \quad \text{1.18}$$

$$(^{208}Pb/^{204}Pb)_m = (^{208}Pb/^{204}Pb)_i + (^{232}Th/^{204}Pb)(e^{\lambda_3 T} - 1) \quad \text{1.19}$$

where,

$\lambda_1 = \lambda_{238U} = 1.55125 \times 10^{-10} yr^{-1}$ (Jaffey et al., 1971).

$\lambda_2 = \lambda_{235U} = 9.8485 \times 10^{-10} yr^{-1}$ (Jaffey et al., 1971)

$\lambda_3 = \lambda_{232Th} = 4.948 \times 10^{-11} yr^{-1}$ (Leroux and Glendenin, 1963)

From these equations, initial Pb-isotopic ratios could be calculated by using measured values of $(^{206,207,208}Pb/^{204}Pb)_m$ and $(^{238,235}U/^{204}Pb)$ and $^{232}Th/^{204}Pb$, when T is known or assumed and the isotopic system is assumed to be closed since T.

Oxygen Isotopes

Measured Oxygen isotope ratios (i.e., $^{18}O/^{16}O = R$) are expressed in δ notation, defined as:

$$\delta^{18}O_{sample} = [\frac{R_{sample}}{R_{SMOW}} - 1] \times 10^3 \quad \text{1.20}$$

The isotopic fractionation factor between two samples, A and B, is defined as:

$$\alpha_{A-B}=R_A/R_B$$

In terms of δ-values this expression becomes:

$$\alpha_{A-B}=\frac{1000+\delta_A}{1000+\delta_B}$$

The mathematical quantity $10^3\ln\alpha$, the permill fractionation, is very useful in stable isotope geochemistry. This quantity is very well approximated by the Δ-value:

$$\Delta_{A-B}=\delta_A-\delta_B\cong 10^3\ln\alpha_{A-B} \quad\text{.......} 1.21$$

In the present work two minerals (quartz and feldspar) have been analysed for oxygen isotope ratios. The measured ratios for these minerals have been normalised according to the eqn. 1.20 and the permill fractionation between the pair qz-fels has been expressed according to the eqn 1.21 i. e.,

$$\Delta_{Qz-Fels}=\delta_{Qz}-\delta_{Fels}$$

2. GEOLOGIC BACKGROUND

2.1 Regional Geology and Tectonic Setting

On the basis of controls in stratigraphy, deformation, metamorphism and magmatism, the Canadian segment of the North American Cordillera has been subdivided into five physiographically distinct belts. These belts which reflect the present geodynamic pattern of the Canadian Cordillera are from east to west (Fig. 2.1):

1. the Rocky Mountain Belt (RMB),
2. Omineca Crystalline Belt (OCB),
3. Intermontane Belt (IMB),
4. Coast Plutonic Complex (CPC) and
5. Insular Belt (IB). (Monger et al., 1972).

However, the Canadian Cordillera is a type of "collision orogen" involving the accretion of a collage of allochthonous terranes or suspect terranes (Coney et al., 1980) to the western margin of the North American continent by convergent and transform plate motions (Price et al., 1981). These allochthonous terranes have been grouped together in two large composite terranes, Terrane I and II (Fig. 2.1)(Monger et al., 1982). Previously Monger et al. (1972) and Dickinson (1977) suggested that the two metamorphic and plutonic welts (OCB and CPC) resulted from the subduction of Pacific Ocean lithosphere beneath the western edge of North America. But the present view is that they resulted from tectonic overlap and/or compressional thickening of crustal rocks during collisions between North America and the two terranes. The eastern composite Terrane I is made up of four smaller, originally independent terranes (Eastern Assemblage, E; Quesnellia, Q; Cache Creek, Cc and Stikinia, St) that apparently coalesced by the end of Triassic time prior to emplacement in their present locations along the continental margin. The western composite terrane II consisting of three smaller terranes (GN, A, W) amalgamated by late Jurassic time. Terranes I and II probably accreted to North America between mid-Jurassic and mid-Cretaceous time and between early Cretaceous and early Tertiary time respectively (Price et al., 1981).

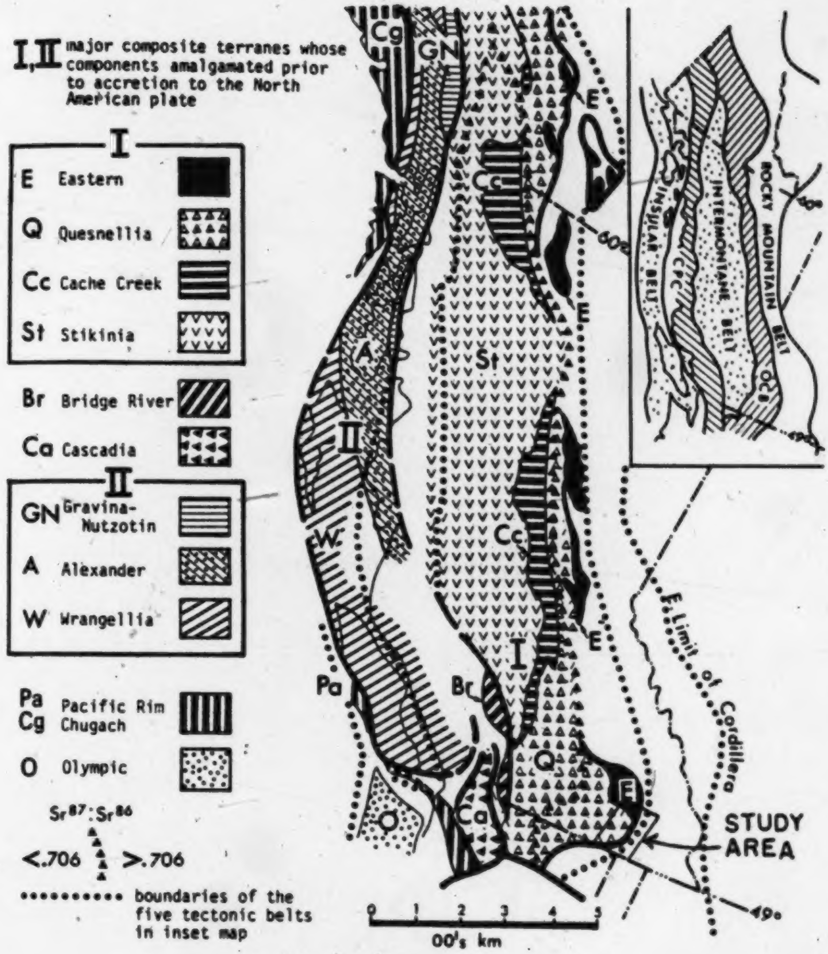
I, II major composite terranes whose components amalgamated prior to accretion to the North American plate
I
E Eastern
Q Quesnellia
Cc Cache Creek
St Stikinia
Br Bridge River
Ca Cascadia
II
GN Gravina-Nutzotin
A Alexander
W Wrangellia
Pa Pacific Rim
Cg Chugach
O Olympic
Sr87:Sr86
<.706 >.706
boundaries of the five tectonic belts in inset map
0 1 2 3 4 5
00's km
STUDY AREA
E. Limit of Cordillera
60°
49°
INSULAR BELT
CPC
INTERMONTANE BELT
ROCKY MOUNTAIN BELT
OCB

Fig. 2.1. The inset box at the right top, shows five physiographic and tectonic divisions of the Canadian Cordillera. The two super terranes I and II of Monger et al (1982), consisting of several smaller alochthonous (or suspect) terranes. Terrane I of E, Q, Cc and St, and Terrane II consists of Gn, A and W. ^{87}Sr/^{86}Sr line (according to Armstrong et al., 1977) indicates possible western extension of Precambrian continental crust or segments that may have rifted away from it. The study area is shown enclosed in a box in the southeastern corner. (Figure modified from Monger et al., 1982).

The Omineca Crystalline Belt and Coast Plutonic Complex appear to have formed at least in part as a result of these accretions, for the following reasons. First these two high-grade metamorphic and granitic belts are roughly coincident with the boundaries between Terranes I and II respectively. Secondly, stratigraphic, isotopic and structural evidence established the fact that much of the metamorphism and granitic intrusion that characterise these belts occurred during the probable times of collisions. The overall pattern of collisions involves the movement of the North American Plate relatively westward into various Pacific Plates from Jurassic time onward and in conjuction with subduction of Pacific Ocean lithosphere.

The regional stratigraphic analysis of the supracrustal rocks forms the fundamental basis for the notion that the Canadian Cordillera is in part a collision orogen. Also the recognition of contrasting terranes in the western Cordillera, and the documentation of large displacements between these terranes from their disjunctive palaeontological and palaeomagnetic records and amounts and times of displacements on major structural features separating them all lend suport to the collision orogen concept.

Each of the terranes, the basic building blocks of the Cordillera (Coney et al., 1980) is characterised by its own distinctive, laterally persistent stratigraphic record that differs from the coeval records in the neighbouring terranes, from which it is separated by major faults and/or structurally complex zones, intrusion or cover of younger rocks (Monger et al., 1982).

Each terrane, as defined on the basis of the integrity of its unique internal stratigraphic record and not on the basis of any genetic or tectonic model, consists of one or more tectonostratigraphic assemblages, each of which can be interpreted by analogy with modern examples as having formed in a particular tectonic setting (Monger and Price, 1979; Tipper and Woodsworth, 1980).

2.2 Local Geology

2.2.1 Introduction

The area under study lies in the southeastern part of the Omineca Crystalline Belt and the southwestern part of the Rocky Mountain belt. It also straddles the boundary between the eastern part of Quesnellia (Q) and the western part of the miogeocline. The study area could be grouped into four tectonic divisions:

1. Purcell Anticlinorium(PA),
2. Kootenay Arc(KA),
3. Nelson-Rossland Arc(NRA) and
4. Gneissic Complex(GNC).

1. The Purcell Anticlinorium(PA)

The low-grade metasedimentary rocks of Helikian and Hadrynian age are exposed in the Purcell Anticlinorium, a broad generally north-trending anticlinal structure between the Rocky Mountains to the east and the Kootenay Arc to the west. It is characterised by large relatively open folds cut by a number of north and northeast trending steep faults. These faults appear to have been active intermittently since at least Hadrynian time and played an important role in controlling the type, distribution and thickness of late Proterozoic and early Paleozoic sediments (Lis and Price, 1976). One of these faults, St Mary's Fault (49°30'N, 116°15'N, Fig. 1.1c, Chapter 1) is now an important right-hand reverse fault in the western Rocky Mountains and follows the locus of an older NE trending structure across which there were up to 13 km of stratigraphic separation with the northwest side down, during the deposition of the Windermere Supergroup (Lis and Price, 1976). The other major right-hand reverse fault in the area is the Moyie-Dibble Creek fault that had a similar stratigraphic separation of same sense but during the deposition of the Lower Paleozoic assemblage (Price, 1972)

2. The Kootenay Arc(KA).

The KA of southeastern British Columbia coincides with the west flank of the Purcell Anticlinorium. It is a curving belt of complexly deformed sedimentary, volcanic and metamorphic rocks, over 400 km long, extending from northwest Washington to north of Revelstoke (Fyles, 1970). This arcuate structural zone has developed in a succession of rocks ranging in age from Hadrynian to early Mesozoic.

The Arc is characterised by penetrative strains and complex tectonic overprinting associated with greenschist and amphibolite facies regional metamorphism and coaxial refolding about north to northwest trending axes (Fyles, 1964, 1967). A marked change in structural level occurs across the Arc from the lowest part of the Belt-Purcell Supergroup in the core of the Purcell Anticlinorium to an extensive tract of exposures of the Triassic-Jurassic rocks, which occur adjacent to the Nelson Batholith and the Shuswap Metamorphic Complex (Price, 1981).

About 20 kms of aggregate thickness of the succession of rock stratigraphic units which occur in superposition between these two horizons are mostly due to change in structural level, though part of it is due to change on stratigraphic levels. This resulted from the tectonic stacking of the continental margin terrace wedge, which accumulated outboard from the Proterozoic rifted margin of the North American craton, over to the top of the craton. Accordingly the KA is basically a simple structure:- a westerly facing monocline of crustal dimension (Price, 1981). This monoclinal step in the supracrustal rocks is coincident with the western edge of the thick (about 40 km) slab of Hudsonian (>1750 Ma) continental crust that forms the undeformed basement of the North American craton in western Canada.

3.Nelson-Rossland Arc.(NRA)

This Arc in the study area basically includes the Jurassic volcanics (the Rossland Volcanic Group) and granitic batholiths e.g., Kuskanax and Nelson batholiths, Bonnington and Trail Plutons. This Arc is part of an allochthonous terrane, Quesnellia, which consists of late Paleozoic and early Mesozoic volcanogenic eugeoclinal strata. A separate definition of the Nelson-Rossland Arc is necessary to distinguish the dominantly volcano-plutonic rocks of this Arc from the miogeoclinal rocks of the Kootenay Arc on the basis of rock-types, degree of metamorphism and different tectonic history of the two regions.

4. The Gneissic Complex(GNC).

The westernmost part of the study area is occupied by the southern part of the Shuswap Metamorphic Complex. This part of the Complex has been provisionally termed as the Okanagan Plutonic and Metamorphic Complex (Okulitch, 1984). In the study area, the Complex includes from north to south, Valhalla Gneissic Complex (Reesor, 1965; Parrish, 1984; Parrish et al., 1985; Carr, 1985), Castlegar Gneiss (Little, 1962; Simony, 1979; Halwas and Simony, 1986) and Trail Gneiss (Simony, 1979; Little, 1982). Drawing analogy with the Monashee Complex, Simony (1979) suggested that the Trail Gneiss is likely to be a partially reworked and possibly allochthonous piece of the Precambrian North American Craton. It probably acted as the basement over which an Upper Paleozoic to Jurassic sequence of 'arc-type' clastic, andesitic volcanic and volcaniclastic rocks accumulated.

The Trail Gneiss and its cover (Mt. Roberts Formation) pass northward, through a zone of increasing metamorphic grade, into the younger Castlegar Gneiss which closely resembles the upper sheet of mixed gneiss in the Valhalla Dome. The Trail and Castlegar Gneisses form a broad antiform continuous with the Valhalla Dome (Simony, 1979).

In the south the Trail and Castlegar Gneisses have a N-S faulted contact (Champion Lake Fault) with the Bonnington Pluton (Little, 1962, Simony, 1979) and in the north the Valhalla dome has similar relationship with the Nelson Batholith (Parrish, 1981, 1984; Carr, 1985).

2.2.2 Stratigraphy

A. Proterozoic

Fig. 2.2 shows the stratigraphic successions in the study area. Rocks of the Purcell Supergroup in the study area occupy the northern part of a large northwest trending basin that developed in an epicratonic re-entrant along the eastern edge of the Cordilleran miogeocline (Harrison, 1972). Thickness and facies changes are more pronounced in the eastern exposures than the western exposures. A shallow-water shelf, tidal-flat, flood plain and deltaic

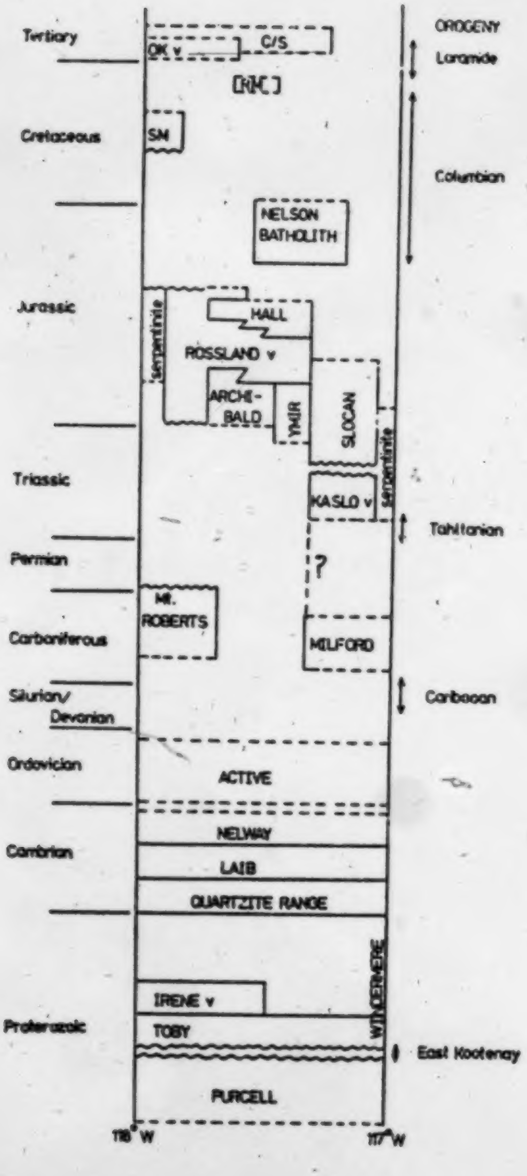
Tertiary
Cretaceous
Jurassic
Triassic
Permian
Carboniferous
Silurian/
Devonian
Ordovician
Cambrian
Proterozoic
C/S
OK v
[RM]
SM
NELSON
BATHOLITH
Serpentinite
HALL
ROSSLAND v
ARCHI-
BALD
YMIR
SLOCAN
Serpentinite
KASLO v
?
MT.
ROBERTS
MILFORD
ACTIVE
NELWAY
LAIB
QUARTZITE RANGE
IRENE v
TOBY
WINDERMERE
PURCELL
118° W
117° W
OROGENY
Laramide
Columbian
Tahltanian
Caribooan
East Kootenay

Fig. 2.2. Generalised stratigraphic succession for the Nelson-Rossland area after Douglas et al. (1970). RM=Rossland Monzonite, SM=Shophi Mt. Formation, C/S=Coryell Syenite.

depositional environment in the east graded into deep-water environment to the west. Price (1964) compared the depositional environment of the Purcell rocks to the present Gulf Coast miogeocline, with sediments derived from a large, low-relief drainage basin in the craton, and deposited on the western edge of the craton on and adjacent to the flood plain of a large subsiding delta.

The oldest rocks of the Purcell Supergroup, the Aldridge Formation, are divided into three formations: lower, middle and upper. The rusty weathering argillite, siltstone and quartzite of the lower Aldridge Formation are overlain by greater than 2000m of dominantly grey turbidite-wacke beds, interlayered with laminated siltstone of the middle Aldridge. Generally rusty weathering laminated argillite and siltstone (300-400m) belonging to the upper Aldridge were deposited over the middle Aldridge.

Metagabbro sills, more extensive in the middle Aldridge, have been used as marker horizons (Høy and Diakow, 1981). Also there are many dykes in the lower Aldridge and these generally constitute more than half of any section.

Overlying the Aldridge is the Creston Formation, consisting of subtidal to supratidal green, grey and maroon argillite and siltstone. Dominantly subtidal to intertidal carbonates and clastics of the Kitchener and Van Creek Formations overlie the Creston Formation. Locally depositional environment changed from sedimentary rocks to the andesitic lavas belonging to the Nicol Creek Formation, exposed only along the eastern flank of the Purcell Mountains. Over the rest of the mountains, grey and green argillite, dolomite and quartzite of the Dutch Creek Formation overlie the "Siyeh" Formation. The uppermost rocks of the Purcell Supergroup belong to the Mount Nelson Formation comprising stromatolitic dolomite and dolomitic limestone, argillaceous limestone and argillite.

Belt-Purcell Supergroup is overlain unconformably by dominantly immature clastic and volcanic rocks of the late Proterozoic Windermere Supergroup (Reesor, 1973; Young et al., 1973; Glover, 1978). This Supergroup forms a north trending belt that markedly decreases in width northward. At the base of the Supergroup lies a polymict conglomerate with a micaceous or sandy matrix, the Toby Formation. Pebbles, cobbles and boulders in the conglomerate are mainly quartzite and dolomite and locally greenstone. The similarity of these clasts to rocks of the underlying Purcell sequence indicates their derivation from the upper part of the Purcell Supergroup (Glover and Price, 1976). Most of the clasts of the Toby conglomerate are characteristically oblate ellipsoids flattened in the plane of the foliation, but in areas of intense deformation, dolomite clasts are hardly recognisable.

Lying above it are dark bluish green mafic tuff and massive to schistose greenstone with minor intercalations of light grey phyllite belonging to the Irene Volcanic Formation. It is succeeded upwards by pelite and limestone of the Monk Formation and then by grit, quartzite and conglomerate of the Three Sisters Formation. East of the Kootenay Lake in the northern part of the Kootenay Arc the Windermere Supergroup is represented only by the Toby conglomerate and Horsethief Creek Group. Here the Toby Formation is much narrower than in the south. The overlying Horsethief Creek Group consists of up to 8500m of pelite, slate and grit with several quartzite and polymict units. Lis and Price (1976) suggested that the deposition of the Windermere Supergroup probably involved contemporaneous faulting along the antecedent of the St. Mary Fault, a northwest dipping reverse fault of regional extent. The fault scarp related to this fault separated the uplifted source area to the south from a deep structural basin on the north. The Horsethief Creek Group thins from greater than 9 km to only a few kms northward within the basin. Southeast of the scarp, lower Cambrian quartzites of the Cranbrook Formation lie unconformably on the upper Purcell rocks. The Upper Proterozoic Windermere Supergroup is missing completely and 4 kms of the Middle Proterozoic strata, exposed further to the northeast, have been eroded away (Høy et al., 1981).

B. Paleozoic

In the south, the Precambrian-Cambrian boundary is taken at the contact between the Three Sisters and Quartzite Range Formations, because of the presence of trilobite fossils near the top of the Quartzite Range Formation (Fyles and Hewlett, 1959). The overlying Reno Formation marks a transition from the comparatively pure arenaceous rocks below through somewhat argillaceous rocks to the more calcareous rocks of the Laib Formation above. In the

Sheep Creek area. Fyles and Hewlett (1959) called the upper part of the Reno the Trueman Member, which contains limestone lenses. But Little (1965, Salmo Map) put the Reno-Laib boundary at the base of the Reeves Member, an extensive limestone bed, because the base of the Trueman Member is very difficult to trace in the Salmo area whereas that of the Reeves Member is easily recognised. Also the Reeves Member abounds in Archaeocyathids of late Lower Cambrian age. Overlying the Laib with a gradational contact is the Nelway Formation of Middle Cambrian age. It consists of grey dolomite, limestone and argillite. There is probable disconformity between the Nelway Formation and overlying Active Formation of Lower and Middle Ordovician age. It consists of black argillite and slate, grey limestone and argillaceous limestone. The Upper Paleozoic rocks are missing in this area, as if sedimentation stopped after Ordovician time.

The Paleozoic of the central KA started with the deposition of Lower Cambrian Hamill Group (micaceous quartzite, quartz-rich-schist, micaceous schist with ortho-quartzite marker unit) and the overlying Archaeocyathid-bearing limestone of the Lower Cambrian Badshot Formation. In the Riondel area, massive amphibolite units in the central part of the Hamill are probably metamorphosed basic volcanic layers (Høy, 1980). Grey phyllite, grit and greenstone characteristic of the Lower Paleozoic Lardeau Group (Lower Cambrian) overlies the Badshot Formation. An unconformity separates the late Mississippian Milford Group, composed of limestone, siliceous metasandstone, grey phyllite and local chert, basic volcanic and basal conglomerate, from the underlying Lardeau Group. Paleozoic rocks of Silurian and Devonian age are absent in the central KA.

In the northern KA, the Mohican Formation, a thin-bedded succession of calcareous rocks, is a gradational unit between the Hamill Group and the Badshot Formation (Høy et al., 1981). Here the Badshot Formation is an extensive relatively pure limestone unit and overlain by dark argillite or micaceous schist at the base of the Index Formation.

C. Mesozoic and Cenozoic

Volcanic and related rocks of the Carboniferous to Triassic Kaslo Group in the central Kootenay Arc form part of the Eastern Assemblage of Monger et al. (1982). This Group overlying the Milford Group is a succession of altered agglomerates, tuffs and flows with localised bodies of serpentinite (Rice, 1941; Klepacki and Wheeler, 1985; Klepacki et al., 1985). The Slocan Group, disconformably overlying the Kaslo Group, consists of predominantly argillaceous sediments with some well developed slaty facies. These two Groups are mostly preserved north and east of the Nelson Batholith. Further south, along the western side of the southern tail of the Nelson Batholith lies the Ymir Group, comprising of argillite, slate, argillaceous quartzite and hornfels. This Group, though unfossiliferous, was thought to be equivalent to the Slocan Group (Little, 1960). The upper part of the Ymir Group is correlated lithologically with the Archibald Formation which occurs 24 kms southwest of Ymir and ammonites of Hettangian to Lower Sinemurian age. Lithologies of this Formation include mainly argillitic siltstone and mudstone, with occasional beds of greywacke, volcaniclastics and quartzites (Beddoe-Stephens, 1979). Presence of K-feldspar and altered ferromagnesian minerals with small amount of quartz suggests a volcanic and/or plutonic source. Also lack of cross-bedding indicates a turbiditic sedimentary environment.

Conformably overlying the Ymir Group and Archibald Formation is the dominantly volcanic Elise Formation of the Rossland Volcanic Group. This Lower Jurassic Volcanic Group outcrops in an arcuate belt some 70 km long and 7-12 km wide near the town of Nelson and Rossland. Rocks of the Volcanic Group form a succession of agglomerates, conglomerates, lavas and fine-grained volcaniclastics and pyroclastics. The lava types are strongly porphyritic and range from augite-rich ankaramites to plagioclase-phyric andesites (Beddoe-Stephens, 1982). He also suggested on the basis of typical rock associations and geochemical work that the lavas formed in an island-arc regime.

The youngest sedimentary rocks of the Hall Formation conformably overlie the volcanics. Elise Formation yielded fossils of lower Sinemurian (early Lower Jurassic) age. Frebold (1959) discovered ammonites of Toarcian (late Lower Jurassic) age in sedimentary beds near the top of the Elise Formation. Hall Formation includes rocks like siltstones, greywackes and conglomerates with volcanic components. Presence of cross-bedding and plant remains and conglomerates suggests a shallow-water environment.

Latter rocks in the area are almost totally intrusive granitic (s.l.) rocks. K-Ar, Rb-Sr and U-Pb zircon dates define three periods of intrusive igneous activity:

1. Emplacement of late-synkinematic to post-kinematic granodioritic plutons in mid-Jurassic time (170-164 Ma) accompanying amphibolite facies metamorphism (e.g., Nelson Batholith, Kuskanax Batholith, Bonnington Pluton, Trail Pluton, Mine and Shaw Creek Stocks).
2. Second phase of igneous activity saw the emplacement of post-kinematic granitic plutons in mid-Cretaceous time (100 Ma) (Bayonne Batholith, White Creek Batholith, Fry Creek Batholith, Summit Stock) and
3. the last and final period of emplacement includes small and large bodies of syenite in Eocene time (50 Ma) in the western part of the area, e.g., Coryell plutons.

2.3 Structure and Metamorphism

The structure and metamorphism are discussed with respect to four areas: Summit Creek, Salmo, Riondel and Lardeau area.

Glover and Price (1976) described the structural evolution of the Summit Creek area: it involves the superposition of two phases of deformations. The overall structure is steep northwesterly plunging Summit Creek Anticline. This fold is characterised by an easterly swing of both bedding and foliation parallel to the southern margin of the Mine Stock. This anticlinal structure formed during the initial phase of deformation during which small-scale northerly plunging Z-shaped folds and an associated penetrative foliation (S_1) developed.

The above deformation is also related to differential reverse movement on the Blazed Creek fault, the probable southern extension of St. Mary's fault. At the same [illegible] the Copper Coin thrust, a westerly verging low-angle reverse fault developed as a result of emplacement of the Shaw Creek Stock. In the southern part of the area large-scale northerly plunging Z-shaped folds developed as deformation continued, together with its weak crenulation cleavage (S_2). A simultaneous external rotation of the entire block mass took place about the same axis as that of the earliest small scale northerly plunging Z-shaped folds (F_1).

A westerly facing local salient of the regional metamorphic culmination involves rocks of the Windermere Supergroup and surrounds the undeformed granodioritic Mine Stock. Pelitic rocks of the Monk Formation show the best development of the metamorphic zones. Highest grade metamorphism attained in the pelite north of the stock is represented by the mineral assemblage sill-ky-gt-staur-musc-bi-qz (Archibald et al., 1983). The preferred orientation of biotite and muscovite defines a penetrative foliation in pelitic schist of both the local salient and the regional metamorphic culmination south of the Shaw Creek Stock. Sigmoidal inclusion trails are found in staurolite porphyroblasts in the staurolite zone south of the Mine Stock and north of the Wall Stock. The above observations suggest that regional metamorphism occurred during the earliest phase of deformation. Parallelism of the metamorphic isograds with the boundaries of granitic stocks demonstrates that contact metamorphism outlasted the penetrative deformation in the southern part of the Summit Creek area. In this area, Archibald et al. (1983) noted that "post-kinematic quenching of prograde metamorphic reactions occured at a temperature of about 500°C and a depth of about 15 km (P=0.38 GPa) south of the Mine Stock, but a temperature of about 600°C and a depth of about 20 km (P=0.55GPa) on the north side".

A well-defined distinctive low-pressure contact-metamorphic aureole has developed in pelitic Monk Formation in response to the emplacement of the Summit Stock, a post-orogenic quartz-monzonite pluton. Andalusite and cordierite porphyroblasts within the andalusite zone of the aureole have overgrown the deformation fabric, whereas rocks from the sillimanite and sillimanite-K-feldspar zones have a granoblastic texture. Overlapping and retrograding effect of the Summit Stock aureole over that of the Mine Stock suggests the emplacement of the Summit Stock took place after the cessation of the penetrative deformation and after significant post-metamorphic uplift and erosion.

Leclair (1982, 1983) studied the area just west of the Bayonne Batholith and discovered a major west-dipping thrust fault that juxtaposes the Windermere Supergroup (hanging wall) over the Hamill Group (footwall). It resembles the west Bernard fault east of Kootenay Lake described by Høy (1980), as it separates a right-hand-up panel of upper Proterozoic to Lower Cambrian rocks to the south and east from a tightly folded and probably up-side-down sequence to the west.

The structure in the Salmo area is dominated by a series of tight isoclinal folds and arcuate thrust faults. Fyles and Hewlett (1959) divided the area into four major structural units. They are from east to west Eastern, Black Argillite, Mine belts and Mesozoic volcanic rocks. From the east isoclinal Laib Syncline complicated by a series of northerly trending steep faults follows westward to Sheep Creek anticline. The youngest rocks exposed within the Laib syncline include Ordovician slate and argillite. In the anticline the whole Cambrian section well down into the Lower Cambrian Quartzite Range Formation is repeated. These structures constitute the Eastern Belt. The Black Bluff Fault separates Sheep Creek anticline from the Black Argillite Belt, represented by a sequence of probable Ordovician black slate and argillite (Active Formation) exposed along the northerly trending belt. These rocks, bounded on the east and west by regional strike faults, are complexly folded and faulted and have an overall synformal form. Across the Black Bluff Fault Middle Cambrian argillaceous limestone, dolomite and phyllite on the east are juxtaposed over tightly folded argillite and slate on the west. The Mine belt on the west is a belt of great structural complexity. Complexly folded and faulted section of the Reeves limestone is on the upper limb of the Jersey Anticline. It is a complicated recumbent fold with an axis which plunges southward on the south slopes of the Iron Mountain, northward on the north slopes, and has a gently dipping axial plane which is broadly folded (Brown et al., 1981). The Mine belt is bounded on the west by a complexly folded and faulted thrust fault, the Waneta fault, which dips southward at low angles west of the Black Bluff Fault but further to the north swings northward and steepens.

These bedding faults form the boundaries between the folded belts, which have been thrust successively from southeast to northwest upon one another and which formed before the emplacement of the Nelson intrusives. Along the Argillite Fault younger rocks have overridden older ones, but elsewhere the reverse is true (Fyles and Hewlett, 1959). Northward in the Ymir area the four structural units are also recognised. From east to west, they are bounded successively by the Porcupine and Oxide faults and an assumed fault west of them. It is probable that the Black Bluff Fault is same as the Porcupine Fault and the Argillite fault is the extension of the Oxide fault. The principal change from Salmo northward is a change in the dips of the foliation, and consequently of the axial planes of phase I folds, from vertical in the south to 30° to 50° to the west, characteristic of the formations in the central 70-80 km of the Kootenay Arc.

Central Kootenay Arc shows drastic change in the structural style from that in the southern part of the Arc. Three phases of folding have regionally developed in the central and northern Arc and northern Selkirk Mountains. In general, oldest or phase I folds produced structures that are tight to isoclinal north-trending recumbent anticlines. They have gently plunging axes and folded axial planes. In the Riondel area, the Riondel nappe, the oldest recognised structure, is a recumbent fold closing to the west (Høy, 1977). A west-dipping reverse fault separates an inverted panel of rocks in the west (the lower limb of the nappe) from a right-way-up panel in the east. The root of the nappe is probably hidden beneath this thrust fault.

In the Lardeau area, a phase I syncline in Lower Paleozoic rocks is truncated by an unconformity at the base of the early Mississippian Milford Group (Read, 1976). Moreover, clasts derived from the Broadview Formation are found in the conglomerate at the base of the Milford Group (Read, 1975). These evidence suggest that phase I structures developed during the Cariboo Orogeny in pre-late Mississippian time.

Phase II folds are more open and comprise of crenulation cleavage folds with north trending axes (parallel with phase I folds) and upright to steeply west dipping axial surfaces superimposed on phase I folds (Fyles, 1964; Høy, 1977, 1980). These folds dominate the structures of the Kootenay Arc and are responsible for pronounced N-S structural grain. This second phase of deformation is apparently restricted to an interval between 178 to 164 Ma in the Lardeau area. Phase II folds commonly have an N-shaped profile looking northward, and cause stratigraphically and structurally higher rocks to outcrop on the western side of the Arc. Phase

III folds of Read (1973) and Brown and Tippet (1978) generally show a reverse N-shapes profile looking northward, a westerly dipping axial plane. They are common in the central and southern parts of the Arc. These phase III folds are generally taken as phase II folds in the central KA (Fyles, 1964; 1967; Høy 1980) as phase II folds in the north appear to die out in this part of the Arc. These phase II folds in the Riondel area are younger and a minimum age of 97 Ma is provided by the age of the post-tectonic Fry Creek Batholith (Høy, 1977).

According to McMechan and Price (1982), the region south of the Moyie Fault has been metamorphosed to greenschist (east) to subgreenschist (west) facies. Here the penetrative cleavage in argillites of the Aldridge Formation is defined by the preferred orientation of muscovite and biotite neoblasts. The present petrographic study shows that the argillites of the Aldridge Formation are in the bi-isograd and bi-musc-albite-qz and are in bi-musc-qz subfácies of the greenschist facies.

Along the western boundary of the Purcell Anticlinorium lies a N-S trending belt of amphibolite facies regional metamorphism that transects major structures of the Kootenay Arc (Crosby, 1968). This belt plunges to the north under the Purcell Anticlinorium, but in the south it merges with a plutonic-metamorphic complex in northern Idaho (Miller and Engels, 1975). Archibald et al. (1983) compiled all the data on metamorphic mineral assemblages in pelitic rocks and have drawn the regional metamorphic isograds in the Kootenay Arc (Fig. 2 of Archibald et al., 1983).

The highest grade of metamorphic rocks is recorded by the presence of sillimanite-K-feldspar gneiss in the Riondel area (Høy, 1976), corresponding to a pressure between 0.5 to 0.6 GPa and a temperature close to 650° C (Archibald et al. 1983). Beside this areally restricted zone, the innermost sillimanite zone (10-15 km across) forms the core of the metamorphic culmination and is recorded in rocks as old as the Aldridge Formation in the south and as young as the Triassic Slocan Group in the north (Parrish, 1981). Isograds of lesser metamorphic grade (St/St-Ky, Gt and Bi) form concentric zones in the area and therefore indicate metamorphic grade decreases both east and westward.

Degree of metamorphic grade decreases westward from the Kootenay Arc to the Nelson-Rossland Arc. Studies of Beddoe-Stephens and Lambert (1981) show that in the rocks of the Rossland Volcanic Group, north of Salmo, virtually all primary minerals have been replaced by greenschist facies hornblende or actinolite, chlorite, epidote, biotite, calcite and secondary plagioclase. South of Salmo, the degree of metamorphism decreases to prehnite-pumpellyite facies. Though plagioclase is frequently sericitised or saussuritised and pseudomorphs of olivine as calcite or chlorite are found, primary amphibole and spinel are common relict phases. Fresh, unaltered clinopyroxenes are also found.

In the Gneissic Complex, the grade of regional metamorphism is low but increases northward from Trail towards the Valhalla Gneiss Dome where sillimanite grade metamorphism is attained (Wheeler et al., 1974).

3. GEOCHRONOLOGY OF SEDIMENTS AND GRANITES

3.1 Rb-Sr dating of Sediments

Many studies have been made to test the applicabilty of whole rock Rb-Sr method for dating of unmetamorphosed to low-grade metamorphosed sedimentary rocks (e.g., shales, argillites). Since the first attempts of Whitney and Hurley (1964), Bofinger and Compston (1967), Bofinger et al. (1968), although resonable ages have been obtained, dating of sediments is beset with many uncertainties. The dates obtained are either older (Choudhuri and Brookins, 1967) or younger (Compston and Pidgeon, 1962) than known stratigraphic age or geologic arguments might allow. Moreover because of our limited understanding of isotopic equilibrium processes soon after deposition and during diagenesis, lithification and low-grade metamorphism (greenschist facies), confusion arises while interpreting the dates as either sedimentary, diagenetic or metamorphic. Such difficulties are related to the detrital component (i.e., presence of inherited radiogenic ^{87}Sr, Whitney and Hurley, 1964), and to the degree of isotopic equilibration of the clay minerals in marine environment with the seawater strontium. Dasch (1969) and Biscaye and Dasch (1971) in their study of deep sea sediments demonstrated clearly that homogenisation of strontium isotopes does not take place as a result of prolonged contact between sediments and seawater.

Metasedimentary argillaceous rocks have been dated by whole rock Rb-Sr method. Powell et al., (1969) obtained a 2730 Ma age for a group of metasediments metamorphosed to cordierite-biotite grade. They interpreted this age as either the age of sedimentation or the time of isotopic homogenisation. Peterman (1966) interpreted a date of 1.75 Ga for metasedimentary rocks of Mahnomen Foramtion of Minnesota as most likely age of metamorphism associated with the Penokan orogeny. Argillaceous sedimentary rocks of this Formation contain 2M polymorph of muscovite and therefore are in the greenschist facies of metamorphism. Also Faure et al. (1968) suggested that low-grade or contact metamorphism may cause isotopic homogenisation of strontium.

However for unmetamorphosed shales, to obtain an Rb-Sr age representing the time of deposition, the sediments must have had a uniform $^{87}Sr/^{86}Sr$ ratio and a reasonable spread in Rb/Sr ratios at the time of deposition and remained isotopically closed system thereafter. Cordani et al. (1978) suggested that "if some criteria are followed regarding the selection of samples (based on their mineral composition and Rb, Sr contents) and that all samples are derived from the same depositional environment, the sedimentation ages can be obtained in practice from any kind of unmetamorphosed pelitic rocks". The mechanical dispersion of the detrital material in the depositional basin should be effective enough to lead to a uniform Sr-isotopic composition for WR samples a few cm in size. Moreover a convenient range in Rb/Sr ratio should also result. Works of Dasch (1969), Biscaye and Dasch (1971) and Hart and Tilton (1966) support such expectations. Homogeneous isotopic composition may also result either from authigenic formation of the bulk of the sample (glauconite, Obradovich and Peterman, 1968; Morton and Long, 1980) or from an isotopically uniform source (Perry and Turekian, 1974)

Sr-isotopic inheritance from the source is possible as the weathering of primary crustal rocks results in an increase of the Rb/Sr ratio but will not largely affect the Sr-isotopic composition (Dasch, 1969). Moreover transport of weathered detritus does not result in significant Sr-isotopic changes in detritus. If such conditions are true, Rb-Sr dating of pelitic rocks consisting of such detritus minerals will result in dates greater than sedimentation (Whitney and Hurley, 1964).

If the above sediments undergo burial or regional metamorphism, equilibration of Sr isotopes between phases may result and age obtained is likely to represent metamorphic age. Initial $^{87}Sr/^{86}Sr$ ratio will be equal to integrated, average ratio inherited from the source region.

During deposition of detritus components, mixing with an isotopically homogeneous phase (e.g., carbonates) will result in "isochron slope" which may be positive, zero or even negative, depending on the composition of the end-members. Such mixing will tend to homogenise the bulk Sr-isotopic composition and lower the Rb/Sr ratios of the samples.

The present study is an attempt to date the sedimentary and/or metamorphic ages of different sedimentary units constituting the miogeocline. The present state of paleontological, structural and metamorphic evidence has been taken into account while interpreting the dates.

3.2 Proterozoic Sediments

3.2.1 Geology

The Purcell Supergroup of southeastern British Columbia and southwestern Alberta, together with its stratigraphic equivalent, the Belt-Purcell series of western Montana and northern Idaho is the most extensive and least disturbed succession of Proterozoic sediments in North America. It crops out over an area greater than 125,000 km^2. Purcell Supergroup in Canada attains a maximum thickness of 14 km (Gabrielse, 1972). The Belt-Purcell Supergroup thins eastward towards the craton where shallow marine and fluvial carbonate and coarse to fine-grained clastic rocks dominate.

Purcell rocks outcrop in three tectonically distinct areas (Clarke Range, Hughes, Lizard and Galton Range and Purcell Anticlinorium) in southeastern B. C. and southwestern Alberta (Høy et al., 1981). The present geochemical study is related to the most western tectonic or structural unit, i.e., the Purcell Anticlinorioum. The Purcell Supergroup in the Anticlinorium consists of seven sedimentary Formations, the oldest and thickest is the Aldridge Formation of siliciclastic rocks probably deposited by turbidity currents (Hamilton et al., 1983, Bishop et al., 1970).

Samples collected for dating come from the middle Aldridge Formation, which is about 3 km thick. The thinner (300-400 m) upper Aldridge consists of generally rusty weathering laminated dark grey argillite and lighter grey siltstone with turbiditic characteristics.

3.2.2 Structure and Metamorphism

The Purcell Anticlinorium is a broad north-plunging structure in rocks of Helikian and Hadrynian age between the Rocky Mountains to the east and the Kootenay Arc to the west.

Central part of the anticlinorium in the southern Purcell mountains is cut by a number of NE-trending faults, e.g., St. Mary's Fault, Moyie Fault. Geology of the Moyie lake area has been worked out in detail by Høy and Dickow (1981). The Moyie fault cuts the western limb of the Moyie anticline, a northeast plunging upright fold, the dominant structure of the "Moyie Block" of Benvenuto and Price (1979). Metagabbro sills define tight to open north to northeast trending folds involving lower and middle Aldridge rocks (Høy et al., 1981).

According to McMechan and Price (1982), the region south of the Moyie Fault has been metamorphosed to greenschist (east) to subgreenschist (west) facies. Here the penetrative cleavage in argillites of the Aldridge Formation is defined by the preferred orientation of muscovites and biotite neoblasts. The present petrographic study shows that the argillites of the Aldridge Formation are in the bi-isograd and bi-musc-albite-qz and bi-musc-qz subfacies of the greenschist facies (Table A.3, Appendix 1).

Samples collected from two localities can be divided into two groups on the basis of mineralogy and structure. The first group shows predominant bedding laminations (or cleavage) consisting of alternate bands of quartz and micas. Plagioclase (albite) is absent. While the second group is devoid of such laminations but contains small amount of plagioclase. The other significant difference lies in the colour of biotite. The first group is dominated by pale brown biotite while the second group by deep brown biotite. There is difference in grain size in quartz, finer in Group 1, and both fine and coarse in Group 2. Such differences are attributable to the differential response to the metamorphic conditions and thereby isotopic homogenisation of originally heterogeneous sediments. Biotite found in these rocks is entirely of metamorphic origin, though very small % of detrital biotite may be present as in the Mount Fisher area (McMechan and Price, 1982). They have studied in detail the degree of metamorphism in this area using techniques based on the illite crystallinity (Kubler, 1967) and on the ratio of muscovite polymorphs. In this area, in argillites, illite crystallinities vary in the range of 2.0 to 3.0 and proportion of 2M muscovites varies from 60 to 100%, increasing with stratigraphic depth. 2M (two-layer monoclinic) form is the stable form at high temperature and the inversion of the 1M (one-layer monoclinic, ordered) and 1Md (one layer, monoclinic, disordered) forms to 2M form occurs between 200 to 300°C at 0.1 GPa (1kbar) total pressure (Yoder and Eugster, 1955). Increase in the relative proportion of the 2M form of muscovite is directly proportional to the increasing metamorphic grade. Many workers (Frey, 1970; Siddans, 1977) observed that muscovites found in rocks in the greenschist facies of regional metamorphism are almost entirely of 2M polymorph. The high proportion of 2M polymorph found in the greenschist facies rocks of the Mount Fisher area should also be found in the present study area (Moyie Lake) as the argillitic rocks show greenschist facies mineral assemblage. If this assumption is correct, then the maximum temperature attained during regional metamorphism in the Moyie lake area can be roughly estimated from the mineral assemblages. A minimum temperature of 300°C (Turner, 1968; Zen and Thompson, 1974) and a maximum temperature of 350°C (Schwarcz et al., 1970), 400°C (Carmichael as quoted in McMechan and Price, 1982) and 440°C (Winkler, 1976) during disappearance of biotite have been estimated for the greenschist facies metamorphism. Therefore both lines of evidence indicate a metamorphic temperature of about 350°C or slightly higher.

3.2.3 Earlier Work

The age of the Purcell system in the Canadian Cordillera is known only within broad limits. Oldest rocks overlie crystalline basement >1.6 Ga old (Burwash et al., 1962) or 1.7 Ga (Zartman et al., 1982). Paleomagnetic studies (Evans et al., 1975, Vitorello and van der Voo, 1977; Elston and Bressler, 1980) suggest that the Belt-Purcell Supergroup was deposited prior to 1300-1350 Ma. Obradovich and Peterman (1968) obtained a K-Ar date of 1330±45 Ma on biotite from the Pichard (correlative to Aldridge) Formation from the Alberton area of northwest Montana and a WR Rb-Sr date of 1325±15 Ma for argillaceous samples from the Big Belt and Little Belt Mountain sequence. A K-Ar biotite date of 995 Ma has been reported from the Moyie Lake area by McMechan and Price (1982).

Andesitic flows and gabbroic to dioritic dykes and sills are volumetrically minor but are widely distributed throughout the Purcell sequence (Gabrielse, 1972). Sills are concentrated in the middle and lower units of the Aldridge Formation in the Purcell Mountains and locally form a high proportion of the stratigraphic successions. Gabbro sills intruded the Purcell Supergroup in southeastern British Columbia in two stages during middle Proterozoic time and in at least three stages in the Belt Supergroup. Zartman et al. (1982) obtained a U-Pb age on zircon of 1433±10 Ma from a basic sill in the Crossport area of northern Idaho. This sill is a typical example of the Moyie intrusions which are slightly discordant sheets and dykes, most commonly developed in the lower part of the Aldridge Formation. Therefore the lower and middle Aldridge Formations must be older than 1433 Ma and the younger dates must be related to deformation and regional metamorphism.

North of the St. Mary's fault in the Mathew Creek area, intrusion of the granodioritic Hellroaring Stock into the Aldridge Formation post-dates the Precambrian regional metamorphism and folding (Leech, 1962). Ryan and Blenkinsop (1971) obtained a Rb-Sr WR isochron date of 1305±52 Ma (recalculated using $\lambda=1.42\text{x}10^{-11}\text{yr}^{-1}$) for this Stock. Therefore the Aldridge Formation here is older than at least 1300 Ma.

3.2.4 Results

Eighteen whole rock samples have been analysed for Rb, Sr concentrations and their isotopic compositions. The analytical results for both the groups are listed in Table 3.1. Fig. 3.1 shows the plot of all data points. Group-I samples give an isochron age of 971±10 Ma(2σ) with an initial ratio of 0.7294±0.0005 and MSWD=45. Group-II samples have a slope with equivalent age of 1142±18 Ma(2σ) and initial ratio of 0.7411±0.0008 and MSWD=158. Therefore the age for Group-I is more precise than that for Group-II.

3.2.5 Discussion

The relatively lower MSWD for Group-I set of samples points to the geological significance of the age. However correct interpretation of this age depends on many factors. In the fine-grained sediments like the Aldridge Formation, isotopic homogenisation must have started soon after deposition and during diagenesis and lithification due to burial. Chemical diagenesis depends essentially on temperature, time and chemical environment (Sibata and

Table 3.1 Rb-Sr data from the Aldridge Formation.

Sample ID	Rb(ppm)	Sr(ppm)	$^{87}Rb/^{86}Sr$	$^{87}Sr/^{86}Sr$
		Group-I		
8001B	64.60	103.42	1.8163	0.75788±3
8001E	247.76	105.26	6.8840	0.81843±3
8001F	203.11	40.46	14.8508	0.93969±12
8002D	252.04	67.80	10.9430	0.88619±3
8002E	210.61	173.32	3.5397	0.77794±3
8002F	148.52	220.74	1.9556	0.75494±3
8002G	45.44	95.88	1.3770	0.75000±4
8002H	149.59	145.54	2.9945	0.76892±3
		Group-II		
8001C	101.50	94.35	3.1370	0.78690±3
8001G	222.93	136.02	4.7994	0.81901±3
8001H	114.48	73.902	4.5330	0.82361±6
8001I	198.09	76.09	7.6406	0.85449±3
8002A	149.64	62.39	7.0465	0.86042±2
8002C	204.22	233.65	2.5487	0.78790±1
8002I	70.61	118.06	1.7405	0.76734±1

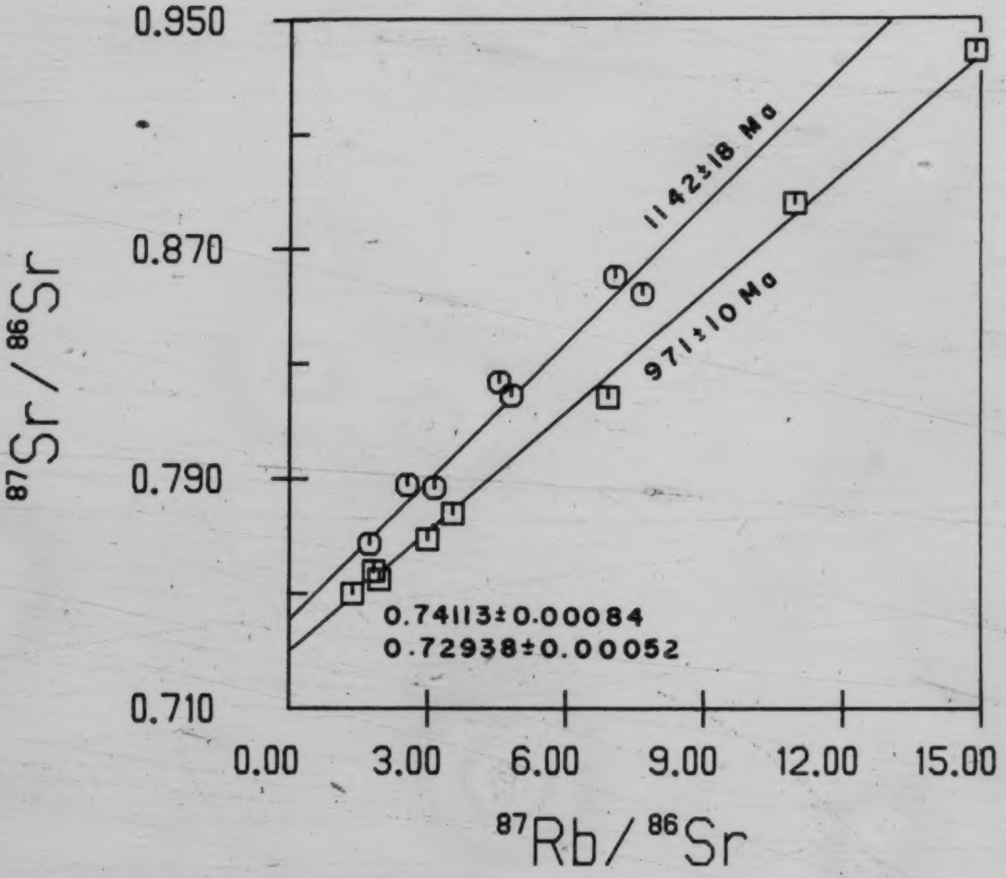

Fig. 3.1. Rb-Sr isochron diagram for the middle Aldridge Formation. Open square symbols are samples belonging to Group-I (8001B, E, F, 8002D, E, F, G, H) and open hexagon symbols represent samples belonging to Group-II (8001C, G, H, I, 8002A, C, I)

Mizutani, 1982). Later low-grade metamorphism led to the formation of new biotite and muscovite crystals under prevailing thermodynamic conditions. As discussed before, on the basis of analogy of the metamorphic grade in the Fisher Creek area (McMechan and Price, 1982) and Moyie lake area (Høy et al., 1981), and present petrographic study of the samples (Table A1.3, Appendix 1), the middle Aldridge Formation was metamorphosed to greenschist facies with the abundant formation of biotite and 2M polymorphs of muscovite. Under such conditions of pressure and temperature (>350°C and 0.1 GPa), and knowing the sensitive behaviour of Sr-isotopes in micas, Sr-isotopic homogenisation is likely to be expected (Peterman, 1966; Faure et al., 1968). The close fit of 8 metasedimentary samples to an isochron line with slope equivalent to 971±10 Ma therefore must indicate timing of such metamorphism. Additional support for this conclusion is obtained from a K-Ar date (995 Ma) on biotite from Moyie Lake area (McMechan and Price, 1982). Similarity of these two independent dates for the argillaceous rocks is significant. This date of 995 Ma is the oldest of all K-Ar dates determined on biotite and muscovite from this area. As resetting of K-Ar dates on biotite and muscovites depends on the degree of Ar-loss during metamorphism, the oldest date of 995±34 Ma is taken to represent the closure of Ar diffusion during cooling of the system.

It is also now known that Aldridge sedimentation was terminated during East Kootenay Orogeny at 1300-1350 Ma on the basis of palaeomagnetic data and dating of gabbroic sills and granitic body (Hellroaring Creek Stock). Therefore the younger WR Rb-Sr age of 971 Ma obtained for Group-I samples must be due to a later episode of metamorphism. According to McMechan and Price (1982), the second episode of metamorphism (Goat River Orogeny during 800-900 Ma) occurred during deposition of the Windermere Supergroup. The present study shows that the metamorphism that affected the middle Aldridge Formation in the Moyie Lake area is older (by ≅80-90 Ma) than the Goat River Orogeny.

The second group of samples plot around a 1142 Ma line with significant scatter. This date is difficult to explain, but is probably partially reset during 970 Ma metamorphic event. On the basis of present study, it is therefore proposed here that an episode of greenschist facies metamorphism took place around 970 Ma. High Sr-initial ratios of 0.729 to 0.741 suggest lack of isotopic homogenisation with contemporary Proterozoic seawater (0.7075 at 1000±50 Ma, Veizer et al., 1983).

3.3 Lower Paleozoic Sediments

3.3.1 Geology

In southeastern B. C. (Salmo area), the base of the Cambrian system is placed at the contact between the Three Sisters and Quartzite Range Formations. Cambrian trilobites have been found near the top of the later Formation (Fyles and Hewlett, 1959). The Quartzite Range Formation is overlain by the Reno and then by the Laib Formation, the Reeves member of which abounds in Archaeocyathids of late Lower Cambrian age. With a gradational contact the calcareous Nelway Formation overlies the Laib. A probable disconformity separates the overlying Active Formation from the Nelway Formation. The upper Paleozoic rocks are missing in this area as if sedimentation stopped after Ordovician time.

Little (1960) summarised the geology of these two Formations. Outcrops of dominantly calcareous Nelway Formation are exposed in the belt bounded by the Ripple Creek Fault in the east, Black Bluff Fault in the north and the Pend-d'Oreille river in the west (Salmo Map area). Total thickness and mineralogy of the Nelway Formation north of the International boundary has been worked out only in comparison to that of the equivalent "Metaline Limestone" well exposed in the United States near the Metaline Falls. The lower part of the Nelway Formation is dominated by mostly black calcareous rocks: limestone, phyllite and calcareous schist. The middle part consists of mainly weathered dolomite, while abundant irregular masses of chert dominate the upper part of this Formation. While no diagnostic fossils have been found in the Nelway Formation north of the border, trilobites of Middle Cambrian age occur in the corresponding Metaline Limestone to the south.

The Active Formation outcrops are found discontinuously in a N-S belt bounded by the Black Bluff Fault on the east and the Argillite fault on the west. It is also exposed in an E-W trending belt south of the Pend-d'Oreille river. Because of the complex structure and absence of top and bottom exposures, Little (1965) could not determine the total thickness of the Active Formation. However a maximum apparent thickness of about 1400m is obtained in the type area, i.e., the Active Creek Valley. The Active Formation correlated with the "Ledbetter slate" of Metaline Quadrangle in USA consists of dolomite, dolomite breccia and limestone, silicified argillite and limestone, grey limestone and argillaceous limestone. Graptolites of probable Deepkill (lower Ordovician) age have been found from the Active Formation and some of Normanskill (early Middle Ordovician) age have been found to occur in the equivalent formation south of the International boundary.

3.3.2 Structure and Metamorphism

Salmo Map area lies in the southern part of the Kootenay Arc where its trend changes abruptly from roughly south to southwestward and locally west. A series of tight isoclinal folds and arcuate thrust faults dominate the structural pattern of the Salmo area. Black Bluff, Argillite and Waneta faults divide the area into four major structural belts (Eastern, Argillite, Mine belts and Jurassic Volcanic Rocks). Samples collected from the Nelway Formation are dominantly calcareous with minor amounts of quartz and muscovite. The rocks show wavy schistose structure with thin muscovite bands complexly folded. Quartz grains are present as small lenses. Beside forming the distinct bands, muscovites also occur as scattered grains within the main carbonate mass. No appearance of biotite has been detected. Therefore the Nelway Formation has not been subjected to greenschist facies metamorphism.

Black slates/phyllites collected from the Active Formation lie above the biotite isograd as first appearance of biotite (though in small amount) has been detected. Unlike the Nelway Formation, Active samples are not carbonate rich but there is a variation in the amount of carbonate (e.g., 8009U: most carbonate rich(20%) and 8009A: without any carbonate). Well developed schistosity consists of alternate bands of quartz and micas. Quartz grains have been flattened to a great extent with the longer axes parallel to the schistosity, implying great load or compressional pressure.

3.3.3 Results

Six whole rock samples were selected from the Nelway Formation for age determination by Rb-Sr method. Analytical results and the isochron plot are shown in Table 3.2 and Fig. 3.2 respectively. Rb-Sr data for whole rock samples give an isochron age of 557±50 Ma (MSWD=1.28), by excluding sample 8010V which is clearly far off the rectilinear plot. According to the time scale of Harland et al. (1982), 557 Ma is correlated to mid Lower Cambrian. The Sr-initial ratio calculated for the Nelway Formation (0.71018±0.00027) is slightly higher than that of contemporaneous seawater (0.7091, Burke et al., 1982).

Analytical data for 7 whole rock samples from the Active Formation are given in Table 3.2 and plotted in Fig. 3.3. Rb-Sr data for seven whole rock samples fall on an isochron line of slope equivalent to 160±8 Ma(2σ) and an initial ratio of 0.71662±0.00034(2σ) and MSWD=7. The initial ratio for this mid-Ordovician Active Formation is much higher than contemporaneous marine Sr isotopic composition (0.70675, Peterman et al., 1970; Burke et al., 1982).

3.3.4 Discussion

Because of absence of any diagnostic fossils in the Nelway Formation, the present study to determine the age of sedimentation is the first attempt using the whole rock isochron method. The indirect evidence that the Nelway Formation in the Salmo area is of Middle-Cambrian age comes from the abundant fossils found in the equivalent Metaline Formation south of the international boundary (Little, 1960). The similarity between the isochron age and the indirect fossil age substantiates the validity and usefulness of the whole rock Rb-Sr dating method to a sequence of unmetamorphosed calcareous and shaly sediments. Therefore the slope age of 557 Ma is interpreted as the age of sedimentation for the Nelway Formation. Deviation of the sample 8010V from the isochron plot is difficult to explain, as it is no different mineralogically from the others. Discounting analytical error as the reason, the sample might contain some undetected detrital component accounting for the high $^{87}Sr/^{86}Sr$ ratio.

Table 3.2 Rb-Sr data from the Nelway and Active Formations

Sample ID	Rb(ppm)	Sr(ppm)	$^{87}Rb/^{86}Sr$	$^{87}Sr/^{86}Sr$
	Nelway	**Formation**		
8010R	81.78	803.19	0.2947	0.71214 ± 1
8010S	44.71	825.88	0.1567	0.71195 ± 1
8010T	21.45	946.97	0.0655	0.71055 ± 1
8010Q	112.48	510.37	0.6381	0.71540 ± 6
8010W	67.23	500.09	0.3892	0.71313 ± 2
8010V	22.39	703.98	0.0920	0.71352 ± 3
	Active	**Formation**		
8009A	101.59	39.88	7.3896	0.73425 ± 2
8009D	58.59	323.76	0.5241	0.71789 ± 5
8009J	93.09	256.84	1.0495	0.71940 ± 2
8009L	93.24	80.79	3.3441	0.72245 ± 1
8009R	52.34	117.82	1.2868	0.71955 ± 1
8009T	39.06	362.98	0.3117	0.71814 ± 2
8009U	16.62	707.81	0.0680	0.71657 ± 2

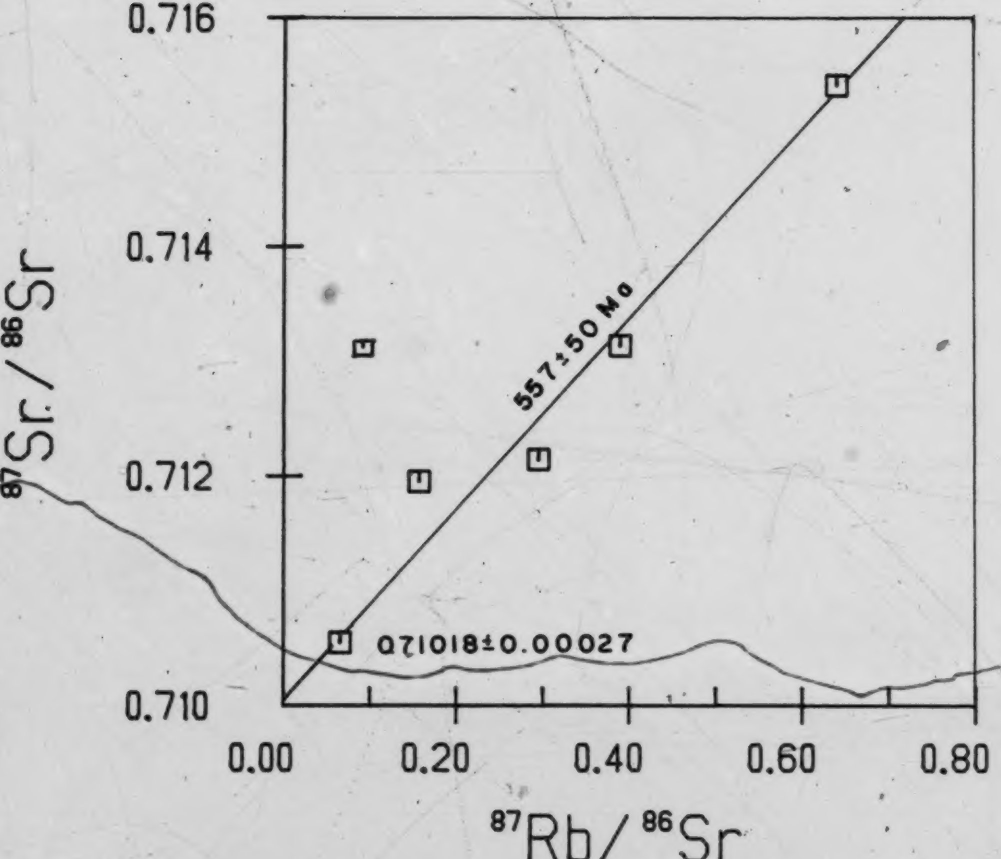

Fig. 3.2. Rb-Sr isochron diagram for the Nelway Formation.

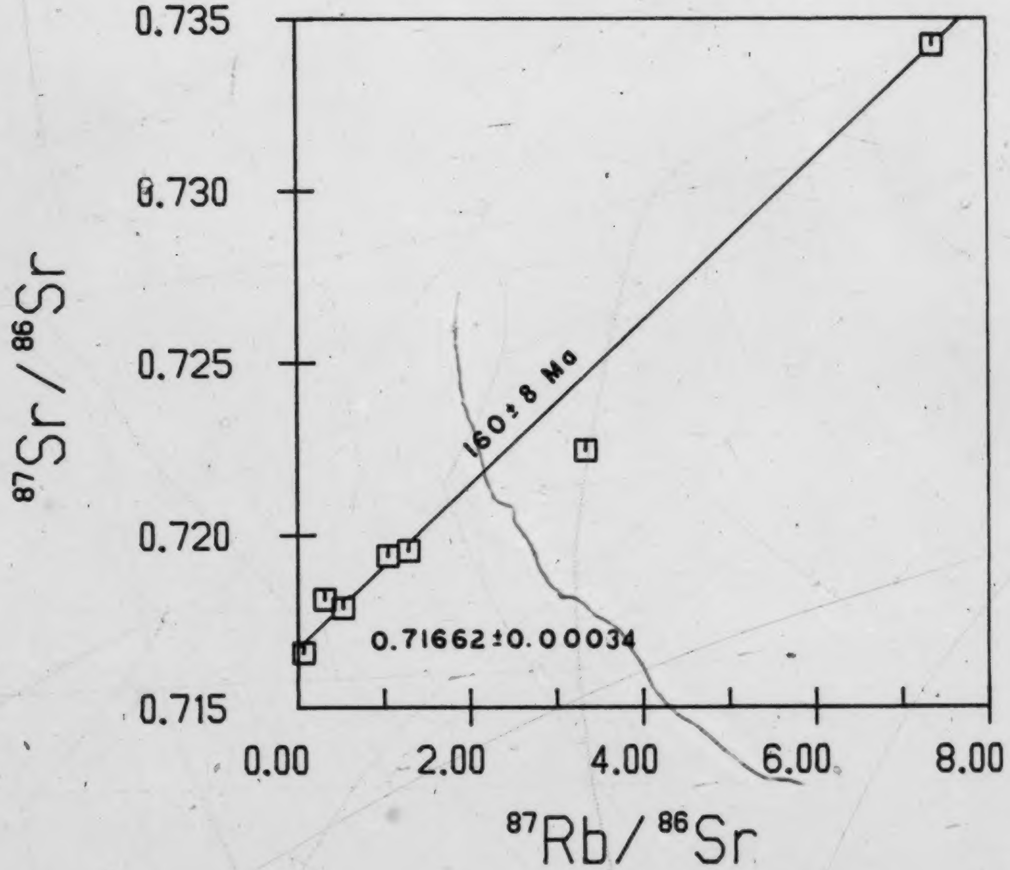

Fig. 3.3. Rb-Sr isochron diagram for the Active Formation.

Because the samples are variable mixtures of carbonates and detrital minerals and because of good fit of the data points to an isochron line, it is very likely that during sedimentation, there was almost complete isotopic homogenisation on the bulk rock scale. Isotopic equilibration between the aluminosilicates detritus as a whole and the marine carbonate may be expected as a result of low-temperature, geologic processes during diagenesis. During this processes, carbonate rocks will loose significant amount of Sr which in turn will flux through the adjacent clays. Veizer and Compston (1974) suggested that Sr isotopic exchange between silicates and carbonate phases may occur during deep burial diagenesis and thereby increase $^{87}Sr/^{86}Sr$ in the carbonate. Slightly higher initial ratio (0.71018) calculated for the Nelway Formation than contemporaneous marine Sr (0.7091) could be the result of such an exchange. Resulting mixing of clays and carbonates must have lowered the Rb/Sr ratios of whole rocks, but the range found (0.06 to 0.63) was significant enough to produce the isochron.

The seven representative samples give an isochron age of 160 Ma much lower than the established stratigraphic age (Lower Ordovician). Mineralogies of these samples also show that the Formation has been metamorphosed to lower greenschist facies (biotite isograd). Therefore the age obtained strongly suggests that the Active Formation has been metamorphosed during mid-Jurassic time. This metamorphic event is probably correlated to the movements along the Black Bluff Fault during or just after emplacement of the Nelson Batholith.

Larger variations in Rb/Sr and $^{87}Sr/^{86}Sr$ ratios are found for the Active Formation (Table 3.2). Sample 8009U is most carbonate rich (20%) and has $^{87}Rb/^{86}Sr$ ratio close to zero(0.06). If the carbonate fraction of this sample had the same Sr-isotopic composition as that of marine Sr during Lower Ordovician (i.e., 0.70675, Burke, et al., 1982), its extremely low Rb/Sr ratio cannot support the growth in $^{87}Sr/^{86}Sr$ to 0.7166 found at 160 Ma. Alternatively its Rb/Sr ratio might have been drastically lowered during upper Jurassic metamorphism from the pre-metamorphic value, though it is very unlikely. Therefore it is suggested here that there was Sr-isotopic exchange between silicates and carbonates during metamorphism supporting Veizer and Compston's(1974) observation.

It is possible to reconcile the juxtaposed occurrence of unmetamorphosed Nelway with the metamorphosed Active Formation along the Black Bluff Fault from the field observations. Along this fault sedimentary formations including the Nelway have thrust over the younger Active Formation to the west, resulting in deeper burial and consequently higher temperature and pressure conditions for the latter. The difference in metamorphic grade also supports this scenario.

3.4 Upper Paleozoic and Lower Mesozoic Sediments

3.4.1 Geology

The Milford, Kaslo and Slocan Groups were originally defined by Cairnes (1934) and the Ymir Group by Frebold and Little (1962). These sedimentary groups have been studied in detail by Little (1960, 1964, 1967), and more recently by Høy (1977) and Høy et al. (1981), Leclair (1983), Klepacki (1983), Klepacki and Wheeler (1985) and Klepacki et al. (1985). The following is a brief geological summary:

The Milford and Slocan Groups outcrop only in the central and northern Kootenay Arc. In the central Kootenay Arc the Milford Group occupies a narrow belt along the west side of the Kootenay Lake, unconformably overlying the Lower Cambrian Lardeau Group.

Leclair (1983) divided the Milford Group in the central Kootenay Arc into three mappable units:

Upper Unit: Thinly bedded grey to light-grey quartzite and chert intercalated with greenstone and amphibolite.

Middle Unit: thin unit of greenstone and amphibolite.

Lower Unit: dark grey to black phyllite and schist and blue grey limestone with minor quartzite and greenstone.

Klepacki (1983) on the basis of detailed mapping in the Roseberry Quadrangle divided the Milford Group into 5 distinct units:

Grey Siliceous Argillite Unit

Phyllite Greenstone Unit
Cherty Tuff Unit
Sandstone Phyllite Unit
Limestone Unit

Sedimentary structures (cross-bed and scour marks) in the sandstone/phyllite unit indicate sediment transport from the east. Upper Mississippian (Chesterian) conodonts have been found in the oldest Limestone Unit and also in the Cherty Tuff Unit. North of the Woodbury Creek and south of the Coffee Creek occurs a strikingly metamorphosed quartzite ("Ribbon Quartzite", Little, 1960).

Dominantly greenstone and amphibolite belonging to the Pennsylvanian-Traissic Kaslo Group separate the underlying Milford Group from the overlying Slocan Group. The Upper Triassic Slocan Group disconformably overlying the Kaslo volcanics consists essentially of grey phyllite and minor limestone, sandstone and tuffaceous sediments. However bulk of this group consists of dark grey to black argillite and slaty argillite (Little, 1960).

The bulk of the Ymir Group outcrops in a north-south trending belt sandwiched between the southern tail of the Nelson Batholith on the east and Rossland Volcanics on the west in the Salmo Map area (Little, 1965). Large blocks of roof pendants belonging to the Ymir Group are found scattered within the southern part of the Nelson Batholith.

Lithologically this Group consists mainly of argillite, slate, argillaceous quartzite, minor limestone and shale and its upper part resembles closely the Archibald Formation which contains ammonites of early lower Jurassic age. Though no diagnostic fossils have been found in the Ymir Group, lithological similarities of the Ymir and Slocan Groups suggest similar conditions of deposition and they probably deposited in the same geoclinal trough and at the same time (Little, 1960). He also suggested that the Ymir Group is mainly Triassic although the lowermost part may be as old as Permian.

3.4.2 Structure and Metamorphism

Though uncertainties in definition of fold phases and their correlations throughout the Kootenay Arc and the northern Selkirks persist, three phases of folding have been recognised on a regional scale in the central and northern Arc. The oldest, large first generation phase I folds are isoclinal with gently plunging axes and folded axial planes (Høy et al., 1981). These folds affected stratigraphic units older than the Milford Group and therefore developed between Middle Ordovician and late Mississippian during the Cariboo Orogeny. First phase folds led to the deformation of quartz laminations in phyllite of the Lardeau Group but not in Milford Group: a fabric difference is the principal criterion for differentiating the phyllites of the two Groups. More open crenulation cleavage folds with steeply dipping axial planes parallel to the first phase folds constitute the phase II folds. Outcrops of stratigraphically and structurally higher rocks have been caused by phase II folds which generally have an N-shaped profile looking north, and an easterly to vertically dipping axial plane (Read, 1973). These second generation folds are best developed in phyllites of the Milford and Slocan Groups (Klepacki, 1983). In the central Kootenay Arc, these folds however die out. Phase III folds (Read, 1973; Brown and Tippet, 1978) well developed in the central and southern parts of the Arc are called phase II folds in Kootenay Arc (Ainsworth-Kaslo area) by Fyles (1964, 1967) and Høy (1980). These folds have a reverse N-shaped profile looking northward and a westernly dipping axial plane.

The enormous shortening in the stratigraphic thickness found in the central Kootenay Arc compared to that found in the northern and southern parts is related to the large number of approximately N-S trending faults (Little, 1967; Høy, 1977; Leclair 1983). This tectonically attenuated zone, viewed as a highly deformed and faulted remnants of an old continuous stratigraphic section, forms the convex eastward belt of the Arc.

Structurally within the southern Kootenay Arc, four structural units analogous to those in the Salmo area are also recognised in the Ymir area. The Porcupine and Oxide faults and another unnamed fault separate these structural units. Largely isoclinal, locally overturned folds (e.g., the Laib Creek syncline and Baldy anticline) probably formed synchronously with the above thrust faults during a period of deformation that took place prior to the emplacement of the Nelson plutonic rocks.

Høy (1976) studied the metamorphism in the Riondel area located within the regional metamorphic culmination in the Kootenay Arc. He established five calc-silicate isograds defined by surface traces across which observed mineral assemblages are related by a specific metamorphic reaction. The metamorphic grade ranges from the upper greenschist facies in the east to the upper amphibolite facies in the west. Metamorphic grade decreases westward on the west side of the Kootenay Lake and lies in the lower greenschist and amphibolite facies for the Milford Group of samples collected along the Woodbury and Coffee Creeks.

Limestone/phyllitic samples of the Slocan Group collected from the Nakusp area have well developed porphyroblasts of garnets randomly distributed with respect to the foliations. The metamorphic grade therefore lies in the garnet zone of the lower amphibolite facies and is not as high as that in the Riondel area.

3.4.3 Results

Results of Rb-Sr analyses of the samples are shown in the Tables 3.3(Milford), 3.4(Slocan and Ymir), plotted in Figs. 3.4(Milford), 3.5(Slocan) and 3.6(Ymir). Samples from the Milford Group have been divided into three groups (I, II and III) on the basis of location and lithology. Groups I and II give almost identical slope ages of 262±46 Ma(2σ) and 264±12 Ma(2σ), but different Sr-initial ratios (0.7116±0.0004, 0.70922±0.00162). The third group however gives much lower slope age of 179±74 Ma(2σ) and Sr-initial ratio (0.7059±0.0005). Group-II and Group-III have very low MSWD's (0.11 and 1.37) compared to that of Group-I (30.6).

Eight samples each from the Slocan and Ymir Groups give similar slope ages of 247±6 Ma and 250±16 Ma respectively. Their Sr-initial ratios however slightly differ: 0.70800±0.00004 (Slocan) and 0.70644±0.00036 (Ymir). Ymir Group has slightly higher MSWD(8.6) than that of the Slocan Group(5.5).

Table 3.3 Rb-Sr data from the Milford Group.

Sample ID	Rb(ppm)	Sr(ppm)	^{87}Rb/^{86}Sr	^{87}Sr/^{86}Sr
		Milford-3		
8003A	133.45	152.23	2.5390	0.71867±8
8003B	70.37	177.56	1.7330	0.71577±8
8003C	144.49	140.50	2.7970	0.72048±6
8003D	7.11	152.59	0.1120	0.70652±3
8003E	43.10	169.01	0.7370	0.70777±9
8003F	2.24	191.32	0.034	0.70574±4
		Milford-27		
8027B	6.32	1320.97	0.0138	0.71182±2
8027C	129.96	636.49	0.5910	0.71313±4
8027D	147.48	152.93	2.8000	0.72340±1
8027F	190.45	173.30	3.1836	0.72097±1
8027H	181.78	531.52	0.9902	0.71559±7
8027P	56.35	40.59	4.0239	0.72589±9
8027S	145.44	790.53	0.0534	0.71048±2

Table 3.4 Rb-Sr data from the Slocan and Ymir Groups.

Sample ID	Rb(ppm)	Sr(ppm)	^{87}Rb/^{86}Sr	^{87}Sr/^{86}Sr
	Slocan	**Group**		
8035A	41.22	556.75	0.2142	0.70877±2
8035B	107.22	443.46	0.6997	0.71017±1
8035C	64.09	603.20	0.3074	0.70914±1
8035D	145.28	261.94	1.6056	0.71362±2
8035E	165.00	154.32	3.0963	0.71734±1
8035F	164.64	260.76	1.8279	0.71444±6
8035G	4.91	1956.61	0.0072	0.70790±3
8035H	2.97	1571.67	0.0054	0.70811±4
	Ymir	**Group**		
8006D	107.04	256.00	1.2099	0.70943±1
8006G	72.81	530.77	0.3969	0.70925±2
8006H	66.92	259.10	0.7475	0.71024±4
8006I	84.47	87.87	2.7836	0.71689±5
8006K	104.34	134.58	2.6412	0.71578±12
8006M	22.84	475.06	0.1391	0.70650±2
8006N	18.32	794.86	0.0666	0.70656±2
8006P	124.38	421.73	0.8498	0.70845±5
8006P	124.38	421.73	0.8498	0.70845±5

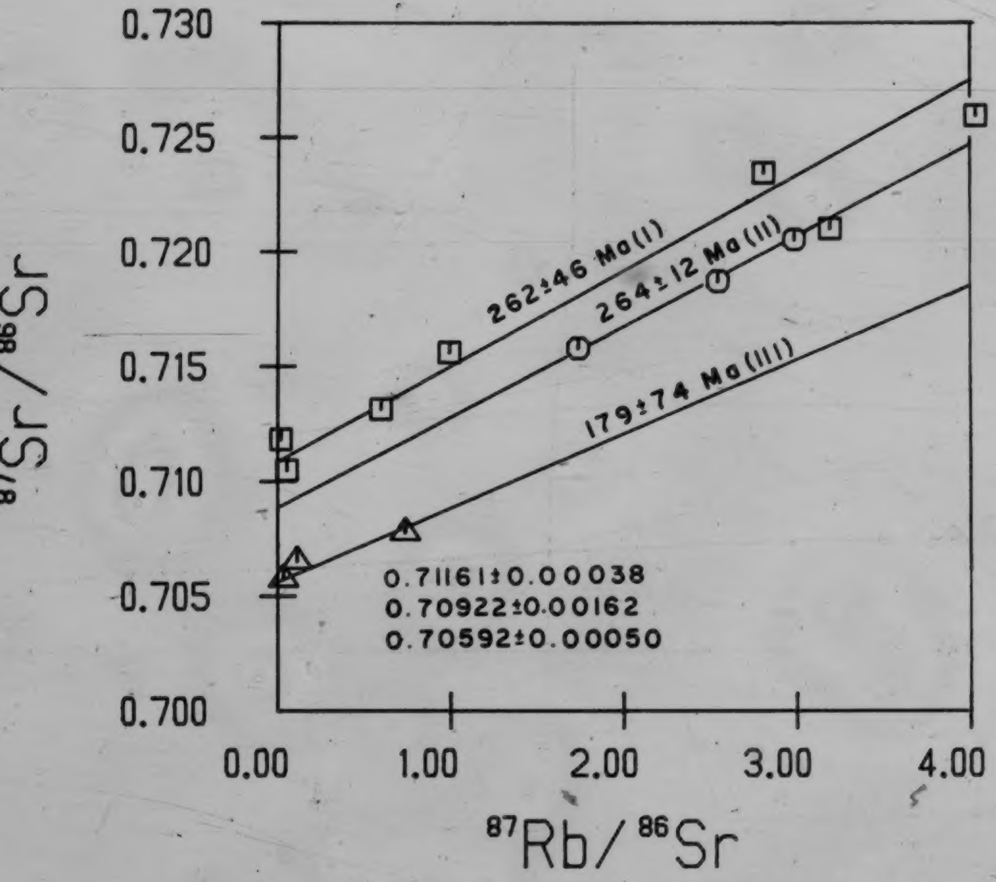

Fig. 3.4. Rb-Sr isochron diagram for three groups of samples from the Milford Group. Square symbols represent Group-I (8027-B, C, D, F, H, P, S), hexagons represent Group-II (8003-A, B, C) and triangles represent Group-III (8003-D, E, F).

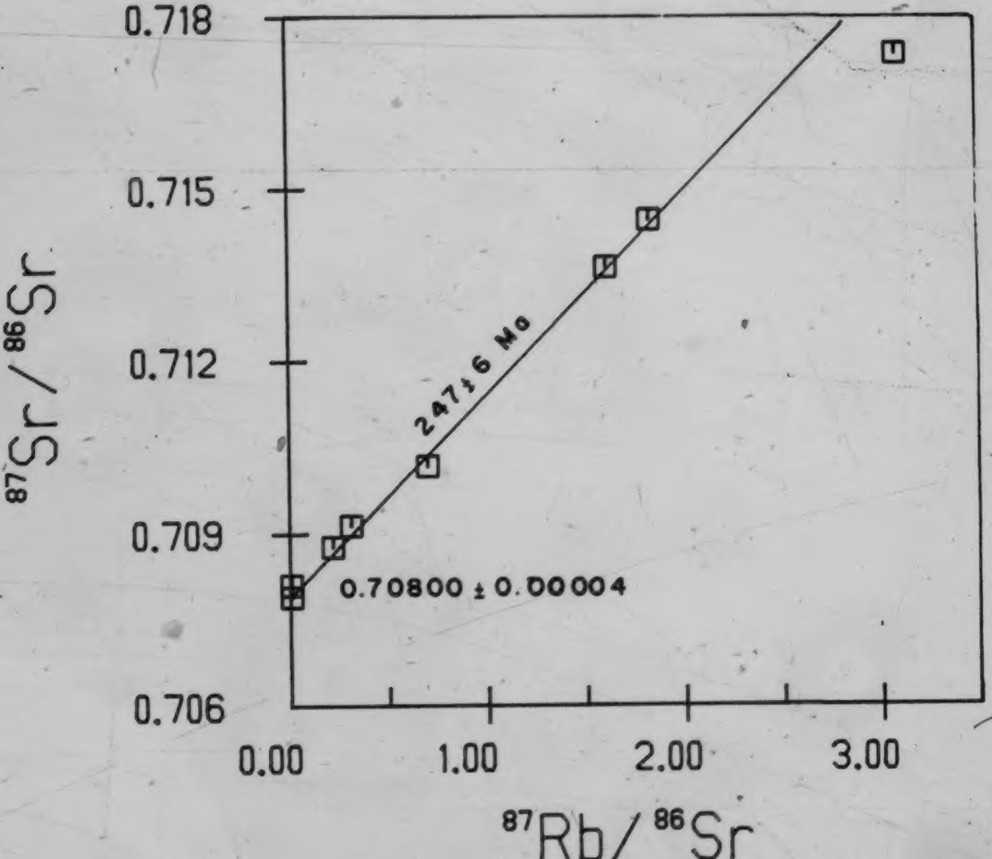

Fig. 3.5. Rb-Sr plot for the Slocan Group samples.

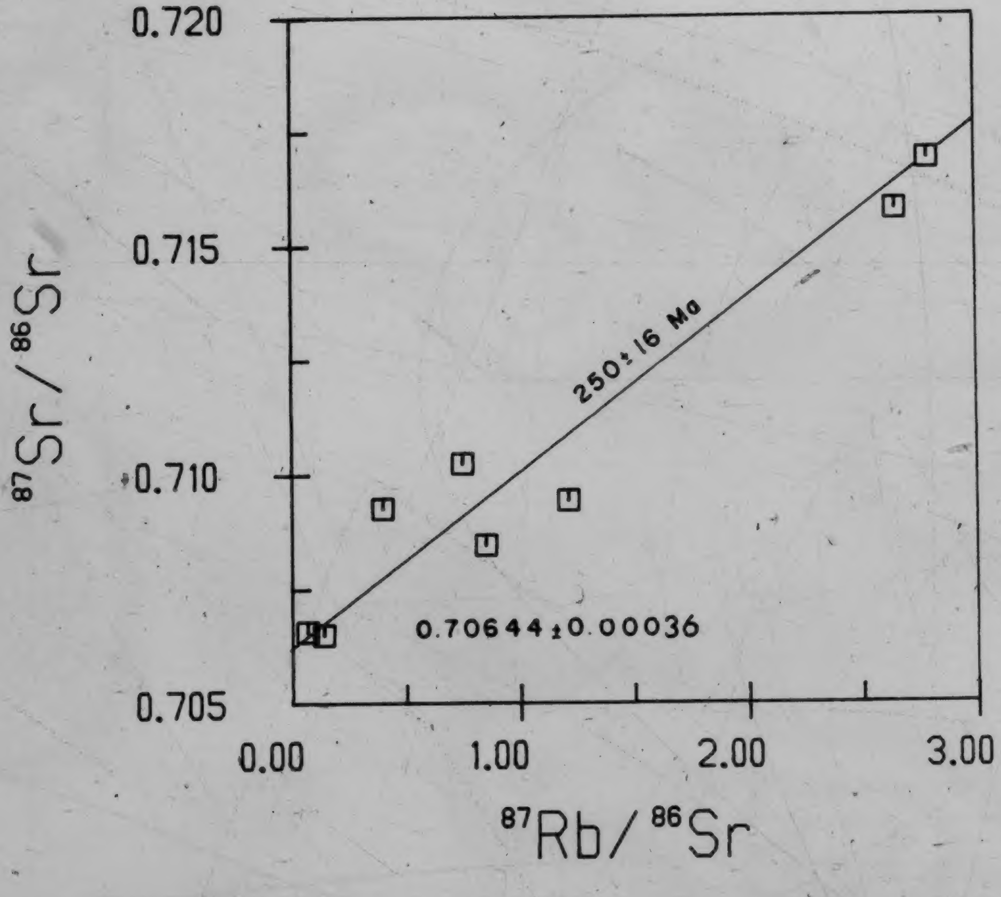

Fig. 3.6 Rb-Sr plot for the Ymir Group Samples.

3.4.4 Discussion

Milford Group

Out of 14 whole rock samples collected from the two localities, seven of them are qz-bi-musc schists (8027-B,C,D,F,H,P,S of Group I), three of them are gt-staur-schist (8003A, B, C of Group II) and three of them are amphibolites (8003D, E, F of Group III). Faunal evidence suggests the Milford Group could be as old as late Mississippian (320 Ma). The positive evidence for resetting of Rb-Sr isotopic systems for the Aldridge and Active Formations metamorphosed to bi-zone of the greenschist facies, strongly suggests that Milford samples must have undergone Sr-isotopic redistribution at the time of metamorphism. The intermediate age of about 263 Ma from the two groups of samples metamorphosed to bi- to gt-staur-grades may therefore indicate a separate metamorphic event for the Milford Group, not previously deduced. If so, this age is however older than the established metamorphic event during 170-164 Ma. Alternatively, it is possible Sr-isotopic homogenisation was not complete during the 170-164 Ma metamorphic event and the samples record an age of no geological significance. Though it is difficult to choose between the two, the latter alternative is however supported by the younger age of 179 Ma obtained from 3 amphibolitic samples. These three samples probably record the beginning of metamorphism as their precursor rock type was basic in nature and therefore more homogeneous than the detrital sediments of the groups I and II, which are less readily susceptible to isotopic homogenisation.

Slocan Group:

For eight samples analysed for this Group the significant range in Rb/Sr is due to large variation in mineralogy. Samples 8035G and 8035H with lowest Rb/Sr and $^{87}Sr/^{86}Sr$ consist almost entirely of carbonates with <1% of muscovite and quartz. $^{87}Sr/^{86}Sr$ ratios in these samples (0.7078, 0.7080) are very close to the Sr-isotopic composition determined for Lower Jurassic seawater (0.7080, according to Peterman et al., 1970, or 0.7077-0.7078, according to Burke et al., 1982). Presence of <1% of muscovite, because of its higher Rb/Sr ratio, must have contributed some amount of radiogenic ^{87}Sr to the whole rock system, but its contribution is probably negligible. If the muscovites were derived from a young source with low $^{87}Sr/^{86}Sr$ ratios, its Sr-initial ratios might have been lower than or equal to that of the carbonate fraction. These two carbonates along with three samples (A,B,C) with increasing amounts of silicates (quartz, muscovite and biotite) and two samples (D,F) consisting entirely of silicates (with garnet porphyroblasts) plot on a line with slope age of 247±6Ma. Incidentally this age is Lower Triassic according to Harland et al.'s (1982) time scale in contrast to the Upper Triassic (Carnian to Norian) age deduced on the basis of fossil record (Klepacki, 1983) for the youngest limestone/phyllite unit. Regional metamorphism that affected the Slocan sediments probably took place during mid-Jurassic time (164-170 Ma). Therefore it appears that this metamorphic episode did not reset the Rb-Sr system on the outcrop scale.

Parrish (1981) obtained a WR Rb-Sr date of 228±42 Ma (2σ) and $Sr_i = 0.7063$ for a group of metasediments in the Nemo Lake Belt (just north of the Valhalla Gneiss Complex), considered to be equivalent to the Slocan sediments. If this date of 228 Ma is taken to be close to sedimentation based on fossil evidence, the excess 19 Ma obtained for the present group of samples must be due to the increasing amounts of inherited radiogenic ^{87}Sr in more silicate-rich samples.

Ymir Group:

An isochron age of 250±16 Ma obtained from 8 samples belonging to this Group (metamorphosed to biotite-zone) is almost similar to that obtained for the Slocan Group. This observation supports Little's (1960) correlation of the two Groups and their deposition in the same sedimentary basin whose original configuration has been destroyed by intense tectonism and plutonism from Jurassic time onwards. Like Slocan, if an age of 228 Ma is taken as the age of sedimentation, its older age also indicates presence of inherited radiogenic ^{87}Sr in the samples during deposition.

3.5 Geochronology of Granitic Rocks

In an attempt to establish the times of crystallization of granitic batholiths/plutons/gneisses in the study area, zircons have been separated from 10 samples from the Nelson Batholith, Bonnington pluton, Castlegar Gneiss and Unit A, and have been analysed for U, Pb isotopic compositions.

3.5.1 Age Determination

Zircon is a highly refractory mineral and therefore once crystallised it strongly resists subsequent geological disturbances, making it possible to survive through metamorphism. Its suitability for U-Th-Pb dating is due to the fact that its crystal structure easily accepts U^{4+}(0.97A) and Th^{4+}(1.02A), but not Pb^{2+}(1.20A), in place of Zr^{+4} (0.80A).

When the mineral, being dated, has remained closed to U and its daughter Pb-isotopes and a common Pb correction is made, two geochronometers should give concordant dates. The equations 1.17, 1.18, (Chapter 1), could be written as:

for ^{238}U to ^{206}Pb decay,

$$^{206}Pb^{*}/^{238}U=e^{\lambda_1 T}-1$$

where

$$\frac{^{206}Pb^{*}}{^{238}U}=\frac{(^{206}Pb/^{204}Pb)_m-(^{206}Pb/^{204}Pb)_i}{^{238}U/^{204}Pb}$$

and for ^{235}U to ^{207}Pb decay

$$^{207}Pb^{*}/^{235}U=e^{\lambda_2 T}-1$$

When plotted in coordinates of $^{206}Pb^{*}/^{238}U$(ordinate) and $^{207}Pb^{*}/^{235}U$(abscissa), the above equations are parametric equations of a curve (called Concordia, Wetherill, 1956), the points on which give concordant dates for chemically closed systems (Fig. 3.7).

Disturbances when present (i.e., $t_{206}\neq t_{207}$) can be studied by means of this diagram, when discordant dates plot away from the concordia. There are three possibilities for generating similar patterns of data array on a concordia diagram:

1. Pb loss or U gain model

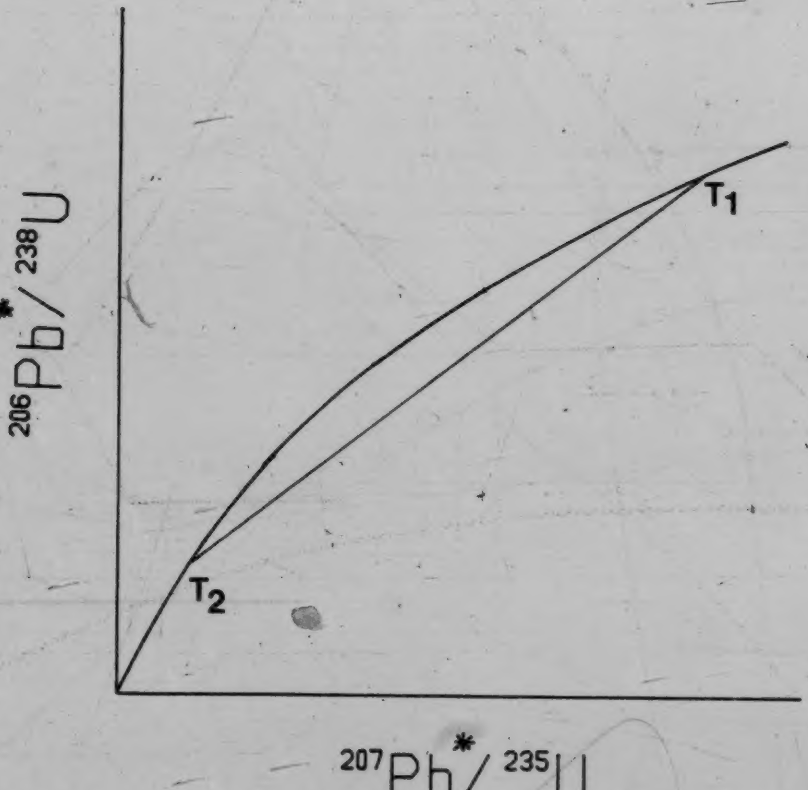
$^{206}Pb^*/^{238}U$
$^{207}Pb^*/^{235}U$
T_1
T_2

Fig. 3.7. Concordia plot (see text for discussion).

2. Inherited phase model
3. New phase model

When Pb loss or U gain happens during a single episode, short compared with the age of the phase, the data will lie along a chord, whose upper intercept T_1 (Fig. 3.7) will give the age of the phase and the lower intercept T_2 represents the time of the episodic event.

During magma genesis, the magma might be contaminated with wall rocks and entrain mineral phases of age (T_1) and the data from such consolidated magma will plot on a chord. The lower intercept in this case indicates the time of crystallization while the upper intercept the age of the old component.

If a rock is subjected to metamorphism which leads to the crystallization of new mineral phases, the mixtures of these new and old phases will also plot on a chord giving the age of original rock (upper intercept) and the age of metamorphic event (lower intercept).

For ages to be concordant, errors introduced through a number of factors are to be evaluated. Sources of error generally come from:

1. Concentration of U and Pb:

Taking known uncertainties in the isotopic ratios (0.04 to 0.06%), spike calibration (0.2%) and weighing (<0.1%), total uncertainties of U and Pb concentrations were estimated to be less than 0.5% for all samples analysed in this study.

2. Common Pb Correction:

Sources of common lead present in the sample include: i) lab blank, ii) true initial lead trapped in the crystal structure and iii) common lead trapped in inclusions. The first two sources of common lead could be measured or estimated from the total blank present in the reagents and from the feldspar which contains very little or no U and Th, but high concentration of Pb. Pb in feldspar separated from the whole rock will give the Pb isotopic composition present in the mineral being dated at the time of crystallization. For samples whose feldspar Pb isotopic compositions have not been measured, whole rock common Pb corrected for in-situ decay could be taken as the best approximation of the common lead (Chen, 1977). This is specially true for young samples, e.g., Jurassic or younger in age found in the study area. For the samples analysed here, $(^{206}Pb/^{204}Pb)_m$ ratios are generally greater than 700 (Table 3.6), except for three gneissic samples whose corresponding ratios lie in the range of 90 to 781. Therefore for zircons from the batholiths, the uncertainty due to not knowing the exact ratios of non-radiogenic lead is negligible.

Following Chen (1977), for samples with $(^{206}Pb/^{204}Pb)_m$ ratios >700, t_{206} and t_{207} ages will be considered concordant if they agree within 1.2 Ma and for samples with the above ratio <200, the two ages are concordant if they agree within 2 Ma.

3.5.2 Results

Analytical results are shown in Tables 3.5, 3.6 and 3.7 and plotted in Fig. 3.8. Six samples analysed for the Nelson Batholith, come from a small granodioritic body (Location# 15) on the west arm of the Kootenay Lake.

Five samples (8004, 8059A,B,D,E) from the Location# 15 have slightly discordant ages. The difference between the two ages lies in the range of 1.1 to 1.6 Ma, which is little more than the accepted limit of 1 Ma for concordancy. Sample 8059C shows moderate discordancy.

Oldest ages so far obtained from northern margin of the Nelson Batholith by other dating methods include a K-Ar biotite date of 174 Ma and a hornblende date of 168 Ma (Nguyen et al., 1968). Mount Carlyle Stock, north of the Nelson Batholith also gives a K-Ar hb data of 164 Ma (Wanless et al., 1968a). The range of U-Pb zircon ages from the least discordant samples is 163.3 to 168.0 Ma and therefore is close to the lower limit of the K-Ar dates. Though the small discordancy is most probably due to inherited zircon component (see e.g., Chen, 1977; Gulson and Krogh, 1973) because of the presence of an old (1.8 Ga) lower crust (see Chapter 7) under the batholith, true emplacement age for the east-central part of the batholith must lies in between 163.9 (8059B) and 167.5 Ma (8004). The lower limit of 164 Ma is used for most of the calculations in Chapters 7 and 8.

Higher K-Ar dates (168 and 174 Ma) from the northern part than the U-Pb zircon dates from the east-central part of the batholith could be explained in two ways:

a) Northern part of the batholith is older than the central part which, in turn, is older than the

Table 3.5 Common Pb isotopic composition.

Sample ID	$^{206}Pb/^{204}Pb$	$^{207}Pb/^{204}Pb$	$^{208}Pb/^{204}Pb$
Pb in	**K-feldspar**		
8004	19.308	15.692	39.149
8059A	19.312	15.710	39.190
8059B	19.272	15.690	39.090
8059C	19.274	15.667	39.069
8059D	19.212	15.636	38.747
8059E	19.306	15.695	39.160
WR-Lead,	**Initial**	**Ratios**	
8075F	19.172	15.670	38.474
8064E	18.245	15.549	38.957
8063A	..	..	..
8069B	..	..	..
8070C	18.858	15.663	38.680
Lab-Blank	19.740	15.680	37.870

Table 3.6 U-Pb isotopic data from Zircon analyses.

Sample	Wt(mg)	$^{207}Pb/^{206}Pb$	$^{206}Pb/^{204}Pb$	U(ppm)	Pb(ppm)
8004	53.3	0.06453	995.12	1024	29.4
8059A	50.9	0.05732	1978.63	985.7	25.4
8059B	50.9	0.05572	2445.58	998.7	25.3
8059C	44.8	0.05418	4237.28	1044	26.2
8059D	41.7	0.05498	2873.56	995	25.3
8059E	34.0	0.05514	2757.85	980.7	27.5
8075F	45.1	0.05600	2849.81	1174	27.5
8064E	53.6	0.23728	92.15	1083	38.0
8063A	68.9	0.21197	89.09	415.4	66.7
8069B	32.5	0.09947	495.61	1578	23.5

Table 3.7 Data for concordia plot and Model ages (Ma)

Sample	$(^{207}Pb/^{206}Pb)^*$	$^{206}Pb^*/^{238}U$	$^{207}Pb^*/^{235}U$	T_{206}	T_{207}	$T_{207/206}$
8004	0.04974	0.02623	0.1799	166.0	168.0	183.0
9059A	0.04988	0.02589	0.1781	164.8	166.4	189.0
8059B	0.04971	0.02566	0.1759	163.3	164.5	181.9
8059C	0.05073	0.02587	0.1810	164.7	168.9	228.0
8059D	0.04987	0.02586	0.1778	164.6	166.2	189.0
9059E	0.04982	0.02607	0.1791	165.9	167.3	187.0
8075F	0.05085	0.02289	0.1605	145.9	151.2	234.0
8064E	0.08546	0.01886	0.2223	120.5	203.8	1326.0
8063A	0.04707	0.00851	0.0556	55.1	55.0	51.0
8069B	0.07054	0.01221	0.1188	78.3	114.0	944.0

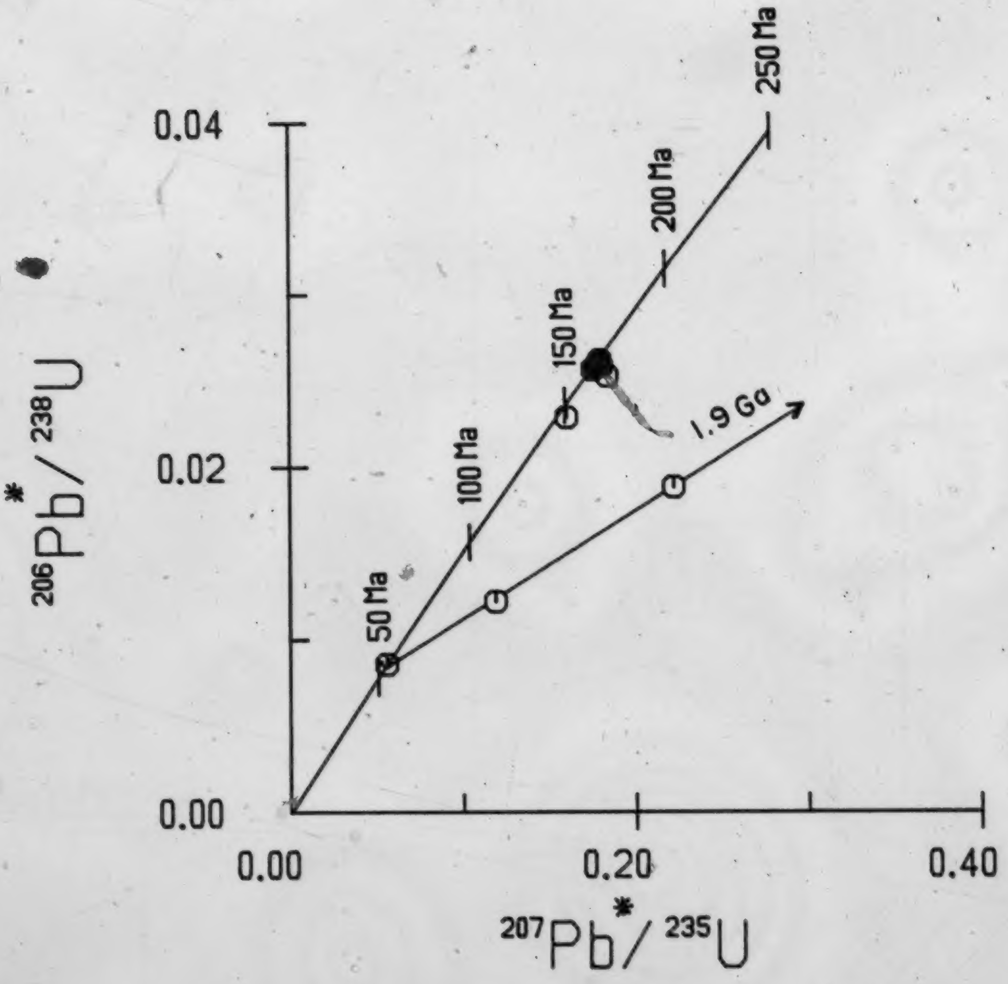

Fig. 3.8. U-Pb concordia diagram showing results for zircons from the Nelson Batholith, Bonnington pluton, Castlegar Gneiss, and Unit A. Discordia shown for the three gneissic samples (8063A, 8064E and 8069A).

southern part (e.g., Rb-Sr date date of 150 Ma and K-Ar bi date of 124 Ma have been obtained from the deformed tail of the Nelson Batholith, Duncan et al., 1979). or

b) Older dates are due to the presence of excess Ar^* in the biotite and hornblende crystals (Hart, 1969; Schwartzman and Giletti, 1968).

Dating of zircon from the northern part is therefore needed to prove the above alternatives.

Geological reasoning brackets the age of emplacement of the Nelson Batholith. It is certainly younger than the Rossland Volcanic Group which has an age span of about 200-185 Ma (Tipper, 1984) and is also younger than the middle Bajocian (about 171 Ma) Hall Formation (Frebold, 1959). Following this geological argument, the K-Ar biotite date of 174 Ma from the northern part of the batholith is suspect and probably supports the excess Ar model.

In this context, it is interesting to note that Parrish and Wheeler (1983) obtained an age of emplacement of the Kuskanax Batholith at 173 Ma with a strong evidence of inherited old Pb component from the local basement (about 2 Ga old)

One sample from the Bonnington Pluton (8075F) shows moderate discordancy. If the emplacement of this Pluton is synchronous with the Nelson Batholith, its lower 206Pb and 207Pb ages (145.9 and 151.2 Ma) than those of NB samples suggests small degree of Pb loss.

Two granitic gneissic samples from the Castlegar Gneiss (8063A, 8069B) and one sample (8064E) from Unit A plot on a discordia that has a lower intercept age of 54 Ma (same as the concordant age of the sample 8063A) and an upper intercept age of 1901 ± 14 Ma. The lower intercept is interpreted as the age of intrusion of the precursor of Castlegar Gneiss and Unit A. The source material for these gneissic samples is most likely the 1.9 Ga old basement. During this early Tertiary melting event, there was 100% Pb loss for the sample 8063A and therefore it was completely reset and gives concordant dates at 55 Ma (Table 3.7). For the other two samples (6069B and 8064E), Pb loss was significant but not complete. Alternatively if the samples were not derived by partial melting of this 1.9 Ga old basement, the discordia could be explained as a mixing line of two components. First alternative is preferred here as Nd-isotopic evidence from sample 8064E (Chapter 8) supports derivation of Unit A by partial melting of 1.9 Ga old basement.

3.5.3 Discussion

Determination of the true age of emplacement of the granitic batholiths and plutons in southeastern British Columbia has important implications for timing of deformation on the Kootenay Arc and time of accretion of terrane Q to III.

For Jurassic granitic bodies, U-Pb zircon dates are available so far from the Nelson Batholith (this study), Kuskanax Batholith (Parrish and Wheeler, 1983), and Mine Stock (Archibald et al., 1983) and Trail Pluton (Corbett and Simony, 1984).

In the southern Kootenay Arc, metamorphism occurred nearly synchronously with deformation and was accompanied by emplacement of late-synkinematic plutons (Reesor, 1973; Gabrielse and Reesor, 1974; Høy, 1977; Glover, 1978), most of which are now known to be of Jurassic in age (Wanless et al., 1968a, b; Archibald et al., 1983). In the north, the main body of the Kuskanax Batholith was emplaced prior to or during second-phase folding, i.e., early in the Mesozoic structural history of the Kootenay Arc (Read, 1973; Read and Wheeler, 1976b). A U-Pb zircon date of 173 Ma interpreted as the age of emplacement, marks the earliest stage of the second phase deformation. In the south, an age of 163 Ma for the Trail Pluton has been reported by Corbett and Simony (1984). An age of 164 Ma (this study) for the emplacement of the Nelson Batholith gives the minimum limit of time span when late-synkinematic plutons were emplaced (i.e., 173 to 164 Ma). As these plutons were emplaced in the lower-grade rocks, the cessation of regional metamorphism probably coincides with mid-Jurassic time at least in the shallower levels (Archibald et al., 1983).

In the southern part, in the Summit Stock area, U-Pb zircon date (upper limit is 171 Ma) and a concordant K-Ar mica date (166 Ma) from the Mine Stock give a narrow age bracket for this Stock which partly coincides with the formation of the first phase fold in this area (Archibald et al., 1983).

An early Tertiary (54-55 Ma) plutonism/tectonism in the study area is supported by the new data. Parrish and Ryan (1983) found U-Pb zircon dates of about 90 Ma and 63 Ma for two core gneiss units from the Valhalla Gneissic Complex (Reesor, 1963 and Parrish et al., 1985). They interpreted 90 Ma age for "Veined Gneiss" and 63 Ma age for the "Mixed Gneiss" as intrusive events and suggested the possibility of small amout of much older inherited Pb in the "Veined Gnessic Unit". Therefore results of all these studies (Parrish and Wheeler, 1983; Parrish and Ryan, 1983; and this work) support the presence of a lower crust (1.9 to 2.06 Ga old) west of the Kootenay Lake. Implications of this lower crust in the genesis of the granitic batholiths in southeastern British Columbia are profound and have been discussed extensively in Chapters 7 and 8 using Sr, Pb and Nd isotopes and trace elements.

4. Nd-ISOTOPIC STUDY OF SEDIMENTS AND CRUSTAL EVOLUTION

4.1 Introduction

A number of different models of crustal growth and evolution have been proposed since the first study made by Hurley et al. (1962). A model for the timing and nature of the formation of the continental crust is needed to understand the evolution of the Earth, being intimately related to the understanding of mantle-evolution and crustal growth. Evidence derived from different isotopic tracers lead to opposing views on the evolution of the continental crust. On the basis of Sr and K-Ar dating, Hurley et al. (1962) and Hurley (1968) proposed a model of linear crustal growth and even an exponentially increasing rate of crustal growth (Hurley and Rand, 1969) through geological time (Fig. 4.1). This view is diametrically opposite to the no-growth crustal-recycling model first proposed by Armstrong (1968) on the basis of Pb-isotopes. According to Armstrong and Hein (1973) and Armstrong (1981), the present mass of the continental crust formed very early in the Earth's history (>2.9 Ga) and has subsequently been recycled through the mantle in a steady-state fashion such that the mass of the crust has not changed during most of the Earth's history. His main lines of arguments for no-growth recycling model are constancy of continental crustal thickness and freeboard with 'age' and evidence of very early terrestrial differentiation.

Models of linear or exponentially increasing growth with time are not currently accepted. After much debate it is now generally believed that continental crust has grown through geological time from the mantle (at rates not yet agreed upon) (Moorbath, 1977, 1978; McCulloch and Wasserburg, 1978; O'Nions et al., 1979; Allègre et al., 1980; Allègre, 1982; Taylor and McLennan, 1981, 1983), and the process of growth involves complex mixing of fresh material derived from the mantle and recycled older continental material.

Much (70-90%) of the crust was in place by 2500 Ma with a particularly active period of crustal growth and differentiation between about 3200 and 2500 Ma (Veizer and Jansen,

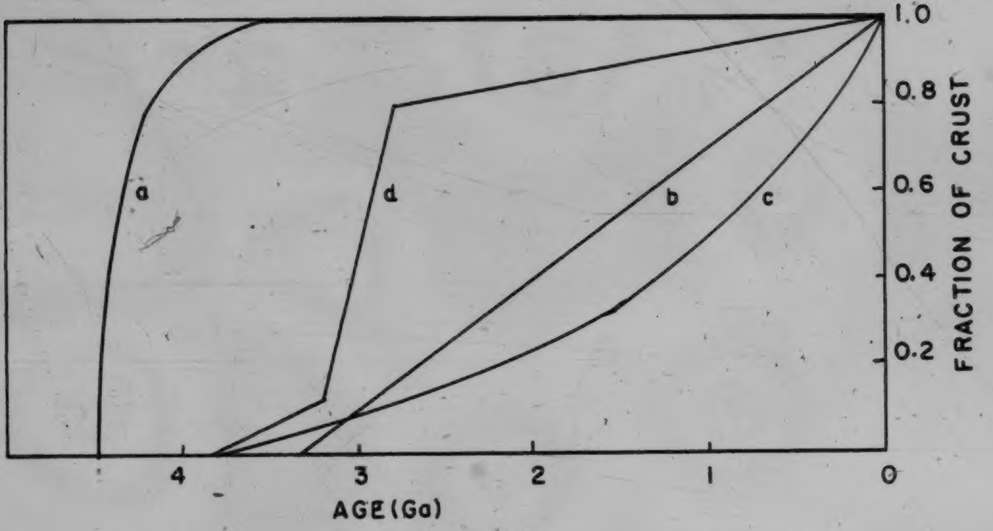

Fig. 4.1. Continental crust growth models: a. Early crustal growth with subsequent recycling of continental crust through the mantle, "constant mass no-growth recycling model" of Armstrong(1981). b. Linear growth through geological time (Hurley et al, 1962). c. Exponentially increasing crustal growth through geological time (Hurley and Rand, 1969) and d. Episodic crustal growth with the major crustal growth occurring between 3.2 and 2.5 Ga (McLennan and Taylor, 1982).

1979; Veizer and Compston, 1976; McCulloch and Wasserburg, 1978; Allègre, 1982; Taylor and McLennan, 1981; Dewey and Windley, 1981; and McLennan and Taylor, 1981). On the basis of changes in trace element distributions in sedimentary rocks to model-changes in area of continental crust during the late Archean, McLennan and Taylor (1982) calculated that 65-75% of the continental crust formed during the period 3200-2500 Ma (Fig. 4.1).

Nd-isotopic investigations on both mantle material (O'Nions et al., 1979; DePaolo, 1980, 1981) and sedimentary rocks (McCulloch and Wasserburg, 1978; O'Nions et al., 1983) also support the above model: during Archean orogenic events, continental crust formed from new mantle material, but the proportion of recycled continental material became progressively more evident during major orogens younger than 2.0 Ga.

DePaolo (1981d, 1983) calculated a present-day recycling rate of 1.0-1.5 km^3/yr. of continental crust to fit Sm-Nd isotopic data for a model of constant-mass continental crust. McLennan and Taylor (1983) calculated that no more than 3.0 km^3/yr. of crustal material is deposited on the oceanic crust. The controversy centering around the no-growth recycling hypothesis (Armstrong, 1981) is the need to carry down 1-3 km^3/yr of sediment flux into the mantle, i.e., removal of all sediments being deposited on oceanic crust. This is highly unlikely given the abundance of deep marine sedimentary rocks in the geological record. Even the lower limit of recycling rate (1.0 km^3/yr) raises severe mass-balance problems (McLennan and Taylor, 1983). Also the no-growth model is heavily dependent on evidence of constant 'freeboard' (Wise, 1974), and plausibility of large scale crustal recycling through the mantle via sediment subduction, both of which are based on assumptions yet to be properly evaluated.

Investigations of crustal evolution are intimately tied to the estimates of crustal residence ages of the sedimentary mass, representative of the average upper crust. The recent surge of interest in the Sm-Nd systematics of shale samples (O'Nions et al., 1983; Allègre and Rousseau, 1984; Goldstein and O'Nions, 1981; Goldstein, 1984; Frost and O'Nions, 1983; Michard et al., 1985) has shown the importance of such studies to the understanding of crustal growth.

Li (1972) and Ronov and Yaroshevsky (1969) estimated that the sedimentary part of the continental mass is $2.4\pm0.4\times10^{21}$kg from O^{18} mass balance calculation and 2.7×10^{21}kg from direct observation of sedimentary thicknesses respectively. About 70% of this sedimentary mass is clastic sediments of which shales are predominant. Shales derived from erosion of continents over large source area can be considered to represent average sampling of large continental segments. It has been repeatedly shown that because of negligible mobility of REE during mixing involved in erosion and deposition processes, relative REE abundance of detrital sediments remains constant and reflects almost perfectly the composition of their source area (Haskin et al., 1966; Nance and Taylor, 1976; McLennan et al., 1978). Hence crustal residence age (see next section for definition) of sediments should reflect the time when their precursor continental material was generated by magmatic processes. Rather constant Nd crustal residence ages of sediments over the last 2.0 Ga have been interpreted by O'Nions et al., 1983, Allègre and Rousseau, 1984, and Goldstein et al., 1984 as a supporting evidence for a decreasing rate of addition of mantle-derived material to growing continents since early Proterozoic.

The present Nd-isotopic study constitutes Sm-Nd isotope analyses of well-preserved stratigraphic units, ranging in age from Middle Proterozoic to Upper Triassic) from southeastern British Columbia. The aim is to understand the evolution of this sedimentary mass and to evaluate the contribution of mantle-derived Nd to these sediments and related tectonic implications.

4.2 Crustal Residence Age

McCulloch and Wasserburg (1978) used the property of constant Sm/Nd ratio in sedimentary rocks, like shales, schists and sandstones to demonstrate the potential of applications of the Sm-Nd system for extracting valuable information on their provenance. They noted that after mantle material is differentiated (accompanying ≅40% fractionation in Sm/Nd, O'Nions et al., 1983) to form a continental segment the modified Sm/Nd ratio remains essentially constant afterwards. If the growth curve of the mantle or that portion of the mantle from which the crustal portion is derived is known, a "model age of differentiation" can be calculated using the measured present day values of $^{143}Nd/^{144}Nd$ and $^{147}Sm/^{144}Nd$ ratios of sedimentary rocks. Though in their work, McCulloch and Wasserburg (1978) used a chondritic Sm/Nd ratio for the mantle growth curve, age of differentiation calculated with respect to such a curve will be inappropriate as the basic rocks presumably derived from the mantle have $\epsilon_{Nd}>0$. Though there are variabilities in ϵ_{Nd} for a particular T, the mantle growth curve proposed by DePaolo (1981b) will be a better reference curve for the calculation of T_{DM} (equated to T_{CR}, O'Nions et al., 1983) as DePaolo (1981a) and Allègre and Ben Othman (1980) have demonstrated that the continental crust is differentiated from an oceanic depleted mantle which is the source of MORB. Such a reference curve has been used by O'Nions et al. (1983) for the calculation of the 'Crustal Residence Age' (T_{CR}).

This crustal residence age is defined as the time when continental material fractionated from the depleted mantle i.e., the time at which the sample possessed the same $^{143}Nd/^{144}Nd$ ratio as the mantle reservoir from which its parental material was derived (O'Nions et al., 1983). Because of the constancy of Sm/Nd ratio during exogenous processes, the model age calculated from Sm-Nd data for sediments may be expected to provide estimates of their average T_{CR} age. This average T_{CR} is closely related to the average age of the continental segments feeding the sedimentary basin.

4.3 Sample Selection

In southeastern British Columbia well-preserved stratigraphic units ranging in age from upper Proterozoic to Triassic constitute the miogeocline and part of the terrane Q. One sample from each stratigraphic unit has been selected and analysed for Sm-Nd isotopic compositions. The primary purpose of the present study is to better understand the evolution of the sedimentary mass in the study area and to complement the data available from sedimentary rocks of various ages (McCulloch and Wasserburg, 1978; Hamilton et al., 1983; O'Nions et al., 1983; Frost and O'Nions, 1984; Allègre and Rousseau, 1984; Michard et al., 1985)

4.4 Results

4.4.1 Precambrian sediments

In the study area, argillites belonging to the Aldridge Formation and Horsethief Group are the only samples of Precambrian age. Only one sample from the middle Aldridge has been analysed for the Sm/Nd isotopic compositions and adds to the detailed study of the Belt-Purcell Supergroup by Frost and O'Nions (1984). The sample analysed here (8001D) has similar $^{143}Nd/^{144}Nd$ and $^{147}Sm/^{144}Nd$ ratios to the Purcell sediment samples analysed by Frost and O'Nions (Table 1, p55). A stratigraphic age of 1.35 Ga has been taken for the sample on the basis of McMechan and Price's study (1982). T_{CR} age of 1.85 Ga is obtained from this sample (Table 4.1). Frost and O'Nions (1984) noted very small spread or range in both $^{143}Nd/^{144}Nd$ and $^{147}Sm/^{144}Nd$ ratios. Such a small range is probably due to a source of uniform composition or to effect of efficient homogenisation of materials from different sources.

Nd-isotopic composition of one sample belonging to the Horsethief Group is markedly different ($\epsilon_{Nd}(0) = -14.9$) from that obtained by Frost and O'Nions($\epsilon_{Nd} = -21.4$) and results in a T_{CR} age of 1.75 Ga compared to 2.63 Ga calculated by them with respect to the same depleted mantle of DePaolo (1981b).

4.4.2 Phanerozoic sediments

Phanerozoic sedimentary rocks in southeastern British Columbia comprise both the miogeocline and the terrane Q (Monger et al., 1979). Brief geology of these sedimentary groups has been described in the previous Chapter (Chapter 3). To better understand their evolution, nature of source provenance and therefore crustal growth, Sm-Nd isotopic compositions have been determined for each stratigraphic unit. One sample from each group has been chosen. They are mostly fine-grained clastic rocks and some are carbonaceous to some extent. Their stratigraphic ages are not uniformly distributed throughout the Phanerozoic, but are confined to the Cambrian (Hamill, Laib, Lardeau, Active), Ordovician (Nelway), Carboniferous (Milford) and Triassic (Slocan and Ymir Groups) periods. In this way time interval covered by the

Table 4.1 Isotopic data and Model ages (in Ga) of sedimentary rocks.

Sample	T(Ga)	f(Rb/Sr)	f(Sm/Nd)	(87Sr/86Sr)m	(143Nd/144Nd)m	Sr(O)	Nd(O)	Sr(T)	Nd(T)	T(Sr)@	T(Nd)@
8001D	1.350+	35.06	-0.41	0.786900	0.511847	1165.2	-15.1	328.4	-1.2	1.91	1.85
8094A	0.850x	75.59	-0.43	0.832001	0.511854	1805.1	-14.9	673.0	-5.7	1.37	1.75
8090A	0.570x	-0.22	-0.42	0.710696	0.512373	83.9	-4.8	-75.7	1.2	0.43	1.00
8037D	0.550x	27.97	-0.43	0.749866	0.511940	639.7	-13.3	369.4	-7.3	1.33	1.62
8084A	0.550x	2.42	-0.46	0.718869	0.511402	199.9	-23.8	176.6	-17.4	4.70	2.32
8010S	0.557#	0.80	-0.49	0.711951	0.511900	101.7	-14.0	94.0	-7.2	7.18	1.52
8009D	0.500x	5.02	-0.38	0.717898	0.511860	186.1	-14.8				
8009D	0.160*	5.02	-0.38	0.717898	0.511860	186.1	-14.8	172.1	-13.3	2.21	1.94
8003C	0.300x	33.24	-0.39	0.720488	0.512102	222.9	-10.1	47.7	-7.2	0.42	1.50
8027C	0.300x	5.79	-0.41	0.713130	0.511579	118.5	-20.3	88.0	-17.2	1.30	2.26
8006G	0.250#	3.56	-0.42	0.709250	0.511902	63.4	-14.0	47.8	-11.4	1.24	1.71
8035C	0.247#	1.46	-0.38	0.708776	0.511897	56.7	-14.1	50.4	-11.8	2.49	1.89

+McMechan and Price (1982), xStratigraphic age, #Present work. *Metamorphic age, @Model age.

present data spans from 1350 to 228 Ma.

There is considerable variation in $^{143}Nd/^{144}Nd$ ratios (0.511402 to 0.512373) or $\epsilon_{Nd}(0)$ values (-23. to -4.8), but mostly cluster around $\epsilon_{Nd}=-14.0$ (Table 4.1). The Laib Formation and one sample from the Milford Group (8027B) have lowest $\epsilon_{Nd}(0)$ i.e., -23.8 and -20.3 and similarly have higher T_{CR} ages (2.32 and 2.21 Ga) than other sedimentary units with T_{CR} ages ranging between 1.50 to 1.89 Ga. One sample from the Milford Group (8003C) has very different Nd isotopic composition with $\epsilon_{Nd}(0)=-10.1$ and $T_{CR}=1.5$ Ga. Thus these two samples from the Milford Group with different Nd-isotopic compositions suggest the heterogeneous source character.

Like the Precambrian sediments, it is difficult to claim the shield as the source for the Phanerozoic sediments except the Laib and part of the Milford Group with T_{CR} ages falling within the range of that of the shield. The difference between the T_{STRAT} and T_{CR} remains in the range of 1.5 to 2.0 Ga.

4.5 Nd Isotopic Evidence for Crustal Growth

The main debate on crustal growth centers around the controversy regarding the degree of and variation in net mantle additions to the continental crust. Studies of O'Nions et al. (1983) and Allègre and Rousseau (1984) suggest decreasing rate of addition of mantle-derived material to the continents and increasing rate of intra-crustal recycling of sedimentary mass since 2 Ga. Evidence was also put forward by Michard et al. (1985) for the preferential incorporation of mantle-derived material took place during the major orogenic events experienced by the European Basement. They found strong evidence of mantle-additions during Hercynian, Caledonian and Cadomian orogenic episodes (0.58, 0.44 and 0.33 Ga).

Since the depleted mantle and the continents are considered to be complimentary, it is possible to deduce the growth curve for the continents from the isotopic evolution curve for the depleted mantle (Allègre, 1982). Therefore mean age of the depleted mantle is equal to that of continental crust (Jacobsen and Wasserburg, 1979). Independent calculation of the mean age[1] of

---

[1] Mean age of continental segment is defined as $<T(t)>=\int_0^t \tau \acute{m}(\tau) d(\tau)$ 4.1
where, $\tau(t)$ is the time and $\acute{m}(\tau)$ is the mass fraction of the continent extracted out

the continental crust can also be obtained by calculating the T_{DM} ages of the different continental segments or shales considered to be representative of the average crust.

Because of the constancy of the Sm/Nd ratio and quasi-linear decay of ^{147}Sm, Allègre et al. (1983) showed that *Mean age = Nd model age for a given portion of continent*. This Nd model age or crustal residence age relative to a depleted mantle reservoir is widely held as the most informative of all the parameters used to quantify the concepts of crustal growth and recycling (McCulloch and Wasserburg, 1978; O'Nions et al., 1983; Goldstein et al., 1984)

Such ages for sediments reflect the timing of differentiation of ultimate igneous source from the mantle unless addition of radiogenic Nd increases the $\epsilon_{Nd}(T)$ values of sediments and therefore decreasing their crustal residence ages.

Fig. 4.2 shows the different theoretical models of continental growth. Hurley et al. (1962) proposed that continents were created continuously at uniform rate (i.e., Uniform Growth Model). However the 'Non-Uniform continuous continental growth' model is gaining more acceptance (O'Nions et al., 1979, 1983; Allègre, 1982; Allègre and Rousseau, 1984). Such a view is supported by Nd-isotopic data obtained from sedimentary rocks (e.g., shales) and granitoid rocks (Allègre and Ben Othman, 1980). Steady-state crust with declining mixing rate (curve 'e') will also have similar growth curve to the 'case b' (Armstrong, 1986, pers. comm.)

4.6 Nd Isotope Evolution in Sediments

Mantle material addition and various recycling rates are most important parameters controlling the Nd-evolution of the sedimentary mass.

Pb isotopic data appear to support continental growth prior to 3.7 Ga, while continual crustal growth from the mantle though at a decreasing rate is supported by both Sr and Nd isotopic data. An internally driven Nd-evolution (Michard et al., 1985) in sediments due to different input rates of mantle-derived materials during major orogenic processes is supported from the study of French Shales. They found significant increase in $\epsilon_{Nd}(T)$ in French sediments during the Hercynian, Caledonian and Cadomian orogenic episodes. O'Nions et al.,

---

[1] (cont'd) of the mantle at time τ.

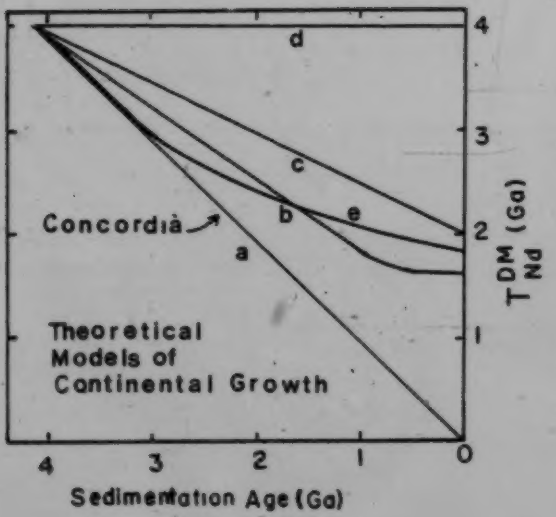

Fig. 4.2. Theoretical models of continental growth as deduced on the basis of Nd model ages vs. sedimentary ages: a. when sedimentation age is equal to T_{Nd}^{DM}; b. Continuous growth with decay (i.e., sedimentary recycling); c. Uniform growth and d. Continental "big bang". e. Steady-state crust with declining crustal recycling rates.

(1983) also found evidence of a high $^{143}Nd/^{144}Nd$ and Sm/Nd component (presumably basaltic, 20-30%) present in Southern Uplands sediments. The present study also shows evidence of mantle input during deposition of the Hamill Group.

Recycling plays a significant role in controlling the present-day distribution of "stratigraphic ages". Blatt and Jones (1975) calculated 66±3.5% to be sedimentary and 34% to be crystalline of the continental rocks on the Earth's surface. Of the total sedimentary rock-mass, about 70% is clastic in nature and the rest consists of carbonates and evaporites (O'Nions et al., 1983). Because of continuous erosion and redeposition of the preexisting sedimentary mass, estimates of the thicknesses and areas of sediments show a trend of increasing sedimentary mass with younger stratigraphic ages. This is due to geologically fast present rate of sedimentary turnover: therefore the half-mass age of all sediments has a depositional age less than 600 Ma (Garrels and McKenzie, 1971; Southam and Hay, 1981). This very young stratigraphic age is however not reflected in crustal residence ages of the sediments which are much older (average is 1.9 Ga, Goldstein et al., 1984). However some portion of sediments would be incorporated into basement as metamorphic rocks and therefore reduce the mean crustal residence age of the recyclable sedimentary mass (O'Nions et al., 1983). This effect will be accentuated through loss of sediments being recycled into granitic rocks, forming parts of cratons. This type of recycling has increased through geological time (Allègre and Ben Othman 1980; Hamilton et al., 1980; DePaolo, 1981a and present study, Chapter 7). Such an effect might also be accomplished through a portion of the sediments being subducted into the mantle along convergent plate boundaries (Kay, 1980; Kraig and Kay, 1981; McCulloch and Perfit, 1981; Nodha and Wasserburg, 1981; Cohen and O'Nions, 1982), though there is uncertainty regarding the amount being subducted (McLennan and Taylor, 1981, 1983) and also the amount of sediment escaping island arc volcanism and passing deep into the mantle (White and Patchett, 1984).

Michard et al., (1985) proposed theoretical evolutionary models of the sediments in terms of different recycling rates, given constant rate of growth from the mantle (Fig. 4.3).

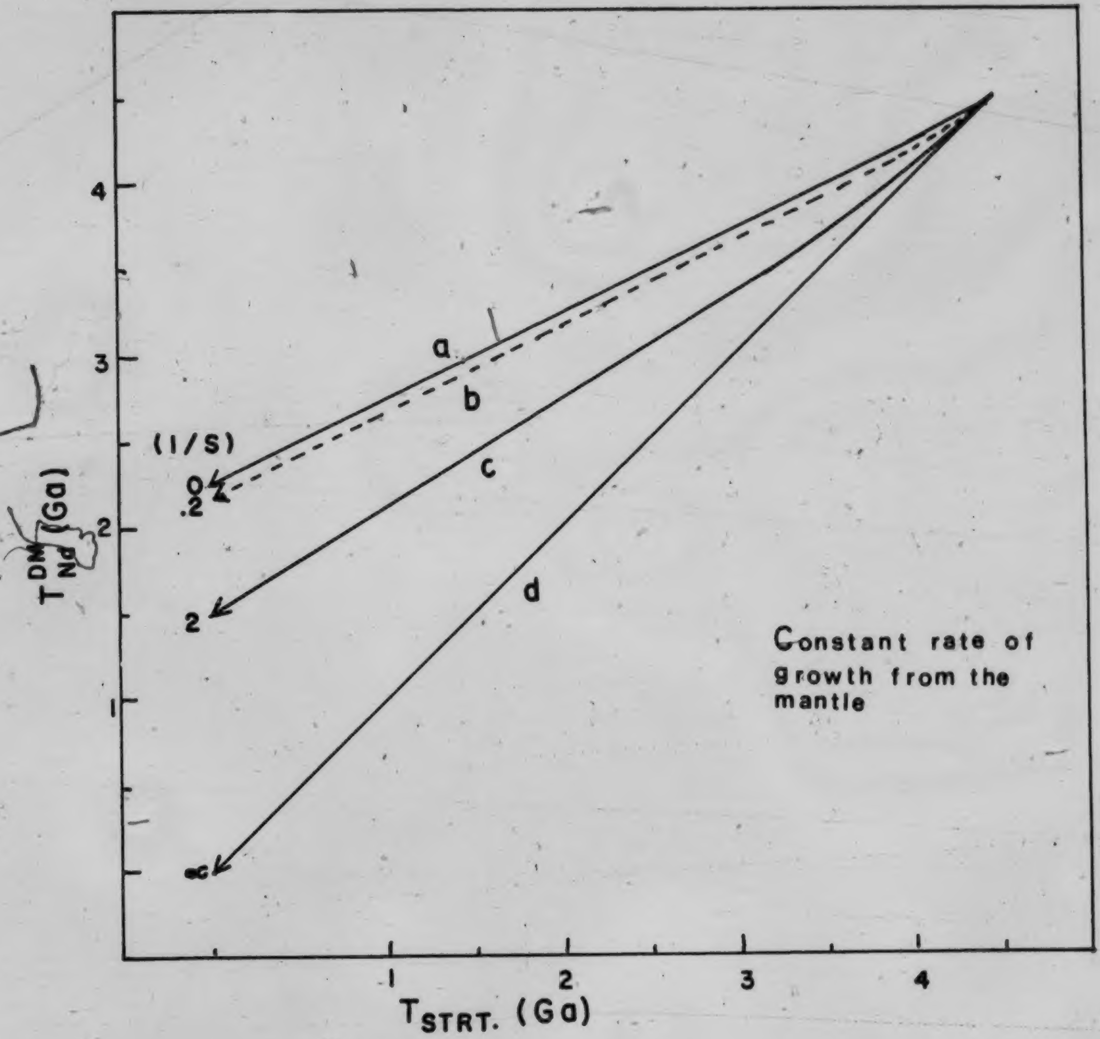

Fig. 4.3. Theoretical evolutionary models of the sediments (Michard, et al, 1985) with a constant rate of crustal growth from the mantle. S is the relative erosion rate and 1/S is the mean survival time of the sediments on the surface of the continents. a. growth with instantaneous recycling forming the homogeneous crust. b. growth with modern recycling rate of 0.2 Ga (Blatt and Jones, 1975) is similar to case a. c. growth with recycling rate much lower than the modern recycling rate. and d. growth with no erosion (i.e., no recycling).

In their models, they neglected the effects of the loss of recyclable sediment on the evolution of sediments. Their model and previous models (Garrels and McKenzie, 1971; Veizer and Jensen, 1979; Zartman and Doe, 1981) share the following characteristics:

1. Mixing of mantle material with continental detritus leads to the formation of new continental segments
2. Areal distribution controls the erosion coefficient i.e. the amount of material removed due to erosion/unit time and
3. MORB-type source (DePaolo, 1980) produces new continental segment.

They related the crustal residence age T_{CR}, to the stratigraphic age (t) and relative erosion rate (s) by the following equation(4.2):

$$T_{CR} = \left(1 - \frac{s.t}{2(s.t + 1)}\right).t \quad \ldots\ldots\ldots\ldots\ldots\ldots\ldots\ldots \quad 4.2$$

Depending on the rate of recycling, two extreme cases can be considered : a) In case of no recycling ($s=0$), crustal residence age is equal to the stratigraphic age (Concordant). Such a scenario is found to be true for Archean sediments. In such a case, due to the volcaniclastic nature of the sediments (Engel et al., 1974; Lowe, 1980) and their resistance to erosion, their crustal residence ages are perfect memories of their geological ages. b) On the other hand, when $s \rightarrow \infty$, recycling tends to be geologically instantaneous and the crust becomes very "stirred". Present day calculated recycling rate of 0.2 Ga (Blatt and Jones, 1975) produces a growth curve very similar to the case of $1/s \rightarrow 0$ (Fig. 4.3).

A plot of all Sm/Nd data on sediments, metasediments, river particulates, atmospheric dusts tend to be bounded by these two curves (see Goldstein et al., 1984).

Interpretation of Nd crustal residence ages of sediments in relation to the crustal growth is possible only if it is assumed that there is a quantitative relationship between the amount of new continental material that is made and the amount of new material that is added to the sedimentary mass (Goldstein et al., 1984). If the relationship is linear then the mean age of the continental crust is same as that of the sedimentary mass, provided that recycling rates of sediments into crystalline crust and vice-versa have constant ratio.

Inspection of all the data (see Goldstein et al., 1984) shows that T_{CR} ages of sediments younger than 2.0 Ga but older than 1.0 Ga tend to reach a steady value of about 1.8 Ga. Such a trend is either best explained by a sharp decrease in the mantle flux (internal-driven evolution) or by a fast sedimentary turnover of previously accumulated crustal rocks. Effects of mantle input are diminished to a great extent due to fast recycling and homogenisation effects (Michard et al., 1985). On the other hand, Allègre and Rousseau (1984) relate the discordance of T_{CR} and T_{STRAT} during the post-Archean era to the decreasing rates of continental growth. Such an interpretation is supported by the evidence summarised by O'Nions et al. (1979) for a crustal growth maximum by the end of the Archean time (see also McLennan and Taylor, 1983). McLennan and Taylor(1982) found a significant change in upper crustal composition at the Archean-Proterozoic boundary, e.g., higher total REE and Th abundances and negative Eu anomaly, $Eu/Eu^{*}=0.65\pm0.03$ compared to 1.00 for the Archean. They ascribed such an anomaly to intra-crustal melting (forming granodiorite and related magma where mainly Ca-rich plagioclase containing abundant Eu is retained in the residue (Taylor and McLennan, 1981b). This geological boundary also coincides with a significant oxygen buildup in the atmosphere (Cloud, 1973; Schidlowski, 1978; Walker, 1977), evidence of which is preserved in replacement of most banded iron-formation to red beds (Cloud, 1973). As the erosion rates are controlled by weathering conditions (due to both inorganic and organic activities), a transition from the Archean steady-state (i.e., heterogeneous crust dominated by igneous rocks and immature sediments) to the modern steady-state (i.e., homogeneous crust dominated by mature sediments) may have been acheived probably by the end of Proterozoic (Michard et al., 1985).

Goldstein et al.(1984) calculated mean residence age of 1.62 Ga for all river sediments and eolian particulates and this overall uniformity of the Sm-Nd systematics of contemporary continental erosion products justifies the use of sediments to evaluate the history of continental crust. Crustal residence ages of the Phanerozoic sediments around 1.8 Ga (Allègre and Rousseau, 1984) and mean T_{CR} age of the entire sedimentary mass around 1.9 Ga (Goldstein et al., 1984) are not very different from those being deposited today. Such observation provides little evidence for a significant amount of crustal growth during the Phanerozoic and intra-crustal recycling is the dominant factor in controlling the average crustal residence ages of the sediments. A recent compilation of all available data on sediments and basement gneisses from the British Isles (Davies et al., 1985) shows that they plot in a tight elongate field with a positive slope suggesting a decreasing rate of crustal growth during last 600 Ma. This is in sharp contrast to the modelled evolution proposed by Allègre and Rousseau (1984) for the North Atlantic Province suggesting a no-growth pattern (Fig 4.4).

Evidence of mantle-input to modern sediments has however been put forward by Michard et al. (1985) on the basis of apparent ages of zircons in sediments and $\epsilon_{Nd}(T)$ values of Phanerozoic French shales. Zircon from sediments can give upper intercept ages in concordia diagrams which represent unbiased mean ages of the ultimate igneous precursors of the host sediments. Such zircon crystallization ages (Vidal et al., 1980; Gebauer and Grunenfelder, 1976) are found to be greater than the T_{CR} ages obtained for the same sediments (Michard et al., 1985). Such age difference between upper intercepts of Zircon-arrays and the crustal residence ages however supports a significant crustal growth from the mantle subsequent to ca. 2 Ga. More work is needed however to sort out the importance of mantle-derived material to the Phanerozoic crust and therefore sediments derived from them.

4.7 Nd evolution in sediments in southeastern British Columbia

Fig. 4.4 shows the plot of Nd model age relative to oceanic mantle and sedimentary ages of shales from southeastern British Columbia. Data for shales from the North Atlantic Province has also been plotted. The growth curve for this province (Allègre and Rousseau, 1984) is shown by the dashed line. The close fit of the growth curve for the North Altantic Province and for sediments in southeastern British Columbia is strong evidence for validity of the crustal growth model 'b' of Fig. 4.2 i.e., continuous growth with decay.

Figure 4.5 shows the plot of $\epsilon_{Nd}(T)$ of sedimentary units vs. their stratigraphic ages. A Nd evolution curve could be drawn through the $\epsilon_{Nd}(T)$ values of the Aldridge, Horsethief, Lardeau, Nelway, Active, Slocan and Ymir Groups. It shows a regular decrease in $\epsilon_{Nd}(T)$

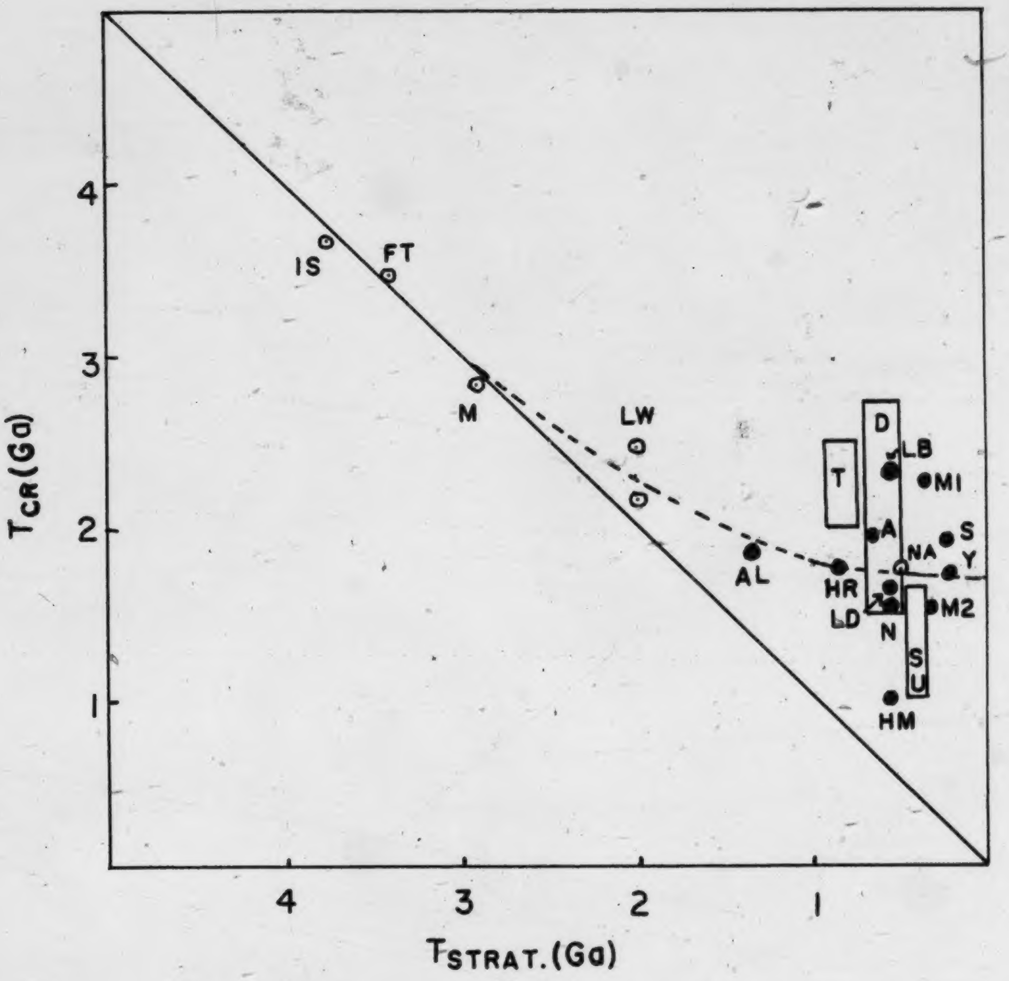

Fig. 4.4. Comparison of stratigraphic (T_{STRAT}) and crustal residence ($T_{CR} = T_{Nd}^{DM}$) ages calculated relative to a depleted mantle of DePaolo(1981b). AL = Aldridge, HR = Horsethief, HM = Hamill, LD = Lardeau, N = Nelway, A = Active, LB = Laib, M1 = Milford-8027, M2 = Milford-8003, S = Slocan, Y = Ymir, IS = Isua metasediments, FT = Fig Tree shale, M = Malene metasediments, LW = Lewisian metasediments, T = Torridonian, D = Dalradian, SU = Southern Uplands (Data from O'Nions et al, 1983). NA = North American Shale Composite (Allègre and Rousseau, 1984). The dashed line represents average Nd-evolution curve for the North Atlantic Province (Allègre and Rousseau, 1984).

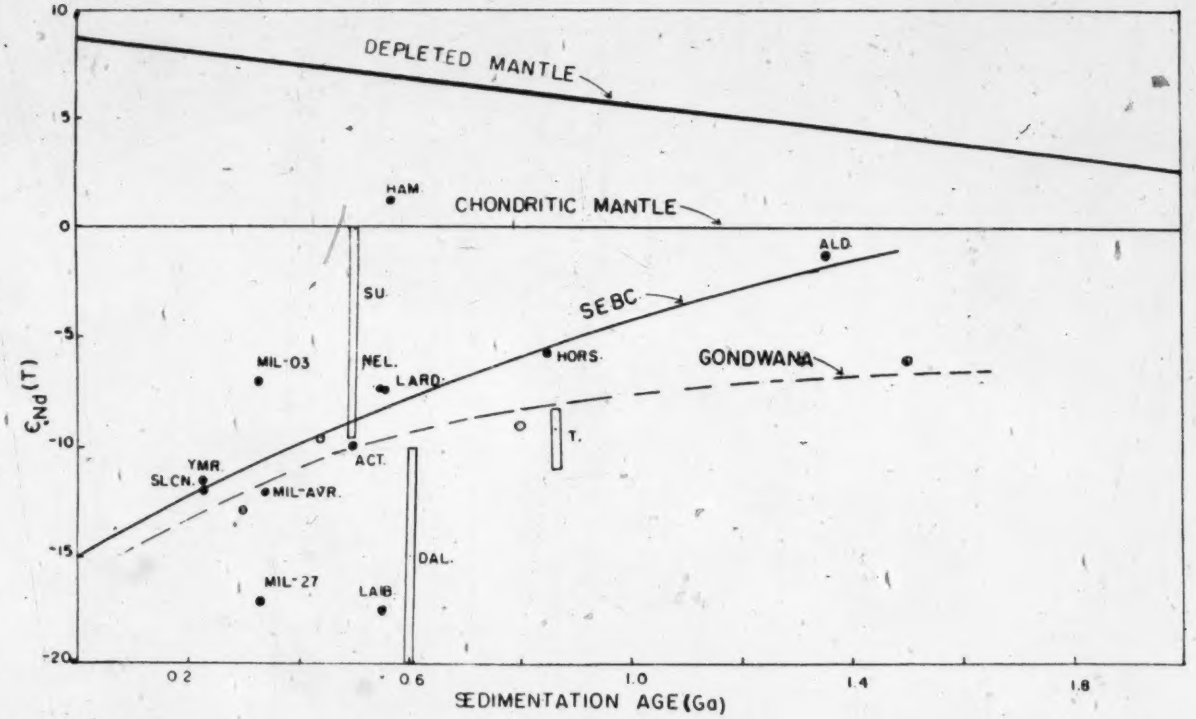

Fig. 4.5. Model of sedimentary evolution in southeastern British Columbia. An average growth curve has been drawn through data points belonging to the Aldridge(ALD), Horsethief(HORS), Lardeau(LARD), Nelway(NEL), Active(ACT), Slocan(SLCN) and Ymir(YMR) Groups). This curve is compared with the sedimentary evolution as deduced for the Gondwana by Allègre and Rousseau (1984). Growth curves for Chondritic and Depleted (DePaolo, 1981b) mantles are also shown. Range in $\epsilon_{Nd}(T)$ values found in Torridonian, Dalradian and Southern Uplands are also shown for comparison. (Data from O'Nions et al, 1983).

through geological time. This fact coupled with observation of almost constant Sm/Nd ratio in these sediments confirms that shales are representative samples of the continental crust, when insoluble elements like REE are studied.

Some of the samples analysed here (8010S, 8009D, 8027C, 8006G and 8035C) contain small % of carbonates. Shaw and Wasserburg (1985) studied isotopic composition of Nd in seawater as a function of time (their Fig. 4, p513) on the basis of Sm-Nd in carbonates and phosphates. Between the time-interval 600 Ma to 200 Ma, $\epsilon_{Nd}(T)$ of seawater varies between -7.0 to -4.0. These values are to some extent higher than the corresponding values obtained from the sediments (-7.0 to -17.0). Bacause of very small amount of carbonates present in the above samples, and extremely low abundance of Sm and Nd in carbonates (Shaw and Wasserburg, 1985), degree of contribution of ϵ_{Nd} in the dominantly shale samples due to carbonates is considered to be negligible and therefore not considered to be very important as far as sedimentary Nd-evolution in SEBC is concerned. Allègre and Ben Othman (1980), DePaolo (1981a) and Ben Othman et al., (1984) have shown that for both granitoid and granulites facies rocks $\epsilon_{Nd}(T)$ values generally decrease through geological time. The present study establishes a local Nd-evolution curve for the sedimentary rocks analogous to one that could be drawn for granitoid rocks (Allègre and Ben Othman, 1980). The simple reason is that shales appear to sample average continental crust. However the Nd-evolution curve derived from the shales from the Australian continent (Allègre and Rousseau, 1984) differs significantly from that in SEBC during the Proterozoic (Fig. 4.5), though they seem to coincide during the Phanerozoic. This evolutionary divergence at least during the late Proterozoic reflects the differential nature of continental source materials for the two continents.

The thick (about 20 kms) succession of the Belt-Purcell Supergroup, the oldest sedimentary rocks in the miogeoclinal belt of southeastern Canadian Cordillera, was interpreted as a continental terrace and aulacogen complex formed along an early Proto-Pacific passive margin in western North America (Gabrielse, 1972; Stewart, 1972; Sears and Price, 1978). A depositional environment in an epicontinental basin has also been proposed for this Supergroup in the western United States. Though original basin configurations, sediment source directions and source areas are not clearly established due to later tectonic movements (e.g., thrust faulting) during Mesozoic (Monger and Price, 1979; Harrison and Kleinkopf, 1980), it is believed that sediment source areas lay to the east, south and southeast of the miogeocline (Harrison, 1972; Gabrielse, 1972). The Belt-Purcell Supergroup overlies >1.7 Ga old crystalline basement (Zartman et al., 1982) and is recognised as a part of the continental crust (Monger and Price, 1979). The detailed Sm-Nd isotopic study of Frost and O'Nions (1983) of the Belt-Purcell Supergroup along with the present study showed that this enormous volume of sedimentary succession has relatively uniform $^{143}Nd/^{144}Nd$ (0.511615 to 0.511204) or $\epsilon_{Nd} = -20$ to -12 and $^{147}Sm/^{144}Nd$ (0.099 to 0.120) and therefore a small range in crustal residence ages (1.85 to 2.1 Ga).

The younger unconformably overlying Windermere Supergroup is, in contrast to the fine-grained, shallow-water deposits of upper part of the Belt-Purcell Supergroup, composed mostly of immature (both texturally and mineralogically) coarse clastic deposits. Stewart (1976) proposed an intra-basinal source for the detritus, and the documentation of the block faulting (with up to 10 km displacements) that occurred during deposition of the Windermere Supergroup oblique to the trend of the Cordilleran miogeocline supports a local supply of detritus. But large volumes of detritus of extra-basinal provenance must be present to account for thick (up to 9 km, Gabrielse, 1972) Windermere Supergroup (Monger and Price, 1979). This Supergroup is considered to be a syn-tectonic complex with mafic intrusive and extrusive rocks near the base of Windermere Supergroup in the southern part of the Kootenay Arc, indicating presence of deep crustal fractures (Monger and Price, 1979; McMechan and Price, 1982).

Unlike the Belt-Purcell Supergroup, only two samples from the Windermere Supergroup have so far been analysed for Sm-Nd isotopic compositions. T_{CR} age of 1.75 Ga from the present study, similar to those obtained for the Belt-Purcell Supergroup, is much lower than that (2.4 Ga) obtained by Frost and O'Nions (1984). These different results support the view that part of the Windermere Supergroup is either recycled Belt-Purcell sediments or derived from the same source area as that of Belt-Purcell and a part came from an older source material.

In order to test the Canadian shield as a potential source provenance, Frost and O'Nions (1984) analysed eight Canadian shield basement samples from southwestern Alberta and obtained crustal residence ages ranging from 2.62 to 3.20 Ga. Their study is in conformity with T_{CR} ages (2.8-3.4 Ga) obtained by McCulloch and Wasserburg (1978) for Canadian shield Composites. Therefore it is clearly seen that no part of the shield has T_{CR} age as young as 1.8 to 2.0 Ga and could not have possibly supplied the sediments to the Cordilleran miogeocline. Then the obvious question arises "if the Canadian shield is not the source of these sediments where do these sediments come from?" The alternative is that they are allochthonous with respect to the Canadian craton. One sample analysed from the Shoreline Stock(8088C) has $\epsilon_{Nd}(0) = -13.1$ similar to the average of the Belt-Purcell sediments. This stock, formed during early Tertiary time (51 Ma), is thought to have derived by partial melting of the local crust (i.e., Craton) (see Chapter 7). Its lower T_{DM} age of 1.55 Ga than the ≃1.8 Ga old basement (the possible source) is simply due to small fractionation in Sm/Nd during partial melting (see also Farmer and DePaolo, 1983). Therefore the cratonic crust underlying the miogeocline is as old as 1.8 Ga similar to the provenance age of the most of the miogeoclinal sediments and this part of the craton (lying in between the Southern Rocky Mountain Trench and the Kootenay Arc), is most likely the continental source for the sediments. The craton to the east of SRMT is geochemically different from that to the west.

Marked deviation from the evolution curve is shown by three sedimentary samples. Most important is that from the Hamill Group (8090A). Its positive $\epsilon_{Nd}(T) = +1.2$ suggests a significant input of mantle-derived material. Unlike the Hamill Group, two other samples that deviate from the Nd-evolution curve are from the Laib (8084A) and Milford(8027C) and have much lower ϵ_{Nd} values (-17.4 and -17.0 respectively). Their crustal residence ages are higher (2.32 and 2.26 Ga) than those so far calculated for any sedimentary and igneous rocks in the study area. A second sample from the Milford(8003C) has much higher $\epsilon_{Nd}(T)$ (-6.9) and a T_{CR} age of 1.5 Ga. Lithological diversities seen in the Milford Group (lower siliciclastic rocks to upper mafic rocks) are also reflected in Nd isotopic composition and therefore diverse nature of the source provenance.

The recent studies of Bond and Kominz (1984) gathered evidence supporting a rifting event in the miogeocline of the southern Canadian Cordillera, not earlier than 600 Ma (probably the event took place between 600 and 550 Ma). Armin and Mayer (1983) also concluded on the basis of tectonic subsidence of the Cordilleran miogeocline in the western U.S.A. that a final rifting phase began about 600 Ma ago. This rifting phase is however younger by about 200 Ma than the one generally inferred at around 750 to 800 Ma on the basis of an episode of block faulting and mafic volcanism that initiated deposition of the Windermere Supergroup (Burchfiel and Davies, 1975; Stewart, 1976; Monger and Price, 1979).

The Lower Cambrian rifting event deciphered by Bond and Kominz (1984) is also supported by petrologic and stratigraphic data from the Hamill Group (Simony and Wind, 1978). This Group consists of pillowed mafic lavas, tuffs, alternated with shales, coarse-grained sandstones, phyllites and schists outcropping within a relatively large area of the miogeocline. Such a lithologic association is suggestive of a continental terrane undergoing rifting (Bond and Kominz, 1984).

The importance of the present Nd isotopic composition for the Hamill Group lies in the fact that rifting is associated with the input of mantle-derived material into the recyclable crustal rocks. The positive ϵ_{Nd} testifies to this fact. An T_{CR} age of 1.0 Ga obtained for this sample is much lower (by 0.8 Ga) than those calculated for the Horsethief Group and Aldridge Formation, suggesting presence of basic components with a high Sm/Nd ratio.

Other Lower Paleozoic sediments (Lardeau, Nelway and Active Formations) have a large range in $\epsilon_{Nd}(T)$ (-13.3 to -14.8, Table 4.1), and T_{CR} ages (1.52 to 1.94 Ga). The Laib sample has almost similar T_{CR} age to that of Windermere as obtained by Frost and O'Nions (1984). Such an older crustal residence age is also obtained for one of the two samples of the Milford Group (2.26 Ga). Though the Laib Formation is lithologically and stratigraphically correlated with the Lardeau Group and therefore thought to have come from the same source, the present Nd isotopic study does not support this and rather points to the fact that they were derived from totally different source provenances. The Laib sediments were derived from much older continental crust (2.32 Ga) than that from which the Lardeau sediments were derived (1.62 Ga). T_{CR} ages calculated for the Lardeau and Nelway are the lowest (1.62 and 1.52 Ga) in the study area. It is interesting to note that T_{CR} ages calculated for the Mesozoic sediments (Slocan and Ymir Groups) are higher than those for the Lower Paleozoic. Similar $\epsilon_{Nd}(T)$ values from these two stratigraphic units suggest that these sediments were deposited in the same basin and were derived from similar source. The source probably lay partly to the west as evidenced by sparse paleocurrent data and facies changes (Cairnes, 1934).

Important conclusions that could be drawn from the present data and those of Frost and O'Nions (1984) are:

1. there are two distinct sources of sediments in the Cordilleran miogeocline: one continental source generated from the mantle at around 2.3 Ga and the other at about 2.0 Ga. Sediments with T_{CR} ages as young as 1.52 Ga (Nelway) might indicate presence of small input of mantle-derived material.
2. the Hamill sample offers supporting evidence for a continental rifting event during Lower Cambrian time (550-600 Ma) and for a mantle input in its provenance.
3. diverse lithological character for the Milford Group is supported by the recognition of multiple source provenances.

The above discussion portrays a very complex picture of Nd evolution in sediments from southeastern British Columbia and attests to the need of detailed Nd isotopic study for all the sedimentary units in order to constrain this preliminary Nd evolution curve drawn on the basis of the present study.

5. PETROGENESIS OF THE NELSON BATHOLITH

5.1 Classification

There are several schemes of classification for granitic rocks (see Barker, 1981, for a review). As granitic rocks (sensu lato) are dominantly made up of quartz and feldspars (two types), a commonly used scheme of classification is that of Streckeisen (1976) when the relative modal abundances (recalculated to 100%) of these three minerals are plotted on a triangular diagram. Chemically, a plot of total alkalies vs. SiO_2 is used to subdivide both volcanic and plutonic rocks into alkaline and subalkaline fields using standard dividing line of either MacDonald (1968) or the line later on proposed by Irvine and Baragar (1971). The sub-alkaline field is further subdivided into a) tholeiitic and b) calc-alkaline fields. These two fields are easily distinguishable on an AFM plot, in which tholeiitic series have greater Fe/Mg enrichment than that shown by the calc-alkaline series.

Many petrologists and geochemists further separate granites into three distinct groups on the basis of molar proportions of several major constituents (Shand, 1951):

Peraluminous: $Al_2O_3 > (Na_2O + K_2O + CaO)$

Metaluminous: $(Na_2O + K_2O) < Al_2O_3 < (Na_2O + K_2O + CaO)$

Peralkaline: $Al_2O_3 < (Na_2O + K_2O)$

Chappell and White (1974) proposed a genetic classification of granitic rocks into two types: a) I-type and b) S-type. I-type granites are derived from igneous rocks and may range from gabbroic to granitic composition and S-types are derived from sedimentary or meta-sedimentary rocks. Though this two-fold classification forms a general mineralogical division, it does not satisfactorily discriminate within-type variations seen between I-types rocks (e.g., Cordilleran granodiorites, Caledonian monzodiorites, Hercynian monzogranites). However Didier et al. (1982) improved this classification by differentiating between crustal and mantle derived I-type magmas. Based upon identification of enclaves as either meta-sedimentary or meta-igneous, they subdivided I-types into Cs (crustal sedimentary) and Ci (crustal igneous).

Petro et al. (1979) developed chemical criteria, for the major elements, to distinguish plutonic rocks generated at compressional plate boundaries from those generated at extensional plate boundaries. According to them, compressional plutonic suites are characterised by intermediate unimodal frequency distributions of differentiation index and normative plagioclase, calc/alkali indices in the range of 60-64, and distinctive patterns on AFM diagrams. Extensional plutonic rocks are characterised by bimodal distribution of differentiation index and normative plagioclase, calc/alkali indices in the range 50-56 and the presence of peralkaline rocks.

The above classification schemes use wt% of major elements. Recently, however, de la Roche and his coworkers (1980) derived a new scheme of classification of volcanic and plutonic rocks using R1-R2 diagrams ($R1= 4Si-11(Na+K)-2(Fe+Ti)$, $R2=6Ca+2Mg+Al$)). Bachelor and Bowden (1985) used this multicationic diagram to determine whether petrogenetic models involving fractional crystallization, partial melting or magma mixing can be readily displayed or identified. They concluded that there is a systematic change through an orogenic cycle which leads progressively to the ultimate development of alkaline magmas. They argued that most granitoid series result from a two-stage processes: first, fractional crystallization of clinopyroxene, olivine and calcic plagioclase from a basic source with tholeiitic affinities, produces a magma of intermediate composition which then suffers periodic mixing with a felsic magma followed by *in-situ* fractional crystallization to generate individual intrusions within a granitoid series. ***A similar scheme will be shown to be valid in producing calc-alkaline granitoid suites in the Nelson-Rossland Arc.***

5.2 Nelson Batholith (NB)

This batholith is a large composite body with polyphase intrusive events that took place in an interval of less than 10 Ma (164 Ma to 174 Ma). It includes rocks ranging in composition from diorite to true granite, but dominated by granodiorite. Because of poor exposure and lack of detailed geological mapping, these different units have no known boundaries. Besides large mineralogical variation, they also exhibit significant textural variation, ranging from coarse grained non-porphyritic types to porphyritic varieties with large K-feldspar megacrysts.

Chemically also, the Nelson Batholith shows wide variation. Fig. 5.1 shows a plot of total alkalies vs. SiO_2 with the alkaline/subalkaline boundary superimposed on it. Though bulk of the samples plot in the subalkaline field, a group of samples (8052-group) is definitely alkaline. This alkaline suite has lowest SiO_2 contents (50.8 to 52.6 wt%) and highest amount of alkalies in the range of 8.27 to 10.43 wt% (see Table A2.2.1, Appendix 2).

Rest of the samples from the batholith collected from widely separated areas (see sample Location Map, Fig.1.1, Chapter 1) are mostly hb-bi-granodiorite. They have limited range in both SiO_2 (62.0 to 68.0) and K_2O+Na_2O (6.0 to 9.9).

Fig. 5.2 is an AFM plot for the NB samples. All the samples fall in the calc-alkaline field and much below the CA/TH boundary. The trend shown is typical of calcalkaline rocks in other island arc tectonic regimes.

Metaluminous character of the NB samples is evident as all the samples do have the following relationships:

$$Al_2O^3/(Na_2O+K_2O+CaO)<1.00.$$

though the degree of metaluminous character varies to some extent. (Table 5.1)

Table 5.1

Sample group	SiO_2 Range	A/NKC*
8013-group	67-68	0.934-0.947
8052-group	50-53	0.467-0.545
8053-group	65-66	0.881-0.921
8057-group	63-66	0.817-0.894
8059-group	61-63	0.750-0.866
8061-group	62	0.945-0.954

*$A/NKC=Al_2O_3/(Na_2O+K_2O+CaO)$

The alkaline 8052-group is strongly metaluminous i.e., low in Al_2O_3 and high in K_2O+Na_2O, while most of the samples are weakly metaluminous.

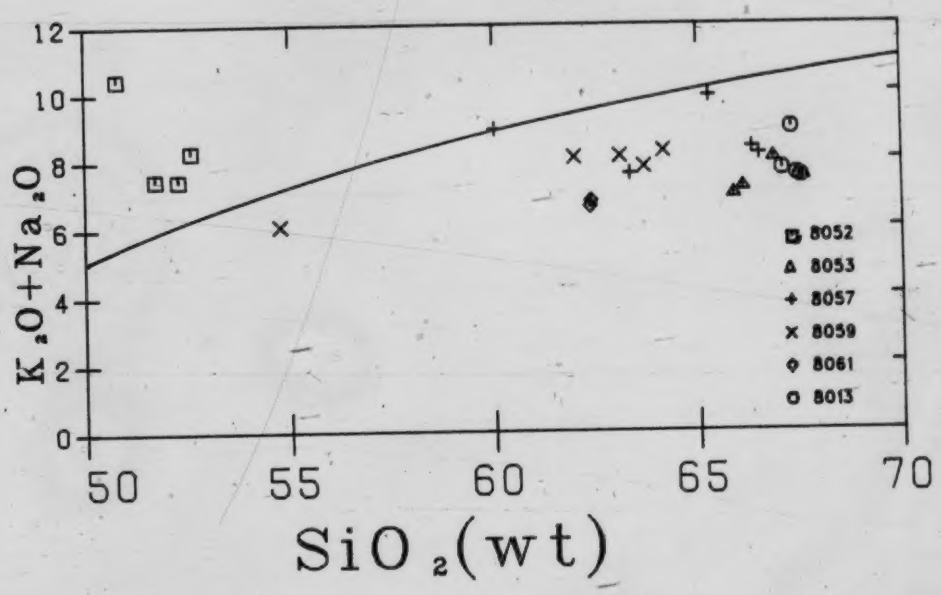

Fig. 5.1. Plot of total alkalis (K_2O+Na_2O) against SiO_2. The line (according to Irving and Baragar, 1971) divides the samples into two groups. All the samples (except those belonging to 8052-Group) plot in the subalkaline field.

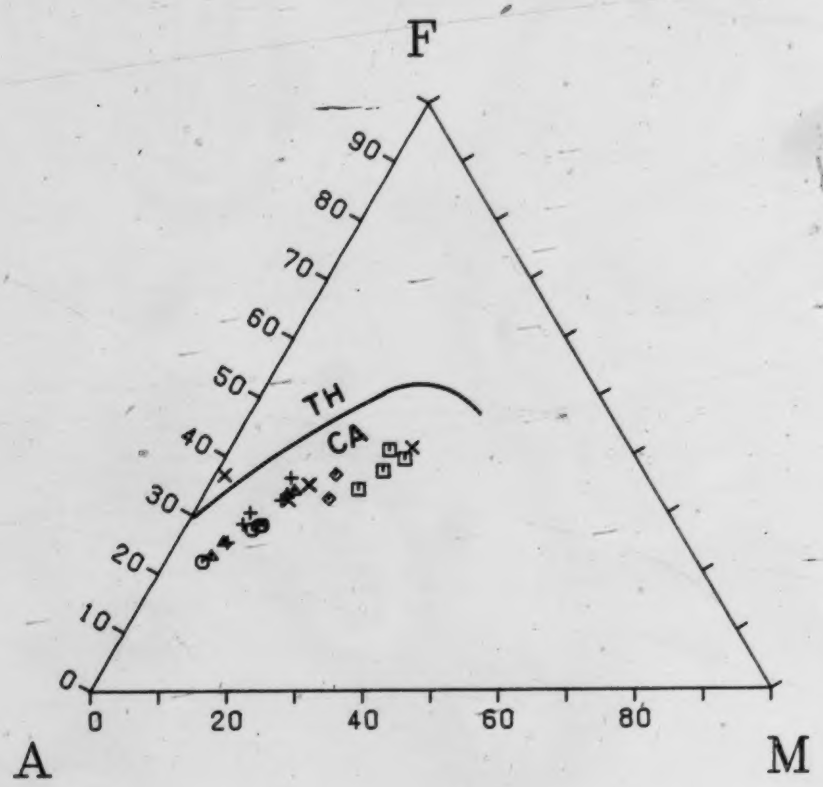

Fig. 5.2. AFM plot for the Nelson Batholith samples. All the samples show typical calc-alkaline trend.

5.3 Results

5.3.1 Major Elements

There is limited variation in SiO_2 (from 60 to 68 wt%) among the Nelson Batholith samples. All the major elements have been plotted against SiO_2, as abscissa, (Harker's diagram) to evaluate nature of the phases controlling major element variation. Good negative correlations are found between FeO-total, CaO, MgO, MnO, TiO_2 and P_2O_5 vs. SiO_2 (Fig. 5.3a-f). In all the above correlations (except TiO_2), the alkaline suite (8052-group) falls on the extension of these slightly curved correlation lines, apparently suggesting a genetic relationship between this alkaline suite and rest of the batholith (though it is not true as discussed later). Except TiO_2, this alkaline suite has higher contents of total FeO, CaO, MgO, MnO and P. Its TiO_2 content is much lower (0.65 to 0.73) compared to rest of the batholith at a given SiO_2 content. Therefore it is proposed here to name this suite as "low-Ti alkaline suite". Weak positive correlations are found between Al_2O_3, K_2O and Na_2O vs. Si_2O for this suite. The slightly curved variations on Harker's diagram for the main Nelson Batholith samples are suggestive of progressive fractional crystallization.

There is a compositional gap of about 9 wt% SiO_2 that separates the alkaline suite from the main calc-alkaline granodiorites. Sample collected from different localities have their own distinctive SiO_2 range, though overlapping to some extent (Table A2.2.1, Appendix 2).

5.3.2 Trace Elements

There are no systematic variations between Rb, Sr, Ba and and SiO_2. On average, Sr and Ba decrease and Rb increases with SiO_2 but there is considerable scatter. Nelson Batholith samples have high concentrations of these elements: Rb (50 to 150 ppm), Sr (600 to 1200 ppm) and Ba (1000 to 1500 ppm). There is also no systematic relationship between K/Rb ratios and SiO_2. There is a wide range in K/Rb ratios varying from 200 to 400. However K/Rb ratios roughly increase with K_2O (Fig. 5.4). High field strength elements (HFS) like Zr (Fig. 5.5a), Nb (Fig. 5.5b) and Ti steadily fall with differentiation. Zr/Nb ratios however increase from 4

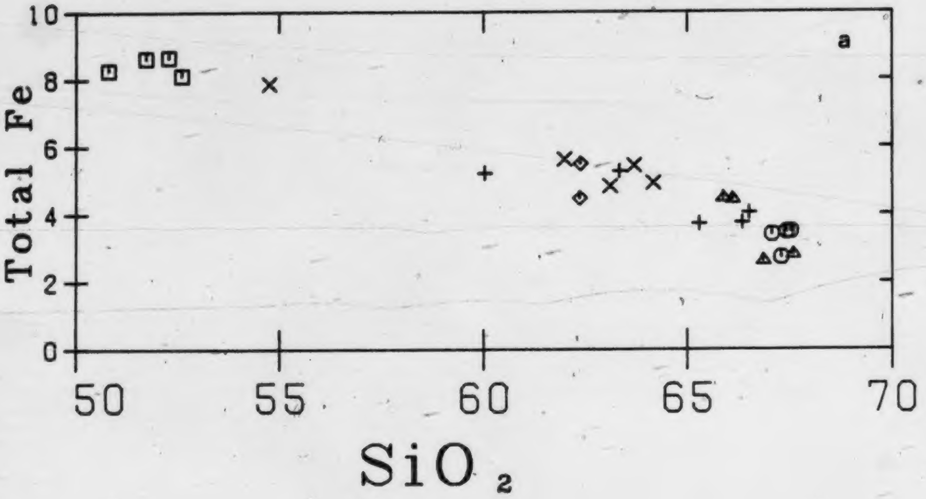

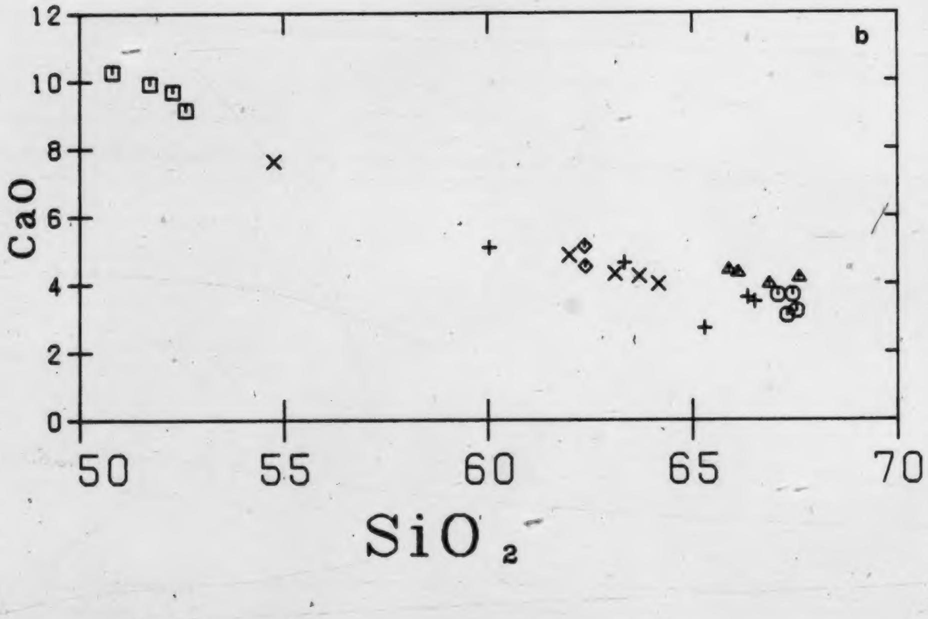

Fig. 5.3a-f. Major element oxide variation plotted against SiO_2 content. a. Total Fe vs. SiO_2, b. CaO vs. SiO_2, c. MgO vs. SiO_2, d. MnO vs. SiO_2, e. TiO_2 vs SiO_2 and f. P_2O_5 vs. SiO_2.

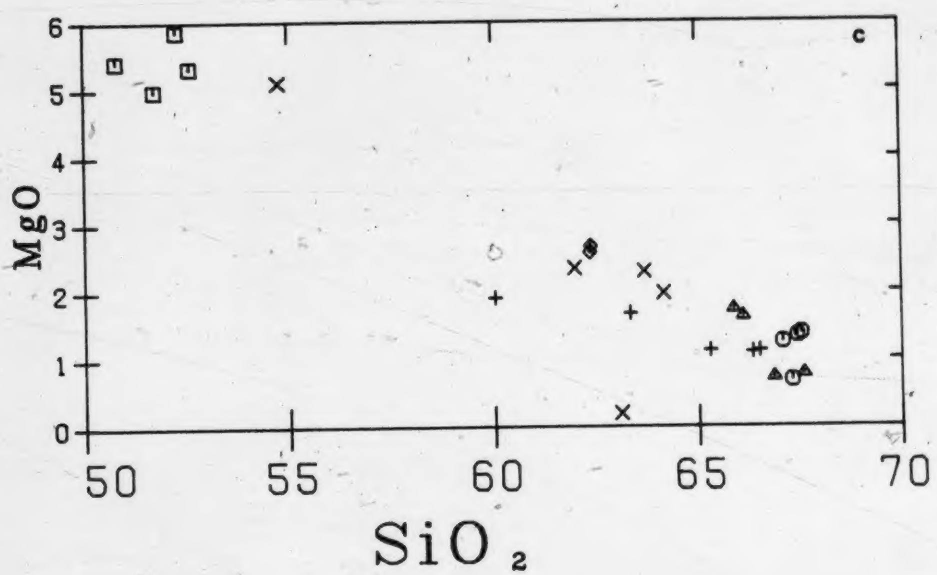
c
MgO
0
1
2
3
4
5
6
50
55
60
65
70
SiO 2

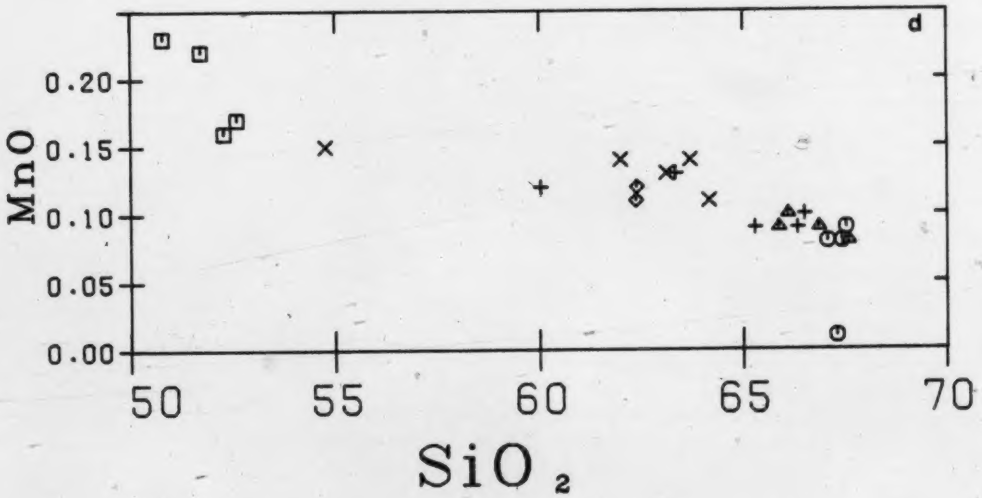
d
MnO
0.00
0.05
0.10
0.15
0.20
50
55
60
65
70
SiO 2

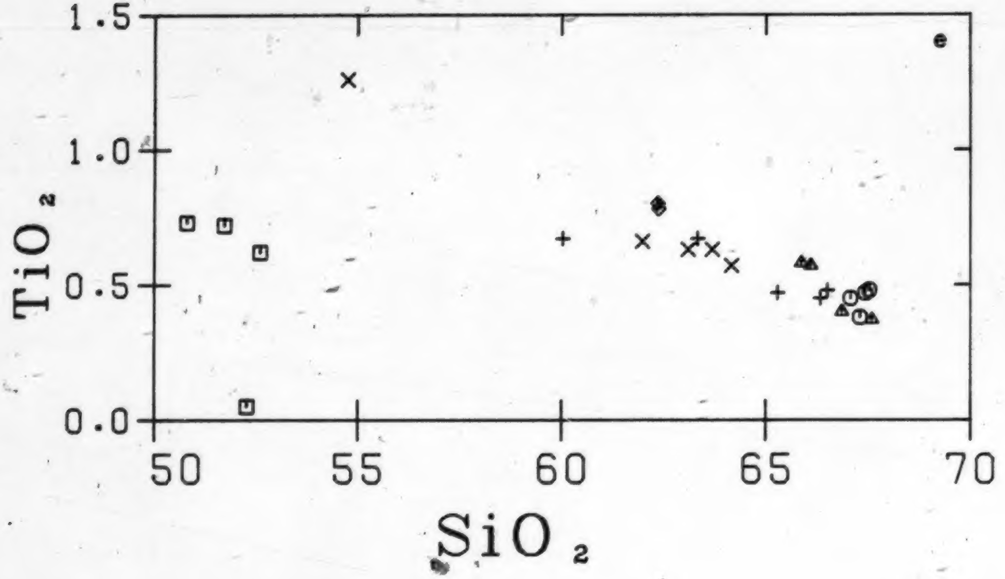
e
TiO₂
1.5
1.0
0.5
0.0
50
55
60
65
70
SiO₂

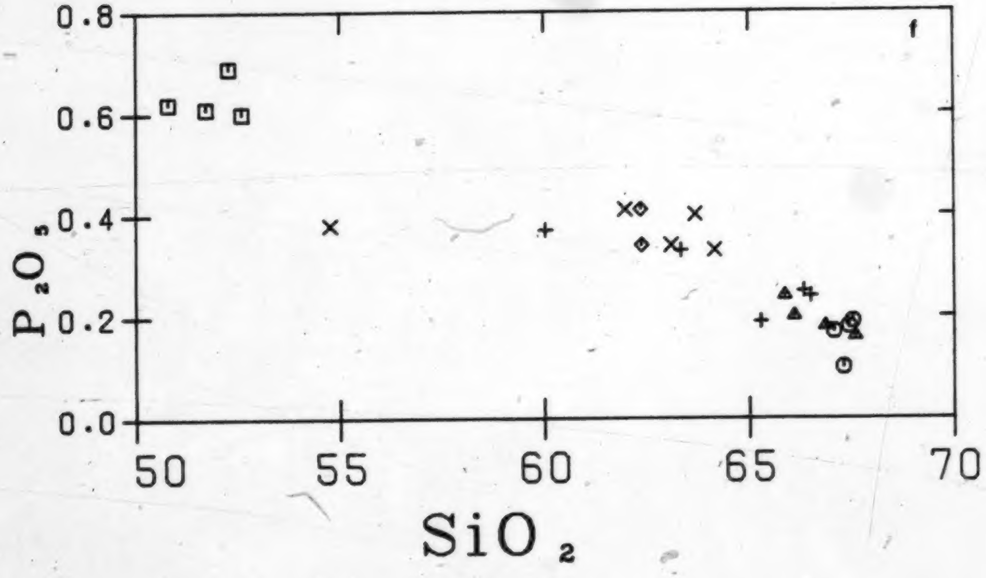
f
P₂O₅
0.8
0.6
0.4
0.2
0.0
50
55
60
65
70
SiO₂

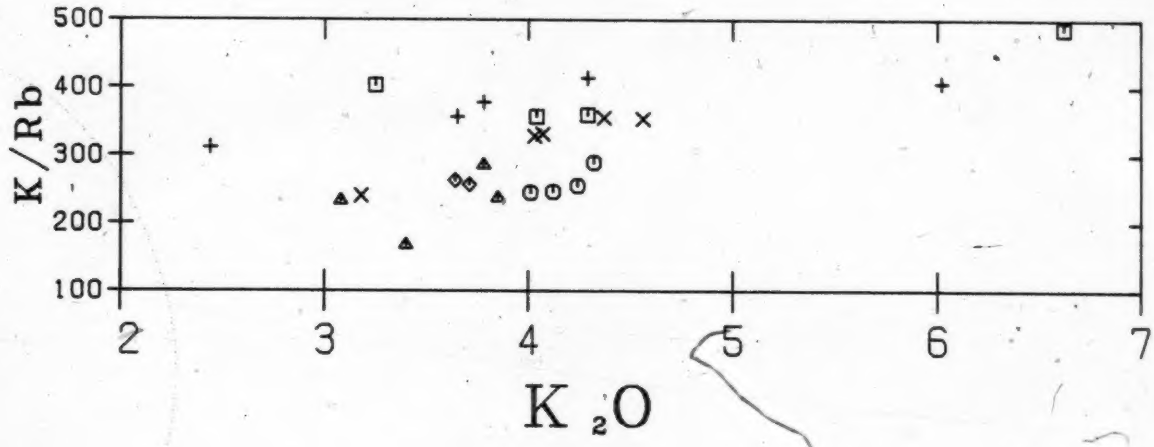

Fig. 5.4. Shows variation in K/Rb ratios vs. K_2O.

to 10 (Fig. 5.6).

Both the light and heavy REEs decrease with increasing SiO_2 (Fig. 5.7a-b). Also Σ(REE) (La+Ce+Nd+Sm+Y(equiv. to heavy REE)) contents fall continuously from basic to acid members (the reverse of normal igneous trends). Covariance of HFS elements (Zr, Nb) with Y (Fig. 5.8a, b) is significant in the granite petrogenesis.

5.4 Petrogenesis

5.4.1 Introduction

This section deals with the variations in major and trace elements seen in the SiO_2 range of 60 to 70 wt%. Detailed isotopic modelling (Chapter 7) conclusively shows that NB magma originated in the mantle and underwent fractional crystallization and assimilation (AFC) with the lower crust. This stage is the first of the two-stage model of isotopic and chemical evolution experienced by the Nelson Batholith magma. The first stage was responsible mainly for both Nd, Sr and to some extent Pb isotopic contamination with the lower crust while undergoing fractional crystallization of variable amounts of amphibole, clinopyroxene and plagioclase. Fractionation of these phases at the lower- to mid-crustal level led to the formation of more siliceous rocks. This evolved magma rose to the higher crustal level and undergone *in-situ* fractional crystallization. Crystallization behaviour at this stage produced various petrographic and chemical units. Limited upper crustal Pb and O isotopic exchange took place at this stage.

The second stage of magma evolution is controlled by the phase equilibria in the four phase compositional space of Qz-Or-Ab-An. Minor mafic phases (bi and hb) are also present and play an important role in controlling some of the major element chemical trends. Recently, increasing importance has been given to minor phases (such as apatite, zircon, sphene and more rarely allanite, monazite and xenotime) that control fractionation trends of REEs, Y, Zr, Nb, U and Th (Tindle and Pearce, 1981; Gromet and Silver, 1983; Mittlefehldt and Miller, 1983)

The second stage of chemical evolution could be best studied in stages with respect to major and minor elements. Firstly, major element distribution is controlled by both felsic

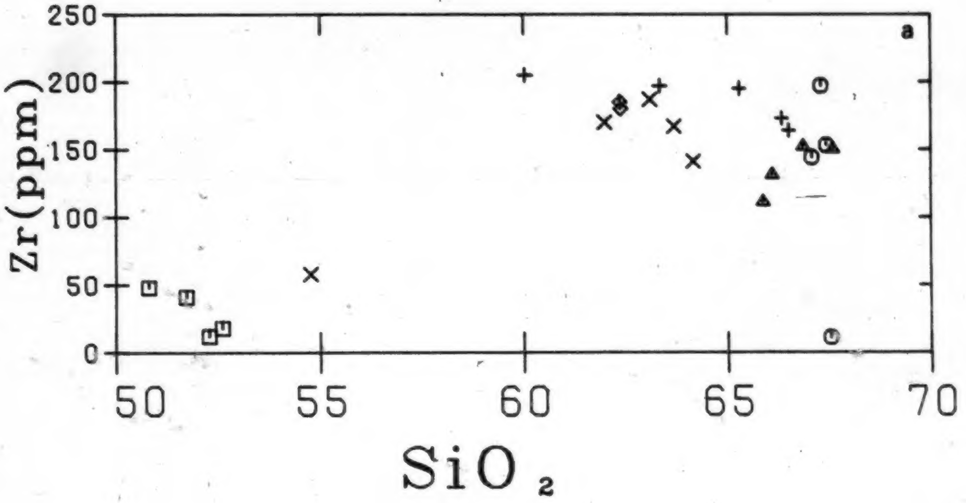

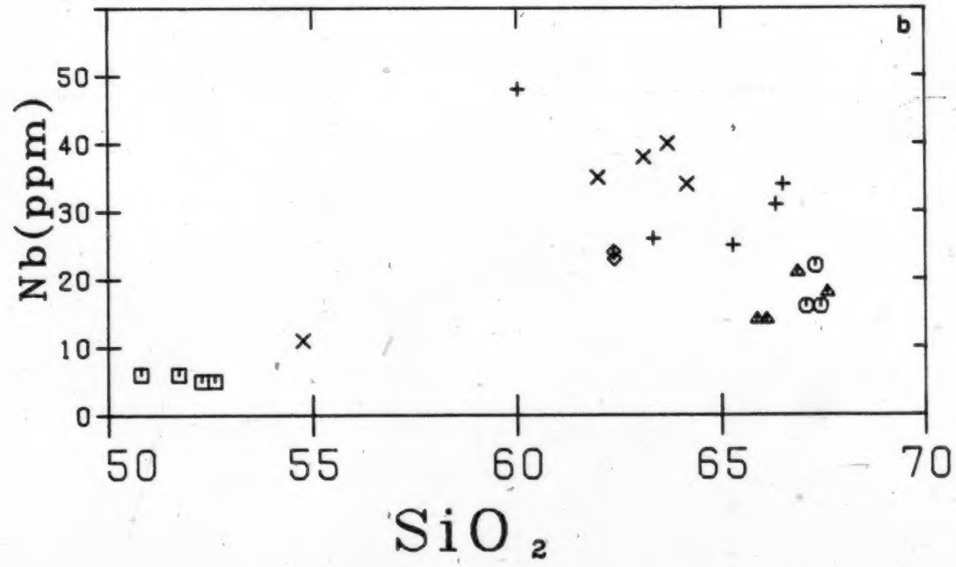

Fig. 5.5a-b. Show variations in high field strength (HFS) elements with SiO_2. a. Zr and b. Nb.

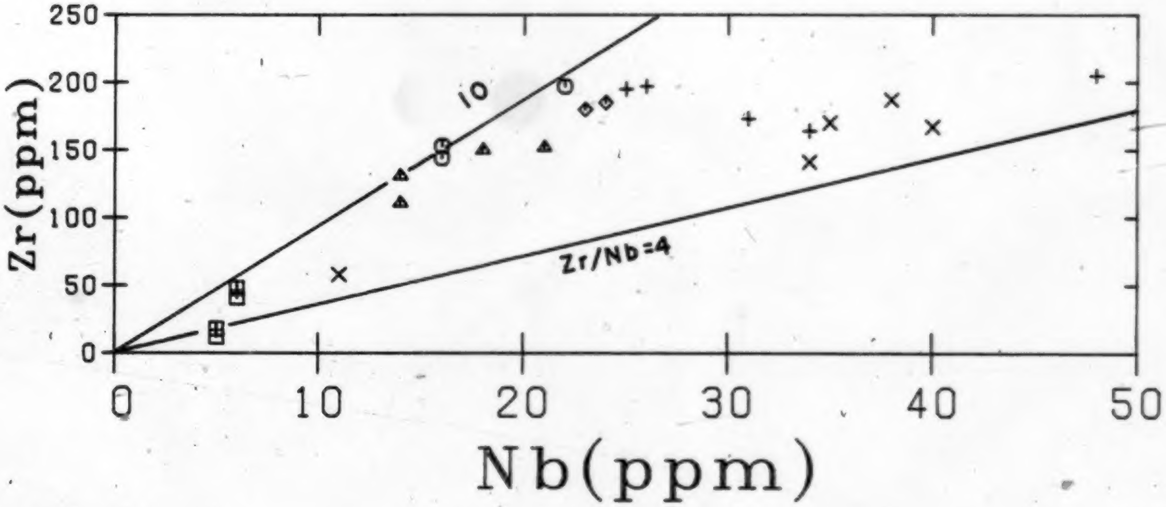

Fig. 5.6a-b. Plot of Nb vs. Zr, Zr/Nb ratio increases from 4 to 10 with differentiation.

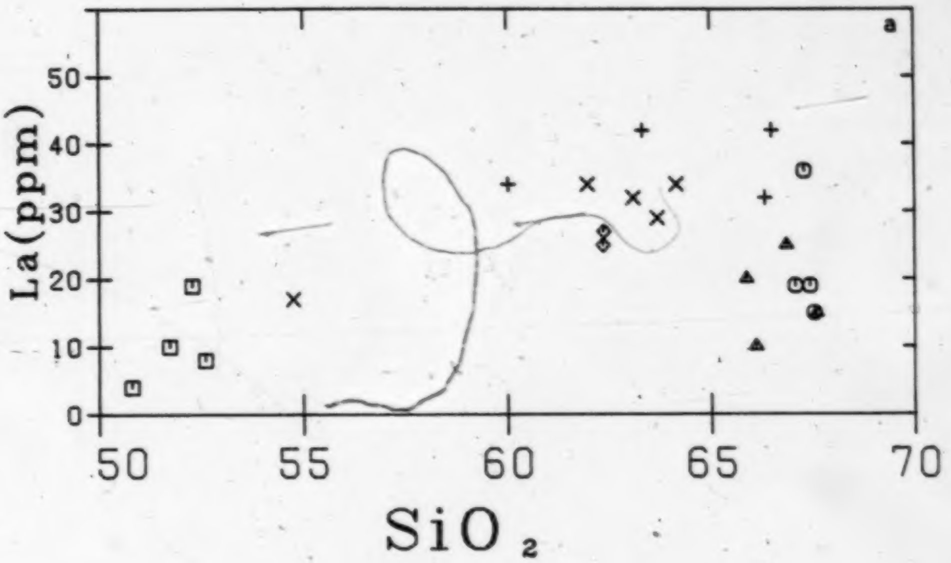

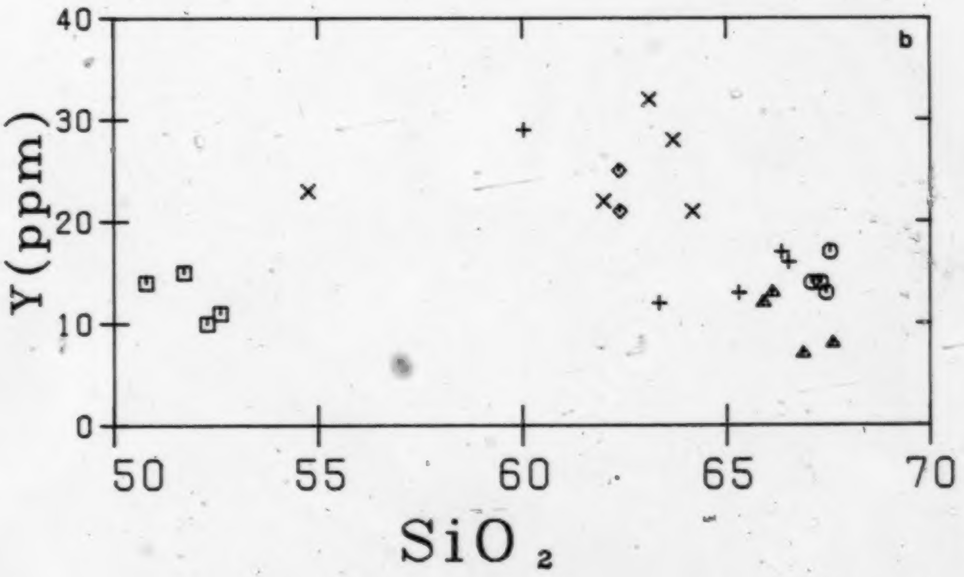

Fig. 5.7a-b. Plots of REEs vs. SiO_2. a. La content decreases with increasing SiO_2, b. Y also decreases.

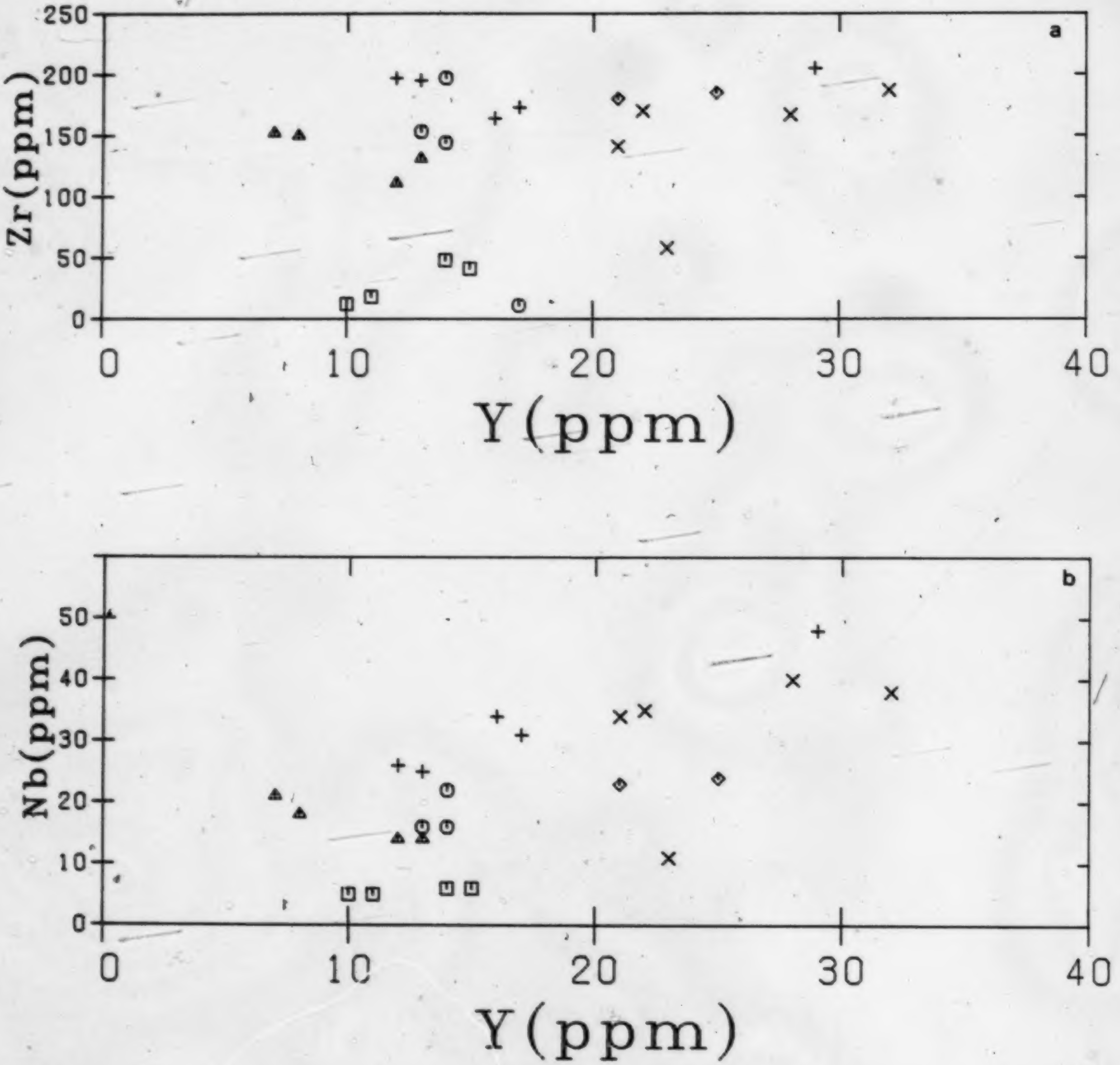

Fig. 5.8a-b. Show covariance of HFS elements with Y, a. Y vs Zr and b. Y vs Nb.

minerals (e.g., feldspar) and mafic minerals (bi and hb). Secondly large ion lithophile (LIL) elements (Rb, Sr and Ba etc.) are mostly partitioned into the major rock forming minerals of granites. REE, Zr and P could be modelled in terms of various minor phases.

Therefore the objectives of this chapter are (1) to qualitatively explain the major elements variation and (2) to quantitatively model some trace elements.

5.4.2 Major Elements

Relatively smooth chemical trends found in the Nelson Batholith granodiorite samples result from elements being constituents of the same minerals that are removed during fractional crystallization. In general, removal of minerals like biotite, hornblende, magnetite and ilmenite through fractional crystallization will decrease Fe-total, TiO_2 and MnO with increasing SiO_2. Biotite has strong preference for Mg over Fe and generally has higher Ti/Fe ratios than coexisting liquid (Miller and Mittlefehldt, 1984) and its preference for Mg over Fe increases in more felsic rocks (Bateman and Chappell, 1979). Depletion of MnO and other transition metal trace elements (Sc, Zn) is also controlled by biotite ($D^{Mn}=10$ between biotite and liquid, Mahood and Hildreth, 1983; Higuchi and Nagasawa, 1969) and other minerals with stronger affinity for Mn (e.g., hb). As most NB samples are predominantly granodioritic, subtraction of mafic minerals must have controlled the continuous depletion of MgO and Fe-total. As no chemical analysis for these mafic minerals is available, no attempt has been made to determine amounts of these mafic minerals using least squares modelling methods developed by Wright and Doherty (1970) or by Stormer and Nicholls (1978). Trends found in the AFM diagram (Fig. 5.2) also support importance of fractional crystallization. Depletion of CaO similar to other major oxides must be due to Ca-rich plagioclase and to some extent by amphibole if it is highly calcic. Behaviour of other major oxides (Al_2O_3, K_2O and Na_2O) is not very clear. Depletion of P_2O_5 must be due to apatite fractionation. Abundance of small grains of apatite in all the samples and its textural relationships prove apatite was on the liquidus all throughout the crystallization history.

The random behaviour of Al_2O_3, K_2O and Na_2O could be very easily explained if it assumed that Nelson Batholith magma was a "crystal mush" before solidification. Study of the crystallization behaviour of a typical granitoid magma in the system, Qz-Or-Ab-An, shows that fractional crystallization of any of the assemblages (1) plagiocalse only, (2) plagioclase + quartz and (3) quartz and two-feldspars will produce definte chemical trends for Ca, Na, K and Al against SiO_2 (see caption of Fig. 5.9). Absence of such expected trends for Al, Na and K mostly contained in feldspars suggests interaction between cumulus and intercumulus melt. Fig. 5.9 is schematic representation of crystallization of a typical granitoid magma in the system Qz-Or-Ab-An. If a granitic liquid (with initial composition at 1) follows a crystallization path 1-2-3-4, the following chemical trends are likely to occur. Due to crystallization of only plagioclase from 1 (plagioclase-only field) to 2 (on the plagioclase-quartz cotectic surface), Al, Ca and Na will fall with concomitant rise in Si and K. As both qz-plag crystallize along the path 2-3, Ca will continue to fall, Si and Na will drop slightly, while Al and K rise. At position 3, when the liquid reaches quartz-two-feldspar cotectic line (with the incoming of K-feldspar as a crystallizing phase), K will fall while Na will rise. Fractionation of mafic phases (bi and hb) and unlikely separation of crystals and liquid will tend to blur the above expected trends. Therefore due to absence of clear chemical trends for K, Na and Al for the Nelson Batholith, *in-situ* fractional crystallization appears to be dominant process where cumulus-intercumulus interaction was extensive (see also trace element modelling).

5.4.3 Trace Elements:

During the crystallization of a magma in a plutonic environment, two extreme types of crystallization are generally considered under conditions where rates of diffusion of ions exceed that of crystal growth. Perfect fractional crystallization is the one when only surface of the crystals is in equilibrium (Rayleigh fractionation) with the liquid. The other type is perfect equilibrium crystallization where the entire solid phase remains in equilibrium with the liquid at all times. For granitoid magma, because of high viscosity, crystals forming by either processes are unlikely to gravitationally settle and therefore perfect separation of crystals (to be called

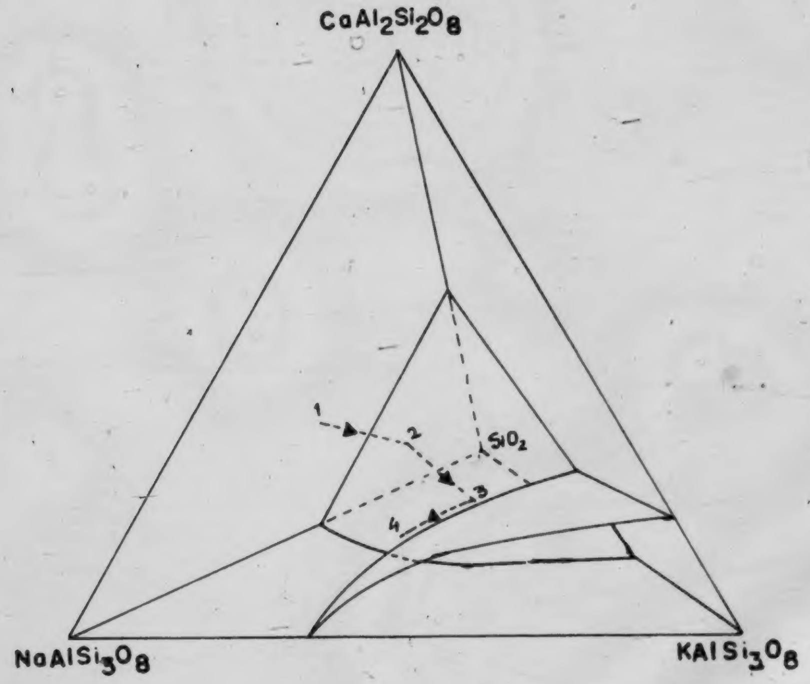

Fig. 5.9. Schematic representation of a typical granitoid magma in the system Qz-Or-Ab-An. If a granitic liquid (with the initial composition at 1) follows a crystallisation path 1-2-3-4, the following chemical trends are likely to occur. Due to crystallisation of plagioclase only from 1 (Plagioclase field) to 2 (on plagioclase-quartz cotectic surface), Al, Ca and Na will fall with concomitant rise in Si and K. As Qz-Plag crystallise along the path 2-3, Ca will continue to fall, Si and Na will drop slightly, while Al and K rise. At position 3, when the liquid reaches Qz-two-feldspar cotectic line (with the incoming of K-feldspar as a crystallising phase), K will fall while Na will rise. Fractionation of mafic phases (bi and hb) and unlikely separation of crystals and liquid will tend to blur the above expected trends. For the Nelson Batholith, behaviour of major elements (Figs. 5.1 to 5.3) shows in-situ fractional crystallisation was the dominant process where cumulus-intercumulus interaction was extensive (see also LIL element modelling).

Cumulate) from melts rarely happens. Therefore there lies a continuum of conditions of crystallization involving partial equilibration between solid and liquid. Many studies of granitoid magma have revealed the dominant effects of *in-situ* fractional crystallization in controlling the major and trace elements behaviour (McCarthy and Hasty, 1976; McCarthy and Groves, 1979; McCarthy and Robb, 1978; Tindle and Pearce, 1981; Stephens et al., 1985). Although some have described igneous sedimentary structures indicative of fractional crystallization (Emeleus, 1963, Smith, 1974), such structures are uncommon in granitic rocks. Also the cumulus-intercumulus textural relationships (expected due to *in-situ* fractional crystallization) are not normally observed in granites as the intercumulus melt will generally crystallize the same mineral assemblages as that of the cumulate phase.

A. Large Ion Lithophile Elements(Rb, Sr and Ba)

Trace element concentrations in coarse-grained granitic rocks are determined firstly by the composition of their parent magma and subsequently by the type of crystallization process. In this section, the distribution of Rb, Sr and Ba and relative proportions of different crystallizing phases and cumulus and intercumulus melt relationships will be modelled. Gravity segregation of crystal from granitic melts is evidently rare. Fractionation could occur either by (1) progressive inward nucleation of crystals from the margins of the magma chamber or (2) by filter pressing (Bateman and Chappell, 1979). Slow diffusion of ions in the solid state prevents requilibration between early formed solids and melt, while the melt remains more or less homogeneous in composition. Definition of cumulus crystals and inter-cumulus melt is the same as those of McCarthy and Robb (1978). The inter-cumulus melt is assumed to crystallize in isolation from the remaining magma mass.

Behaviour of trace elements during fractional crystallization has been given mathematical expressions by many workers (e.g., Neuman et al., 1954; Greenland, 1970; Hanson, 1980 and Allègre and Minster, 1978 for a review). Modal or non-modal removal of crystallizing phases from the melt has been discussed by Hartogen and Gijbels (1976).

Two extreme modes of crystallization will be considered here.

1). Perfect (or Rayleigh type) Fractional Crystallizaton:

$$C_m^i = C_{0,m}^i F^{(D_i-1)} \quad \text{(5.1a)}$$

$$C_s^i = D_i C_m^i \quad \text{(5.1b)}$$

2). Equilibrium Crystallization:

$$C_m^i = C_{0,m}^i / [F + D^i(1-F)] \quad \text{(5.2a)}$$

$$C_s^i = D^i C_m^i \quad \text{(5.2b)}$$

Where $C_{0,m}^i$ = concentration of element i in the original melt,

C_m^i = concentration of element i in the residual melt,

C_s^i = concentration of element i in the solid,

F = weight fraction of melt remaining.

D^i = bulk distribution coefficient for element i

$[D^i = K_1^i X_j]$ where,

K_1^i = distribution coefficient for element i in phase j, and

X_j = weight fraction of phase j.

Figs. 5.10 and 5.11 illustrate the application of these equations to modelling LIL element variations. In Fig. 5.10a-b, the solid phase consists of 20% quartz, 20% K-feldspar, 50% plagioclase, 5% biotite and 5% hornblende (see discussion later on for choosing the above mode). Partition coefficients for Rb, Sr and Ba used are listed in Table 5.2. During equilibrium crystallization curves BC and AB represent changes in the melt and 'cumulate' composition. It is seen that first cumulate to separate from the melt is enriched in both Sr and Ba, but depleted in Rb, while the reverse is true for the melt. This is because bulk K_D's for Sr and Ba are greater than 1 (for the above mineral assemblage), while that of Rb is less than 1. Melt and cumulate formed due to fractional crystallization change composition along the straight line vectors BE and AD. Products of crystallization in between these two extremes will be bounded by these curves.

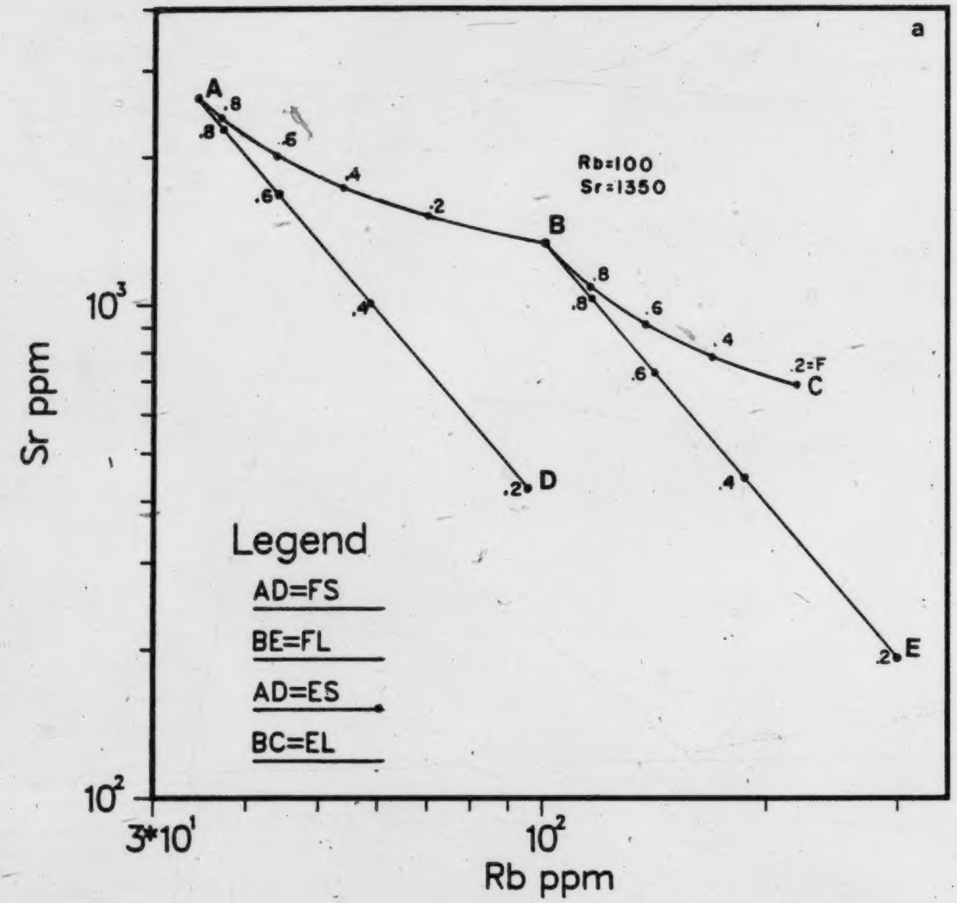

Fig. 5.10a-b. Methods of modelling Large Ion Lithophile(LIL) element (Rb, Sr and Ba) variation in granitic rocks. An initial liquid composition is taken at B (see text for explanation). Solid phase to crystallise consists of 20% Qz, 20% Kf, 50% Plag, 5% Bi and 5% Hb. Distribution coefficients used are listed in Table 5.2. During progressive equilibrium crystallisation, the liquid changes in composition along BC and the corresponding solid along AB. Dots along the curves show crystallisation intervals of 20%. For fractional crystallisation, the solid and liquid change along AD and BE. Points D and E represent the solid and melt compositions at 80% crystallisation. (FS =fractional solid, FL = fractional solid, ES = equilibrium solid and EL = equilibrium liquid). a. Rb-Sr and b. Rb-Ba.

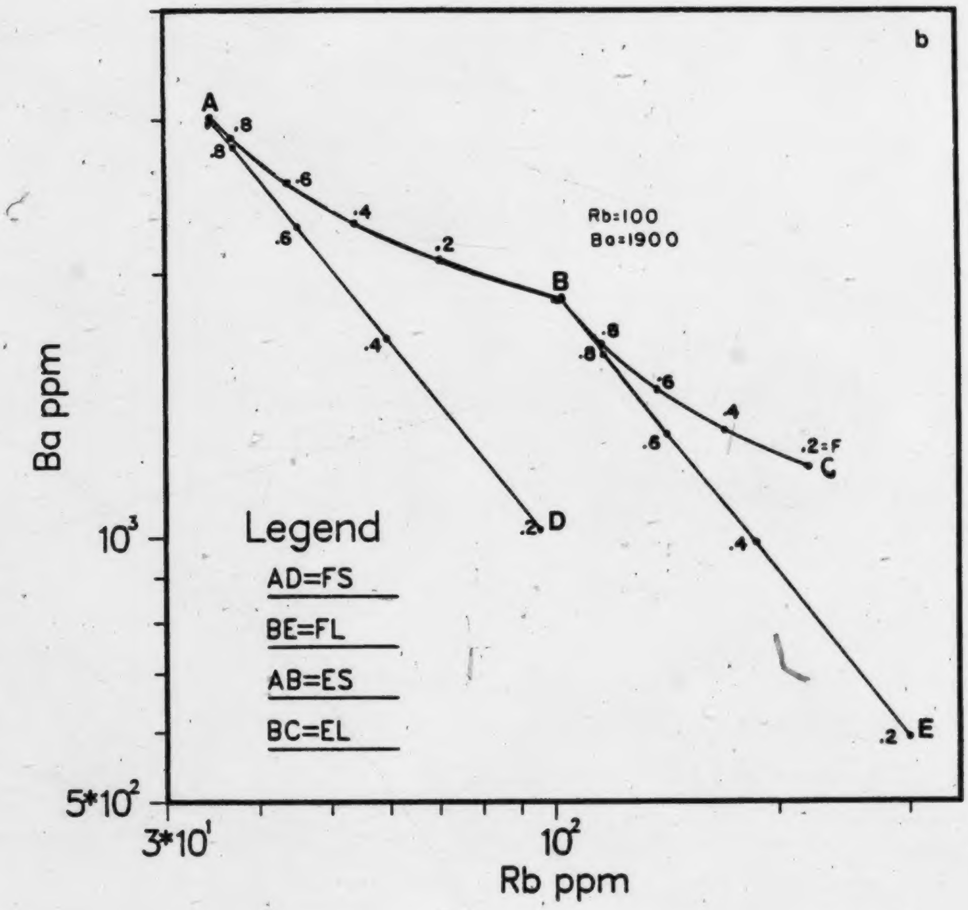
b
A
B
C
D
E
.8
.6
.4
.2
.2=F
Rb=100
Ba=1900
Legend
AD=FS
BE=FL
AB=ES
BC=EL
Ba ppm
Rb ppm
10³
5*10²
3*10¹
10²

Table 5.2[*]

Element	Qz	K-fels	Plag	Horn	Bi
Rb	0.0001	0.659	0.048	0.014	5.26
Sr	0.0001	5.87	2.84	0.22	0.120
Ba	0.0001	6.12	0.36	0.044	6.36

[*] Taken from Hanson (1978) and Arth (1976).

Figs. 5.11a-b illustrate the effects of intercumulus melt on the trace element distribution. Intercumulus melt once trapped by cumulus phase remains isolated from and crystallizes independently of the bulk of the melt. This melt can be regarded as an additional phase with unit partition coefficients for all elements (Greenland, 1970; McCarthy and Hasty, 1976). Therefore trapped intercumulus melt, result of *in-situ* fractional crystallization, will tend to bring cumulus composition curve closer to the melt composition curve and decreases the range of composition in the solid formed. For example, in Fig. 5.11 curves AD and BE follow the change in pure cumulate and melt composition as discussed before. The other curves marked 2-2', 4-4' and 6-6' parallel to AD/BE, are solid compositions due to removal of 20%, 40% and 60% intercumulus melt by the cumulate respectively.

LIL trace element modelling has recently been applied to granite petrogenesis by McCarthy and Hasty (1976), McCarthy and Robb (1977), McCarthy and Groves (1979), Michael (1984) and Tindle and Pearce (1981). The usefulness of such modelling lies in the fact that these trace elements are partitioned into the major rock forming minerals of granites. In the following discussion, therefore, a mineral assemblage (comprising mainly of quartz, K-feldspar, plagioclase and minor biotite and hornblende) has been chosen on the basis of observed modes of the most mafic granodiorite sample (8057G with SiO_2=60.03%). Though it is possible that modal proportions of crystallizing minerals might vary in practice, they are assumed to remain constant for modelling purposes. As the Nelson Batholith samples considered are mostly bi-hb-granodiorite with a small SiO_2 range (60 to 68%), the assumption of constant mode will not alter the conclusions very much. The other requirement for modelling is a need to know the initial concentrations of Rb, Sr and Ba of NB magma at about SiO_2=60 wt%. These concentrations are taken to be 100, 1350 and 1900 ppm respectively, close to those of the sample

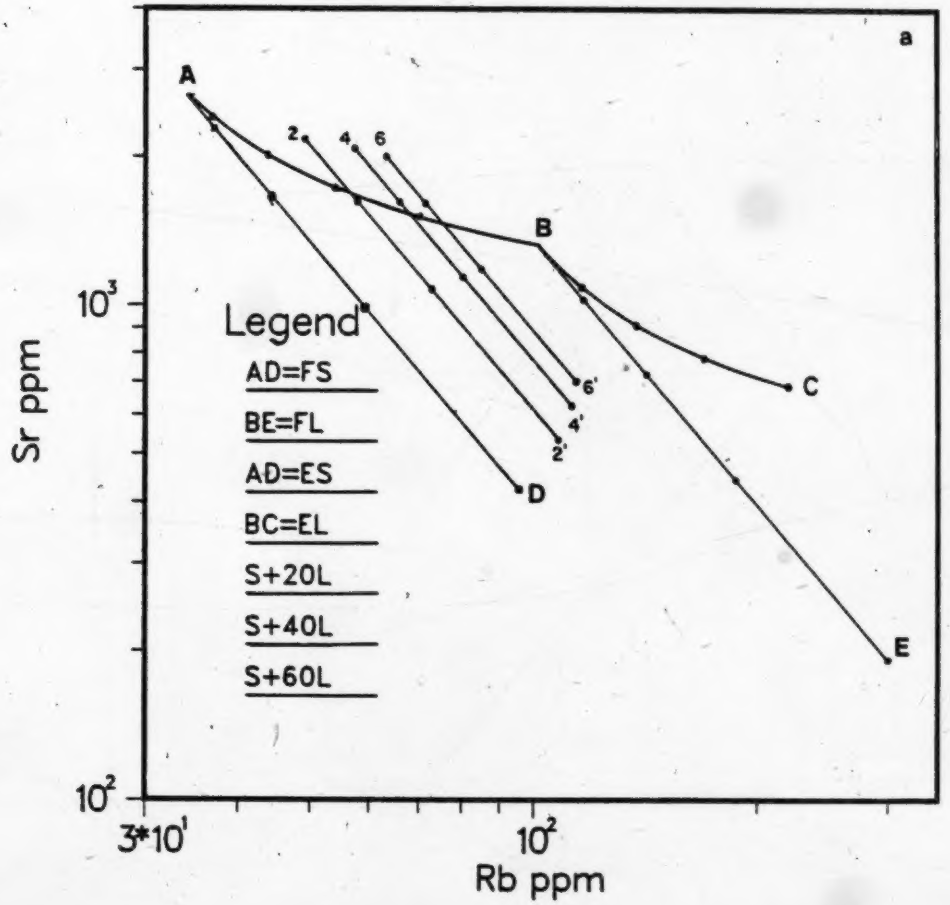

Fig. 5.11a-b. Illustrates the effects of trapped intercumulus melt with the cumulate on Rb, Sr and Ba during fractional crystallisation. Melt compositions lie along the vector BE. The curves marked 2-2', 4-4' and 6-6' are solid compositions due to removal of 20%, 40% and 60% intercumulus melt by the cumulate. Curve AD represents solid compositions not trapping any intercumulus melt. (S+20 = solid +20% liquid, S+40% = solid+40% liquid and S+60= solid + 60% liquid). a. Rb-Sr and b. Rb-Ba.

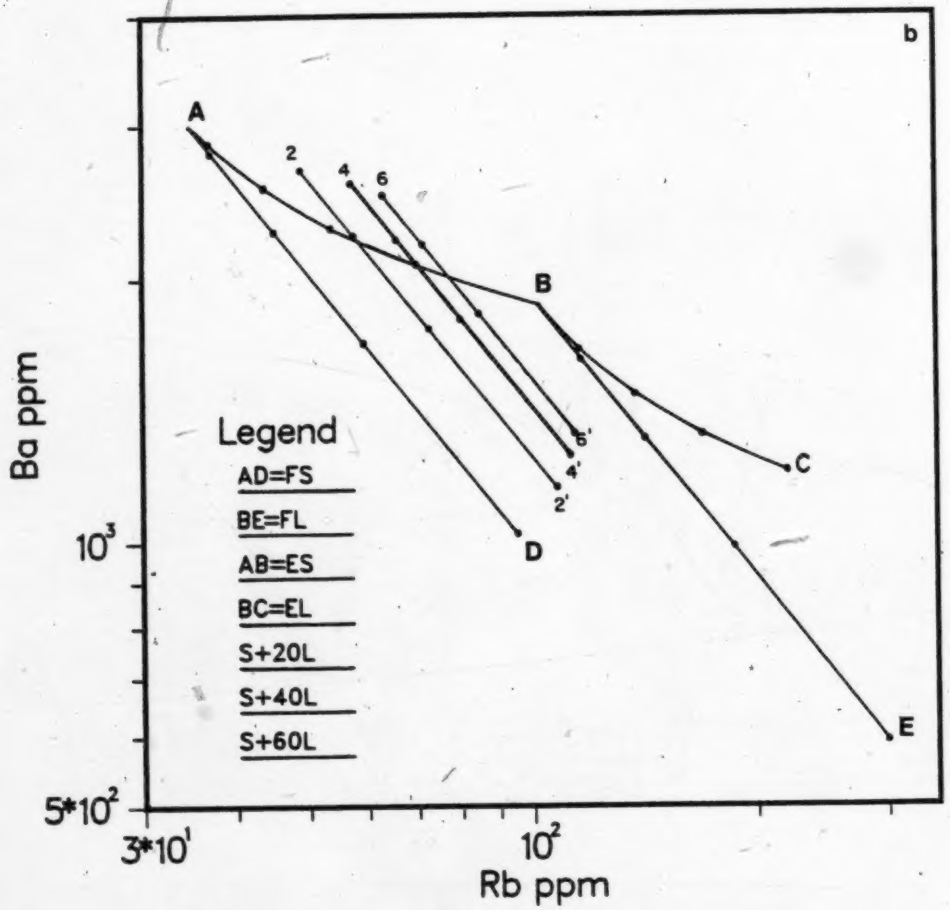
b
A
B
C
D
E
2
4
6
2'
4'
6'
Legend
AD=FS
BE=FL
AB=ES
BC=EL
S+20L
S+40L
S+60L
Ba ppm
Rb ppm
10^3
$5*10^2$
$3*10^1$
10^2

8057G.

Lastly, the factor that influences the modelling results is the choice of mineral-melt partition coefficients used in the calculation. Table 5.2 shows the distribution coefficients for Rb, Sr and Ba for those minerals used in the modelling. Many factors that affect trace element distribution coefficients include temperature, melt composition and melt structure. Therefore other values than those in Table 5.2 are also available (for example, Leeman and Phelps, 1981). Sun et al. (1974) and Drake and Weill (1975) have shown that distribution coefficients for most trace elements studied are inversely proportional to temperature. During fractionation, increasing polymerisation of the melt will decrease solubilities of Sr and Ba but will increase that of Rb (Watson, 1976) and consequently for the present case of constant proportions of crystallizing phases $D^{Sr,Ba}$ will increase and D^{Rb} will decrease. The above observations necessitate continual change in K_D's to be taken into account for modelling calculations. For both practical purposes and lack of our knowledge regarding the change in D_i, mean melt distribution coefficients (Arth, 1976; Hanson, 1978) have been used. Therefore modelling should be treated with some caution.

Figures 5.12a and b show Rb-Ba and Rb-Sr models for fractional crystallization with various proportions of intercumulus melt along with the NB data superimposed. Curves AD and BE are pure solid and melt compositions. Curve 2-2' shows the composition of the solid if 20% intercumulus melt is repeatedly trapped, curve 4-4' and 6-6' are solid compositions if 40% and 60% melt are repeatedly trapped. Marked dots on the curves represent different intervals of crystallization. From both the figures, it is clear that NB samples are cumulate-melt mixtures: the proportions of intercumulus melt vary widely. The 8013-group of samples with highest SiO_2 contents (around 67%) plots on or close to the pure melt curve BE at about 40% fractional crystallization. The other groups (8053-, 8057- and 8059-) of samples have trapped intercumulus melt varying from 0% (i.e., pure cumulate) to 95%. The overall agreement between the two diagrams and model calculation and observed data show predominant effects of in-situ fractional crystallization. Also trapping of intercumulus melt took place at different levels of fractional crystallization (50 to 80%). Again these high values of crystallization levels

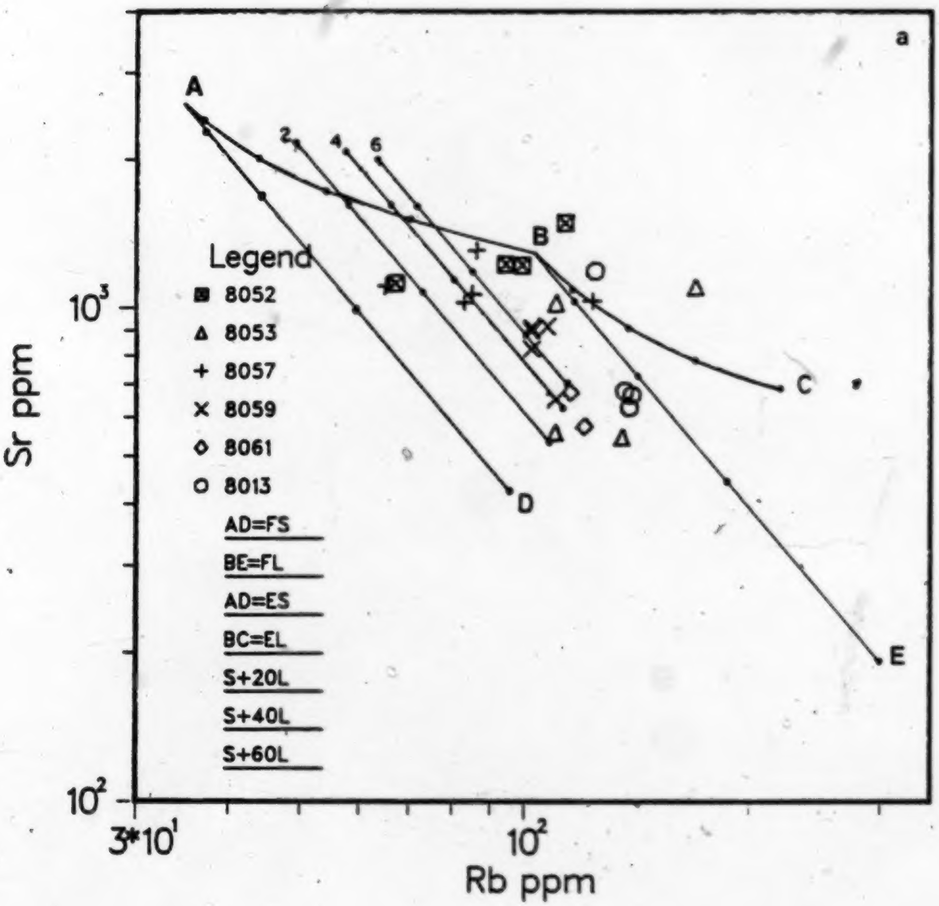

Fig. 5.12a-b. Illustrate the effects of intercumulus melt and cumulate on the Rb, Sr and Ba contents of the granitic samples from the NB. Model curves from the Figs. 5.11a-b have been superimposed. a. Rb-Sr and b. Rb-Ba.

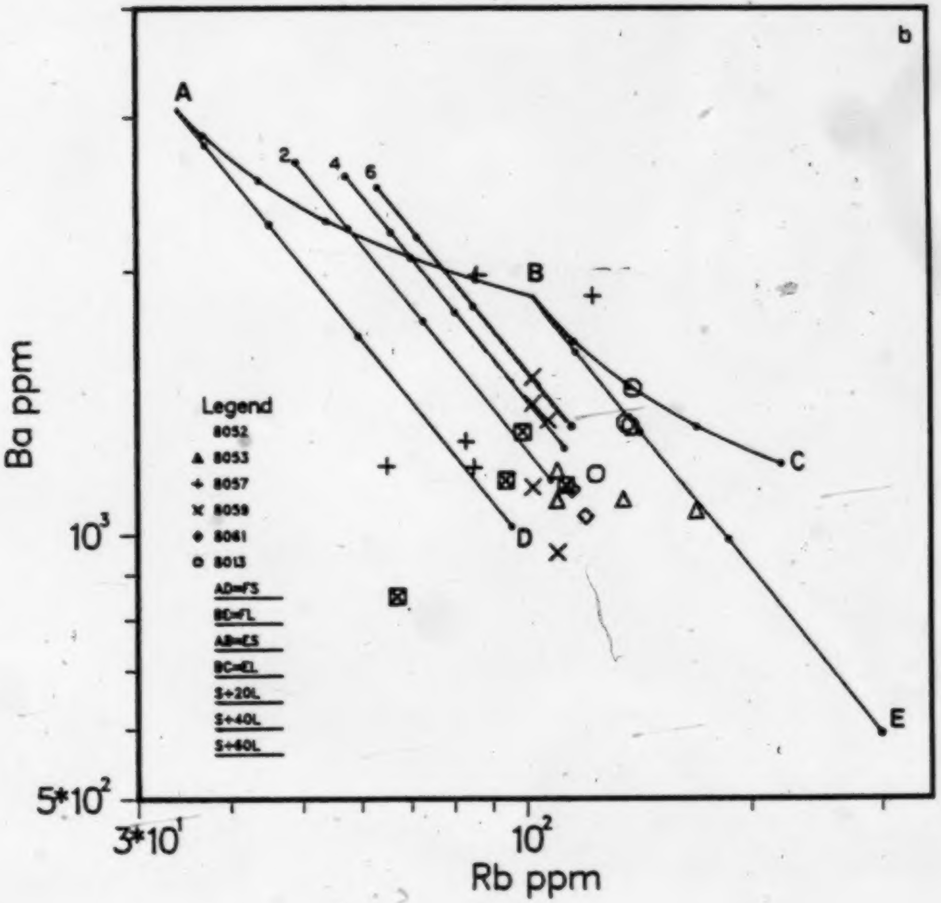
b
A
B
C
D
E
2
4
6
Legend
8052
▲ 8053
+ 8057
× 8059
● 8061
○ 8013
AD=FS
BD=FL
AB=ES
BC=EL
S+20L
S+40L
S+60L
Ba ppm
10^3
$5*10^2$
Rb ppm
$3*10^1$
10^2

needed to produce NB granodiorites required large volumes of original magma. This problem could be easily circumvented if high K_D's for Rb, Sr and Ba for feldspars are used in the calculation. Whalen (1983) and Michael (1984) discussed this problem with respect to more evolved granites ($SiO_2 > 70\%$) than the NB samples. Presence of small amounts of intercumulus melt required to produce Rb-Ba distributions in some samples suggests efficient separation of crystals from melts does sometimes occur. Examples of such efficient separation include a case study of the Blue Tier Batholith, Tasmania (McCarthy and Groves, 1979). They suggested well defined vertical and or concentric zonings were produced due to latter stages of crystallization on the magma chamber's roof, walls and floor inwards. Absence of very evolved rock-types in and around the Nelson Batholith rules out operation of filter-pressing which would have squeezed out vapour-rich more evolved liquids to form aplites, alaskites etc. On the other hand, NB magma appears to have crystallized or solidified at depth without perfect separation of crystals and melt. Due to the highly viscous nature of acidic magmas, gravity induced fractionation of crystals is not considered to be very important (Rice, 1981).

B. Ti, P, Zr, Nb and REE

Unlike LIL elements, these elements are concentrated in minor phases. Therefore enrichment or depletion of these elements will depend on the crystallization behaviour of these phases. NB samples have been found to contain trace (though significant) amounts of zircon, apatite, sphene and allanite. Monazite and xenotime are also large depositories of REEs, but, their presence in NB samples has not been proven. Therefore behaviour of the above elements is considered in terms of fractionation of zircon, apatite, sphene and allanite. Opaque minerals like ilmenite and magnetite will also control Ti.

Figs. 5.3(e,f) and 5.5(a,b) and 5.7(a,b) show continuous decrease in Ti, P, Zr, Nb, La and Ce throughout the magma evolution. Depletion of Ti could be due to either biotite or ilmenite separation. Abundance of sphene might also have contributed to Ti depletion to some extent, while depletion of P is certainly due to apatite. Presence of apatite in the samples as an early crystallizing phase (on textural grounds) supports this conclusion. Zircon is abundant in the NB samples. Therefore fractionation of zircon (with high K_D for Zr) will deplete Zr. However Zr/Nb ratio (Fig. 5.6) increases with differentiation and therefore Nb is depleted faster than Zr. Nb is believed to be removed by biotite and also by sphene and ilmenite (Tarney and Saunders, 1979). It is known that zircon has very large distribution coefficients for middle and heavy REE (Table 5.3, Arth, 1976; Condie, 1978), but at its normal abundance levels (<.1 wt%) its D^{HREE} is too low (300 to 600) to induce much depletion. However its removal will cause an increase in $(Ce/Y)_{Ch}$, equivalent to $(Ce/Yb)_{Ch}$) although fractionation of other minerals having high K_D's for LREE and HREE will mask the zircon effect.

The depletion of LREE in granitic magmas is not expected due to normal fractionation of major minerals and therefore has been cited as contrary to probable trends in magma undergoing fractional crystallization (Scott and Vogel, 1980). Recent studies (Gromet and Silver, 1983; Mittlefehldt and Miller, 1983; Miller and Mittlefehldt, 1984), however have gathered enough evidence on the importance of accessory phases controlling the REE distribution. The accessory minerals recognised in the NB samples are, in the order of abundance, sphene, epidote, apatite, zircon, allanite and monazite(?), though their absolute abundances slightly vary from sample to sample and from most basic to most acidic rocks. Detection of monazite is doubtful at this moment as it is commonly confused with zircon (see also Mittlefehldt and Miller, 1983). Both minerals occur as inclusions in biotite crystals. Some grains show radiation damage haloes. Electron microprobe analyses are needed to distinguish between monazite and zircon.

LREEs with larger ionic radii do have distribution coefficients <1, for most major minerals (quartz, K-feldspar, biotite and hornblende) and therefore will behave as incompatible elements during magmatic crystallization. On the other hand HREEs (including Y) may not behave incompatibly if amphibole is crystallizing (Arth and Barker, 1976; Frey et al., 1978). NB samples exhibit continuous depletion in REEs (La, Ce, Y) though there is considerable scatter. Modelling done for Rb, Sr and Ba using only major minerals can not explain REE data. Therefore alternative means of LREE depletion must be explored. There are large number of chemical processes likely to be responsible for LREE depletion. These are a)

Autometasomatism, b) Liquid state thermogravitaion diffusion (LSTD), c) Increase in K_D for LREE vs. liquid, d) Loss of LREE-rich vapour phase and e) Fractionation of LREE-rich accessory phases (Miller and Mittlefehldt, 1982).

Most of the samples are relatively fresh and do not exhibit strong alteration as expected due to reaction with late stage HREE-rich fluids. If such HREE rich liquids are present and autometasomatise the parent rock, it will simulate a LREE depleted pattern (Dodge, 1979; Bowden and Whitney, 1974). However their suggestion is not supported by the experimental studies on vapour-liquid REE partitioning (Flynn and Burnham, 1978; Mysen, 1979). Their study suggests that at crustal pressures water-halide vapours have K_D for LREE between vapour/liquid greater than K_D for HREEs between vapour/liquid, but K_D for LREE is less than 1 and consequently the liquid will not be depleted in LREE due to loss of a vapour phase. Though it is difficult to rule out any effect of such a vapour phase, the intermediate SiO_2 contents of NB samples and absence of any late stage highly silicic rock-types such as pegmatites, aplites etc. do not support production of vapour-rich phases during solidification of NB magma. CO_2 rich vapour has also high distribution coefficients for LREE (e.g., $D^{Ce}=50$, $D^{Sm}=10$, $D^{Tm}=20$, Wendlandt and Harrison, 1979). Therefore loss of such a vapour will deplete the liquid in both light and heavy REE more than MREE. Chondrite-normalised REE patterns for the NB samples show (Fig. not shown, see Table A2.2.1, Appendix 2) clear depletion of MREE(e.g., Nd, Sm) relative to LREE(e.g., La). Therefore loss of CO_2 rich vapour was not responsible for LREE depletion for NB samples. Recent studies (Hildreth 1979, 1981; Whalen, 1983) on high SiO_2 granitic rocks have established the importance of liquid state processes (convective circulation and Soret diffusion) in the chemical zonation of magma chambers without separation of crystalline and vapour phases. Such processes have been successfully apllied to the Bishop Tuff which shows marked LREE enrichment (Hildreth, 1979) and the Ackley City Batholith (Whalen, 1983) which shows LREE depletion from granites to aplites. The cooler more felsic cap of a magma chamber will be enriched in HREE relative to LREE due to stronger complexing of the former (because of their smaller ionic radii). Such a process of ascent of felsic cap must be taking place before extensive crystallization. In plutonic environments, the magma composition appears to have been controlled by crystal liquid equilibria which will mask the effects of liquid state diffusion (if any). As the NB samples have intermediate composition (SiO_2 = 60 to 68 %) and the modelling on LIL elements showed conclusively the importance of in-situ fractional crystallization, it seems unlikely that LSTD was operating in the case of the NB magma.

As mentioned before, major minerals in a granitic magma have very low K_D for REE. With decreasing temperature and increasing felsic composition of the magma, even though increasing polymerisation might increase K_D's for REE to some extent for the major minerals, the bulk K_D's will still be less than 1. Therefore LREE will still behave as incompatible elements unless they are taken up by some accessory phases with K_D's for LREE >1. Separation of significant amounts of such phases must have operated for the NB magma. The following Tables (5.3a-b) show the distribution coefficients for some selected REE.

The NB samples are unusually rich in sphene and apatite. Zircon is also moderately abundant. Allanite is generally found as cores of epidote and only few grains (2 to 5) have been identified in thin sections. If an average modal abundances of 1% sphene, 0.05% apatite, 1.0% epidote, 0.01% zircon and 0.001% allanite are taken along with modal abundance of major minerals as used for LIL element modelling and recalculated to 100%), bulk K_D for La, Ce becomes greater than 1. Therefore these accessory minerals played an important role in depleting the LREE in the NB samples.

Even though separation of these accessory minerals is required to explain the REE behaviour, problem arises regarding their efficient separation from the melt. Gravity induced fractionation by crystal settling is generally considered unimportant in granitic magmas (Rice, 1981; McCarthy and Robb, 1978). Because of large grain sizes of sphene and epidote, they might easily settle out of the magma. However, other minerals like apatite and zircon which are very small might not separate as efficiently as sphene. Allanite is large compared to apatite or zircon. These accessory minerals occur as inclusions in larger minerals (e.g., biotite and feldspar) and therefore their separation must be related to the separation of host minerals. As discussed before, granites are undoubtedly mixtures of minerals fractionated from the melt and

Table 5.3a*

Element	Qz[a]	K-fels	Plag	Bi	Hb
La	0.0001	0.08[b]	0.34[b]	0.33[b]	0.30
Ce	0.0001	0.044	0.027	0.32	1.52
Nd	0.0001	0.025	0.21	0.29	4.26
Sm	0.0001	0.018	0.13	0.26	7.77
Yb	0.0001	0.012	0.049	0.44	8.38

* Taken from Arth (1976)

a- assumed.

b- from Mittlefehldt and Miller (1983)

Table. 5.3b**

Element	Sph	Apat	Zirc	Allan	Mon	Xen
La	50	25	3	5.10^3	10^4	500
Ce	80	25	3	5.10^3	10^4	700
Sm	125	25	4	$1.2x10^3$	5.10^3	$1.4x10^3$
Eu	60	25	3	800	10^3	$1.2x10^3$
Tb	75	25	50	100	$1.5x10^3$	$6.5x10^3$
Yb	60	25	250	100	200	10^4
Lu	50	25	300	100	200	10^4

** Taken from Condie (1978).

the trapped melt. It is also possible that the LREE depletion trend is some artifact of the relative mixture of cumulus minerals and intercumulus melt.

6. PETROGENESIS OF THE BONNINGTON PLUTON

6.1 Introduction

Exposed south and southwest of the Nelson Batholith is a large granitoid body known as the Bonnington Pluton. This pluton is cut along its western boundary by the Champion Lake Fault (Simony, 1979) which separates it from the Castlegar and Trail Gneisses. The Rossland Volcanic Group lies along its southern, eastern and northern edges and separates this pluton from the Nelson Batholith lying to the north. Like Nelson Batholith, the Bonnington Pluton also shows wide variation in petrography, mineralogy and texture (see Table A1.2, Appendix 1). Both porphyritic and non-porphyritic varieties are present and though rock-types ranging from diorite to granodiorite in composition are present, quartz-diorites dominate the petrographic varieties (Little, 1960 and the present work). For the present work, both quartz-diorite and granodiorite samples were collected mainly from two localities. Four groups (8021-, 8022-, 8067- and 8068-) of samples were collected from a small area, north of Castlegar (see Fig. 1.1d and Table 1.1 for sample location). Another group of samples (8075-) was collected from the central part of the main body along a newly-built highway connecting Castlegar and Salmo.

All these samples have been analysed for both major and trace elements by the XRF method (Table A2.2.2, Appendix 2). Like the 8052-series of the Nelson Batholith, a group of samples (8022-) is alkaline in nature. On a plot of total alkalies vs. SiO_2, (Fig. 6.1) they fall in the alkaline field, while all other samples from this pluton fall in the sub-alkaline field. This alkaline group is slightly richer in SiO_2 (by about 2-3%) than the 8052-group. Mineralogically this alkaline suite consists of clinopyroxene, micro-perthite and biotite. Hornblende is typically absent unlike 8052-group which contains abundant quantities of both biotite and hornblende. Also the 8052-series does not contain much K-feldspar.

The rest of the BP samples have only about 5 wt% range in SiO_2 (60 to 65) and about 1 wt% range in alkalies (7 to 8). On an AFM plot (Fig. 6.2) BP samples fall in the calc-alkaline field like NB. Therefore calc-alkaline nature of both these granitoid bodies and close temporal and spatial relationships suggest their development in a similar tectonic setting. Table 6.1 shows

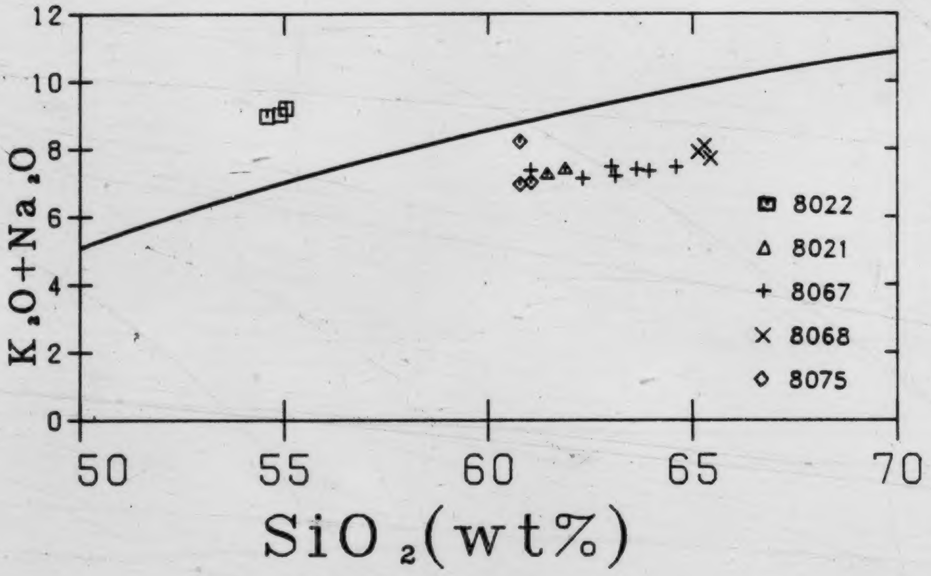

Fig. 6.1. Plot of total alkalis (K_2O+Na_2O) against SiO_2. The line (according to Irving and Baragar, 1971) divides the samples into two groups. All the samples (except those belonging to 8022-series) plot in the subalkaline field.

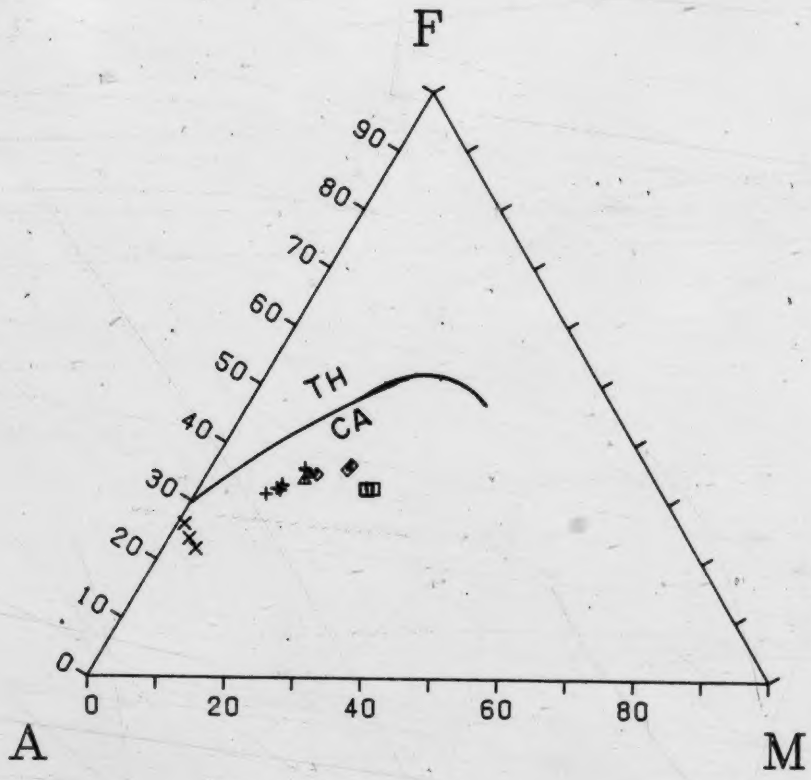

Fig. 6.2. AFM plot for the Bonnington Pluton samples. All the samples show typical calc-alkaline trend.

that all the samples from this pluton are metaluminous in character.

Table 6.1

Sample-Group	SiO_2-Range	Al/NKC*
8022-group	54.59-55.05	0.642-0.672
8021-group	61.44-61.88	0.845-0.849
8067-group	61.04-64.59	0.798-0.854
8068-group	65.13-65.43	0.897-0.915
7075-group	60.77-61.05	0.806-0.935

6.2 Results

6.2.1 Major Elements

Though we are dealing with a SiO_2 interval of only about 6 wt%, distinct variations are seen on the Harker's diagrams. Inter-element relationships seen among the major elements establish 8021- and 8067-groups (to be called main group) as a coherent group. This group intermediate between the low-SiO_2 group of 8075 and high-SiO_2 group of 8068 shows relatively smooth chemical trends. FeO, CaO, MgO, TiO_2 and P_2O_5 (Figs. 6.3a-e) decrease with increasing SiO_2. For this group, Al_2O_3 decreases, K_2O increases, while Na_2O remains almost constant at about 4 wt%. 8075-group differs from the main group in having higher MgO, Na_2O, (Fig. 6.4a) and lower Al_2O_3, K_2O (Fig. 6.4b) contents. Distinct chemical breaks exist between the main group and 8068-group of samples. This higher SiO_2-group(8068) has FeO, MgO and TiO_2 contents plotting below the main trend. Similarly, significantly higher Al_2O_3, Na_2O and Na_2O/K_2O but lower K_2O are also important characteristics of this group.

6.2.2 Trace Elements:

There are no consistent trends among the LIL elements (Rb, Sr and Ba) with respect to SiO_2. The 8068-group though higher in SiO_2 than the main group (8021+8067) has lower Rb(Fig. 6.5a) and higher Sr(Fig. 6.5b) and Ba contents. The main group, however, shows increasing Rb and decreasing Sr and Ba contents with differentiation. K/Rb ratios vary from

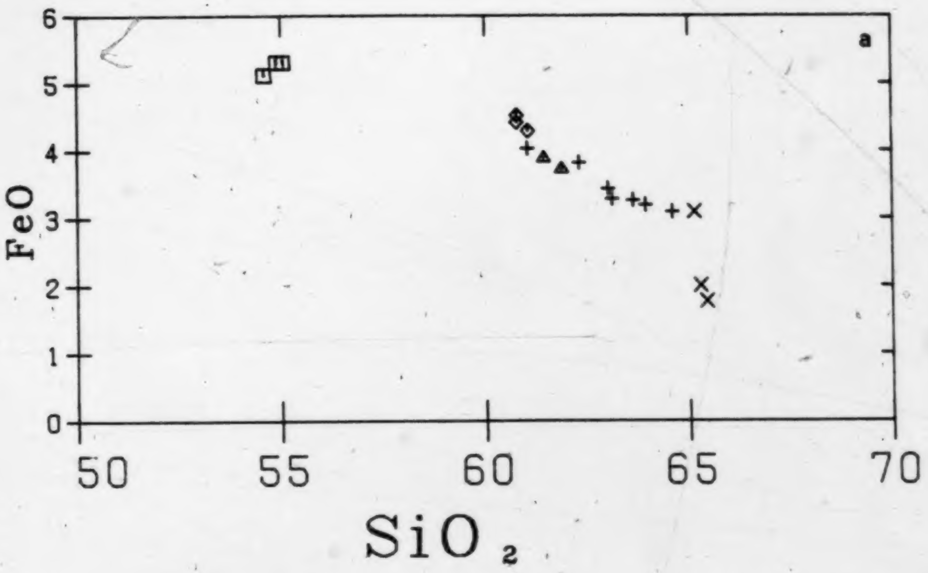

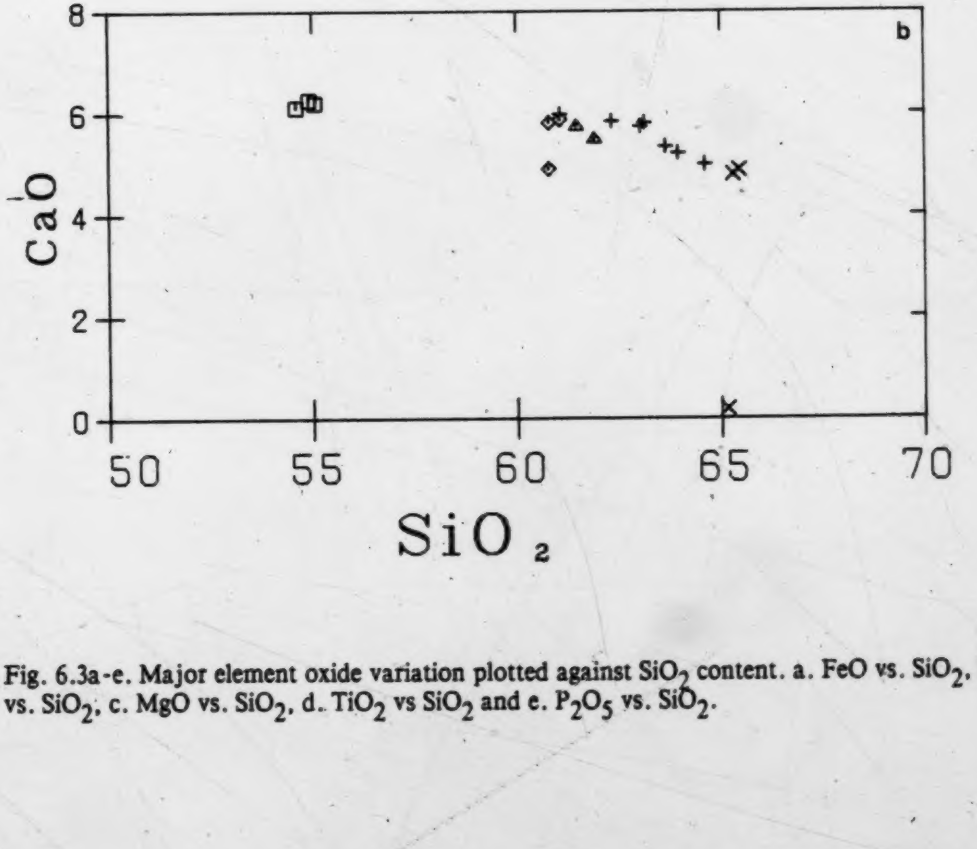

Fig. 6.3a-e. Major element oxide variation plotted against SiO_2 content. a. FeO vs. SiO_2, b. CaO vs. SiO_2, c. MgO vs. SiO_2, d. TiO_2 vs SiO_2 and e. P_2O_5 vs. SiO_2.

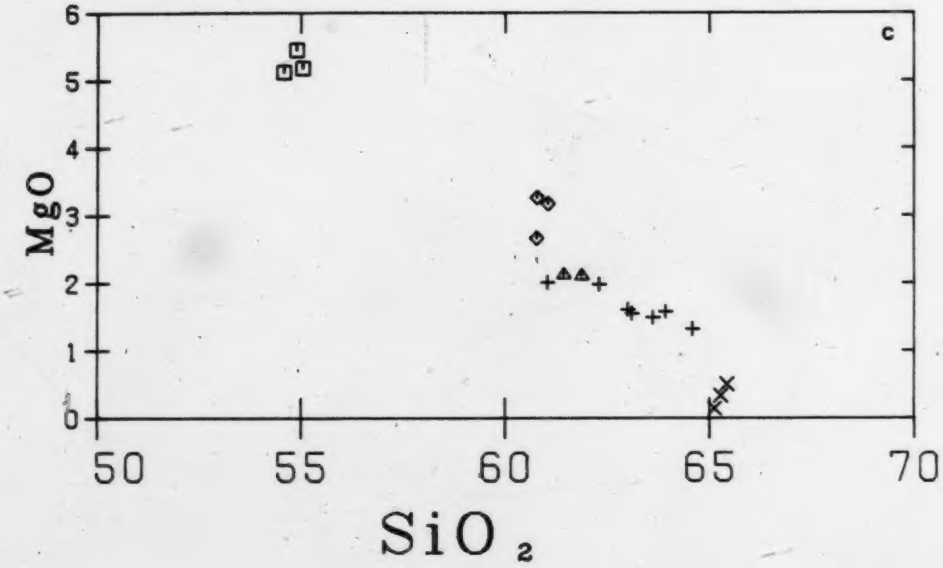
c
MgO
0
1
2
3
4
5
6
50
55
60
65
70
SiO₂

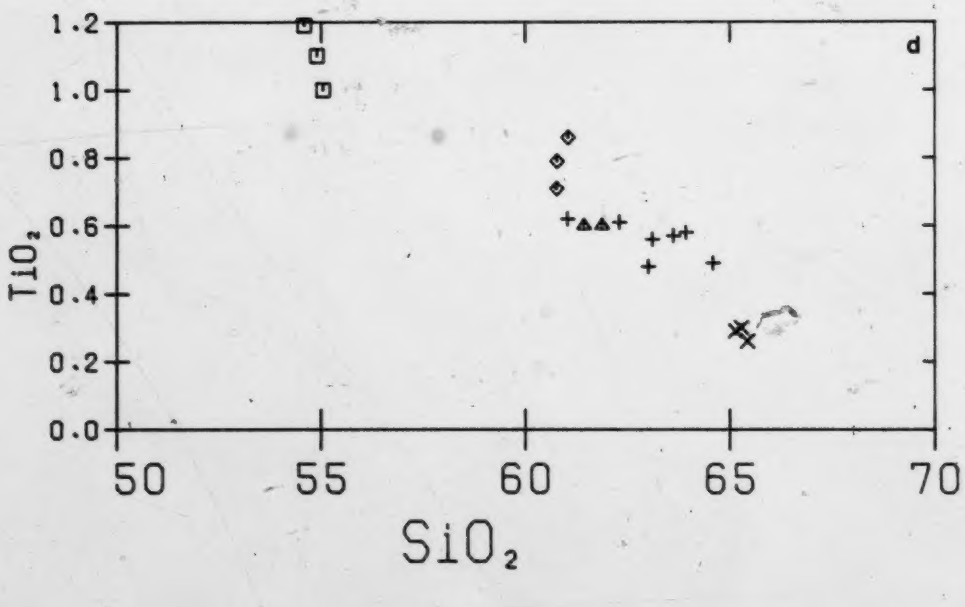
d
TiO₂
0.0
0.2
0.4
0.6
0.8
1.0
1.2
50
55
60
65
70
SiO₂

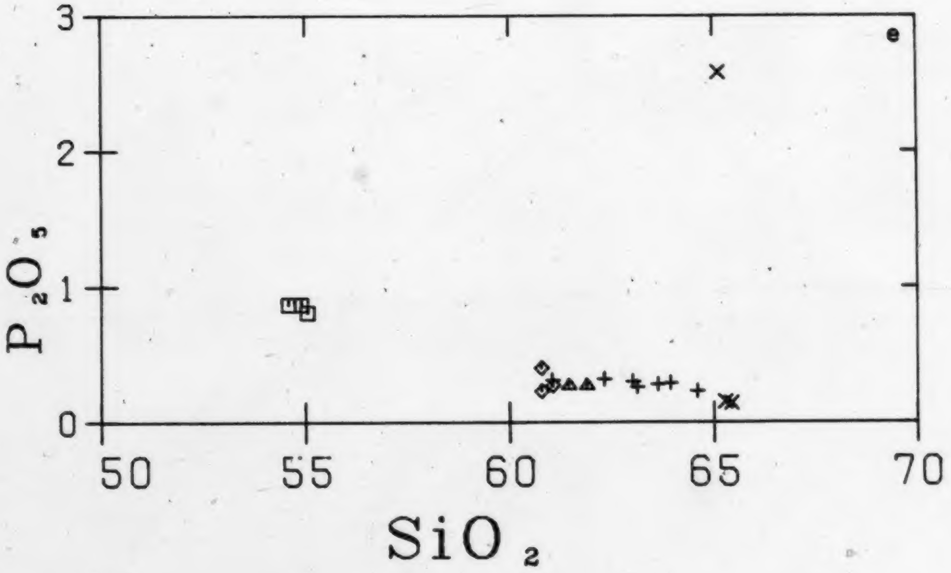
e
3
2
1
0
50
55
60
65
70
P_2O_5
SiO_2

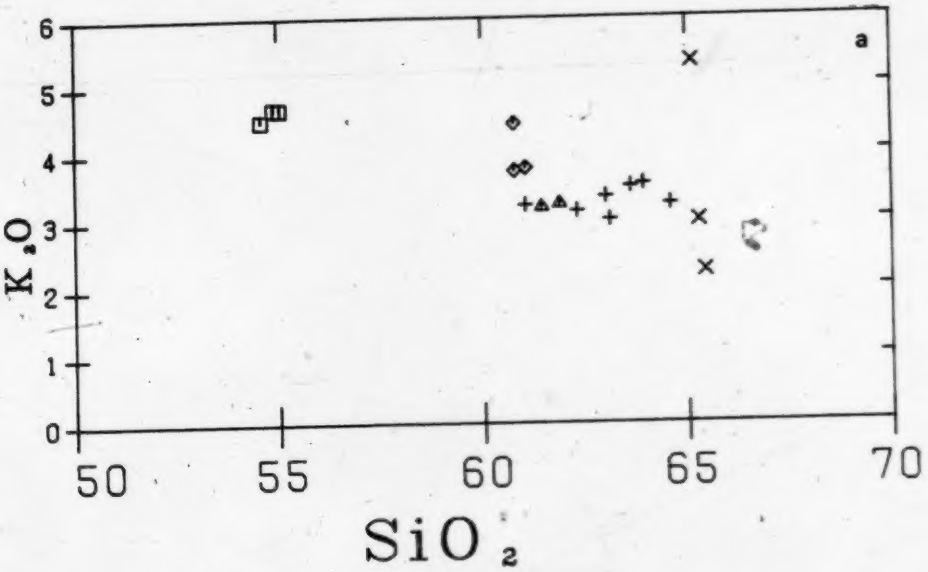

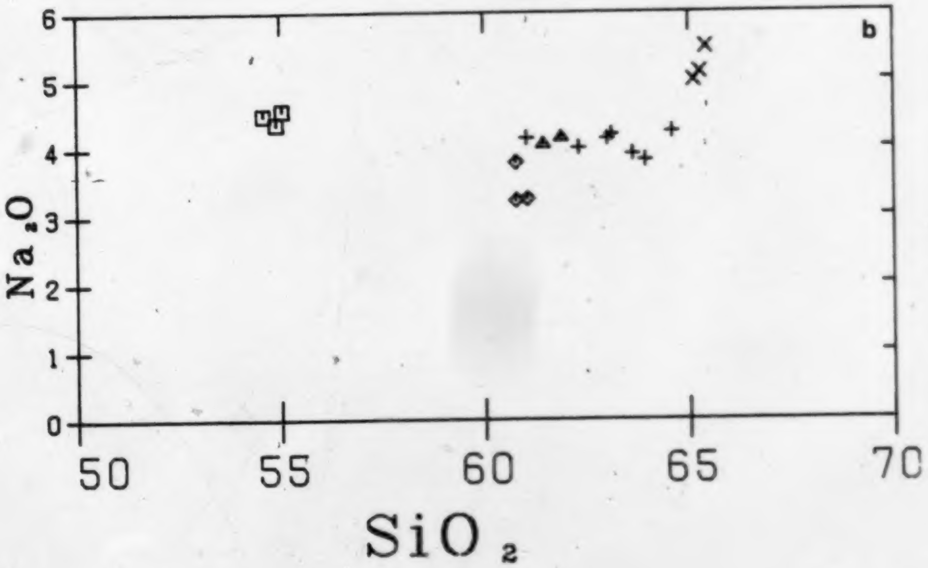

Fig. 6.4a-b. a. K_2O vs. SiO_2 and b. Na_2O vs. SiO_2.

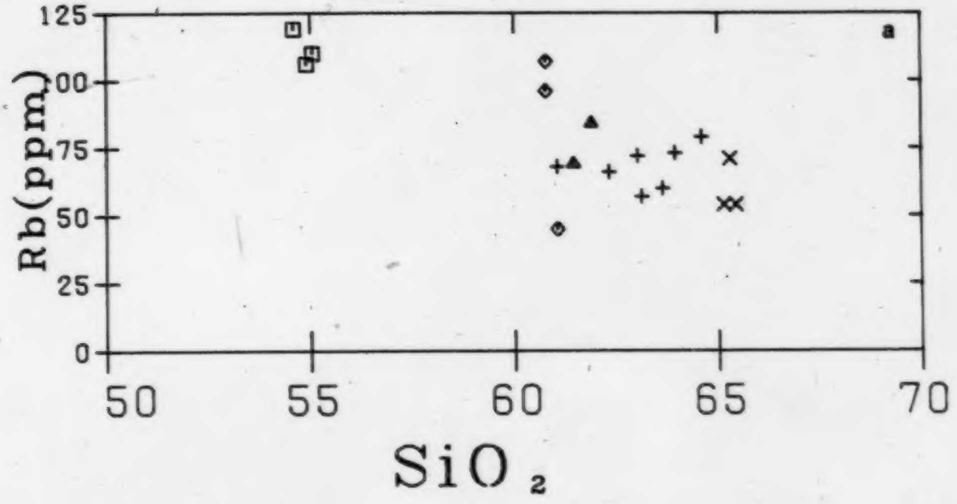

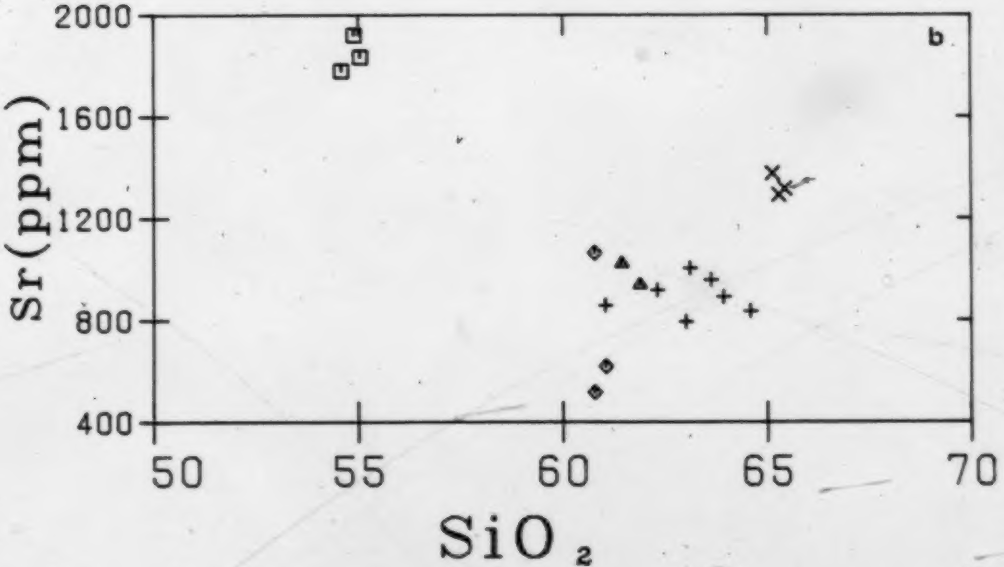

Fig 6.5a-b. a. Rb vs. SiO_2 and b. Sr vs. SiO_2.

about 250 to 500 with 8067-group of samples having highest ratios. For the main group, Rb/Sr, Ba/Sr ratios increase, Ca/Sr ratio decreases while K/Ba remains almost constant (Table A2.2.2, Appendix 2).

No systematic change (Figs. 6.6a and b) is found among the HFS elements (e.g., Zr, Nb), though Zr decreases for the main group, without any relationships to the other groups. On the other hand, Nb contents of the main group remains constant at about 16 ppm. 8068-group has slightly higher Nb contents (=20 ppm) and Zr contents (=100 ppm). Behaviour of Zr and Nb for the Bonnington Pluton is in marked contrast to that of the Nelson Batholith (Chapter 5).

Figs. 6.7a and b show REE behaviour. La varies between 16 to 28 ppm without any definite trend, while Y (equivalent to HREE) decreases for the main group. The 8075-group of samples has highest Y contents.

6.3 Petrogenesis

6.3.1 Introduction

This section deals with the variations in major and trace elements. Lack of smooth chemical trends (unlike NB) suggests a fundamental difference in petrogenesis for the BP particularly with respect to trace element distributions. However, the inter-element chemical trends shown by the Bonnington Pluton samples also correspond to the second stage of the two-stage chemical evolution model proposed for the Nelson Batholith (see Chapter 5). Chapter 7 discusses how AFC processes affected the original magma, assumed to have originated in the mantle. Separate discussion of the petrogenesis for BP is warranted on the basis of field relationships. U-Pb zircon dating (Chapter 3) shows both NB and BP were emplaced at about the same time (=164Ma). Chapter 8 will also show that Pb-isotopic composition of all the BP samples (except 8075-group) is a variable mixture of mantle and lower crustal Pb. Absence of any upper crustal Pb-isotopic signature in BP samples suggests that the second stage evolution is purely chemical. This is not so however for the 8075-group as its Pb-isotopic composition

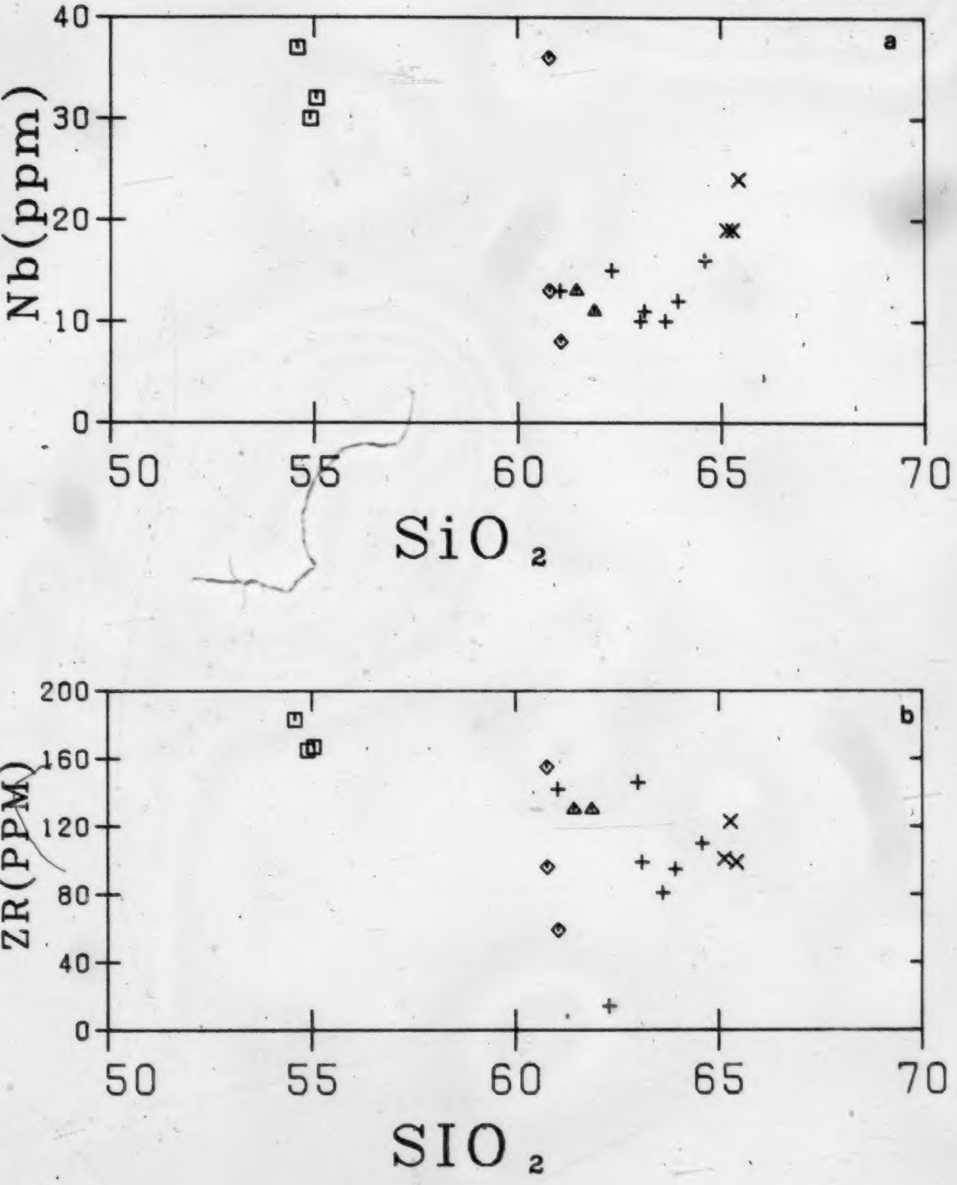

Fig. 6.6a-b. Shows variations in high field strength (HFS) elements with SiO_2. a. Zr and b. Nb.

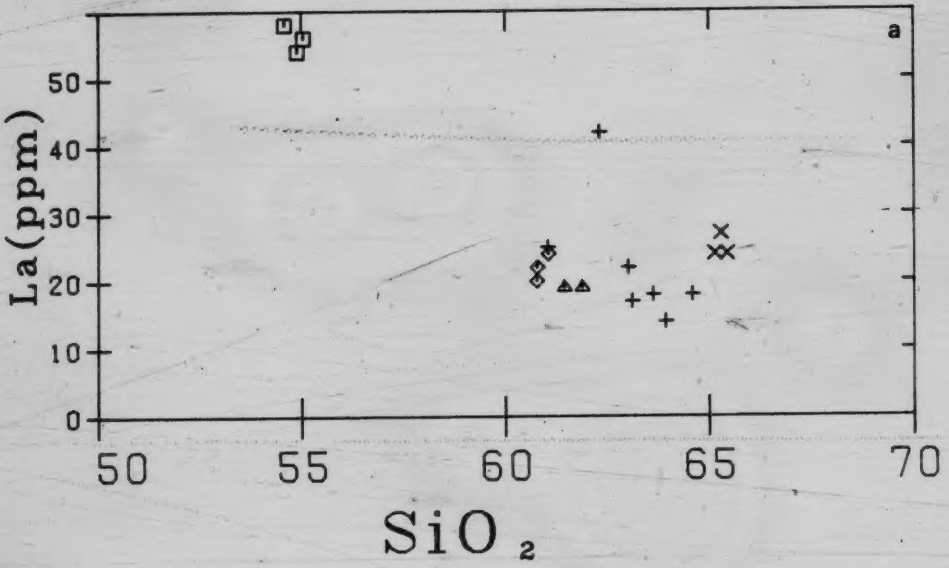

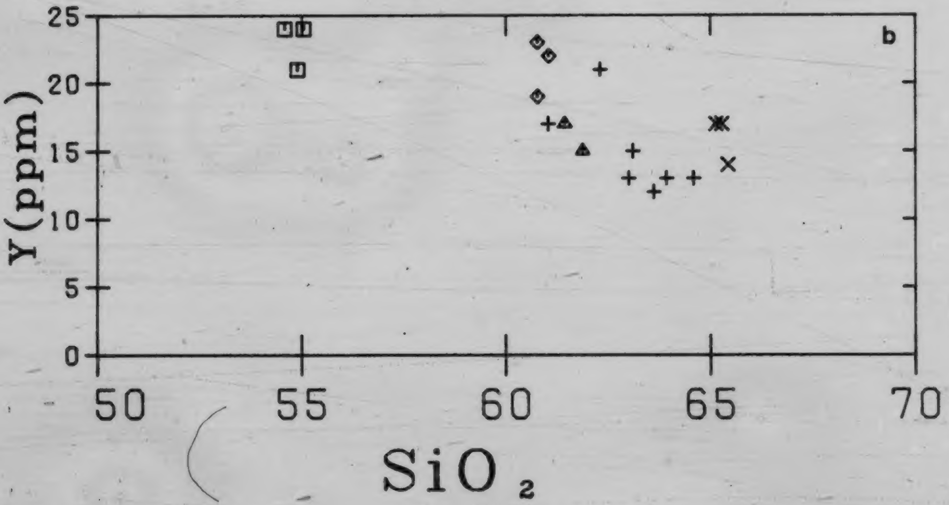

Fig. 6.7a-b. Plot REEs vs. SiO_2. a. La and b. Y.

suggests interaction with the upper crustal sediments. Petrogenesis is discussed first with respact to major elements and then trace elements.

6.3.2 Major Elements:

As 8021 and 8067-groups of samples are hb-bi-granodiorites, continuous decrease in FeO, MgO, TiO_2 and MnO must have been controlled by separation of mafic minerals like biotite and hornblende as was shown for NB. Modal abundances of these minerals decrease with increasing SiO_2. Though the 8075-group plots at the lower SiO_2 end of the main chemical trends, it is not considered to be the parental magma as it will be shown later on while discussing LIL element modelling. Similarly higher SiO_2-group (8068) is dominantly hb-granodiorite (biotite is either absent or present in trace amounts). This explains their lower FeO, MgO and TiO_2 contents than would be expected if they are related to the main group by fractional crystallization. This group has more K-feldspar and is expected to contain more K_2O than the main group if it represents the cumulate products of the magma after K-feldspar has started to crystallize. As was discussed with respact to granitic magma crystallization in the system Qz-Or-Ab-An (see Chapter 5), after K-feldspar begins to crystallize the resultant liquid will be depleted in K_2O, but enriched in Na_2O. This is as seen for this group (8068) with respect to the main group (Figs. 6.4 a and b). However higher modal abundances of K-feldspar and LILE modelling (discussion follows) suggest that 8068-group is not genetically related to the main group either as a fractionated liquid or as the cumulate products.

6.3.3 Trace Elements:

A. Large Ion Lithophile Elements:

Section 5.4.3A of Chapter 5 discussed behaviour of trace elements (in particular LILE) during equilibrium or fractional crystallization. The effects on trace element behaviours due to interaction of intercumulus melt were also discussed. For NB petrogenesis, modal abundances of crystallizing phases were assumed to be constant throughout the crystallization history.

However, in the case of BP, different petrographic units (bi-hb-granodiorite, and hb-granodiorite) require modelling with changing modal abundances of crystallizing phases. This is done to test if the different petrographic units are genetically related either through fractional crystallization or cumulate formation.

Figs. 6.8a and b show only the fractional liquid and solid compositions for two stages of fractional crystallization. During the first stage, the liquid is on the quartz-plagiocalse surface and therefore mainly quartz and plagioclase were crystallizing along with small amounts of biotite and hornblende in the following proportions: quartz=20, K-feldspar=0, plagioclase=50, biotite=15 and hornblende=15 wt%. Initial concentrations of Rb, Sr and Ba in the liquid were taken to be 60, 1000 and 1400 ppm respectively. These concentrations are close to those found in the most basic sample (8067E, with SiO_2=60.77 wt%) of the main group. Sample 8075F with SiO_2=60.77 wt% was not taken as the initial magma composition because of its distant spatial relationship (see sample location map) to the main group. Distribution coefficients for Rb, Sr and Ba are same as those listed in Table 5.2 (Chapter 5).

Fractional crystallization of a magma starting at composition B will produce liquids and solids lying along the vectors BE and AD. Crystallization of quartz, plagioclase, biotite and hornblende was allowed to proceed till 30% (F=0.3) liquid was left (i.e., liquid E and solid D). Tick marks on the vectors BE and AD give % of crystallization at 20% interval. The first solid to form is enriched in Sr and Ba but depleted in Rb while the reverse is true for the liquid. With increasing fractionation both solid and liquid will however be enriched in Rb but depleted in both Sr and Ba. This is so because solid consisting of qz+plag+bi+hb in the proportions mentioned above has effective distribution coeffitients for Rb <1 and Sr and Ba >1. At 70% crystallization (i.e., F=0.3) modal abundances of crystallizing minerals will change, due to incoming of K-feldspar as a major mineral. The new assemblage consists of the minerals in the following proportions: quartz=40%, K-feldspar=40%, plagioclase=30%, biotite=5% and hornblende=5%. These mineral proportions are similar to those of 8068-group except biotite whose percentage is much lower than that assumed above. Crystallization of these minerals from the new liquid at E will push the liquid composition along the vector EF of different

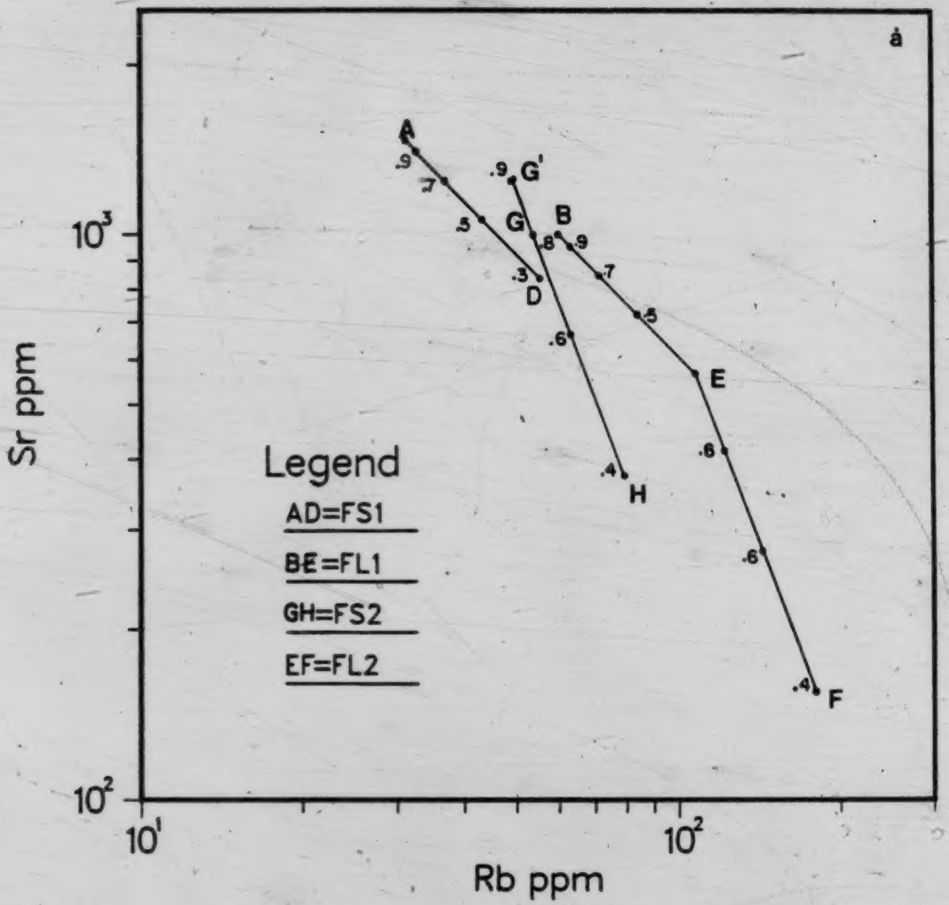

Fig 6.8a-b. Effects of fractional crystallisation on Rb, Sr and Ba contents of a granitic melts. From the initial melt composition at B, the following mineral assemblage (Qz=20%, Kf=0%, Plag=50%, bi=15% and hb=15%) is removed, causing the liquid to move towards E, The composition of the solid phase lies along AD. At E, which represents 70% crystallisation of melt B, K-feldspar starts crystallising, changing the liquidus mineralogy to Qz=20%, Kf=40%, Plag=30%, Bi=5% and Hb=5%. The new liquid composition now changes towards F and the fractionally separated solid composition changes along GH. Solid formed at 10% crystallisation (i.e., F=0.9) is also shown at G' for Sr-Ba model. Crystallisation of the liquid is arbitrarily stopped at 60% crystallisation. It is important to note that there is compositional gap in the fractional solids unlike the liquid which is continuous but with a inflexion at E. a. Rb-Sr and b. Rb-Ba.

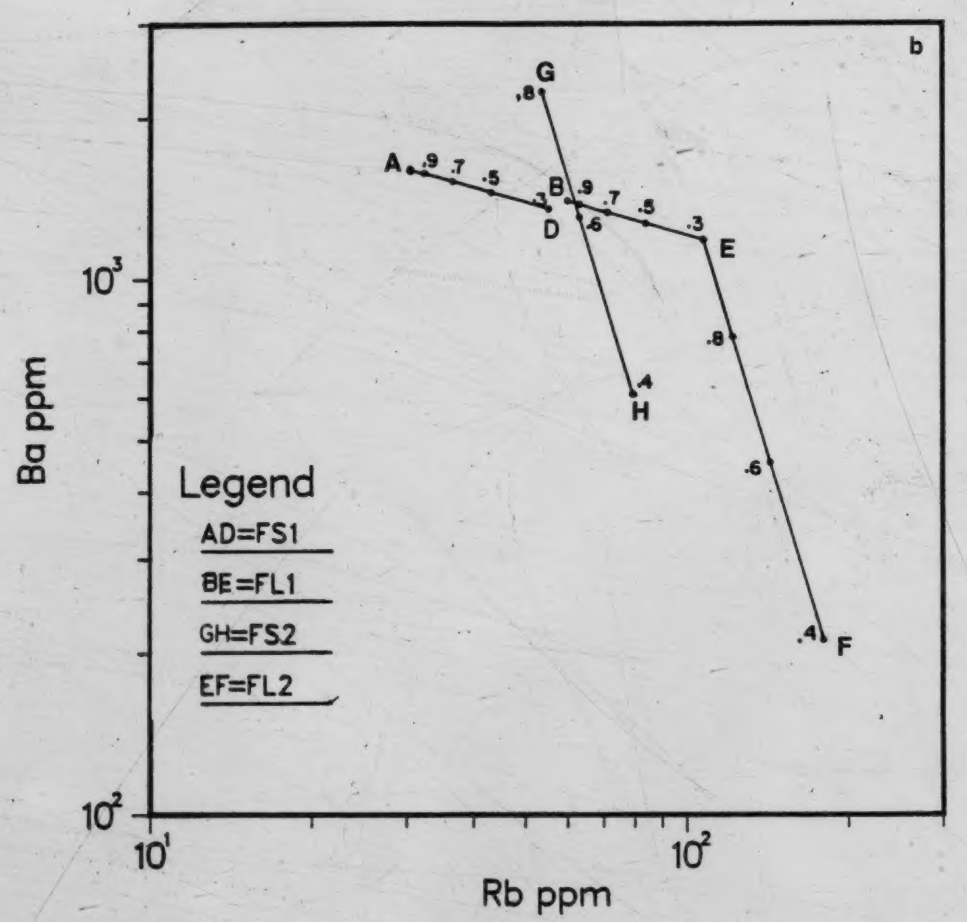
b
G
.8
A
.9
.7
.5
.3
B
.9
.7
.5
.3
D
.6
E
.8
.4
H
.6
.4
F
Ba ppm
10³
10²
10¹
10²
Rb ppm
Legend
AD=FS1
BE=FL1
GH=FS2
EF=FL2

slope. Correspondingly the solid composition will change along GH. Crystallization of this new liquid is arbitrarily stopped after 60% (i.e., F=0.4) crystallization. The model predicts a distinct compositional hiatus for the solid at the point where K-feldspar becomes a liquidus phase. Therefore solid compositions are discontinuous (AD and GH), while the liquid compositions form a continuous trend (BEF) but with inflexion at E indicating a major change in the liquidus mineralogy. Important points to note are that the initial solid formed from the second liquid (i.e., E) will have more Sr and Ba than the original liquid at B. This is more pronounced for Ba than Sr. In the Sr-Rb model (Fig. 6.8b) solid formed at only 10% crystallization of liquid E is also shown. Therefore cumulate composition due to the second liquid will overlap that of the first liquid. Such relationships were actually observed for the Blue Tier Batholith (McCarthy and Groves, 1979).

Figures 6.9a and b show the relationships of modelled variations in solid and liquid to the analysed data from BP. It was argued in Chapter 5 that separation of cumulates from the melt is generally not very effective in the case of a granitic magma particularly at high SiO_2 levels. At first, this does not appear to be so for the 8067-group of samples as they plot slightly above (Ba-Rb diagram) or along (Sr-Rb diagram) the fractional liquid trend BE due to qz+plag+bi+hb fractionation. However slight scatter above or along the liquid trend BE suggests these samples do not represent pure liquid compositions. Samples 8021A and B, having similar SiO_2 as that of 8067E, have much higher Sr and Ba contents than that predicted by the liquid trend. This deviation might be related to incorrect assumption of the initial magma composition or crystallizing mineral assemblage. For example, by changing proportions of crystallizing minerals it is possible to have liquid compositions depleting in Sr but enriching in Ba (McCarthy and Robb, 1978). In the present case, samples having higher Sr and Ba contents than the predicted liquid could be produced if the liquid (after some degree of fractional crystallization e.g., at F=0.5) interacts with the solid produced due to change in the liquidus mineralogy (i.e., after K-feldspar becomes an important liquidus phase). Difficulty arises in such an interpretation as the SiO_2 contents of such products will be higher than those of 8021A and B. Therefore it is suggested here that even samples 8021A and B might represent a different

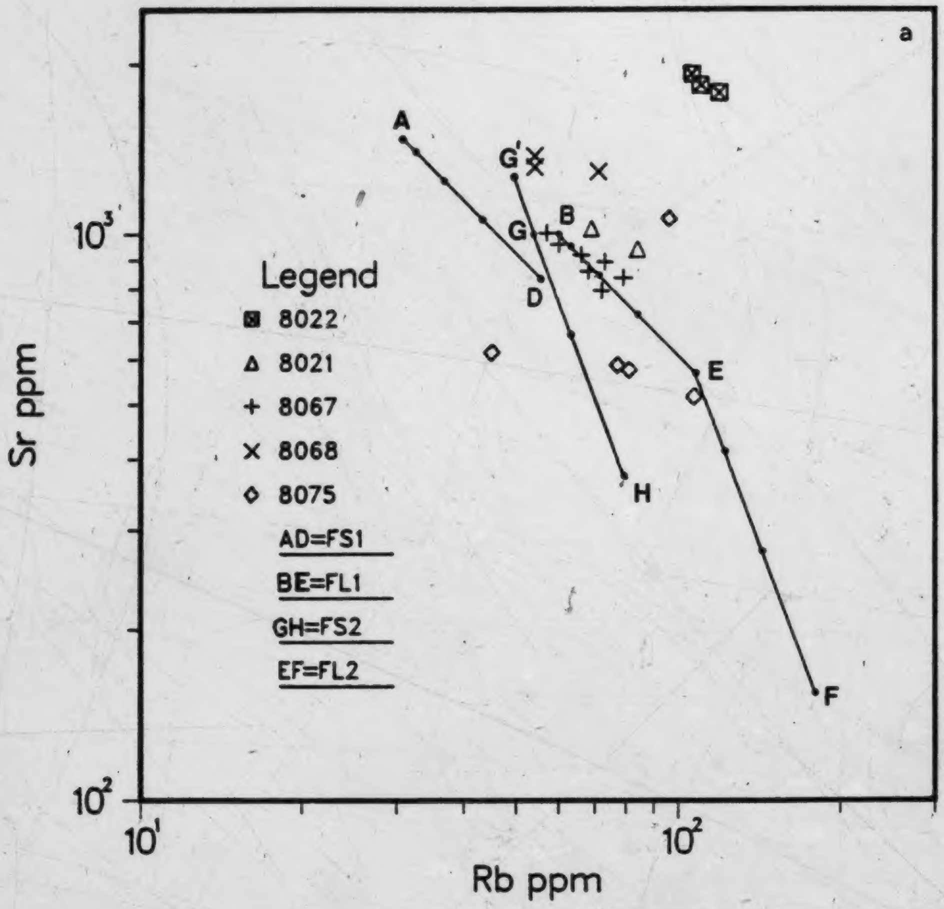

Fig. 6.9a-b. Calculated fractionation curves for melt and solid superimposed on the analysed data of the Bonnington Pluton. (See text for discussion). a. Rb-Sr and b. Rb-Ba.

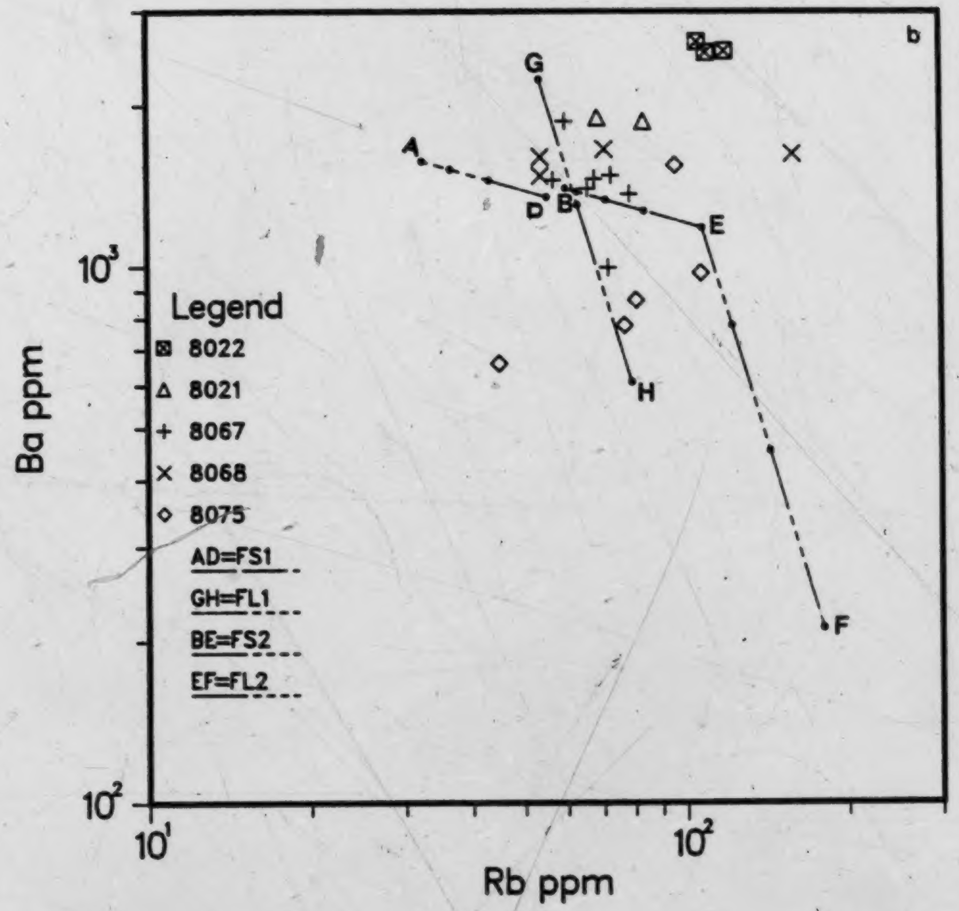
b
G
A
D
B
E
H
F
Legend
⊠ 8022
△ 8021
+ 8067
× 8068
◇ 8075
AD=FS1
GH=FL1
BE=FS2
EF=FL2
Ba ppm
10^3
10^2
Rb ppm
10^1
10^2

magma than that responsible for 8067-group, though they appear to be genetically related on the basis of major element correlations.

Close similarity between the modelled second stage solid (GH) and 8068-group suggests they could be early cumulate products of the liquid E after K-feldspar became the liquidus phase. However, this is difficult to reconcile with the observation made from major elements (particularly with respect to alkalies). For the 8068-group of samples to be cumulate products of such liquid as E, they should have higher K_2O and similar to or lower Na_2O contents than the sample with highest SiO_2(8067C) in the 8067-group i.e., at 64.59wt%. As discussed before, 8068-group of samples has lower K_2O and higher Na_2O contents than 8067C. Therefore for this group (8068) major elements and LILE controlled by major minerals show conflicting relationships. While LILE modelling suggests they could be cumulate products, major elements (alkalies) suggest they are liquids, because at the point when K-feldspar appears on the liquidus, the liquid will be depleted in K_2O but enriched in Na_2O.

Similarly low SiO_2 contents and wide LILE distributions for 8075-group suggest they are not also related in any way to the initial magma assumed for 8067-group. This is also supported by their spatial relations to the other groups.

Therefore it may be argued that apparently independent behaviour of different groups of samples on the basis of both major elements trends and LILE modelling is suggestive of different chemical patterns of successively more evolved liquid compositions. This alternative interpretation requires that the different groups are the results of an equilibrium mode of crystallization. In such a case the parental magma composition controlled the final trace element patterns instead of being controlled by in-situ processes. Magma undergoing equilibrium crystallization results in solid having identical composition to its parental liquid. If it is valid for BP samples, it requires that each group represents a separate, chemically isolated magma. Distinctly different mineralogies, texture and major and LIL elements distributions for 8021-, 8068- and 8075-groups tend to support such a view. For 8067-group, in-situ fractional crystallization was however the dominant process.

B. Ti, P, Zr, Nb and REE

It was discussed in Chapter 5 that the above trace elements (except Ti) are mostly concentrated in accessory mineral phases e.g., sphene, apatite, zircon, allanite, monazite and xenotime. Whereas it was found that the NB granodiorite samples had significant amounts of trace minerals like sphene, apatite, zircon and few crystals of allanite, they are not found in abundance in the BP samples. Granodiorites from 8021- and 8067-groups have trace amounts of only zircon and apatite. Sphene is even less abundant, whereas allanite was not detected at all. Therefore unlike NB, these accessory minerals did not play an important role in controlling the abundances of the above elements. Slight decrease in P (by only about 0.1 wt%) is due to apatite fractionation. Increase in Zr for 8067-group (Fig. 6.6a) suggests absence of zircon fractionation. Nb remains almost constant suggesting sphene or ilmenite fractionation did not occur in significant amount.

Lower Ti and P contents in 8068-group are probably due to absence of biotite and lower modal abundance of apatite. For this group Zr contents fall within the range of that of 8067-group and Nb abundance is slightly higher. Absolute contents of these trace elements are related to the modal abundances of the accessory phases. Therefore lack of any systematic relationships with respect to these trace elements supports the conclusions drawn before that different groups of BP samples are not related to each other by in-situ fractional crystallization process.

REE abundances are distinct for different groups (Figs. 6.7a and b). La contents do not exhibit much inter-group variation. Y decreases for 8067-group suggesting some hornblende fractionation, while other groups have Y contents unrelated to 8067-group.

Scattered and apparently unrelated behaviours of trace elements for different groups of BP are in marked contrast to those observed in NB. Also absolute modal abundances of accessory minerals in BP relative to NB indicate different P-T-X conditions of crystallization for the Bonnington Pluton.

7. Nd-Sr ISOTOPE GEOCHEMISTRY OF GRANITIC ROCKS

7.1 Introduction

Granitic rocks are essential constituents of the upper crust throughout the geological time. It is generally accepted that average composition of the upper crust is granodioritic (Taylor and White, 1965; Taylor, 1977), though there is considerable disagreement regarding the chemical nature of the lower crust (Tarney and Windley, 1979; Taylor and McLennan, 1979; Kay and Kay, 1980). A proper understanding of the crustal evolution is heavily dependent upon the recognition of the source material of granitic rocks and their subsequent chemical and isotopic evolution. This understanding is essential to develop any geologically feasible crustal evolution model. Models of crustal evolution range from a continuous growth of continental crust throughout the geological time (Hurley et al., 1962; DePaolo, 1979, 1980; O'Nions et al., 1979; Jacobsen and Wasserburg, 1979) to a single stage episodic growth during Archean-Proterozoic time followed by recyling (Armstrong, 1968; Armstrong and Hein, 1973; Armstrong, 1981). Petrological, chemical and isotopic studies of the Phanerozoic voluminous granitoid batholiths found in linear plutonic belts point to the fact that development of continental crust is a continuous process and is intimately related to the subduction of oceanic lithosphere, a process responsible for development of the oceanic and continental margin island arcs and also continental margin magmatic arcs (Ringwood, 1975, 1982). But the processes of initial magma generation to final crustal accretion are very complex and therefore our understanding of crustal evolution is far from correct.

Post-Archean crustal evolution has been understood to a great extent through detailed isotopic studies of the granitic rocks exposed along the western margin of the North American Cordillera, the Andes, the French Hercynian and the Japanese tectonic belts. A reconnaisance isotopic study of the granites in the above tectonic belts by Allègre and Ben Othman (1980) indicated contributions from older continental crustal components.

As the batholiths represent deeper levels of erosion of mature island arcs, both oceanic and continental, (Dickinson, 1970) they should be the final products of the continental accretion processes. In most island arc related magmatism, the dominant calc-alkaline plutonic rock series is genetically related to the volcanic rock series. This observation is mostly substantiated on the basis of extensive isotopic studies. Petrological and mineralogical differences are assigned mostly to the complex P-T-X conditions of crystallization. Generalised models often invoke generation of basaltic magmas through partial melting of mantle sources. Subsequent evolution is likewise more complex and involves a multitude of processes. An increasing body of isotopic data indicates complex crustal contamination of original basaltic magma to produce the gabbro-diorite-tonalite-granodiorite-granite plutonic associations or the equivalent volcanic associations. Such models suggest a continental growth via marginal accretion of volcano-plutonic terrains continued thoughout the Phanerozoic.

Such continental margin accretion may also involve the sedimentary appron surrounding the continent and sometimes overlying the crystalline basement. Consequently newly added crust may represent reconstituted older crustal material (Wyllie, 1983; Allègre and Ben Othman, 1980; DePaolo, 1981a). Fortunately combined study of Nd, Sr, Pb and O isotopes is helpful in distingushing presence of and estimating the amount of relative mantle and crustal material (Allègre and Ben Othman, 1980; Hamilton et al., 1980; DePaolo, 1980, 1981a; Farmer and DePaolo, 1983, 1984; James, 1982). This has been possible due to the fact that isotopic characters of both mantle and different crustal segments are quite distinct and relatively well established. Primitive island-arc magmas have low ϵ_{Sr} (= -20.0, or $^{87}Sr/^{86}Sr$ = 0.7033) and high ϵ_{Nd} (= +8.0) while crustal rocks have high ϵ_{Sr} (LC: +28 to 60, UC: 80 to >400) but low negative ϵ_{Nd} (-10.0 to -30.0). Variations in ϵ_{Sr} in crustal rocks depend on both Rb/Sr ratios and age, while those in ϵ_{Nd} effectively depend only on age, as fractionation in Sm/Nd ratios is almost independent of crustal depth.

This overall contrast in Nd and Sr isotopic compositions between the continental crust and mantle magma sources provides valuable framework for studying relative importance of crustal contamination processes (DePaolo, 1981a).

The present isotopic study (Nd, Sr, Pb) of the volcanic, plutonic and metasedimentary rocks in southeastern British Columbia has been initiated to evaluate extent of crust-mantle interaction in the generation of the plutonic batholiths, their ages and structure and evolution of the crust. Better insight into the above aspects will eventually help clarify the petrogenesis of these large volumes of granitic rocks, chemical composition of the continental crust, and the structure and evolution of the mantle.

7.2 Previous Work

No systematic geochemical study has been done on the plutonic and sedimentary rocks in southeastern B.C.. The largest volcanic group in the area, the Rossland Volcanic Group, has been studied in detail with respect to petrology, major and trace element geochemistry (Beddoe-Stephens, 1979; Beddoe-Stephens and Lambert, 1981; Beddoe-Stephens, 1982). Limited Sr- and mineral O-isotopic study of these volcanics show that the source magma originated in the mantle and formed in Mesozoic island-arc settings.

Several geochronological studies have been completed to establish ages of crystallization of the different batholiths/plutons in this area (Nguyen et al., 1968; Baadsgaard et al., 1961; Duncan and Parrish, 1979; Duncan et. al., 1979; Archibald et al., 1983, 1984). These studies include mostly K-Ar mineral dates (having a large range) and recent zircon dates (Archibald et al. 1983, 1984 and the present study). Extensive Sr-isotopic study of granitic rocks all across the Canadian Cordillera (for data compilation, see Le Couteur and Templeman-Kluit, 1976) established the strong geographic variations in $^{87}Sr/^{86}Sr$ conforming to the paleogeographic boundaries. Similar geographic variations have been noted along the U. S. Cordillera (Armstrong et al., 1977; Kistler and Peterman, 1973, 1978) and recently modified by Farmer and DePaolo (1983, 1984). An arbitrary boundary ($^{87}Sr/^{86}Sr=0.7060$, i.e., $\epsilon_{Sr}=17.0$) has been chosen to infer regions underlain by Precambrian basement (with higher $\epsilon_{Sr}>17.0$) and regions underlain by oceanic crust (with lower $\epsilon_{Sr}<17.0$) crust. This boundary line lies west of the present study area. Le Couteur and Tempelman-Kluit (1976) have shown a regular increase in $^{87}Sr/^{86}Sr$ from 0.7028 (west) to 0.709 (east). The present study does not support this general regular variation.

7.3 Isotopic Models

Isotopes (Sr, Nd and Pb) are powerful geochemical tracers in deciphering chemical characteristics of the source materials and subsequent evolution. As the systematics of Nd and Sr isotopic variations in the crustal and mantle rocks are well known, isotopic modelling using different pairs of isotopes have been developed to answer some of the questions posed above. Fig. 7.1 shows such isotopic systematics of mantle and crust of different ages. It is commonly found that the average ϵ_{Nd} value of island arc magmas is 8±2 (Hawkesworth, 1979, 1982; DePaolo and Wasserburg, 1976). From Fig. 7.1, it is seen that old crustal rocks have large range of ϵ_{Nd} (from -10 to -30) and ϵ_{Sr} (-40 to >400). Very low ϵ_{Sr} values are found in high grade (granulite facies) metamorphic rocks. Lower crust is depleted in incompatible elements like Rb, U, K compared to the upper crust (Heier, 1973). This type of chemical stratification of the crust is generally accepted today. This pattern is shown by the 1.8 Ga old Colorado Front Range Basement (DePaolo, 1981b) and the 2.9 Ga old Lewisian Gneisses (O'Nions, 1979). Upper crustal sedimentary rocks have high Rb/Sr ratios and therefore high ϵ_{Sr} values (Fig. 7.1). Initial isotopic ratios falling in intermediate positions in an isotope vs. isotope diagram could be simply explained as variable mixtures of end-member components or in extreme cases each sample was derived from a distinct source. The latter is very unlikely as the degree of variations in isotopic compositions exceeds known heterogeneity in the mantle. Alternative explanations of simple or complex mixing are therefore more probable. First, simple binary mixing results will be discussed and then complex mixing processes (Assimilation Fractional Crystallization, AFC model of DePaolo, 1981c) will be discussed.

Mixing could occur in different ways:

1. mixing in the source regions before melting
2. mixing of magmas produced from two different sources
3. mixing of parental magmas (mantle-derived) with wall-rocks (bulk-assimilation) and
4. any combination of the above.

On the basis of isotopes, it is not always possible to distinguish the processes from one another, but it is certainly possible to sort out the processes if detailed isotopic study of all rock types

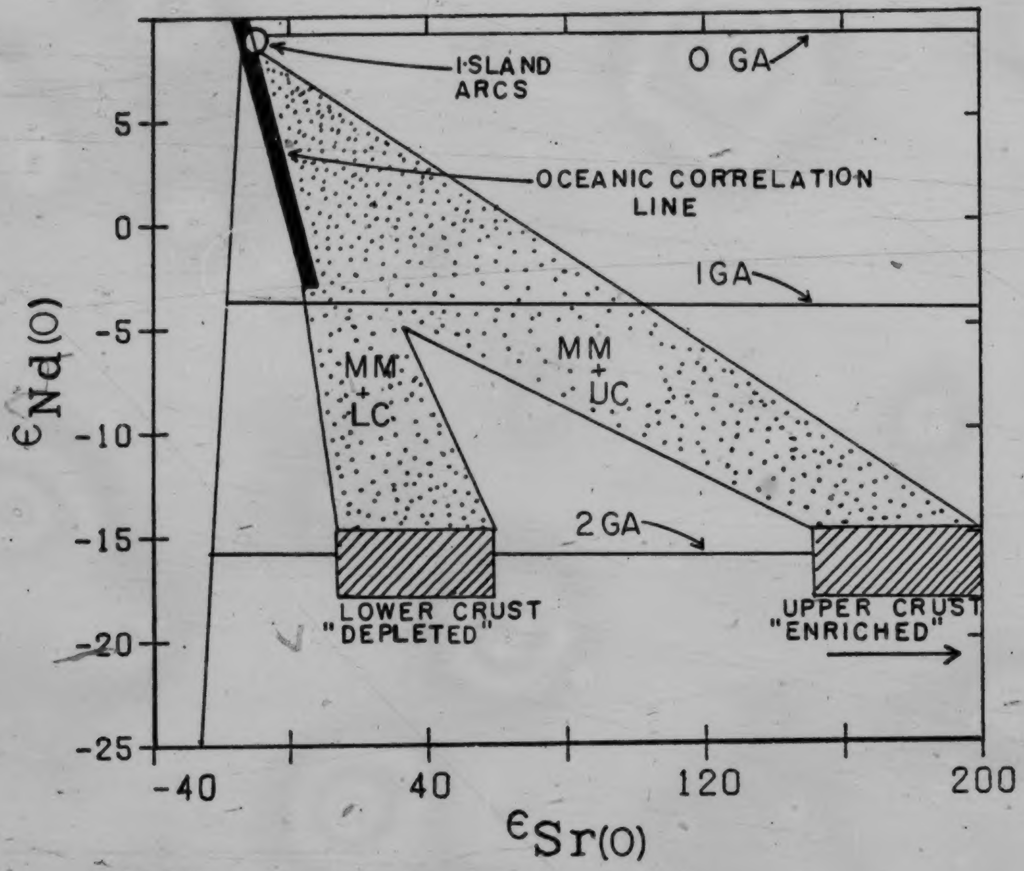

Fig. 7.1 Shows present day $\epsilon_{Sr}(0)$ and $\epsilon_{Nd}(0)$ values for mantle-derived rocks (Mantle Array) and the crust. With increasing age, ϵ_{Nd} values in crust decreases as Sm/Nd is almost constant for both the lower and upper crusts. While ϵ_{Sr} increases differently for the two crustal segments depending on Rb/Sr ratios. In general highly metamorphosed lower crust (granulite facies) is Rb depleted and weakly metamorphosed or unmetamorphosed upper crust is Rb enriched. Rocks produced by mixing mantle magmas and different types of crusts plot in the fields marked MM+LC/UC. Generalised time divisions (horizontal lines) taken from DePaolo, 1981a).

likely to influence the magma character is available. The present study spreads over all possible rock types in the area and therefore it is possible to develop a comprehensive model.

7.4 Results

Isotopic and selected trace element (Sr and Nd) data for the granitic batholiths and sediments are summarised in Tables 7.1, 7.2, 7.3 and 7.4. $\epsilon_{Sr(0)}$ and $\epsilon_{Nd}(0)$ refer to measured isotopic compositions of Sr and Nd (normalised to a model chondritic reservoir (CHUR) for Nd and to a model whole earth uniform reservoir (UR) for Sr. $\epsilon_{Sr}(T)$ and $\epsilon_{Nd}(T)$ refer to initial isotopic compositions. For sedimentary rocks, ϵ_{Sr} and ϵ_{Nd} values at 164 Ma are only shown. Though the ages of emplacement of the batholiths/plutons vary from mid-Jurassic (164 Ma) to Tertiary (51 Ma), for sediments $\epsilon_{Sr}(T)$ and $\epsilon_{Nd}(T)$ values have been calculated only at 164 Ma for comparision with corresponding values of the granitic samples.

7.4.1 Volcanic Rocks

Irene Volcanic(IV), Kaslo and Rossland Volcanic(RV) Groups represent the volcanic or basic rock-types in the study area. Two samples from RV, one each from IV and Kaslo have been analysed for Sr and ~~Nd~~-isotopic compositions. All have positive $\epsilon_{Nd}(T)$ values unlike the granitic rocks. One sample from RV (74/054) has the highest $\epsilon_{Nd}(T)$ value (+6.5), very close to the average island arc magmas (+8). Unlike $\epsilon_{Nd}(T)$, $\epsilon_{Sr}(T)$ values vary significantly.

7.4.2 Nelson Batholith(NB)

The Nelson Batholith is most voluminous in the study area, and displays wide variations in both Sr and Nd isotopic compositions. $\epsilon_{Nd}(T)$ ranges from -2.8(8057B) to -8.8(8012B) and $\epsilon_{Sr}(T)$ ranges from -13.8 (8052A) to 55.4 (8061A). Here the most basic sample 8052A (SiO_2=51.72 wt%) does not have highest $\epsilon_{Nd}(T)$ but has lowest $\epsilon_{Sr}(T)$ (see Table 7.3). It has lowest Pb isotopic composition which is very similar to the probable mantle value (Table 8.1, Chapter 8). Therefore it is clear that different isotopes apparently exhibit dissimilar proportions of contamination. The sample 8057B having highest $\epsilon_{Nd}(T)$=-2.8 is a porphyritic bi-hb

Table 7.1 Selected trace elements and their ratios.

Sample	Rb	Sr	Sm	Nd	87Rb/86Sr	147Sm/144Nd	Sr/Nd
8049A	168.16	1246.85	9.15	11.71	0.3900	0.4897	99.00
8052A	72.80	1123.67	3.54	15.80	0.1873	0.1344	71.00
8053A	133.13	1099.41	3.24	17.94	0.3503	0.1084	61.28
8057B	89.73	1065.94	6.12	38.99	0.2434	0.0938	27.33
8059A	107.00	919.49	6.74	37.43	0.3366	0.1116	24.56
8061A	122.39	573.76	5.67	27.47	0.6173	0.1234	20.88
SB29.7	124.00	1369.57	4.79	28.01	0.2618	0.1022	48.11
8012B	121.42	533.55	5.15	30.32	0.6587	0.1017	17.59
8021B	83.95	939.62	3.77	19.84	0.2584	0.1138	47.35
8021D	214.00	386.75	2.75	14.72	1.6069	0.1117	26.27
8022A	119.14	1780.10	10.12	62.43	0.1941	0.0975	28.51
8075F	116.90	1064.64	5.75	31.72	0.3177	0.1084	33.56
8033G	93.00	1649.56	3.93	22.27	0.1631	0.1056	74.07
8033P	84.00	1305.82	2.72	16.22	0.1860	0.1003	80.50
8038E	139.00	634.56	8.69	46.44	0.6336	0.1119	13.66
8038D	142.99	671.46	5.95	38.38	0.6161	0.0928	17.49
8038A	154.65	517.33	5.00	30.00	0.8650	0.1000	17.24
8096E	73.78	722.21	5.78	32.81	0.2955	0.1054	22.01
8072A	120.01	740.99	3.63	19.75	0.4685	0.1099	37.51
8073A	80.45	762.98	2.02	19.58	0.3050	0.0616	38.96
8070C	132.17	1160.36	5.00	30.28	0.3294	0.0987	38.32
8064E	152.64	833.15	8.26	64.17	0.5301	0.0770	12.98
8007A	99.84	376.76	2.37	13.33	0.7667	0.1065	28.26
8065A	128.52	1423.15	7.00	37.65	0.2612	0.1119	37.79
8088C	244.76	643.42	3.18	18.13	1.1007	0.1050	35.48
74/054	24.00	515.86	2.87	10.36	0.1345	0.1658	49.79
75/116	63.00	774.02	3.10	12.29	0.2353	0.1510	62.97

Table 7.2 Selected trace elements and their ratios for sedimentary rocks.

Sample	Formn	Rb(ppm)	Sr(ppm)	Sm(ppm)	Nd(ppm)	$^{87}Rb/^{86}Sr$	$^{147}Sm/^{144}Nd$	Sr/Nd
8001D	ALD	101.5	94.35	9.05	46.44	3.1370	0.1166	1.44
8094A	HORS	141.17	62.04	3.96	21.17	6.6634	0.1120	2.93
8090A	HAM	185.44	330.0	17.03	89.60	0.0676	0.1136	3.68
8037D	LARD	127.00	146.36	ND	ND	2.5204	(0.1120)*	
8084A	LAIB	93.74	81.00	3.70	20.81	0.2978	0.1065	3.89
8010S	NEL	44.71	825.88	1.85	11.00	0.1567	0.1006	75.08
8009D	ACT	58.59	323.76	3.36	16.50	0.5241	0.1220	19.62
8003C	MIL	144.49	140.50	11.00	58.33	2.979	0.1200	2.408
8027C	MIL	129.96	639.49	1.34	6.93	0.5910	0.1158	91.84
8006G	YMR	72.81	530.77	6.00	33.18	0.3969	0.1139	15.99
8035A	SLCN	41.22	556.75	2.94	14.34	0.2142	0.1229	38.3

ND=Not determined, *Assumed.

Table 7.3 Isotopic data and model ages (in Ga)

Sample	T(Ga)	f(Rb/Sr)	f(Sm/Nd)	(87Sr/86Sr)m	(143Nd/144Nd)m	Sr(O)	Nd(O)	Sr(T)	Nd(T)	T(Sr)x	T(Nd)x
Granitic Rocks:-											
8012B	0.164	6.57	-0.48	0.709270	0.512066	63.7	-10.8	44.8	-8.8	0.71	1.31
SB29.7	0.164	2.01	-0.48	0.707004	0.512205	31.6	-8.1	25.8	-6.1	1.29	1.12
8049A	0.063*	3.48	1.49	0.705023	0.512705	3.4	1.7	-0.4	-0.7	0.38	
8052A	0.164	1.15	-0.32	0.704040	0.512348	-10.5	-5.3	-13.8	-4.0	0.45	1.30
8053A	0.164	3.03	-0.45	0.707367	0.512292	36.7	-6.4	28.0	-4.6	0.99	1.06
8057B	0.164	1.80	-0.52	0.706712	0.512366	27.4	-5.0	22.2	-2.8	1.30	0.85
8059A	0.164	2.87	-0.43	0.707053	0.512361	32.3	-5.1	24.0	-3.3	0.96	1.00
8061A	0.150+	6.10	-0.37	0.709815	0.512226	71.4	-7.7	55.4	-6.3	0.83	1.35
8065A	0.054	2.01	-0.43	0.706517	0.512215	24.6	-7.9	22.7	-7.3	1.12	1.21
8064E	0.054	5.09	-0.61	0.709360	0.511889	65.0	-14.3	60.2	-13.4	0.91	1.27
8021B	0.163	1.97	-0.42	0.705208	0.512380	6.1	-4.7	0.4	-3.0	0.69	0.99
8021D	0.054	17.47	-0.43	0.710845	0.511902	86.1	-14.0	69.5	-13.4	0.35	1.68
8022B	0.164	1.23	-0.50	0.706666	0.512327	26.8	-5.7	23.2	-3.6	1.75	0.92
8075F	0.164	2.65	-0.45	0.707389	0.512385	37.0	-4.6	29.4	-2.7	1.12	0.93
8072A	0.164	4.39	-0.44	0.707668	0.512200	41.0	-8.2	28.4	-6.4	0.76	1.21
8073A	0.164	2.51	-0.69	0.707442	0.512182	37.8	-8.5	30.6	-5.7	1.19	0.85
8070C	0.164	2.79	-0.50	0.706987	0.512195	31.3	-8.3	23.3	-6.2	0.97	1.10
8038A	0.090#	8.94	-0.49	0.708919	0.512300	58.7	-6.2	44.6	-5.1	0.50	0.98
8038D	0.090	6.08	-0.53	0.707492	0.512396	38.5	-4.4	28.9	-3.2	0.54	0.80
8096E	0.090	2.40	-0.46	0.706837	0.512151	29.2	-9.1	25.4	-8.1	1.06	1.23
8038E	0.090	6.28	-0.43	0.707965	0.512344	45.2	-5.4	35.3	-4.4	0.58	1.02
8033P	0.173$	1.14	-0.49	0.705839	0.512139	15.0	-9.4	11.6	-7.3	1.41	1.19
8033G	0.173	0.87	-0.46	0.706221	0.512084	20.4	-10.5	17.8	-8.4	1.97	1.33
8007A	0.102#	7.81	-0.46	0.709493	0.512249	66.9	-7.2	52.9	-6.1	0.62	1.11
8088C	0.051	11.65	-0.47	0.710882	0.511919	86.6	-13.7	76.2	-13.1	0.52	1.55
Volcanic Rocks:-											
IV-1A	0.164	3.80	-0.16	0.705078	0.512741	4.2	2.4	-6.7	3.0	0.37	0.91
8106B	0.190	2.77	-0.09	0.708991	0.512667	59.7	0.9	50.5	1.4	1.49	1.54
74/054	0.170	0.55	-0.16	0.705014	0.512920	3.3	5.9	1.7	6.5	1.59	0.39
75/116	0.170	1.70	-0.23	0.704622	0.512722	-2.2	2.0	-7.3	3.0	0.55	0.75

*Parrish (1983), +Duncan et al. (1979), $Parrish and Wheeler(1983), Archibald et al. (1983), xModel age with respect to Model Depleted Mantle (DePaolo, 1981b).

Table 7.4 Isotopic data and Model ages (in Ga) of sedmentary rocks.

Sample	T(Ga)	f(Rb/Sr)	f(Sm/Nd)	(87Sr/86Sr)m	(143Nd/144Nd)m	Sr(O)	Nd(O)	Sr(T)	Nd(T)	T(Sr)	T(Nd)
8001D	0.164	35.06	-0.41	0.786900	0.511847	1165.2	-15.1	1064.6	-13.4	1.91	1.85
8094A	0.164	75.59	-0.43	0.832000	0.511854	1805.1	-14.9	1588.0	-13.2	1.37	1.75
8090A	0.164	-0.22	-0.42	0.710696	0.512373	83.9	-4.8	81.7	-3.1	0.43	1.00
8037D	0.164	27.97	-0.43	0.749866	0.511940	639.7	-13.3	559.4	-11.5	1.33	1.62
8084A	0.164	2.42	-0.46	0.718869	0.511402	199.9	-23.8	193.0	-21.9	4.70	2.32
8010S	0.164	0.80	-0.49	0.711951	0.511900	101.7	-14.0	99.5	-12.0	7.18	1.52
8009D	0.154	5.02	-0.38	0.717898	0.511860	186.1	-14.8	172.6	-13.4	2.21	1.94
8003C	0.164	33.24	-0.39	0.720488	0.512102	222.9	-10.1	127.2	-8.5	0.42	1.50
8027C	0.164	5.79	-0.41	0.713130	0.511579	118.5	-20.3	101.8	-18.6	1.30	2.26
8006G	0.164	3.56	-0.42	0.709250	0.511902	63.4	-14.0	53.2	-12.3	1.24	1.71
8035C	0.164	1.46	-0.38	0.708776	0.511897	56.7	-14.1	52.5	-12.6	2.49	1.89

granodiorite with large megacrysts of K-feldspar and comes from further east of 8052A, though its both Sr and Pb isotopic compositions are higher than that of 8052A. Overall, there are negative and positive relationships between the degree of differentiation (%SiO_2) and $\epsilon_{Nd}(T)$ and $\epsilon_{Sr}(T)$. More differentiated samples 8061A ($SiO_2=62.38$), 8012B ($SiO_2=67.00$) and SB29.7 ($SiO_2=67.30$) have lower $\epsilon_{Nd}(T)$ values, -6.3, -6.1, -8.8 respectively. Such a relationship is also seen with respect to Sr isotopes whose corresponding values expressed as $\epsilon_{Sr}(T)$ are 55.4, 25.8 and 47.8 for the above samples. The ranges in $\epsilon_{Nd}(T)$ and $\epsilon_{Sr}(T)$ found in the Nelson Batholith encompass those of all other batholiths/plutons.

One sample (8049A) analysed from the Valhalla Gneissic Complex(VG), west of the Slocan Lake, has very distinct $\epsilon_{Nd}(T) = -0.7$ and $\epsilon_{Sr}(T) = -0.4$.

7.4.3 Bonnington Pluton(BP)

Bonnington Pluton occupies an area that extends on both sides of the Pb boundary line (see section 7.6 and Fig. 7.3a). Samples from 8021- and 8022-groups coming from west of the Pb-line have almost identical $\epsilon_{Nd}(T)$ (-3.0 and -3.7) values, but very different $\epsilon_{Sr}(T)$ values (0.4 and 23.2). The sample(8075F) from the east of the line has slightly higher $\epsilon_{Nd}(T) = -2.7$ and $\epsilon_{Sr}(T) = 29.4$ values. A peraluminous granitic sample (8021D) coming from the same area as 8021-group, has the corresponding isotopic compositions equal to -13.4 and 55.4. Isotopic compositions of this sample are similar to that of an 1.8 Ga old model lower crust.

7.4.4 Kuskanax Batholith(KB)

Two samples (8033G and 8033P) from this batholith have following Nd and Sr isotopic compositions, -8.4, -7.2 and 17.8, 11.6 respectively, falling in the lower range of that of the Nelson Batholith.

7.4.5 Bayonne Batholith(BB)

Samples from the Bayonne Batholith show wide variations in ϵ_{Nd} ranging from -3.2 to -8.1. Mineralogically, Bayonne Batholith has two distinctive groups: 1) bi-musc granite and 2) bi-hb granodiorite. Sample 8096E (a two-mica granite) has $\epsilon_{Nd}(T) = -8.1$. On the other hand, 8038-group (bi-hb granite) has higher $\epsilon_{Nd}(T)$ values.

7.4.6 Trail Pluton(TP) and Trail(TN) and Castlegar Gneiss(CGN)

These gneissic samples have similar Nd and Sr isotopic compositions. It is interesting to note that one sample from the Trail Gneiss (8070C) analysed is isotopically almost indistinguishable from the Trail Pluton. $\epsilon_{Nd}(T)$ values cluster around -6.0 ± 0.4 and $\epsilon_{Sr}(T)$ ranges from 23.0 to 30.6.

One sample from the Unit A(UA, 8064E), a small granitic stock, has very similar Nd and Sr isotopic compositions (i.e., -13.4 and 55.4) similar to 8021D.

7.4.7 Summit Stock(SS) and Shoreline Creek Stock(SLCS)

The Summit Stock, a small stock in the southern part of the study area, is a two-mica granite with $\epsilon_{Nd}(T) = -6.1$, $\epsilon_{Sr}(T) = 52.9$. On the other hand, the Shore Line Creek Stock, though a two-mica granite, is isotopically very different from the Summit Stock. The only sample analysed for Nd (8088C) has very low $\epsilon_{Nd}(T) = -13.1$, similar to the other two samples (8064E and 8021D). This very low Nd isotopic composition and also moderately low ϵ_{Sr} (76.2) suggest its derivation from partial melting of the lower crust.

7.5 Identification of the End-Members

7.5.1 Mantle End-Member

Considerable amount of data are available on basaltic rocks presumably derived from the mantle (Hawkesworth, 1979, 1982). Basalts from the mid-ocean ridges have highest ϵ_{Nd} values (+12) and therefore have derived from most LREE depleted source regions. Intraplate island basalts have lower ϵ_{Nd} and extend down to +4 (O'Nions et al., 1977; DePaolo and Wasserburg, 1979) falling along the mantle array with correspondingly higher ϵ_{Sr} values. Continental flood basalts (like Columbia River Basalts, Decan Traps) and some alkalic oceanic islands (Kerguelen) extend this range further down to -2. This large range in ϵ_{Nd} and correlated ϵ_{Sr} therefore suggests either unique mantle reservoirs having their own isotopic characteristics or mixing of two end-members (DePaolo and Wasserburg, 1979). However, average $\epsilon_{Nd} = +8.0 \pm 1.5$ observed for oceanic island arcs (DePaolo and Johnson, 1979; Hawkesworth, 1982) suggests that the mantle reservoirs responsible for island arc magmas have a well defined ϵ_{Nd} compared to the total range observed in the mantle reservoirs. On Figure 7.2, Nd and Sr data of all granitic and sedimentary samples have been plotted. It is seen that each pluton/batholith occupies a distinctive position, though close to each other. The samples form a data array that starts from close to the average island-arc on the mantle array (DePaolo and Wasserburg, 1976) and extends towards both lower and the upper crustal values. Sample 74/054 of the Rossland Volcanics, having highest $\epsilon_{Nd}(T)$, plots slightly off to the right of the Mantle Array, indicating some effects of sea-water alteration or wall rock contamination. Sea water interaction will not affect Nd isotopes (due to its very low Nd ppm=3×10^{-5}, Høgdahl et al. 1968), but will alter Sr isotopic composition. If the sea water alteration effects are subtracted, this sample would have had $\epsilon_{Sr}(T)$ equal to -11.0 to fall on the Mantle Array. This type of isotopic signature most likely represents participation of an incompatible element depleted mantle reservoir in the production of Rossland magma. Now, the question arises, can these measured compositions be taken to represent the original uncontaminated magma source or an even more depleted mantle like oceanic island-arc with $\epsilon_{Nd} = +8.0$ (DePaolo and Johnson, 1979, Hawkesworth, 1982) interacted with wall rocks to produce the present values? The latter alternative is preferred here for the Rossland Volcanics, because the other sample (75/116) analysed has even lower $\epsilon_{Nd}(T) = 3.0$. This variation in isotopic composition might be due to mantle heterogeneity also. But this is extremely unlikely as the scale of heterogeneity is too large to exist beneath such a relatively small volcanic composite.

Slightly lower ϵ_{Nd} values than oceanic island arc rocks appear to be characteristic of continental margin arc-type volcanic rocks (Carmichael and DePaolo, 1980; DePaolo, 1981a). Presence of small crustal component in the magma source or contamination of mantle derived magma at shallow levels could be the possible explanations. In a recent isotopic study of the

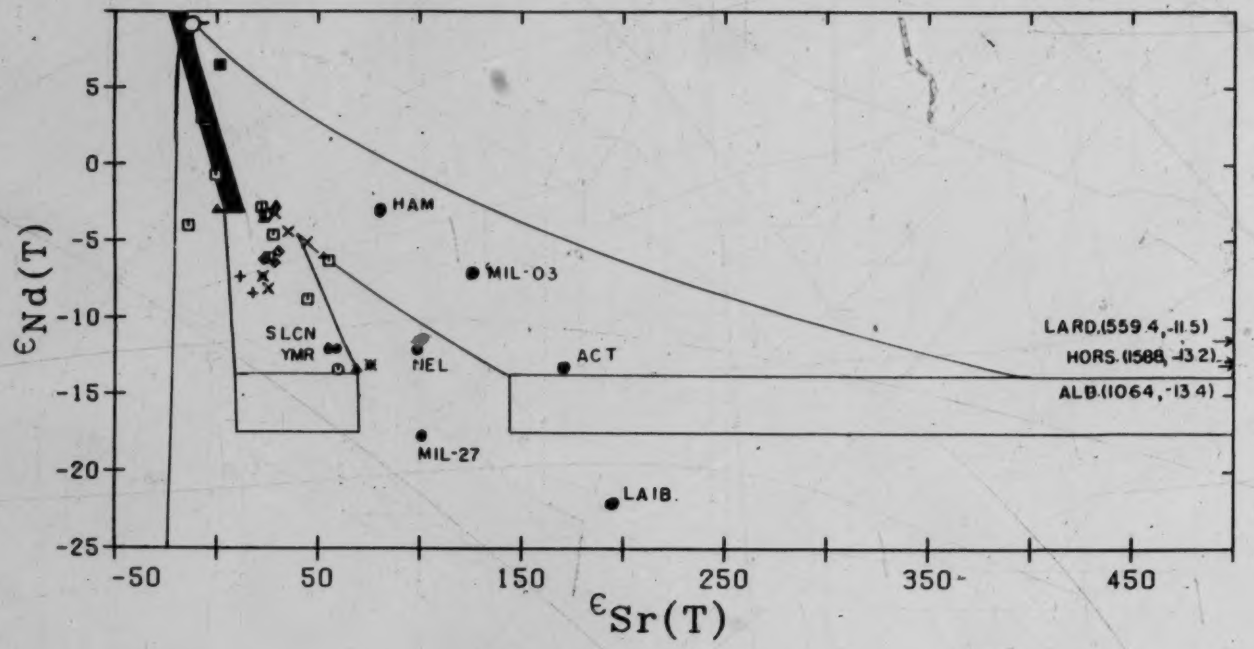

Fig. 7.2. $\epsilon_{Sr}(T)$ vs. $\epsilon_{Nd}(T)$ plot. Shows data points of all granitic rocks and associated sediments and their relation to the general divisions of mantle and crustal mixing zones and model crusts of different ages.

Columbia River Basalt(CRB), Carlson (1984) proposed a depleted mantle reservoir with $\epsilon_{Nd}=6.5$ and $^{87}Sr/^{86}Sr=0.7035$ preserved in the Imnaha and Picture Gorge basalt units, though he could not conclusively demonstrated that these isotopic compositions (his component C1) did not result from crustal contamination of a more depleted MORB-like primary magma. Variable isotopic nature of the Rossland Volcanic samples suggests variable degrees of crustal mixing rather than extremely heterogeneous nature of the local mantle. Therefore for subsequent petrogenetic modelling, a model depleted mantle similar to average island arc ($\epsilon_{Nd}=+8.0$, $\epsilon_{Sr}=-20.0$) is taken as the mantle end-member.

The two RV samples however show similar Pb isotopic compositions. As there are no fixed or accepted Pb isotopic composition for island arc magma like Nd and Sr, Pb isotopic ratios of the RV samples, after a small correction due to crustal contamination, have been taken to represent the mantle values. Therefore a model mantle $^{206}Pb/^{204}Pb=18.88$, $^{207}Pb/^{204}Pb=15.60$, $^{208}Pb/^{204}Pb=38.00$, will be taken to be the mantle end-member.

7.5.2 Crustal End-Members

Several models of paleogeography and evolution of the Kootenay Arc have been proposed (Monger et al., 1972, 1975, 1982; Okulitch, 1984; Archibald et al., 1983, 1984; Chamberlain and Lambert, 1985). All of these models greatly differ from one another, though their essential agreement is on the allochthonous nature of the rocks exposed west of the Kootenay Lake, except for Chamberlain and Lambert's (1985) model which suggests the allochthonous nature of the Belt-Purcell Supergroup.

Monger and Price (1979) summarised the geophysical and tectonic evidence around the Kootenay Arc and concluded that 1.8 Ga old Canadian craton extends as far as the Kootenay Lake. The sedimentary appron overlying this cratonic basement probably extended further west and probably deposited over an oceanic crust (Monger et al., 1972; Monger, 1979; Price, 1981), though no western geological limit can be drawn because of later intense tectonic movements and associated metamorphism that led to considerable telescoping of the Paleozoic and younger sedimentary strata in the Kootenay Arc. But from the field evidence it is clear that the Rossland

Volcanics and asociated granitic batholiths (Nelson, Bonnington, Kuskanax) have intrusive relationships with the adjacent sediments. For example, the Nelson Batholith intrudes along its northern and eastern margins sedimentary formations such as the Slocan, Milford, Lardeau and Ymir Groups. It also has abundant roof pendants of the rocks belonging to the Slocan and Ymir Groups. As granitic plutonisms took place during or shortly after some of these sedimentary units (i.e., Slocan) were accreted to the miogeocline then there is a great possibility that the protoliths of granitic magmas interacted with wall rocks with wide variation in both chemical and isotopic character. However, it can be concluded that paleogeography east of the Pb-line (see section 7.6 and Fig. 7.3a) was occupied by continentally derived sedimentary rocks along its entire length. In the north, the older Kuskanax Batholith has intruded the Upper Paleozoic to Triassic(?) Milford and Kaslo Groups (Parrish and Wheeler, 1983). In the south and the east of the Nelson Batholith, both the Jurassic (Mine Stock) and Cretaceous (Bayonne Batholith, Summit Stock) and Tertiary (Shore Line Creek Stock) batholiths/stocks have definitely intruded the miogeoclinal sedimentary sequence. In the west, the Trail Pluton and Gneiss, the Castlegar Gneiss and the western part of the Bonnington Pluton show no intrusive relationships with any sediments and thus their isotopic compositions are particularly different. In this region Pb isotopes suggest presence of lower crustal type rock. Simony (1979) proposed that the Trail Gneiss is a part of the torn-apart segment of the 1.8 Ga old continental craton. But the present isotopic study does not support his suggestion as its Nd isotopic composition is similar to the nearby Trail Pluton. In general, Pb isotopic data supports his contention that there is lower crust hidden underneath. Therefore it is seen that granitic rocks in the Nelson-Rossland Arc interacted with both the lower and upper crustal rocks.

On the basis of Nd isotopes (see Chapter 4), the miogeoclinal sediments appear to have derived from 1.8 Ga old crystalline basement except those from the Laib (from 2.32 Ga) and the Milford Groups (from 1.5 Ga and 2.26 Ga, see Table 7.3 for T_{Nd} model ages). ϵ_{Nd} values of 1.8 Ga craton derived sediments fall in between -12.0 to -13.4 at 164 Ma while 2.3 Ga old craton derived sediments are around -20.0. Corresponding ϵ_{Sr} values have a large range (100.0 to 1500 at 164 Ma). But because of predominance of 1.8 Ga old craton-derived sediments a

ϵ_{Nd} value of -13.2 is taken for the upper crustal end-member.

7.5.3 Subducted Materials

Materials subducted along with the sinking lithosphere could represent another possible source for the magma. Two types of subducted materials might be considerated: 1) deep sea or continental margin sediments and 2) hydrothermally altered oceanic crust. There is some controversy regarding the possibility of sediments being subducted and, if so, the nature and the amount of sediments (Kay, 1980; Kraig and Kay, 1981). Their study suggests that amount of sediments needed for subduction to explain some island-arc volcanic magma is only 1-2 wt% of the total magma mass. Hydrothermally altered oceanic crust will have elevated $\delta^{18}O$ (Muehlenbachs and Clayton, 1972, 1976) and ϵ_{Sr} but ϵ_{Nd} similar to mantle derived magmas (McCulloch et al., 1980; Jacobsen and Wasserburg, 1979). This is so because seawater has very low Nd ppm ($3x10^{-5}$, Høgdahl et al., 1968) and ϵ_{Nd} ($=-9.0$, DePaolo and Wasserburg, 1977) but comparatively very high Sr ppm ($=8$, Mason, 1966) and ϵ_{Sr} ($=64$, DePaolo and Wasserburg, 1979). Given a water-rock ratio, ϵ_{Sr} will increase while ϵ_{Nd} will remain almost unaffected. Mantle-like $\delta^{18}O$ values (4.8 to 6.5) obtained from clinopyroxene separates from the Rossland Volcanics (Beddoe-Stephens and Lambert, 1981) argue against derivation of magma by partial melting of hydrothermally altered oceanic crust. Sample 74/054 falls to the right of mantle array while sample 75/116 plots exactly on the array. Shift to the right for the former sample might be due to later hydrothermal alteration or low grade metamorphism. Nodha and Wasserburg (1981) showed that involvement of deep sea sediments may be responsible for a shift of only 1 to 2 ϵ-units in Nd between island arc basalts and MORB. The large negative ϵ_{Nd} values for the granites and a general increase in ϵ_{Sr} and Pb isotopes from west to east necessitate an eastward (i.e., away from the trench) increase in the degree of contribution from the subducted sediments. This is unlikely. Therefore all subducted materials appear to be poor candidates for the source of the batholiths. Moreover, the fact that the geographic patterns in Pb isotopic data are related to paleogeographic boundaries rather than to the loci of magmatic intrusions and magma types, rules out the involvement of subducted sediments.

7.5.4 Mixture of Volcanic and Sedimentary Rocks

The only other conceivable source of ϵ_{Nd} and ϵ_{Sr} equal to the range found in the batholiths, is a physical mixture of volcanic and sedimentary rocks. Beside the Rossland Volcanics, there is a lack of widespread volcanic rocks in the area. Sedimentary clastic materials likely to melt are Cambrian or older from a depth of burial consideration (Lardeau, Laib, Hamill, Horsethief Groups and Aldridge Formations). These sedimentary formations are not stratified with any volcanic rocks except the ≅1.0 Ga old Irene Volcanics, only exposed in the southeastern part of the area. Iv-1a has $\epsilon_{Nd}=3.0$ and $\epsilon_{Sr}=-6.7$ at 164 Ma. Therefore to produce granitic rocks with ϵ_{Nd} in the range of -2.0 to -8.0, the amount of the volcanic rocks needed to be melted along with the associated sedimentary rocks (with average $\epsilon_{Nd}=-13.0$) should vary between 70% to 40%. Geological evidence does not support this. Therefore it is concluded that the granitic source is not likely to be a volcano-sedimentary mixture.

7.6 Nature of Crystalline Basement

The isotopic data require presence of a crustal layer all across the study area with a mean $\epsilon_{Nd}(0)=-14.0$. Whether this crustal layer represents a continuous layer consisting of upper crustal sedimentary package or a lower crust of high grade rocks (granulite facies) or a combination of both is a matter of debate. But Pb, Sr and Nd isotopic data can help resolve this problem. The three unique granitic samples from west to east (8064E, 8021D and 8088C) suggest a crustal layer with ϵ_{Nd} values similar to what is expected for a 1.8 Ga old model cratonic crust. Their $\epsilon_{Sr}(164)$ values are also low (55.4 to 76.0) and fall within lower crustal range (Figure 7.2). As $\epsilon_{Sr}(164)$ values of all miogeoclinal sedimentary rocks are invariably greater than 76.0, it is very unlikely that these three samples formed by partial melting of pelitic miogeoclinal sediments as Nd data might suggest. Pb isotopic data however gives more clearcut evidence of the nature of the source material of these three samples. Sample 8021D has the least radiogenic Pb isotopic composition ($^{206}Pb/^{204}Pb=17.692$, $^{207}Pb/^{204}Pb=15.504$ and

$^{208}Pb/^{204}Pb=38.487$) followed by 8064E (18.245, 15.549, 38.956) and 8088C (19.102, 15.671 and 39.223). Slightly higher Sr and Pb isotopic compositions for 8088C than the other two samples are propably due to interaction of granitic melt with the enclosing sedimentary rocks with generally higher values for both Sr and Pb isotope ratios. Samples 8064E and 8021D still retain isotopic ratios closest to their source rocks. If it is true, Pb isotopic data strongly suggest a lower crustal origin for "Unit A" (8064E) and the granitic unit near Castlegar dam (8021D).

From geophysical and tectonic interpretations, it has been shown that the Canadian cratonic basement undoubtedly extends as far west as Kootenay Lake. Therefore isotopic compositions of 8088C (SLCS) are certainly due to the melting of this craton. It is interesting to explore the possibilities of producing SLCS by melting of the Aldridge Formation or by melting a combination of the Aldridge Formation and Horsethief Group, both having $\epsilon_{Nd}(164)$ values close to that of 8088C. On the basis of Pb isotopes a 78:22 mixture of Aldridge to Horsethief is required to produce SLCS. Major problem arises when Sr isotope is considered. Average $\epsilon_{Sr}(164)$ for the two groups from the Aldridge Formation (8001- and 8002-groups) are 1622 and 1138 respectively. One sample analysed for the Horsethief Group has $\epsilon_{Sr}(164)=1586$. If these values are representative of these two sedimentary units at the depth of melting, it completely rules out the possibility of generating SLCS from melting of these sediments. Very low $\epsilon_{Nd}(164)$ for the Hamill Group (-3.1) also rules out its involvement in this melting process. Sr isotopic evidence against SLCS's derivation from sediments could be nullified if it is assumed that the sedimentary units at greater depth (>10 km) undergone high grade metamorphism before at least Cambrian time and were thus depleted in LIL elements (U, Rb etc.) and thus acquired very different isotopic compositions compared to the exposed section. If this is true, then the Aldridge Formation might have had similar isotopic compositions to the lower crust with respect to Pb and Sr. Even though chemically it is feasible, the evidence for this tectonic burial soon after its deposition is lacking. According to Archibald et al. (1983, 1984) and Monger et al. (1982), tectonic burial of the miogeoclinal rocks to a depth of 20-25 km took place only during late Jurassic and early Cretaceous time. Therefore it is very difficult to decipher the nature of the sedimentary rocks at the depth of melting, when

SLCS was formed. From these difficulties, it is suggested here that the Shore Line Creek Stock formed certainly due to partial melting of cratonic basement rather than the miogeocline itself. This peraluminous granitic stock therefore supports the other geophysical evidence of the extension of the craton at least as far as the Kootenay Lake. Very young age (51 Ma) of this stock clearly demonstrates its "autochthonous nature" with respect to the craton, i.e., it formed after the Jurassic accretion of Q to the western margin of the North America. The strong isotopic evidence (provided by 8064E and 8021D) for the presence of a lower crust west of the Kootenay Lake suggests that it might be related to the crust sampled by 8088C, east of the Lake.

Figures 7.3a-c. show the plot of initial isotopic compositions of Pb, Sr and Nd projected onto 49°10' latitude to see isotopic variations from west to east. Systematic geographic variation in Pb-isotopes, is of major tectonic significance. There have been many speculations about the extent of the western edge of the North American craton in this region. From Fig. 7.3a, a geographic boundary could be drawn along a N-S line running parallel to the Slocan Lake in the North and the Champion Lake Fault in the south on the basis of Pb isotopic compositions. If a mantle magma of such Pb isotopic composition as $^{206}\mathrm{Pb}/^{204}\mathrm{Pb}=18.88$, $^{207}\mathrm{Pb}/^{204}\mathrm{Pb}=15.60$, $^{208}\mathrm{Pb}/^{204}\mathrm{Pb}=38.00$ is assumed to exist (evidence discussed later), then Pb isotopic compositions found in samples coming from west of this boundary line represent variable mixtures of mantle Pb and lower crustal Pb, while those samples coming from the east of this line represent variable mixtures of mantle Pb and upper crustal Pb (i.e., from the sediments, see Chapter 8). This geographic division based on Pb isotopes is independent of the mineralogy of the samples. This is very important as this type of geographic division is found neither in Sr nor in Nd isotopic compositions.

Figure 7.3b shows the geographic variations in $\epsilon_{Nd}(T)$. Samples 8021D, 8064E and 8088C define the lower envelope at about $\epsilon_{Nd}(T)=-13.0$ All other granitic samples have $\epsilon_{Nd}(T)$ values in between this lower envelope of -13.0 and the average island-arc magma (+8.0). As both the lower crust and sediments have values close to -13.0, no granitic plutons/batholiths could be derived by partial melting of either source.

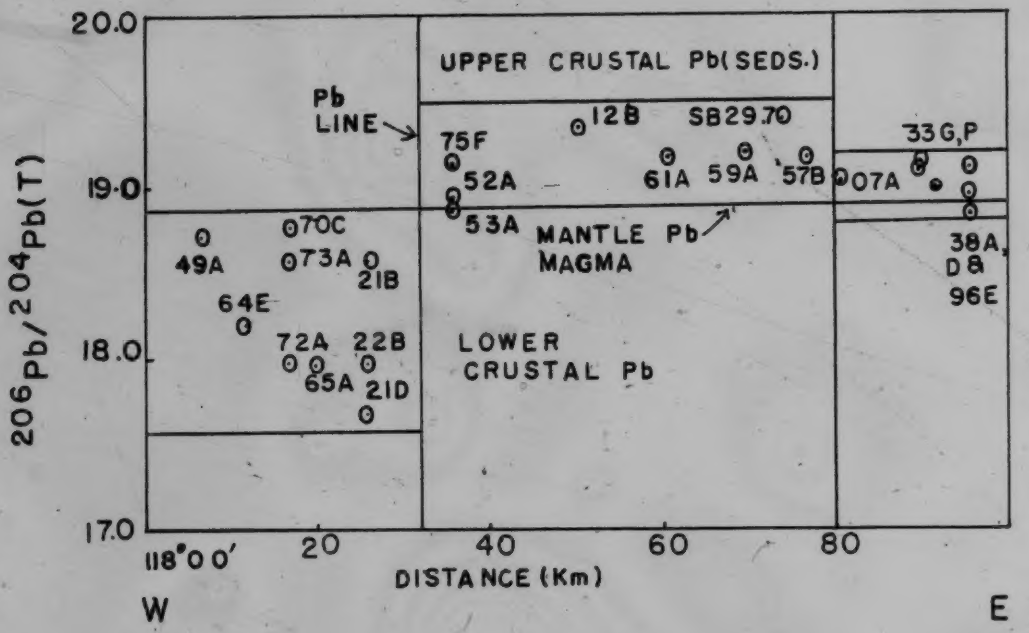

Fig. 7.3a-c. Show geographic variations of initial isotopic compositions of Pb, Sr and Nd in southeastern British Columbia. a. for $^{206}Pb/^{204}Pb$, it shows the mantle value at 18.88, and two distinct geographic breaks. Across the western break (to be called Pb-line), all the samples west of the line have Pb-isotopic compositions lower than the assumed mantle value (see text) and those east of the line have higher values. This line runs N-S along the Slocan Lake in the north and the Champion Lake Fault in the south and is thought to define the western limit of the Pre-Mesozoic migeoclinal sediments. The eastern break is not as prominent as the Pb-line, but the samples from the Bayonne Batholith east of the line tend to be less radiogenic from those to the west and indicates involvement of old unradiogenic crust (e.g., Craton(A)). The source of dominantly unradiogenic lead west of the Pb-Line lies in the hidden lower crust in the area. b and c. Such a 3-fold divisions are not however shown by either Nd or Sr isotopes. For Nd, three samples (8064E, 8021D and 8088C) have lowest $\epsilon_{Nd}(T)$ and form the lower envelope for the rest of the samples. ϵ_{Nd} for the mantle magma forms the upper envelope, suggesting granitic rocks in the study area are mixtures of mantle magma amd the lower crust. For Sr, those three samples have highest $\epsilon_{Sr}(T)$ values and form the upper envelope and the mantle ϵ_{Sr} defines the lower envelope.

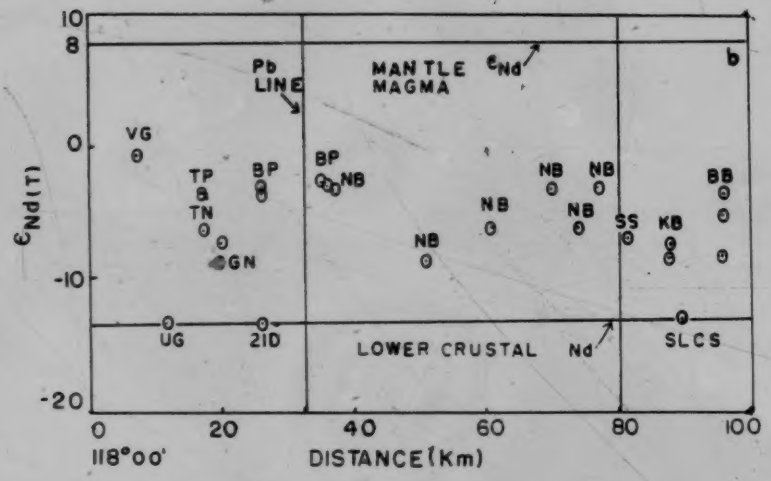
b
10
8
0
-10
-20
$\epsilon_{Nd(T)}$
Pb LINE
MANTLE MAGMA ϵ_{Nd}
VG
TP & TN
GN
BP
BP
NB
NB
NB
NB
NB
NB
SS
KB
BB
UG
21D
LOWER CRUSTAL Nd
SLCS
0
20
40
60
80
100
118°00'
DISTANCE(Km)

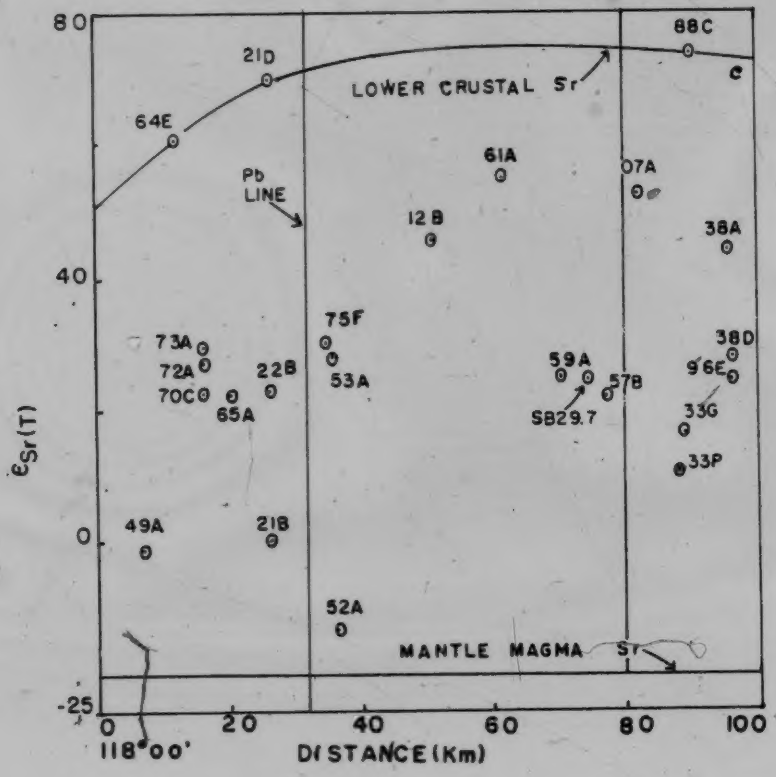
c
80
40
0
-25
$\epsilon_{Sr(T)}$
88C
21D
LOWER CRUSTAL Sr
64E
61A
07A
Pb LINE
12B
38A
75F
73A
72A
70C
65A
22B
53A
59A
SB29.7
57B
38D
96E
33G
33P
49A
21B
52A
MANTLE MAGMA Sr
0
20
40
60
80
100
118°00'
DISTANCE(Km)

Figure 7.3c shows a similar plot with respect to $\epsilon_{Sr}(T)$. From this plot it is also seen that those three samples (8084E, 8021D and 8088C) have higher ϵ_{Sr} values than most granitic samples and therefore form the upper envelope. All other samples are bounded by this upper limit and the depleted mantle ϵ_{Sr} value (-20.0, i.e, 0.7033)

These observations strongly suggest that initial granitic source magma originated in the mantle with a depleted (LILE) mantle isotopic compositions like average island-arc and then interacted with either lower or upper crust or both.

7.7 Petrogenetic Modelling

Petrogenetic models deal with separately or in combination four general categories of processes: (1) fractional crystallization from a mafic parent magma (Bateman and Chappell, 1979; Bateman and Nokleberg, 1978; Gill, 1981; Cawthorn and O'Hara, 1976) (2) melts contaminated with xenolithic debris, including both mafic magmas that have assimilated silicic crustal rocks (Harker, 1904; Daly, 1933; Kuno, 1950) and silicic magmas that have incorporated xenolithic dioritic material (Wilkinson et al., 1964) as well as dark shales (Lee and Loenen, 1971). (3) restite model of White and Chappell (1977) and (4) mixing of mafic and silicic magmas (Wilcox, 1944; Eichelberger, 1978). It is generally found that more than one of the above processes operate together. For, example, Grove et al. (1982) found the mafic lavas at Medicine Lake Highland, California, are related dominantly by fractional crystallization, while the felsic rocks have evolved through a combination of crustal assimilation and magma mixing.

Even though field, geological and petrographic evidence for magma mixing were known since the turn of the century, isotopic and trace element patterns of magma mixing have been given mathematical expressions only recently (Steiger and Wasserburg, 1969; Langmuir, et al., 1978; DePaolo and Wasserburg; 1979). The mixing equations derived by the above workers are simply related to two-component binary mixing. Recently it is becoming obvious that magma mixing also accompanies fractional crystallization (Taylor, 1980; DePaolo, 1981c). Bowen (1928) discussed at length the effects of assimilation on silicic liquids and concluded that heat required for heating and melting the contaminants could be supplied by the heat of fusion of the crystallizing assemblages.

Before detailed isotopic studies were done, AFC processes appear not to have been given serious consideration as assimilation of most common rock types does not seriously alter the liquid line of descent and the major element chemistry for a differentiated series (Bowen, 1928). Taylor (1980), however, showed for the first time, that the effects of combined AFC on isotope ratios and trace element concentrations are significantly different from those produced by either two component mixing or fractional crystallization alone (James, 1982)

In the island arc setting, the conditions for assimilation are all the more favourable as the heat flow is higher than the normal. Magma produced from the low melting components of the subducted slab or the fluids enriched in LIL elements released from it (Ringwood, 1975, 1982) induce melting of mantle above the Benioff zone. These magmas (basaltic or andesitic) rise upwards till arrested by the crustal layer. This is due to the fact that the basaltic or andesitic magmas at >10 kb pressure have higher densities than the granodioritic/sedimentary rocks of the crust (Herzberg et al., 1983). This results in the underplating of mantle derived magmas that undergo crystallization and consequently supply enough heat to melt the overlying crustal layer (cratonic or sedimentary or both). This type of situation is most conducive to crustal contamination.

Isotopic trends generated in this scenario have been mathematically derived by DePaolo (1981c). These models have been successfully applied to explain isotopic characteristics of calc-alkaline granitic batholiths in western USA (DePaolo, 1981a; Farmer and DePaolo, 1983, 1984) and of volcanic rocks (Bacon et al., 1984) and of French granites (Ben Othman et al., 1984a)

From the discussion of the chemical nature of the possible underlying crust and of the known mantle tapped by "island arc volcanics" it is certain that the granitic batholiths present in the study area are composed of materials having inputs from two or more sources. Though it is problematical to deduce the primary nature of the complex mixing processes responsible for generating the observed isotopic trends, as the mixing phenomena are controlled by large number of factors. Most important of these are :

1. nature of the source materials or magmas produced from them.
2. temperature contrast or difference between the magma and wallrocks
3. viscosity of the magma
4. density contrast between the magma and wallrocks.
5. degree of difference in isotopic composition between the end-members.
6. rate of ascent of the source magma and
7. overall tectonic setup.

Many of these factors could be deduced by studying rocks present in the area, particularly the nature of the contaminants. The nature of the mantle end-member could be worked out from the most primitive rock unit (volcanic or plutonic) or generating a mantle magma by partial melting of a model mantle.

7.7.1 Modelling Parameters and Assumptions

It is necessary to make some assumptions about the mixing processes as there are more unknowns than needed to have a unique solution to the observed data.

1. Crystallizing phases are assumed to be some combinations of plagioclase, amphibole and clinopyroxene at mid- or lower crustal levels. Only these crystal phases are considered because of their presence as phenocrysts in the basaltic rocks of the RV Group (Beddoe-Stephens, 1982). Plagioclase is an important phase controlling the Sr abundance and its isotopic compositions. Amphibole plays an important role in the evolution of calc-alkaline suites (Cawthorn and O'Hara, 1976; Gill, 1981). Both clinopyroxene and amphibole are important in fractionating Sm from Nd. All these phases are found in the granitic batholiths/plutons in the study area. Olivine and orthopyroxene are not taken into model calculations as both have got very low K_D's for the elements considered (Rb, Sr, U, Th, Pb, Sm and Nd), though they might be important fractionating phases controlling major element abundances.

2. Latent heat of crystallization of the fractionating phases is mainly responsible to dissolve the assimilated rocks. It is assumed here that wall rocks were already elevated to higher temperature from the heat supplied by the underplated magmas, so that large amount of assimilation can

take place [evidence supporting this conclusion is found in the model results].

3. Crystallization could be either fractional (Rayleigh type) or equilibrium. Fractionating phases obeying Rayleigh crystallization form the cumulates at the bottom of the magma chamber. Nature of the crystallizing phase depends on the P-T-X conditions of the magmas. For example, plagioclase crystallization is controlled by P_{H_2O} in the magma. High water pressure generally found in wet island arc magmas at lower crustal depth, suppresses plagioclase fractionation (Yoder and Tilley, 1962; Gill, 1981).

4. Distribution coefficients of the elements for the phases considered are assumed to be constant even though there is enough evidence on the contrary. Relative proportions and types of the phases also change with the ascent of the magma and also the value of r($=M_a/M_c$, i.e., rate of assimilation vs. rate of crystallization) is not constant.

5. Isotopic ratios of the crystallizing phases are the same as that of magma.

7.7.2 Mathematical Background

a). *Simple Binary Mixing:*

The isotopic composition of the mixture of two reservoirs is calculated according to the following equation (Steiger and Wasserburg, 1969):

$$\epsilon^m_\alpha = \left[\frac{X_1[\alpha]_1[\epsilon_\alpha]_1 + (1-X_1)[\alpha]_2[\epsilon_\alpha]_2}{X_1[\alpha]_1 + (1-X_1)[\alpha]_2} \right] \quad \ldots\ldots (7.1)$$

where $[\alpha]$ = the concentration of Nd or Sr or Pb,

X_1 = weight fraction of component 1 in the binary mixture,

$X_2(=1-X_1)$ = weight fraction of component 2,

$[\epsilon_\alpha]_i$ = normalised isotopic ratio in component i.

For example in the case of Nd isotopes, eqn. (7.1) takes the form:

$$\epsilon^m_{Nd} = \left[\frac{X_c[Nd]_c[\epsilon_{Nd}]_c + (1-X_c)[Nd]_m[\epsilon_{Nd}]_m}{X_c[Nd]_c + (1-X_c)[Nd]_m} \right] \quad \ldots\ldots (7.2)$$

where c = crustal end member

m = mantle end member

$[Nd]_{c,m}$ = concentration of Nd in c or m.

$[\epsilon_{Nd}]_{c,m}$ = normalised Nd isotopic ratio in c or m.

DePaolo and Wasserburg (1978) modified this mixing equation by taking into account the concentration of the stable isotopes of the particular element concerned. If for an element, α(Nd, Sr,Pb) a radiogenic isotopic α^r and a stable isotop α^S are considered, then the isotopic ratio (α^r/α^S) expressed in the normalised form can be written as:

$$\epsilon_\alpha^m = \left[\frac{X_1[\alpha^S]_1[\epsilon_\alpha]_1 + (1-X_1)[\alpha^S]_2[\epsilon_\alpha]_2}{X_1[\alpha^S]_1 + (1-X_1)[\alpha^S]_2} \right] \quad \text{.......... (7.3)}$$

[definition of the respective terms is similar to those of eqn.(1)].

Statistically, ϵ_α^m is equivalent to the weight mean of the isotopic compositions of two end members and obeys the mass balance constraints.

Vollmer (1976) also formulated a mixing equation in the form of a hyperbola:

$$A(\epsilon_\beta)_m + B(\epsilon_\beta)_m(\epsilon_\alpha)_m + C(\epsilon_\alpha)_m + D = 0 \quad \text{.......... (7.4)}$$

where A , B, C, D are constants and are defined as:

$A = a_2b_1(\epsilon_\beta)_2 - a_1b_2(\epsilon_\alpha)_1$

$B = a_1b_2 - a_2b_1$

$C = a_2b_1(\epsilon_\alpha)_1 - a_1b_2(\epsilon_\alpha)_2$

$D = a_1b_2(\epsilon_\alpha)_2(\epsilon_\beta)_1 - a_2b_1(\epsilon_\alpha)_1(\epsilon_\beta)_2$ and

ϵ_β = isotopic ratios of one element, e.g., $^{143}Nd/^{144}Nd$ or ϵ_{Nd}

ϵ_α = isotopic ratios of the other element, e.g., $^{87}Sr/^{86}Sr$ or ϵ_{Sr}

a_i = concentration of ^{86}Sr of component i = 1, 2.

b_i = concentration of ^{144}Nd in component i

Shape of the mixing curves following eqns (7.1) and (7.4) will depend on the effective elemental fractionation factor $(K_{\alpha/\beta})$ between the two components:

$$K_{\alpha/\beta} = \left[\frac{(\alpha^S/\beta^S)_1}{(\alpha^S/\beta^S)_2} \right] \quad \text{.......... (7.5)}$$

or for the isotopic pairs Sr and Nd:

$$K_{Sr/Nd} = \left[\frac{(Sr/Nd)_1}{(Sr/Nd)_2} \right] \quad \text{.......... (7.6)}$$

If $K<1$, the curve is convex upward (Fig. 7.4) and if $k > 1$, the curve is convex downward. Straight line will be obtained only if $K = 1$, i.e., elemental ratios are same for the two components. In this case, it is important to remember that absolute elemental abundances in the two components need not be same, even though it might be one of the special cases.

The above equations for binary mixing will only apply to those cases where melts derived from two sources mix. They are neither valid for (1) mixing involving selective migration of the isotopes nor (2) for the bulk assimilation as well as for assimilation coupled with fractional crystallization (AFC).

b). ***Assimilation and Fractional Crystallization***

Taylor (1980) studied the effects of AFC models on isotopic systems (e.g., O and Sr in the Peninsular Ranges Batholith in USA) and found that the isotopic patterns in such cases are drastically different from simple binary mixing. He also showed his results graphically. Later on, DePaolo (1981) developed detailed mathematical formulations describing the isotopic trends and changes in trace element concentrations. As in this Chapter AFC model has been used frequently, it is necessary to describe the equations.

Some of the mathematical symbols or notations frequently used are defined as follows:

$r = \dot{M}_a/\dot{M}_c$ = ratio of rate of assimilation to rate of crystallization,

M_m° = original mass of the magma,

$M_m(t)$ = mass of magma at any time t,

M_a = mass of assimilated wall rocks,

D = bulk solid/liquid partition coefficient for the element between the fractionating crystalline phases and the magma,

C_a = elemental concentrations in wall rocks,

C_m° = elemental concentrations in original magma,

$C_m(t)$ = elemental concentrations in the remaining magma at time t.

F = fraction of magma remaining at any time $= M_m(t)/M_m^{\circ}$.

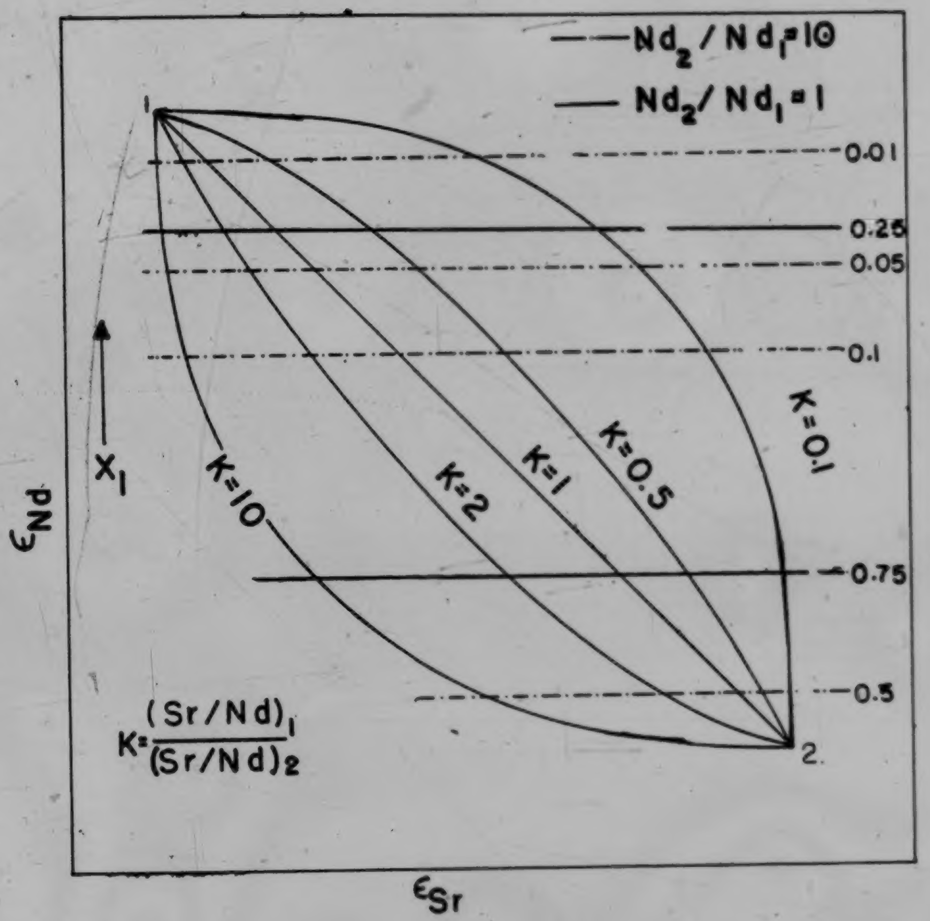

Fig 7.4. ϵ_{Nd} vs. ϵ_{Sr}. Curves (schematic) describing changes in ϵ_{Nd} and ϵ_{Sr} in mixtures of two components for different values of $K_{Sr/Nd}$, the ratio of Sr/Nd in the two end-members. Curves with $K<1$, are concave towards the origin, and those with $K>1$, are convex towards the origin. Dashed ($[Nd]_2/[Nd]_1) = 10$) and dotted ($[Nd]_2/[Nd]_1 = 1$) lines give the wt. fractions of component 2 in the mixture. All the mixing curves terminate at the end-member compositions.

Two different cases have been considered:

1). when $r = 1$, i.e., $M_a = M_c$ or constant magma mass,

2). when $r \neq 1$,

For case 1). Following equations are used to calculate elemental concentration:

$C_m/C_m^\circ = (C_a/DC_m^\circ)[1-\exp(-DM_a/M_m)]+\exp(-DM_a/M_m)$ .... (7.7)

Special cases:

if $D<<1$, eqn. (7.7) reduces to:

$C_m/C_m^\circ = 1+M_aC_a/M_mC_m^\circ$ .... (7.8)

if $D >> 1$, eqn (7.7) rapidly converges to

$C_m \approx C_a/D$ .... (7.9)

when DM_a/D_m becomes large.

For case 1), i.e., $r = 1$, normalised isotopic ratios are calculated using the following equations:

$\epsilon_m = \{C_a/D[1 - \exp(-DM_a/M_m)]\epsilon_a + C_m^\circ\exp(-DM_a/M_m)\epsilon_m^\circ\}.$

$\{C_a/D[1 - \exp(-DM_a/M_m)] + C_m^\circ\exp(-DM_a/M_m)\}^{-1}$ .... (7.10)

Or,

$\Delta\epsilon_m/(\epsilon_a-\epsilon_m^\circ) = 1 - (C_m^\circ/C_m)\exp(-DM_a/M_m)$ .... (7.11)

A limiting case arises when $D < 1$, and eqn (7.11) simplifies to:

$\Delta\epsilon_m/(\epsilon_a-\epsilon_m^\circ) = (1 + C_m^\circ M_m/C_aM_m)^{-1}$ .... (7.12)

In a physical sense, small shifts in isotopic composition may occur even with large amounts of assimilation. The reverse happens only when $D >> 1$, and ϵ_m goes to ϵ_a as soon as M_a/M_m becomes large relative to $1/D$.

Case (2), i.e., $r \neq 1$, a general case.

In this case $M_a \neq M_a$, concentrations of elements change according to the following eqn (7.13):

$C_m/C_m^\circ = F^{-z} + [r/(r-1)]C_a(1-F^{-z})/zC_m^\circ$ .... (7.13)

where $z = (r+D-1)/(r-1)$ If $r+D = 1$, then $z = 0$, and therefore for this special case,

$C_m/C_m^\circ = 1 + [r/(r+1)]C_a\text{Ln}F/C_m^\circ$ .... (7.14)

Other special cases occur when

a) $D << 1$, eqn(7.13) will reduce to eqn(7.15) as F becomes small:

$$C_m/C^{\circ}_m \approx F^{-1}[\,1 - (C_a/C^{\circ}_m)(r/(r-1))] \quad \text{.......... (7.15)}$$

and b) $D >> 1$, $r < 1$, eqn (7.13) becomes

$$C_m \approx rC_a/(r+D-1) \quad \text{.......... (7.16)}$$

This case has a special significance. Eqn (7.16) gives the minimum value of C_m for a magma obeying AFC, i.e., a steady state value is reached, when the elements are not depleted beyond this value.

Isotopic patterns produced during this general case obey the following eqns:

$$\epsilon_m = \left[\frac{[r/(r-1)](C_a(1-F^{-z})\epsilon_a/z + C^{\circ}_m F^{-z}\epsilon^{\circ}_m}{[r/(r-1)](C_a(1-F^{-z}) + C^{\circ}_m F^{-z}} \right] \quad \text{.......... (7.17)}$$

Or,

$$\frac{\Delta\epsilon_m}{\epsilon_a - \epsilon^{\circ}_m} = \frac{\epsilon_m - \epsilon^{\circ}_m}{\epsilon_a - \epsilon^{\circ}_m} = 1 - \frac{C^{\circ}_m}{C_m} . F^{-z} \quad \text{.......... (7.18)}$$

The advantage of writing eqn (7.17) in the form of (7.18) is that it gives the maximum shifts in $\epsilon_{Sr,Nd}$ as a fraction of total isotopic difference between the end members.

Special cases:-

a). when $D << 1$, $r < 1$,

$$\lim_{F \to 0} \frac{\Delta\epsilon_m(\max)}{\epsilon_a - \epsilon_m^{\circ}} = \left[\, 1 - \frac{r+D-1}{r-1} . \frac{C^{\circ}_m}{C_a} \right] \quad \text{.......... (7.19)}$$

This built-in-limit in the shift ($\Delta\epsilon_m$) is a function of the heat balance during assimilation and crystallization expressed through the parameter r.

7.8 Simple Binary mixing

First the isotopic data will be considered in terms of simple binary mixing and it will be shown that such mixing fails to explain the data. The mantle end-member has been taken as LREE depleted island arc type magma with the chemical compositions as tabulated in Table 7.5. The crustal end-members are the different sedimentary rock units present in the area. The

following sedimentary Groups/Formations have been used as possible contaminants:
1. Aldridge Formation(ALD), 2. Horsethief Group(HORS), 3. Hamill Group(HAM) 4. Lardeau Group(LARD), 5. Laib Formation(LAIB), 6. Nelway Formation(NEL), 7. Active Formation(ACT), 8. Milford Group(MIL), 9. Model Lower crust(LC) and 10. Model upper crust(UC).

. Table 7.5 shows the chemical parameters used for these crustal end-members. Model curves calculated according to eqn. (7.1) have been superimposed on the experimental data in Figs. 7.5 to 7.10. Fig. 7.5 shows that binary mixing curves do not generally pass through the area where most of the data cluster. Most of the mixing curves plot to the right of the data array, except those for the LC, UC and Laib. Because of this, sedimentary units are not considered to be potential contaminants for the granitic batholiths. Only the mixing curves due to the LC, UC and Laib pass close to the samples belonging to the Kuskanax Batholith, Bonnington Pluton (one sample, 8021B), NB (8052A) and VG (8049A). These observations suggest that the granitic batholiths do not contain sedimentary units as the major crustal components, but probably contain large amounts of lower crustal (Rb depleted, with low Rb/Sr ratios) material. This conclusion will be supported later by the AFC modelling.

Figs. 7.6a-b show binary mixing models using Pb and Nd isotopes. Potential contaminants are the Liab, Lardeau, Nelway and Milford(8027-group) [Fig. 7.6a], none [Fig. 7.6b] and Aldridge, Lardeau, Laib and Milford Groups [Fig. 7.6c] respectively. Therefore it is seen from these three Figs. that for different pairs of isotopes different contaminants are required:- a fact self-contradictory in itself. The validity of these observations exists only if it is assumed that different isotopes behave differently, particularly Pb isotopes. But this is very unlikely. From Fig. 7.7, the likely contaminants are the (Lardeau, Laib, Nelway, LC, Fig. 7.7a), (Lardeau, Laib, Milford, LC, Fig. 7.7b) and (Lardeau, Laib, Nelway, Active, Milford and LC, Fig. 7.7c) respectively. Therefore again it is seen that different sedimentary units are required to explian the same data set. The above observations are put in a table form (Table 7.6):

Table 7.5 End-member compositions.

Formn	$^{\epsilon}$Nd	$^{\epsilon}$Sr	Pb6/4	Pb7/4	Pb8/4	Nd	Sr	Pb
Ald	-13.4	1064.0	18.191	15.592	38.761	46.4	124.0	25.0
Hors	-13.2	1586.7	22.654	15.993	42.53	21.1	62.0	4.0
Ham	-3.1	81.4	21.143	15.795	41.127	90.0	330.0	13.0
Lard	-1.5	559.8	19.192	15.691	39.254	2.6	253.0	15.0
Laib	-21.9	192.9	19.128	15.718	38.370	20.8	81.0	5.7
Nel	-12.0	99.5	18.845	15.807	39.410	11.0	714.0	22.0
Act	-13.4	172.7	22.011	15.873	39.002	16.5	353.0	18.0
Mil	-18.6	101.7	19.294	15.713	39.163	6.9	322.0	14.0
UC	-13.0	150.0	19.516	15.740	38.962	26.0	270.0	20.0
LC	-13.0	60.0	17.120	15.446	38.464	26.0	430.0	15.0
MM	+8	-20.0	18.88	15.60	38.80	10.0	500.0	2.0

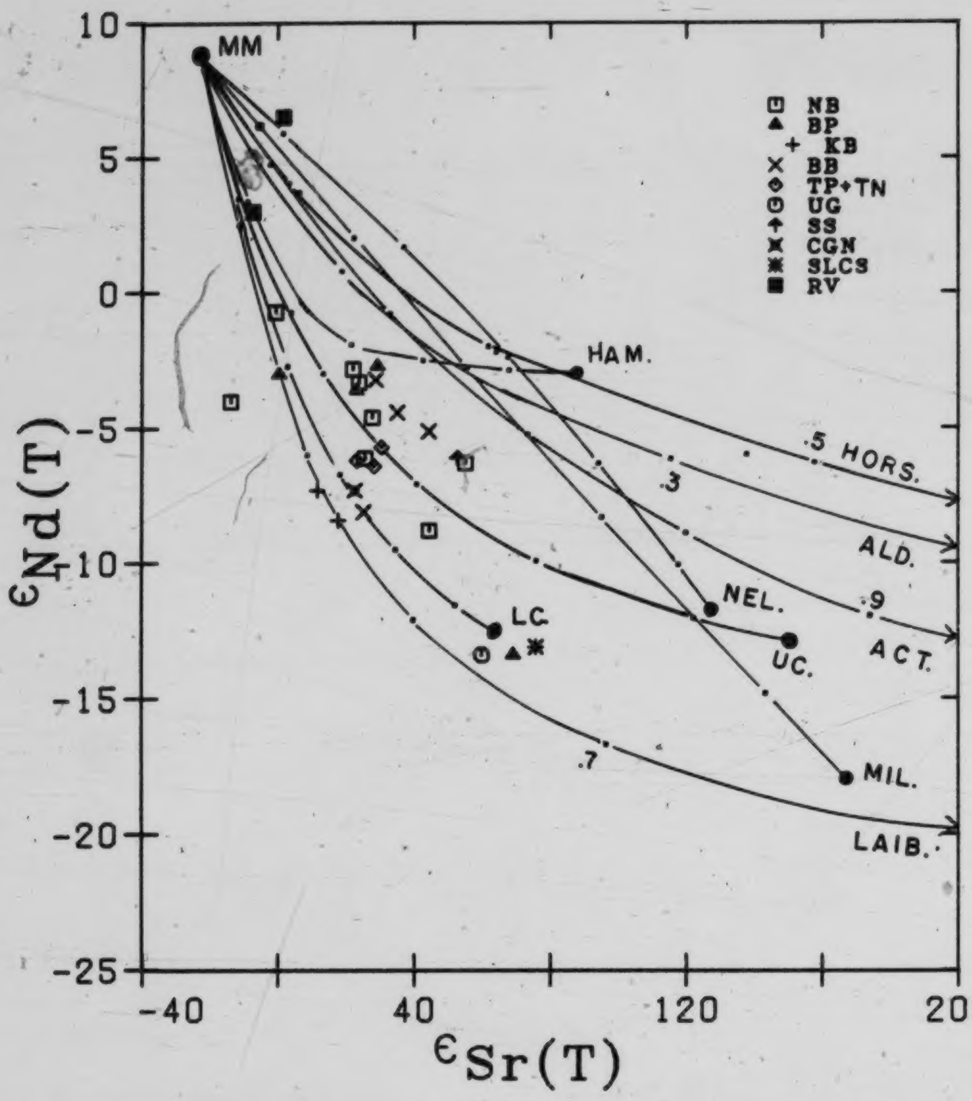

Fig 7.5. Simple binary mixing models: ϵ_{Nd} vs. ϵ_{Sr}. Each curve shows the result of mixing of mantle derived magma ($\epsilon_{Nd} = +8$, $\epsilon_{Sr} = -20$) and the particular crustal end-member. Table 7.5 shows the chemical parameters for all the crustal end-members used. From this Fig., it is seen that crustal end-members like the Aldridge Formation, Horsethief and Hamill Groups, Active and Nelway Formations are not likely to be potential contaminants. Only the model Lower and Upper Crusts are potential contaminants for some of the samples. Dots on each curve show the wt. fractions of crustal endmember at 10% interval.

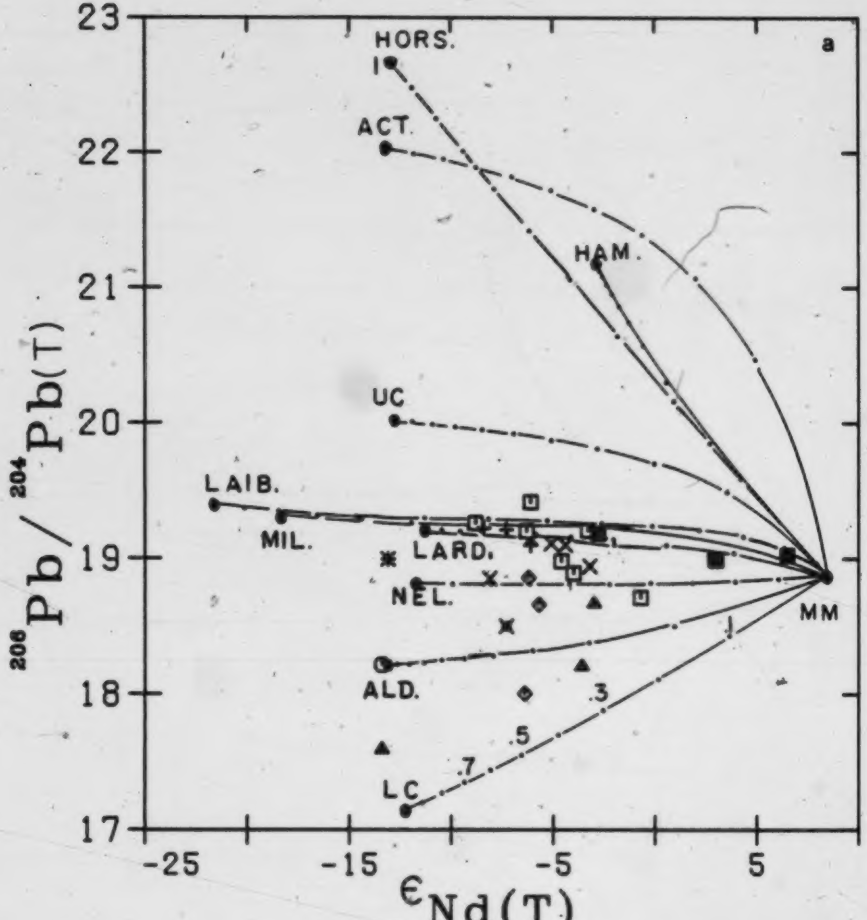

Fig. 7.6a-c. Binary mixing models: Pb vs. Nd. a. Mixing curves joining the mantle magma and the crustal show that the Laib, Lardeau, Milford-27 and Nelway sediments are the likely contaminants. b. Shows none of the sedimentary groups as a potential contaminant. c. Sedimentary groups like the Aldridge, Lardeau, Laib, Nelway and Active are the potential contaminants.

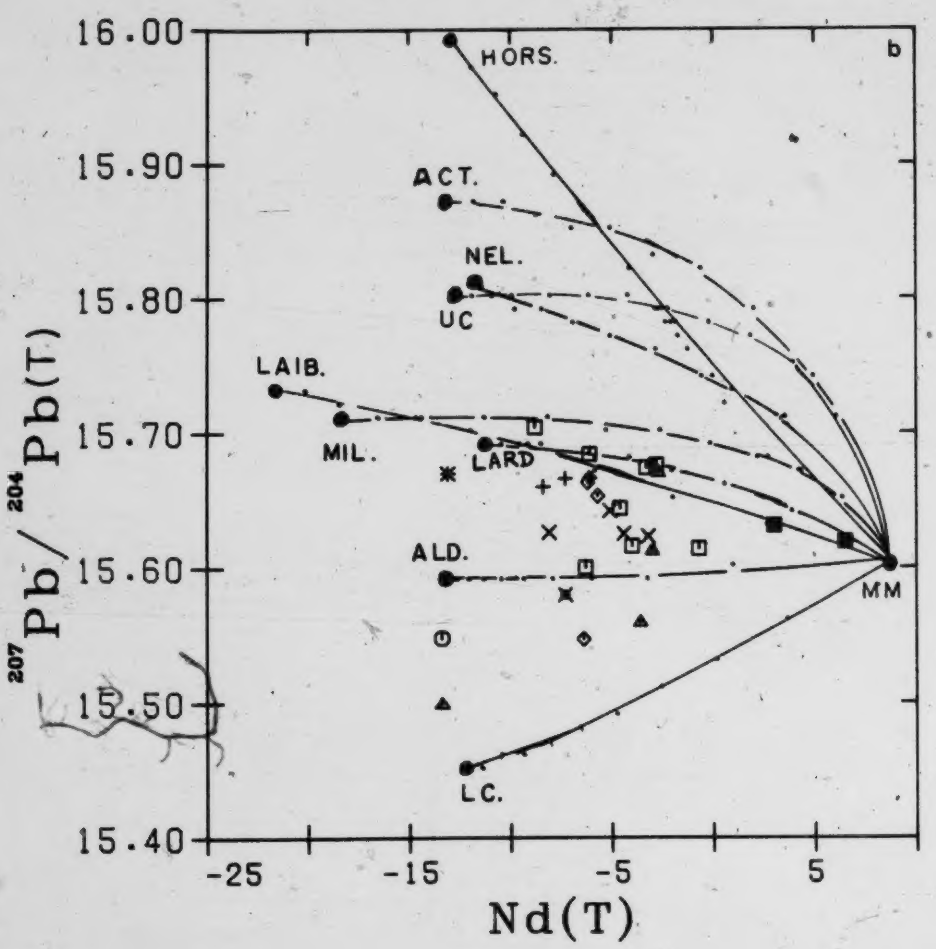
b
HORS.
ACT.
NEL.
UC
LAIB.
MIL.
LARD
ALD.
LC.
MM
16.00
15.90
15.80
15.70
15.60
15.50
15.40
-25
-15
-5
5
$^{207}Pb/^{204}Pb(T)$
Nd(T)

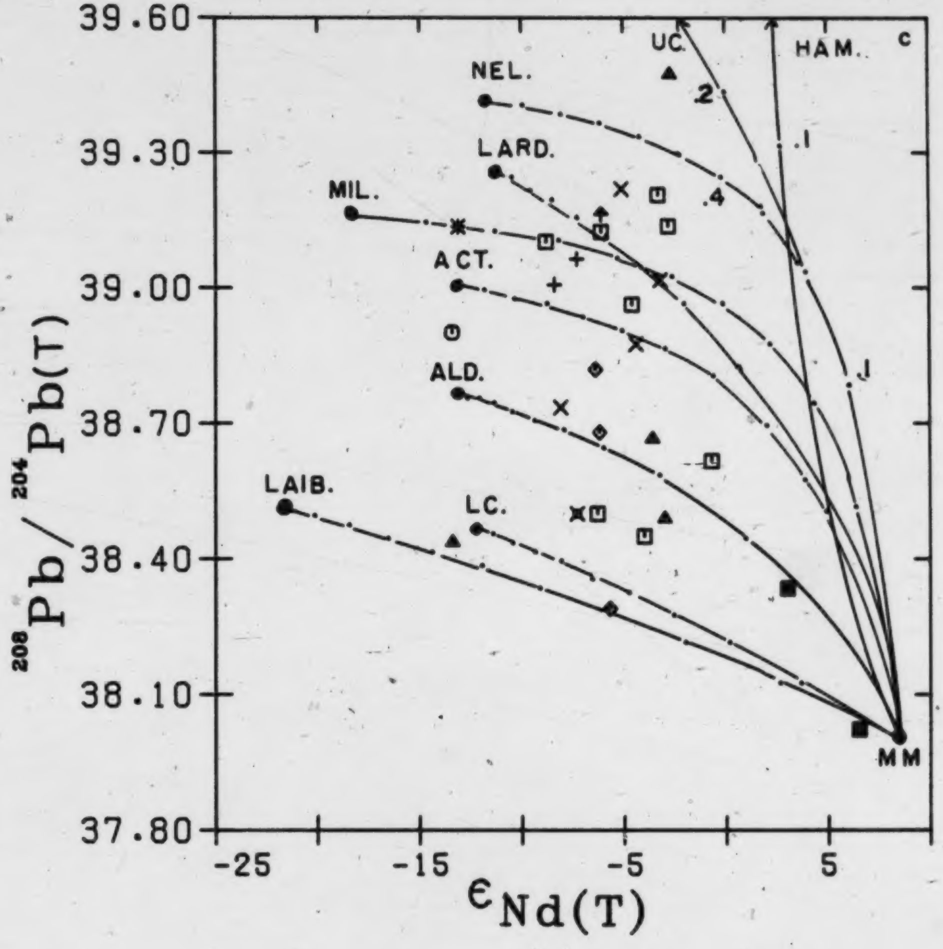
C
UC.
HAM.
NEL.
LARD.
MIL.
ACT.
ALD.
LAIB.
LC.
MM
.2
.1
.4
.1
39.60
39.30
39.00
38.70
38.40
38.10
37.80
-25
-15
-5
5
$^{208}Pb/^{204}Pb(T)$
$\epsilon_{Nd(T)}$

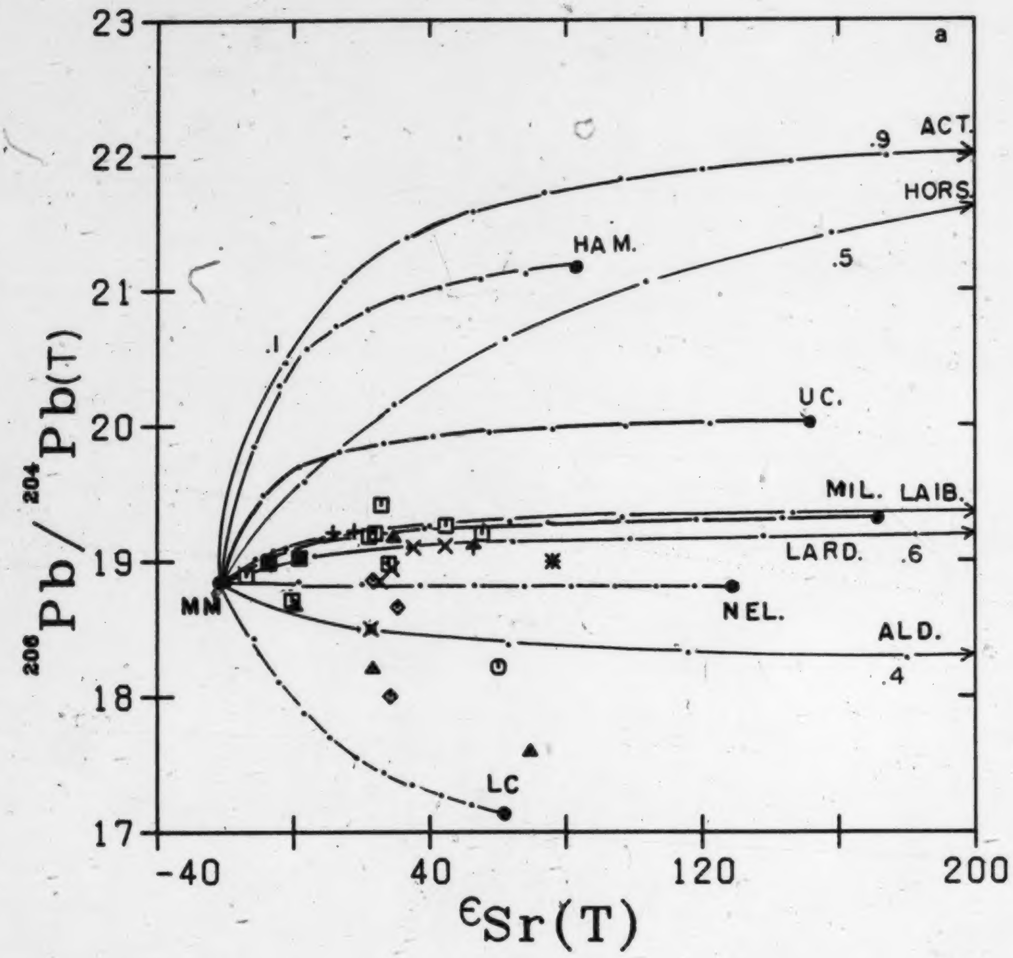

Fig. 7.7a-c. Binary mixing models: Pb vs. Sr. Likely contaminants are: a. Lardeau, Laib, Nelway, Milford and Lower Crust. b. Lardeau, Laib and Milford. c. Lardeau, Laib, Nelway, Active, Milford and Lower Crust.

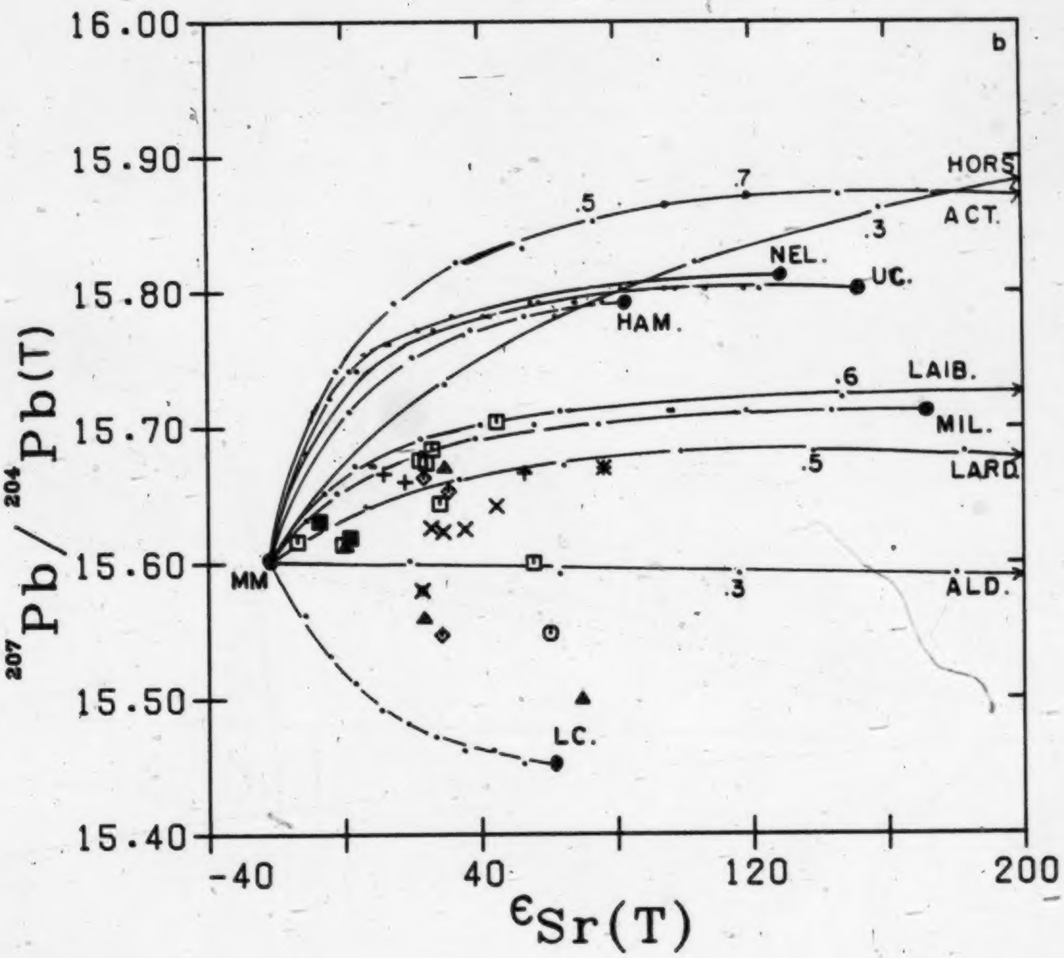
b
16.00
15.90
15.80
15.70
15.60
15.50
15.40
$^{207}Pb/^{204}Pb(T)$
-40
40
120
200
$\epsilon_{Sr}(T)$
HORS
ACT.
NEL.
UC.
HAM.
LAIB.
MIL.
LARD.
ALD.
LC.
MM
.7
.5
.3
.6
.5
.3

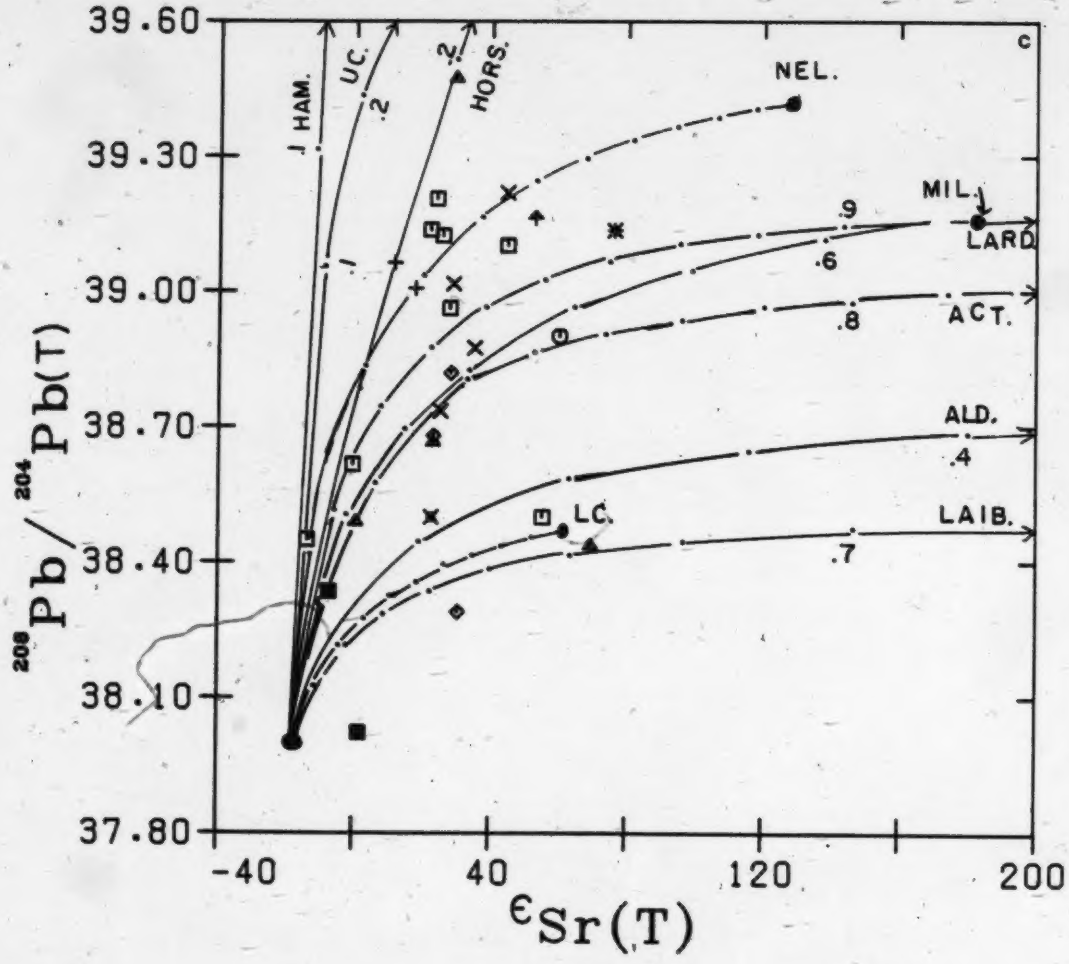
c
39.60
39.30
39.00
38.70
38.40
38.10
37.80
-40
40
120
200
$^{208}Pb/^{204}Pb(T)$
$\epsilon_{Sr}(T)$
HAM.
.1
UC.
.2
.2
HORS.
NEL.
MIL.
LARD
.9
.6
ACT.
.8
ALD.
.4
LC.
LAIB.
.7

Table 7.6 Summary of Results of Simple Binary Mixing Models

Diag.	ϵ_{Nd}-ϵ_{Sr}	Pb6/4-Nd	Pb7/4-Nd	Pb8/4-Nd	Pb6/4-Sr	Pb7/4-Sr	Pb8/4-Sr	ϵ_{Nd}-Nd	ϵ_{Sr}-Sr	Pb6/4-Pb
Fig.#	7.5	7.6a	7.6b	7.6c	7.7a	7.7b	7.7c	7.8	7.9	7.10
Ald	x	x	x	y	x	x	x	x	x	x
Hors	x	x	x	x	x	x	x	x	x	x
Ham	x	x	x	x	x	x	x	x	x	x
Lard	x	y	y	y	y	y	y	y	x	y
Laib	y	y	x	y	y	y	x	x	x	y
Nel	x	y	x	x	y	x	y	x	y	x
Act	x	x	x	y	x	x	y	x	x	x
Mil	x	y	x	y	y	y	y	x	x	y
UC	y	x	x	x	x	x	x	y	x	x
LC	y	x	x	y	x	x	y	y	x	x

y = possible contaminant, x = not a contaminant

From the above table, it is clear that the sedimentary rocks from the Milford and to some extent Lardeau, Laib and Nelway are the most likely contaminants. The other interesting point to note is that ^{208}Pb behaves very differently from the other two Pb isotopes. All the sedimentary units from the Lardeau to Milford Groups and the lower crust are required to explain ^{208}Pb data.

Similar mixing curves have been calculated for isotopes vs. elements as well. The three Figs. 7.8, 7.9 and 7.10 show the mixing curves for ϵ_{Nd} vs. Nd, ^{206}Pb/^{204}Pb vs. Pb and ϵ_{Sr} vs. Sr. From Fig. 7.8 it is seen that the UC, LC and Lardeau are possible contaminants. Figs. 7.9 and 7.10 show that the mixing with Nelway, Active, Milford and lower crust can explain a fraction of data. These commonly observed contradictory observations are taken to imply that the simple binary mixing models fall short of the complicated processes responsible for the isotopic and trace element compositions of the various batholiths/plutons. Therefore the next section discusses the AFC models.

7.9 Assimilation Fractional Crystallization(AFC) Models

7.9.1 ϵ_{Nd} vs. ϵ_{Sr} correlation

Fig. 7.11 shows the mixing lines for AFC modelling using Sr and Nd isotopes. Distribution of curves originating from the mantle end-member indicates that with different values of such parameters as r, F, nature of fractionating phases and related K_D's, a mantle magma undergoing fractional crystallization and assimilating a particular crustal end-member can acquire wide range of isotopic compositions. This is in contrary to simple binary mixing results when products of two-component mixing fall on a particular curve whose slope is determined by K-values (Fig 7.4). If D^{Nd} and D^{Sr} are of similar magnitudes, the curves will follow closely the simple mixing trajectory (DePaolo and Wasserburg, 1979). For the present case, it has been assumed that the fractionating phases are 35:65 mixture of cpx and hb in one extreme and only plag in another extreme. Even though the nature of the fractionating phases could be identified from the theoretical modelling, exact extent of the degree of fractionation

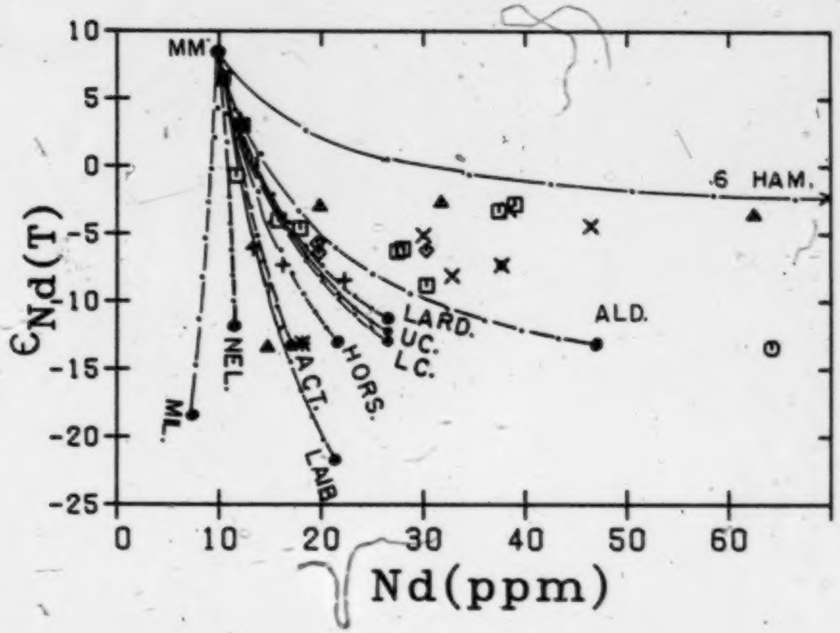

Fig. 7.8. Simple binary mixing model using the isotopes and elements. pair. $\epsilon_{Nd}(T)$ vs. Nd. Most sedimentary groups fail to explain the data. Only model crusts are seen to be the possible contaminants.

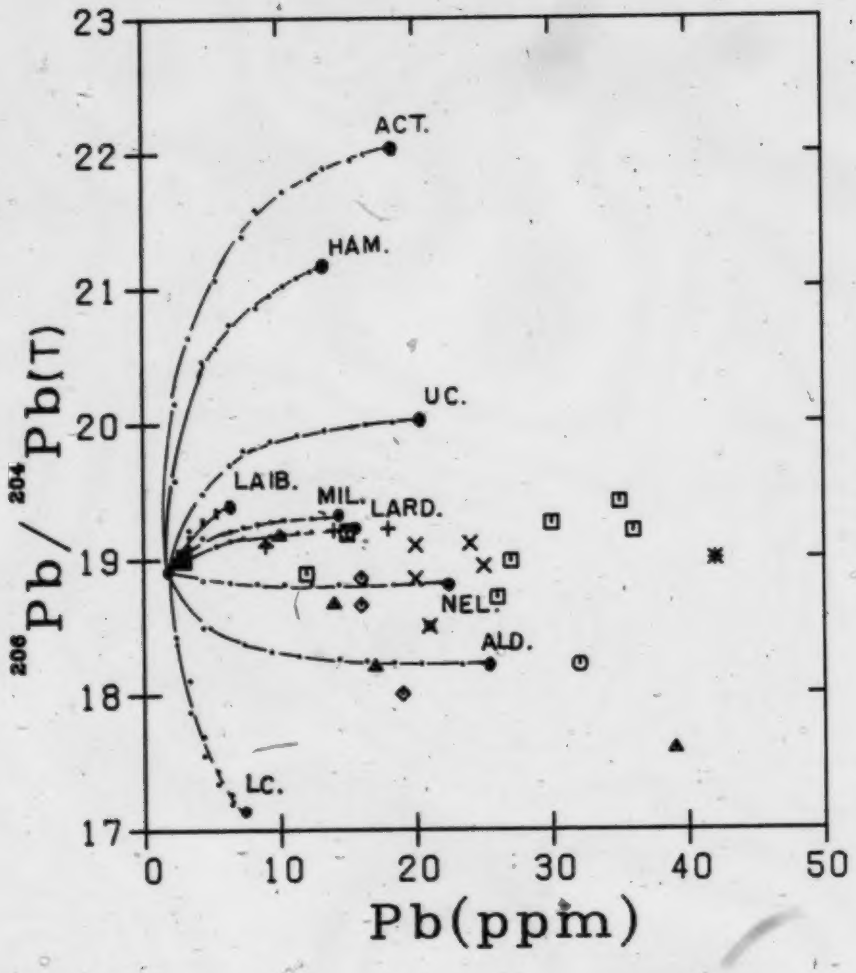

Fig. 7.9. ^{206}Pb/^{204}Pb(T) vs. Pb. Possible contaminants are Lardeau, Nelway and Milford.

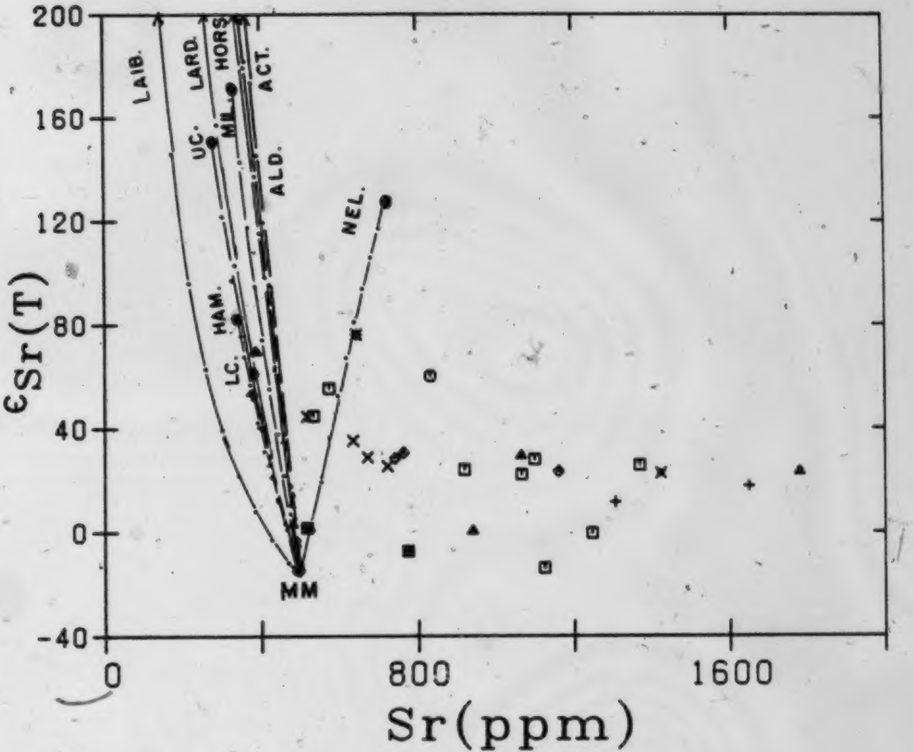

Fig. 7.10. $^{\epsilon}$Sr(T) vs. Sr. Only Nelway is the likely contaminant. A model LC with very high Sr ppm(1700), can explain bulk of the data, but such a Lower Crust composition is very unlikely.

can not be determined, but a close approximation can be given.

For low values of r (less than 0.3), if D^{Sr} is greater than D^{Nd} (i.e., only plagioclase is fractionating) there is a greater effect on ϵ_{Sr} than on ϵ_{Nd}. On the other hand, if $D_{Nd} >> D^{Sr}$ (i.e., if cpx or hb or both are fractionating) the reverse is true. For example, for $r=0.1$, with only plag fractionating, for F ranging from 0.1 to 0.9, there is only about 3 ϵ-units change in Nd, compared to 70 units change in ϵ_{Sr}. This limitation is controlled by eqn. (7.19): For this case $r=0.1$, $D^{Nd}(\text{plag})=0.14$, $C^{m}_{0}=10.0$, and $C_a=26.0$ the r.h.s. of the above eqn. becomes 0.25. The denominator on the l.h.s. is equal to -21.0, therefore $\Delta\epsilon_{Nd} = 0.25(-21.0) + 8.0 = +2.75$.

With r increasing however (>0.5) i.e., greater rate of crustal assimilation, the mixing curves converge towards each other, but still have very different isotopic effects. In general, plagioclase fractionation causes greater effects on ϵ_{Sr} (increasing) as well as Sr contents (decreasing) and combined cpx+hb fractionation decreases ϵ_{Nd} and Nd contents. The trends in isotopic patterns change drastically at low values of F (with $r>0.5$). For example, for the case of cpx+hb fractionation with $r=0.7$, the mixing curve flattens out at $F=0.3$ and ϵ_{Sr} increases dramatically without any effect on ϵ_{Nd}. The value of the parameter r probably depends on the depth of magma assimilation and also on heat balance considerations. At greater depth (lower crustal) mantle magma will be arrested due to its higher density than the overlying crust (Herzberg, et. al., 1983). and will undergo considerable fractionation and assimilation. The lower crust at this depth (>20 kms or >7 kbs) will be at a temperature close to melting. This underplating and consequent intrusion of basic magma into continental crust is likely to cause anatexis at the deeper regions producing granodioritic or granitic melts (Wyllie, 1983). The intermediate ϵ_{Nd} and ϵ_{Sr} values of the granitic samples (whether they are bi-hb or bi-musc granites) between the two end-members are the strongest evidence of the mantle input in the generation of the Cordilleran batholiths.

If it is assumed that the RV magma interacted with the lower crust, the two samples analysed have undergone least amount of assimilation. Sample 74/054 has much higher ϵ_{Sr} than the mantle array at $\epsilon_{Nd}=6.5$. If this deviation is due to later hydrothermal alteration, as

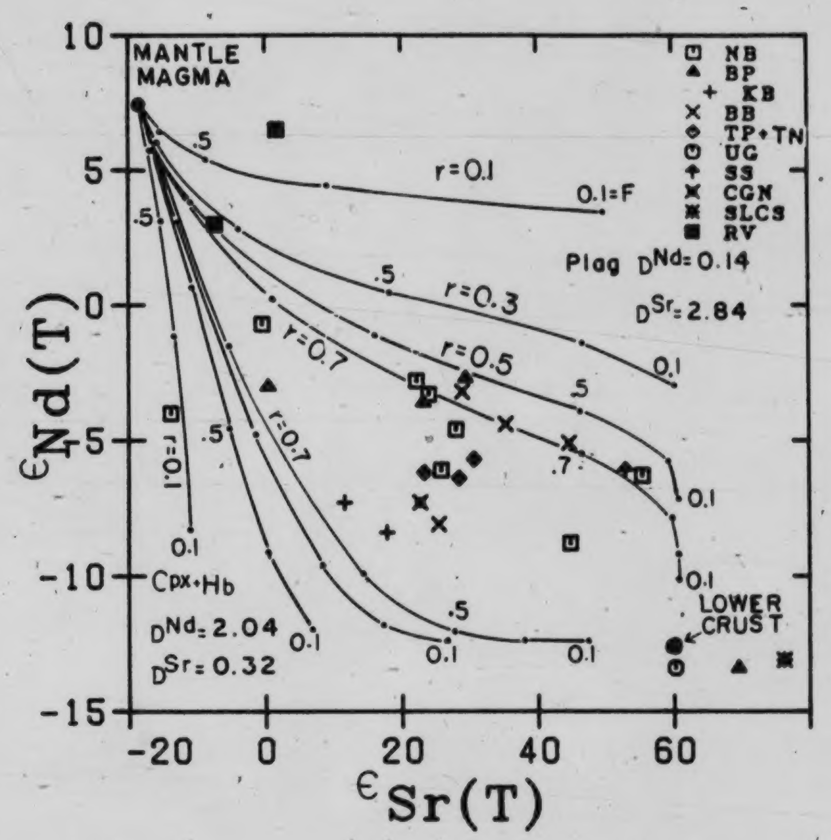

Fig. 7.11. ϵ_{Sr}-ϵ_{Nd} mixing lines for a mantle magma undergoing fractional crystallisation and assimilation with a lower crust. Solid circles represent the isotopic compositions of initial magma and wallrock. Two sets of curves have been drawn for fractionation of (i) plag. (right hand side) and (ii) cpx+hb (left hand side). For each curve r ($=M_a/M_c$) value and F (the relative amount of magma remaining) values are shown by dots. Mantle magma ($\epsilon_{Nd}=+8$, $\epsilon_{Sr}=-20$, Nd=10 ppm and Sr=500 ppm) is assumed to have undergone some fractionation before interacting with the lower crust ($\epsilon_{Nd}=-13.2$, $\epsilon_{Sr}=+60.0$, Nd=26 ppm and Sr=430 ppm). For modelling, $D^{Sr,Nd}$ for plag, cpx and hb are taken from Hanson (1978, 1980). See Fig. 7.12, for sample identification. Note that curves do not necessarily connect the endmembers, unlike binary mixing models.

discussed before, this sample represents a magma with only less than 10% (F=0.9) crustal contamination at r=0.1 (Fig.7.11) and undergoing small amount of plagioclase fractionation. The other sample 75/116 has undergone larger degree of contamination (r=0.3, F=0.75). This contradicts with its higher Sr ppm (722 compared to 515 ppm of 74/054) (Fig. 7.12). But if it is assumed Rossland magma interacted with upper crust, then its higher Sr abundance is due to cpx or hb fractionation. This is borne out by the fact that hb is present as phenocrysts in this sample whereas it is absent in 74/054. Both have similar Nd contents, however. This hypothesis of upper crustal contamination is also supported by geological evidence that the volcanic rocks ascend fast to the surface and therefore having least chance of assimilation with the lower crust. Pb isotopes also support this conclusion (see Chapter 8). But the presence of cpx and hb as phenocrysts suggests that ascent of magma chamber was temporarily halted at lower or mid-crustal depth. On the other hand, a lower crustal assimilation for the granitic batholiths is more viable considering the large degree of assimilation required on the basis of the isotopic data. Petrographically (see Table A1.1 and A1.2, Appendix 1) most of the metaluminous granites contain clinopyroxenes (though in small amounts) in their mode. Even some peraluminous granites have embayed cpx grains.

On Fig 7.3, a Pb-line has been drawn dividing samples into two groups: 1. those having Pb isotopic compositions less than (west of the line) and greater than (east of the line) the assumed mantle value. This Pb line is identified with a fundamental change in the paleogeography in the area as discussed before. This line has also been drawn on Fig. 7.12. Exception to this general trend are the two samples from the Kuskanax Batholith (with + symbols) and 8022B (alkaline rock from BP) which have Pb-isotopic compositions greater and less than the mantle value respectively.

It is seen from Fig. 7.11 that the samples which have assimilated the lower crust but have undergone predominantly cpx+hb fractionation are: 8052A(NB), 8021B(BP), 8049A(VG), 8033G and 8033P (KB). Samples which have undergone mainly plag fractionation are: 8053A, 8057B, 8059A, and 8061A from NB, 8075F(BP), 8038A, 8038D, 8038E from BB and 8007A from SS. The remaining samples (8065A(CGN), 8072A, 8073A from TP, 8070C

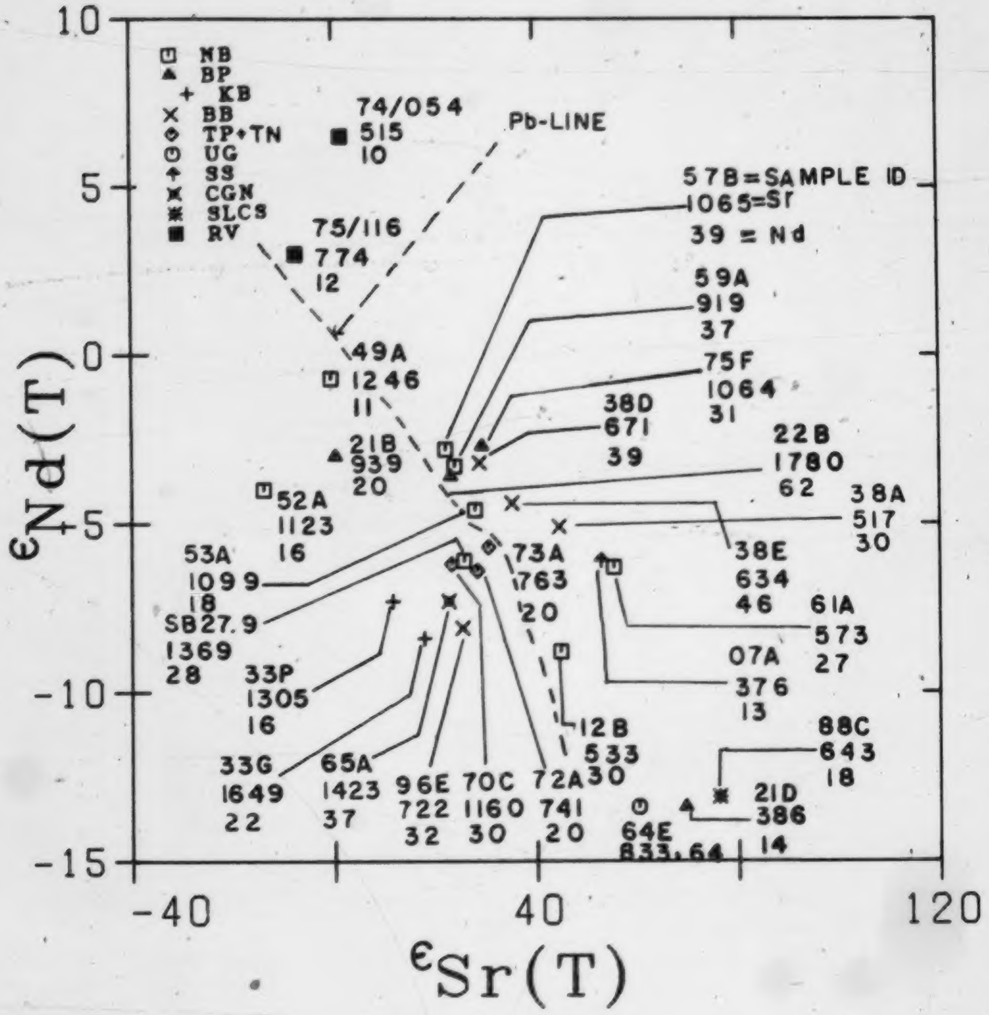

Fig. 7.12. Sr and Nd concentrations are shown for each sample.

(TG) and 8096E (BB), 8012B(NB)) show even greater rate of crustal assimilation ($\simeq$1.0). The r values vary from 0.1 to 0.9 for those samples whose isotopic compositions and trace element abundances have been controlled by cpx + hb fractionation. Sample 8052A (an alkaline rock) with $r=0.1$ represents about 20% of the original magma. Its low SiO_2 content (51.72 %) contradicts this observation. Its $\epsilon_{Sr} = -13.8$ and mantle-like Pb isotopic composition are strong evidence for its derivation from the mantle except its significantly low ϵ_{Nd} value($=-4.0$).

With further discussion it will be seen that the change in ϵ_{Nd} is not simply related to the degree of fractionation of the granitic samples. Samples 8049A and 8021B have undergone greater degree of assimilation ($r=0.7$ but with $F=0.88$). The Kuskanax Batholith samples show also higher rate of crustal assimilation ($r=0.9$ and $F=0.75$).

The samples which have undergone definitely plagioclase fractionation have a very narrow range in r (0.5 to 0.7) but represent different amounts of remaining magma (indicated by variable F).

It is interesting to note that the samples affected by plagioclase removal have lower Sr ppm and higher Nd ppm than those samples affected by cpx + hb fractionation. Both Sr and Nd ppms are shown on Fig. 7.12. This observation supports the validity of AFC model which could explain simultaneously both the isotopic compositions and trace element abundances. But it is not yet well understood how AFC will control major element chemistry of the evolving magmas.

Cpx + hb (35:65 mix) have greater D^{Nd}(2.04) and smaller D^{Sr}(0.32) than those for plagioclase ($D^{Nd}=0.14$, $D^{Sr}=2.84$) (Table 7.7). Therefore it is expected that the samples affected by cpx + hb will have higher Sr and lower Nd concentrations than those affected by plagioclase only. This expected pattern is clearly evident from the Fig. 7.12 (see also Table. 7.1). In this case, samples affected by cpx + hb separation have Nd ppm less than 22 and those affected by plag. separation have Nd > 27 ppm. There are some execptions. For example, sample 8021B has lower Sr ppm (939) than the sample 8022B (1780) and 8075F (1064), contrary to what is expected. But their Nd concentrations follow the expected trend. These observations might suggest either (1) they had different source compositions or (2) they have

Table 7.7 Distribution Coefficients used for AFC modelling.

Element	Plag	Cpx	Hb	35Cpx + 65Hb	Reference
Rb	0.048	0.032	0.0077		Hanson, 1978.
Sr	2.84	0.516	0.22	0.32	,,
Sm	0.11	0.95	3.99		Hanson, 1980.
Nd	0.14	0.65	2.80	2.04	,,
Pb	0.01	0.01	0.01		Leeman, 1981.

undergone more complex AFC than being envisaged here. The evidence for the former idea comes from the very alkaline nature of the sample 8022B and also its trace element chemistry (Table 7.1 and also Table A2.2.1 A2.2.2, Appendix 2). The other interesting observation is that the samples can acquire higher and lower concentrations of Nd and Sr than the end-members themselves. This is only possible in case of AFC models. Simple binary mixing will produce compositions having values for all the elements and isotopes intermediate between the two end-members.

7.9.2 ϵ_{Sr} vs. Sr correlation.

A negative correlation between Sr-initial ratios and Sr concentrations for a suite of batholithic samples from an area is thought to indicate crustal assimilation and fractional crystallization (Cox el. al., 1979, Halliday, 1983). Granitic batholiths exposed in the Nelson-Rossland Arc have generally very high Sr and Ba concentrations. (Table A2.2.1 and A2.2.2, Appendix 2). In particular a suite of samples (8022-group) from the Bonnington Pluton have Sr concentrations >1700 ppm and Ba >2500 ppm but with only about 55% SiO_2. Samples from the Kuskanax Batholith also have Sr >1200 ppm and Ba >1700 ppm. These unusually high contents of Sr and Ba and some other trace elements are not generally found in calc-alkaline batholiths produced at the continental margins (Atherton et al., 1979; Hawkesworth, 1979; Tarney and Saunders, 1979).

Two general models beside AFC could be invoked to explain these unusually high Sr and Ba abundances: (1) either almost total melting of a source with extremely high Sr and Ba concentrations i.e., having plagioclase as the main constituent and (2) or partial melting of less plagioclase-rich source followed by extensive fractionation of phases with $D^{Sr} \simeq 0$. Both the alternatives could be discarded on the basis of isotopic evidence. A simple two component mixing model will be adequate only if a component is found with a very high Sr ppm (>2000) and Ba ppm (>2800). This is extremely unlikely. Following is a discussion of AFC models using Sr-initial ratios and Sr concentrations. Figs. 7.13a-e show the ϵ_{Sr} values and Sr concentrations and the curves describing possible shifts in ϵ_{Sr} and Sr at various values of r (0.1

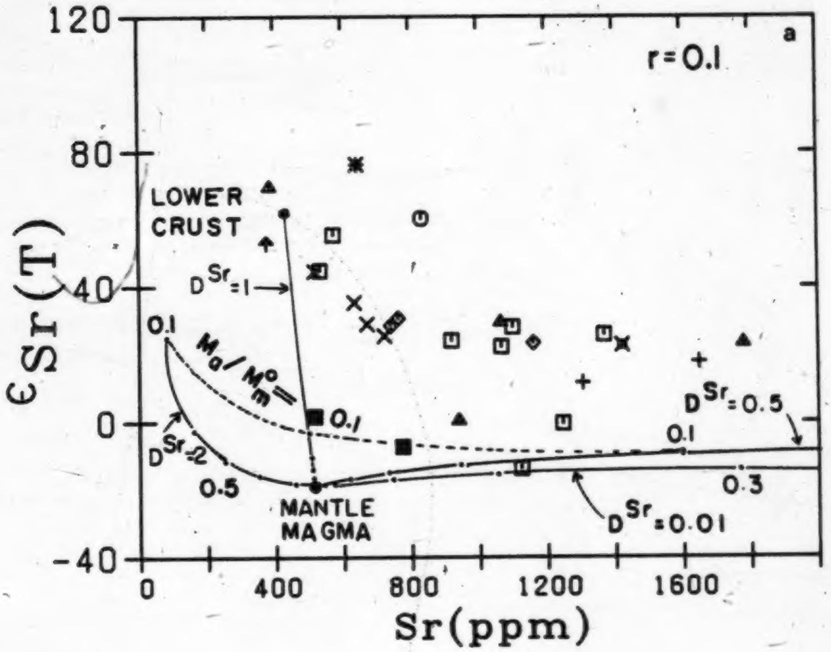

Fig. 7.13. The ϵ_{Sr}-Sr mixing curves for a mantle magma affected by AFC. Mantle and crustal endmember compositions are the same as those of Fig. 7.11. Five different cases are shown (a to e) for different r values (0.1 to 0.9). D^{Sr} values used were those tabulated by Hanson (1978). For each r value, AFC mixing curves are shown for D^{Sr} values from 0.01 to 2. Dots on each curve are F values at intervals of 0.2. With r value increasing or D^{Sr} approaching 1, AFC curves converge to the simple mixing line ($D^{Sr}=1$). The dashed-dotted lines represent isopleths for the relative amount of assimilated crust. M_a/M_m° values at each r value are also shown.

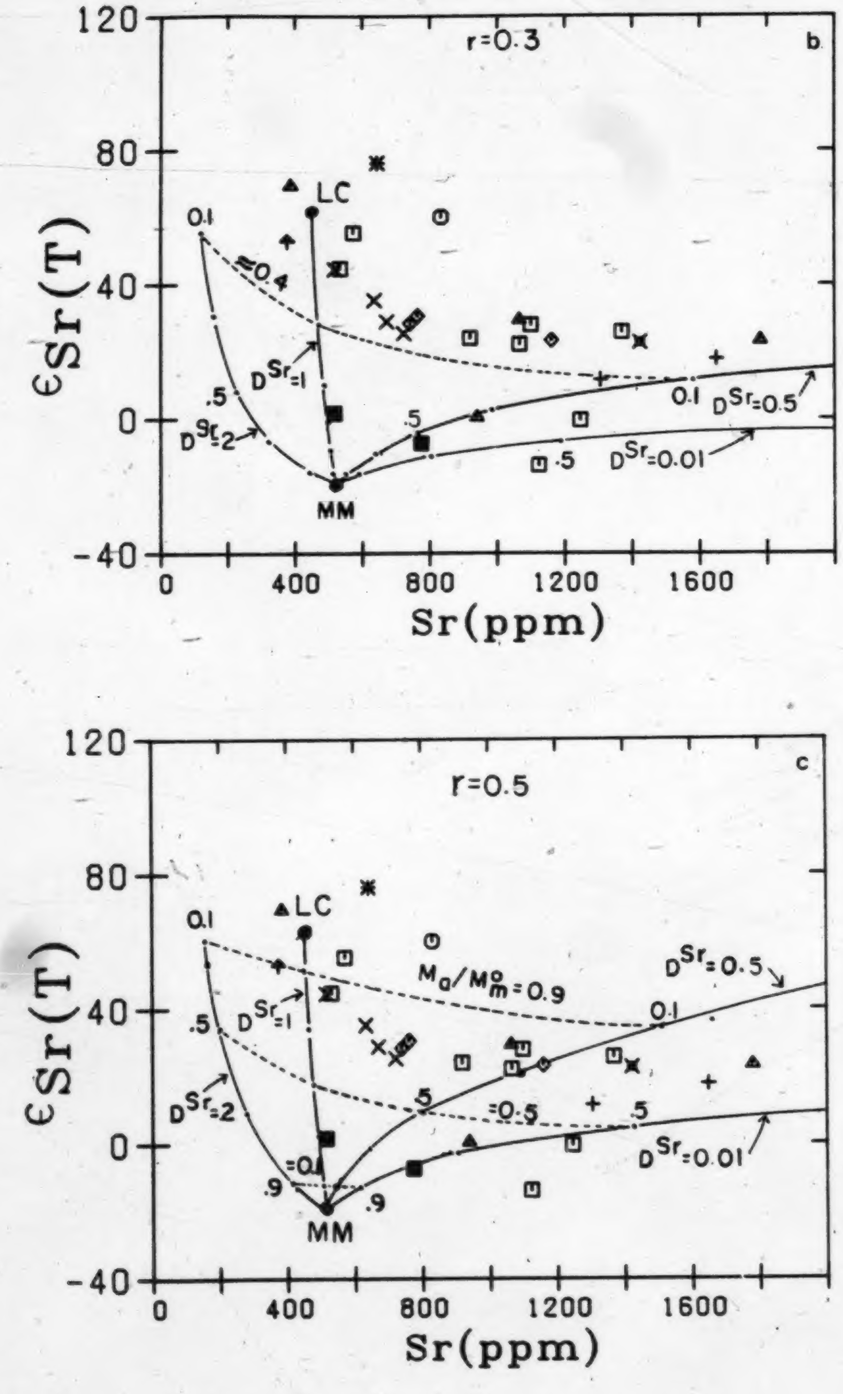
r=0.3
b
LC
MM
0.1
=0.4
.5
$D^{Sr}=1$
$D^{Sr}=2$
.5
0.1
$D^{Sr}=0.5$
.5
$D^{Sr}=0.01$
$\epsilon_{Sr}(T)$
Sr(ppm)
120
80
40
0
-40
0
400
800
1200
1600
r=0.5
c
LC
MM
0.1
.5
$D^{Sr}=1$
$D^{Sr}=2$
$M_a/M_m^o=0.9$
$D^{Sr}=0.5$
0.1
.5
=0.5
.5
=0.1
.9
.9
$D^{Sr}=0.01$
$\epsilon_{Sr}(T)$
Sr(ppm)
120
80
40
0
-40
0
400
800
1200
1600

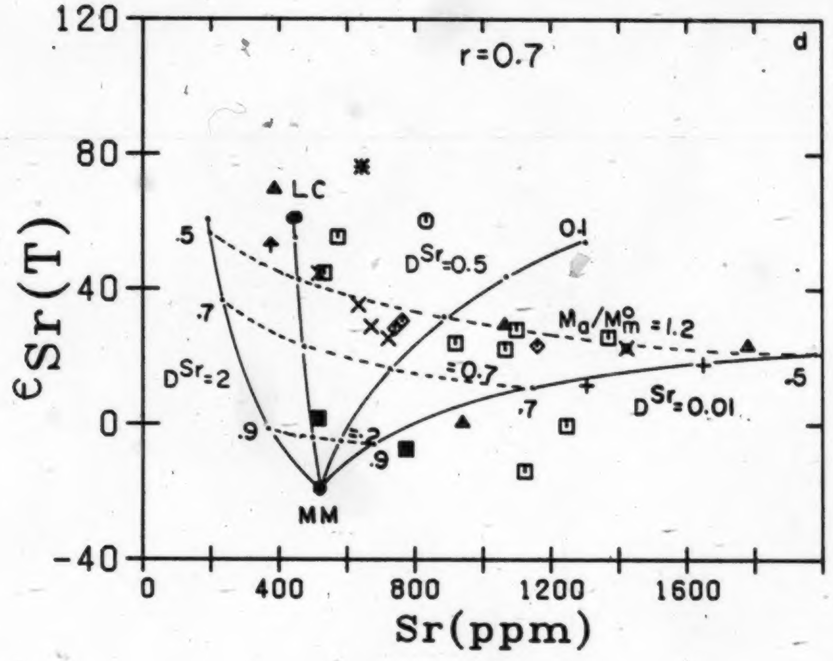
r=0.7
d
120
80
40
0
-40
0
400
800
1200
1600
εSr(T)
Sr(ppm)
LC
MM
.5
.7
.9
D^Sr=2
D^Sr=0.5
0.1
Ma/M°m=1.2
=0.7
=2
.7
.9
D^Sr=0.01
.5

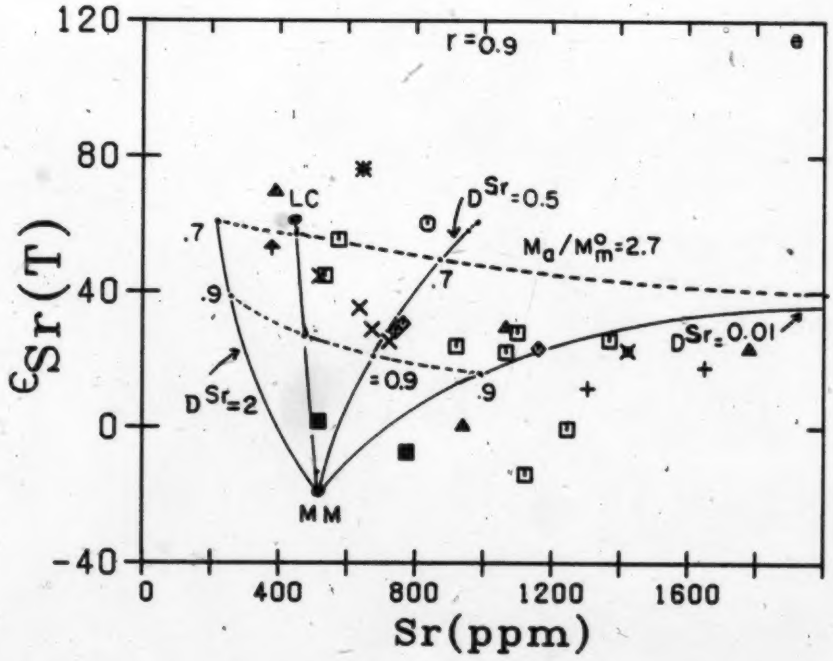
r=0.9
e
120
80
40
0
-40
0
400
800
1200
1600
εSr(T)
Sr(ppm)
LC
MM
.7
.9
D^Sr=2
D^Sr=0.5
Ma/M°m=2.7
.7
=0.9
.9
D^Sr=0.01

to 0.9), for a mantle magma (ϵ_{Sr} = -20.0, Sr = 500.0 ppm) undergoing concomitant fractional crystallization and assimilation of a model crust (ϵ_{Sr} = 60.0, Sr = 430.0 ppm). From the earlier diagram (Fig. 7.11), it was shown that most samples had r values >0.5 . It will be also shown here that greater r values (>0.5) are required to explain the data.

The parameters that control the shape of the curves are r, the ratio of the mass rate of assimilation to the mass rate of crystallization, D^{Sr}, the bulk solid/liquid partition coefficient for the crystallizing (fractionating) phases from the magma. Tick marks on the curves are the F values ($F = M_m(t)/M_m^o$ i.e., ratio of the mass of magma remaining at any time to the original mass). This F value could be converted to another important parameter M_a/M_m^o by using the following equation:

$$M_a/M_m^o = r(F-1)/(r-1) \quad \text{.......} \quad (7.20)$$

Farmer and DePaolo, 1983). Isopleths with a particular value of M_a/M_m^o are also shown on each diagram with a particular r value. These isopleths clearly show the rate of increasing assimilated mass away from the mantle end-member.

From the Figs. 7.13a and 7.13b, with r = 0.1 and 0.3, it is seen that though the data could be explained theoretically but only with unrealistic values of such parameters as F and M_a/M_m^o. For example with r = 0.1, all the samples with Sr >800 ppm needs D^{Sr} = 0.75, indicative of significant plagioclase fractionation) and M_a/M_m^o >0.9 and F less than 0.4. Similarly for r = 0.3, most of the samples plot above the isopleth M_a/M_m^o = 0.9, and samples with very high Sr ppm represent only about less than 30% of the original magma mass. These high values of M_a/M_m^o required to explain the data with low r values (0.3) are not compatible with the conclusions drawn from Fig. 7.11 where r values >0.5 were needed. And also F values in the range of 0.7 to 0.9 required to explain the data in Fig. 7.11 are higher than very low values (less than 0.4) obtained from Fig. 7.13c. Therefore low r values (0.1 and 0.3) cannot satisfactorily explain the data. Only sample(8052A) compatible with very low rate of assimilation (r = 0.1) and virtually no plagioclase fractionation comes from the most basic unit of the Nelson Batholith (8052-group). This sample has lowest ϵ_{Sr} = -13.6 among all other granitic samples. This observation has also been confirmed from Fig. 7.11. For most of the samples, if larger r values are considered (0.5 to 0.9), similar values of other parameters such as D^{Sr}, F and M_a/M_m° are obtained from both types of diagrams (Figs. 7.11, 7.13c, d and e).

In Fig. 7.13c ($r=0.5$), samples with low $\epsilon_{Sr}(T)$ values and moderately high Sr concentrations between (600 to 1400) [i.e., samples 75/116, 8021B, 8049A, 8033G, 8033P] plot close to the mixing curve with $D^{Sr}=0.01$ i.e., these samples did not undergo any plagioclase separation as was confirmed from ϵ_{Sr} vs. ϵ_{Nd} correlation. They also have M_a/M_m° values lying between 0.7 and 0.1, indicative of lesser mass of crust assimilated. These samples represent 45% to 80% of the original magma mass. Samples with higher $\epsilon_{Sr}(T)$ values plot above or close to the $M_a/M_m^\circ = 0.7$ isopleth (not shown) and have corresponding F values around 0.3. They have undergone significant plagioclase fractionation ($D^{Sr} \approx 0.5$). Samples in this group include 8059A, 8057B, 8053A, 8075F, 8070C, SB29.7 and 8065A.

Granitic samples having even higher $\epsilon_{Sr}(T)$ and lower Sr ppm belong to the Trail Pluton, Bayonne Batholith, Summit Stock and the central part (8012B) and the southern tail (8061A) of the Nelson Batholith. These samples must have undergone predominantly plagioclase fractionation with $D^{Sr} > 0.5$ to 1.1. They also contain significant mass of of assimilated material ($M_a/M_m^\circ = 0.7$ to 0.9), if $r=0.5$ is correct. These high M_a/M_m° values are consistent when considered in combination with Nd isotopes, as these samples have much lower $\epsilon_{Nd}(T)$ values i.e., closer to the lower crustal value ($= -13.0$).

Similar conclusions are arrived at when the case $r=0.7$ (Fig. 7.13d) is considered. At this high r value, most samples plot between the isopleths, $M_a/M_m^\circ = 1.2$ and 0.7 and between F values from 0.5 to 0.7. These moderate values of the model parameters are probably more consistent with intermediate isotopic compositions of the samples.

If the case of $r=0.9$ (Fig. 7.13e) is considered, samples with lowest $\epsilon_{Sr}(T)$ cannot be explained by AFC as they fall outside the area affected by AFC. Also most of the samples plot in between the M_a/M_m° isopleths 0.1 and 0.2 and have very high F values (≈ 0.85). These parameter values are either too low or too high to be realistic and also contradict observations made in Fig. 7.11.

From the above discussion it is now clear that intermediate values of r (0.5 to 0.7 or up to 0.9 in some cases) could best explain the data array even though there are minor discrepancies among conclusions drawn from the two sets of Figs. 7.11 and 7.13c, 7.13d.

Nelson Batholith samples have a wide range in Sr concentrations from 500 to 1400. This variation could be due to a single stage contamination and crystallization process as discussed above. Alternatively an upper level plagioclase fractionation could also be responsible to lower Sr abundances. This stage could represent a chemical (but not isotopic) evolution. It is not possible to establish these processes on the basis of Sr-isotopes only. Clear evidence of upper crustal isotopic contamination exists for Pb isotopes.

There is a general tendency for $\epsilon_{Sr}(T)$ to increase eastward (inland). For example, the Bayonne Batholith samples have higher $\epsilon_{Sr}(T)$ than other batholiths to the west. Though the increase is small there remains two possibilities for this increase: (1) a regular inland increase in ϵ_{Sr} in the crustal end-member or (2) an inland increase in the proportion of incorporated crustal rocks. Case (2) has been discussed with respect to ϵ_{Sr} vs. Sr correlation, where a single lower crustal end-member has been considered. If it is true the crustal end-member has a fixed composition, then for Bayonne Batholith samples an inland increase in M_a/M_m° is required to explain the data.

7.9.3 $\epsilon_{Nd}(T)$ vs. Nd correlation.

Similar to $\epsilon_{Sr}(T)$ vs. Sr, an AFC model has been tested for $\epsilon_{Nd}(T)$ vs. Nd correlation. Fig. 7.14 shows the data array and the mixing curves as a result of AFC. Only two cases of $r=0.5$ and 0.7 have been considered here with different D^{Nd} values (from 0.1 to 1.0). It is seen that the data are compatible with r values between 0.5 and 0.7 but with a wide range of D^{Nd} values. For $r=0.7$, most of the samples fall in between curves with D^{Nd} values of 0.3 to 0.65. Samples of lower Nd concentrations (less than 25 ppm) are due to significant cpx ($D^{Nd}=0.65$) or cpx+hb fractionation. Samples with increasing Nd concentrations correspondingly show effects of less and less cpx an hb fractionation. This general pattern is consistent with what has been established from Sr and Nd isotopic correlation. Again for a two component

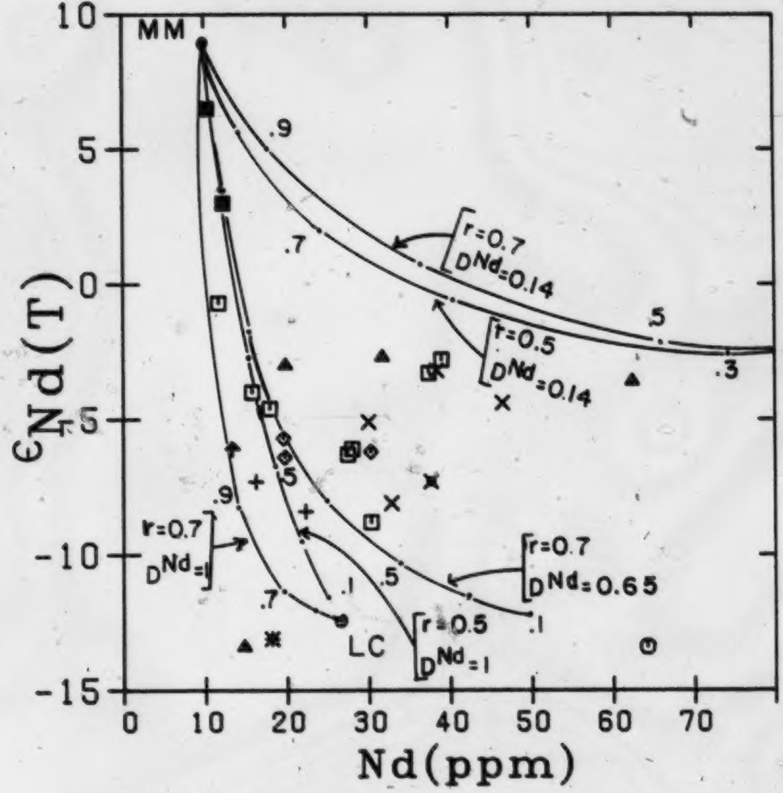

Fig. 7.14. ϵ_{Nd}-Nd mixing curves for assimilation fractional crystallisation in a magma chamber. For plagioclase fractionation ($D^{Nd}=0.14$), two curves are shown for two r values (0.5 and 0.7). For cpx+hb fractionation, for $r=0.5$, curve for $D^{Nd}=1.0$ and for $r=0.7$, curves for $D^{Nd}=0.65$ and 1.0 are shown. F values are shown by dots on each curve. For endmember compositions see Fig. 7.11.

mixing to be valid the crustal end-member will have to have very high Nd contents similar to the sample (8064E, 65ppm). Even though a lower crust with such a high Nd ppm might exist, it is not likely on the basis of Nd contents of the two samples representing the local lower crust (8021D and 8088C) and a large number of studies made on the lower crustal composition (Taylor, 1977; Jacobsen and Wasserburg, 1979; McCulloch and Wasserburg, 1978). Lower crust has an average Nd concentrations of 26 ppm (Bielski-Zyskind et al., 1984). Increasing Nd concentrations but with similar ϵ_{Nd} values are compatible with a petrogenetic model where differentiation postdates or is contemporaneous with mixing.

One discrepancy observed here is that D^{Nd} as high as 2.04 (due to 35% cpx and 65% hb) is not required. Maximum D^{Nd} needed to explain the lowest Nd concentrations is about 1.00. As D^{Nd} for cpx is 0.65 (Hanson, 1978), a greater bulk distrbution coefficient for Nd than 0.65 suggests fractionation of another phase with higher D^{Nd} than 0.65. Such a likely phase is amphibole ($D^{Nd}=2.80$, from Hanson, 1980). This supports the fact that hb was fractionating along with Clinopyroxene. In modelling granitic samples using combined Nd and Sr isotopes, a D^{Nd} value of 2.04 (corresponding to 35% cpx + 65% hb) was used. This relative proportion of the two phases has been arbitrarily fixed to represent an extreme case. In reality other combinations are possible as liquidus phase relationships undergo considerable change during evolution of a magma body.

7.9.4 ϵ_{Sr} vs. Rb/Sr relationship

Fig. 7.15 shows shifts in ϵ_{Sr} and $^{87}Rb/^{86}Sr$ in a magma affected by assimilation and fractional crystallization. For the calculations an initial magma with Rb=20 ppm and Sr=500 ppm has been mixed with a model crust having Rb=24 ppm and Sr=430 ppm (Bielski-Zyskind et al., 1984). $^{87}Rb/^{86}Sr$ ratios for the two end-members are therefore 0.117 and 0.163 respectively. (see also the Fig. caption). Trajectories shown are for $r=0.5$ and 0.7 and for different values of $D^{Sr}=0.01$, 0.25, 1.0 and 2.0. A small but constant value of $D^{Rb}=0.05$ was assumed for simplicity. Curves with very small D^{Sr} (0.01), fall on the left hand side of the simple mixing line. Samples plotting on this side will be in theory plagioclase cumulates, while

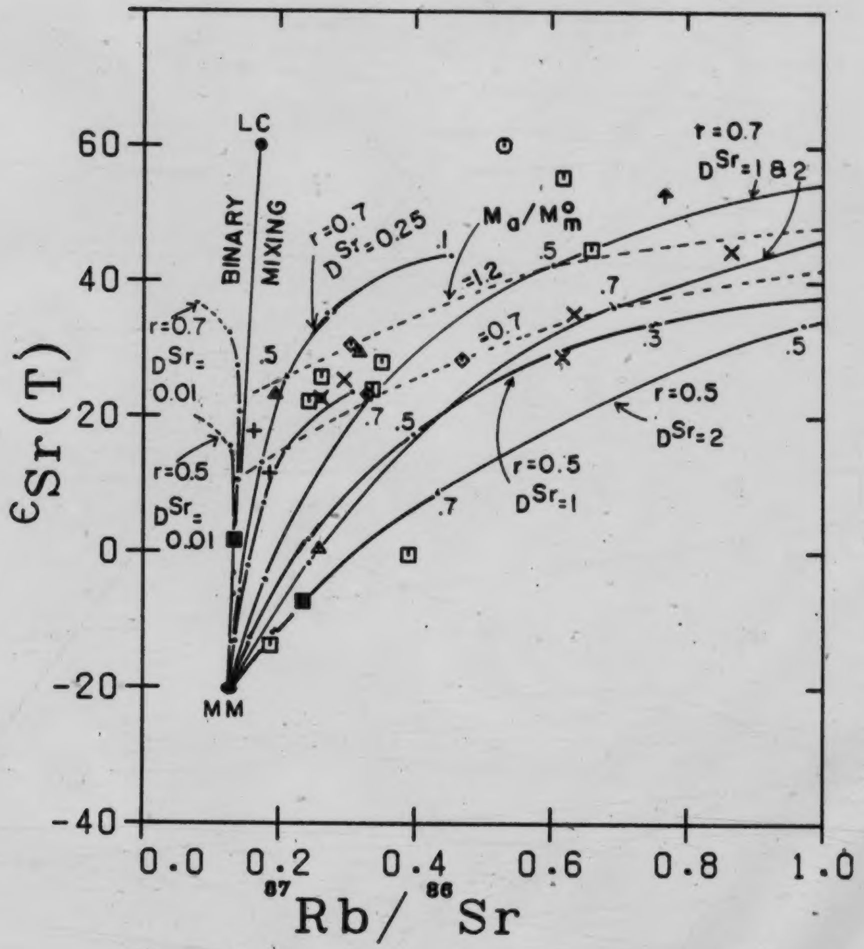

Fig. 7.15. The ϵ_{Sr} vs. Rb/Sr plot showing the curves describing the possible shifts in ϵ_{Sr} and $^{87}Rb/^{86}Sr$ at various r values and D^{Sr} (0.01, 0.25, 1.0 and 2.0). All the samples plot to the right of the two-component mixing line, and are bounded by the two isopleths, for the relative amount of crust assimilated, M_a/M_m° (0.5, 0.7). F values at intervals of 0.2 are shown by dots. End-member compositions are same as those mentioned in Fig. 7.11. D^{Rb} was taken to be 0.05 for simplicity. Plagiclase-rich cumulate rocks could lie to the left of the simple mixing line, e.g., curves with $r=0.5$ and 0.7 and $D^{Sr}=0.01$.

position of a sample on the right hand side of this line is controlled by physical parameters inherent in the model (e.g; D^{Sr}, D^{Rb}, F, M_a/M_m^o). DePaolo (1981c, Fig. 4) has shown that for a given r value, increasing $\epsilon_{Sr}(T)$ is associated with increasing Sr concentrations and low Rb/Sr as long as D^{Sr} is small (<0.25). For example, for the trajectory r=0.7 and $D^{Sr}=0.25$, samples plotting above the trajectory (8033G and 8033P) have higher Sr concentrations than those samples plotting below. Most of the samples plot to the right of the simple mixing line and therefore have undergone variable degrees of plagioclase fractionation. Samples with high Sr concentrations lie in between the trajectories with $D^{Sr}=0.25$ and 1.0 for r=0.7, while samples with low Sr concentrations plot far to the right and are bounded by curves with $D^{Sr}=$ 1.0 and 2.0 and r=0.7, suggesting significant plagioclase fractionation. These samples also tend to have higher $\epsilon_{Sr}(T)$, a fact in conformity with their low F values (less than 0.7) and consequently higher M_a/M_m^o.

For the trajectory r=0.7, M_a/M_m^o isopleths have been drawn for two values 0.7 and 1.2. Most of the samples are bounded by these two isopleths and therefore a 1.5 to 0.8:1 mixture of mantle and crust is suggested. This observation is also supported by AFC modelling of Fig. 7.13. A major discrepancy between Fig. 7.15. and Fig. 7.11 is with respect to the samples 8049A and 8021B. Both seem to have undergone significant plagioclase fractionation (r=0.5, D^{Sr} >2.0 and r=0.7, D^{Sr} >2.0) according to Fig. 7.15, but none at all according to Fig. 7.11. This type of contradictory behaviour is also observed for samples with respect to Sm/Nd fractionation (see below).

It has been known for a long time that good WR Rb-Sr isochron is difficult to obtain for a suite of samples from any batholith in the Nelson-Rossland Arc (Nguyen et al., 1968, Duncan et al., 1979, and this study). This failure is now fairly well understood if AFC modelling is accepted as a major geochemical process responsible for the variations in most chemical parameters. In particular, the AFC model explains the very high Sr concentrations of the granitic samples with very low Rb/Sr ratios and generally high Sr-initial ratios.

7.9.5 Oxygen Isotopes

A note of caution probably comes from oxygen isotopic data. Even though the present study on O-isotopes (Table 7.8) shows some samples of BP and BB have undergone hydrothermal O-isotopic exchange, no systematic relationships have been found between O and other isotopes. For example, both the hydrothermally unaltered (8038D) and altered (8038A) samples from the Bayonne Batholith have similar Nd and Pb isotopic compositions. For the Bonnington Pluton, the sample 8021B (unaltered) has similar $\epsilon_{Nd}(T)$, and $^{208}Pb/^{204}Pb(T)$, but slightly higher $^{207,206}Pb/^{204}Pb(T)$ values than the altered sample (8022B). They have however very different $\epsilon_{Sr}(T)$ values, i.e, 8021B (unaltered) has lower $\epsilon_{Sr}(T)$ than 8022B (altered), exactly opposite to that seen in the Bayonne Batholith samples. The highly siliceous sample (8021D, with $SiO_2=73.88$) has lowest Nd and Pb and high Sr isotopic compositions, similar to those of a lower crust. As its Nd isotopic composition clearly shows its derivation from the melting of a lower crust, highly altered nature with respect to O-isotopes probably did not affect other isotopic compositions. Moreover oxygen isotopic exchange is very selective on meter scale. Therefore even though it remains a possibility, systematic Nd and Sr isotopic behaviour of the granitic samples from different batholiths/plutons suggests predominant effects of AFC. It remains to be seen or proved that such hydrothermal alteration mostly taking place at the shallow level could explain all the aspects of both isotopic and trace element chemistry. Decoupling of Pb isotopic contamination from both Sr and Nd is sometimes related to upper crustal hydrothermal effects as shown by Vitrac et al., 1981.

The most recent and extensive oxygen isotopic study of Magaritz and Taylor (1986) shows that strong ^{18}O depletions are seen only locally in NB, and such depletions are confined to areas close to the Tertiary intrusions and along the N-S trending Lakes (e.g., Slocan). Though values of $\delta^{18}O$ quartz in granite samples from the Nelson Batholith vary considerably, they attain highest values of 11.4 to 13.3 near Nelson town. It is intersting to note that $\epsilon_{Nd}(T)$ value for the sample (8012B) from this area is also very low (-8.8). In general, their data suggest that a maximum whole rock $\delta^{18}O$ value of 11 to 12 is attained in the area between Slocan Lake and the Nelson town, but it decreases to 9.5 to 10.0 east of the Kootenay Lake.

Table 7.8 Oxygen Isotopic data from the Bayonne Batholith and Bonnington Pluton.

Sample	δ_{qz}	δ_{fels}	Δ(Qz-Fels)	ϵ_{Sr} (T)	ϵ_{Nd}(T)	Pb6/4	Pb7/4	Pb8/4
8038A	9.67	4.83	4.84	44.6	-5.1	19.10	15.64	39.21
8038D	10.25	8.72	1.53	28.9	-3.2	18.93	15.62	39.01
8021B	10.48	9.18	1.30	0.4	-3.0	18.66	15.61	38.48
8021D	10.01	4.39	6.62	69.5	-13.4	17.69	15.50	38.48
8022B		5.57		23.2	-3.6	18.04	15.52	38.55

Such a picture matches exactly with that of Pb-isotopic variation across the region (Fig. 7.3a) substantiating the earlier conclusion that an upper crustal sedimentary contaminant is necessary to explain the Pb-data. That such a component is not the Purcell sediments (e.g., middle Aldridge) as concluded by Magaritz and Taylor (1986) has been clearly shown by both simple binary mixing and AFC models. However the conclusion made from the decrease of Pb-isotopic composition east of the Kootenay Lake that the lower crust was involved in the generation of the Bayonne Batholith is supported by their oxygen isotopic data.

7.9.6 ϵ_{Nd} vs. Sm/Nd relationship

Figs. 7.16a-b show the relationship between ϵ_{Nd} and and $^{147}Sm/^{144}Nd$ ratio in a model mantle magma undergoing fractional crystallization and assimilation with a model lower crust. Sm/Nd atomic ratio in the model magma has been taken to be 0.18 (corresponding to Sm = 3.0 ppm and Nd = 10.0 ppm). This value is typical of island arc tholeiites (DePaolo, 1981a) and is very close to the Sm/Nd ratio of the RV sample 74/054 (0.164) which is least contaminated. As previously shown, RV samples have also undergone some fractionation of cpx and plag, so its Sm/Nd ratio must also be fractionated relative to the primitive magma derived from the mantle. For modelling granite petrogenesis in the western USA Farmer and DePaolo (1983, 1984) took a mantle magma (with Sm/Nd ratio equal to 0.161) generated by 1% partial melting of the mantle (for details see their papers). Value chosen here is slightly higher than the model magma used by them as in this case model magma responsible for contamination is taken similar to the RV andesitic magma, because of the close geological associations. This fact does not necessitate generating a model magma by only 1% batch melting of the mantle as it is probably very unlikely for this small amount of melt to segregate and rise upward. Physics of melting and separation of the melt requires at least a few percent of melting before the melt can escape the residue (Turcotte, 1982; Sleep, 1984).

A model lower crust with Sm = 5.0 ppm and Nd = 26 ppm has been taken to calculate the mixing trajectories. Sm/Nd ratios of three samples likely to represent the lower crust on the basis of their Nd isotopic compositions are 0.1117 (8021D), 0.0770 (8064E) and 0.1050 (8088C)

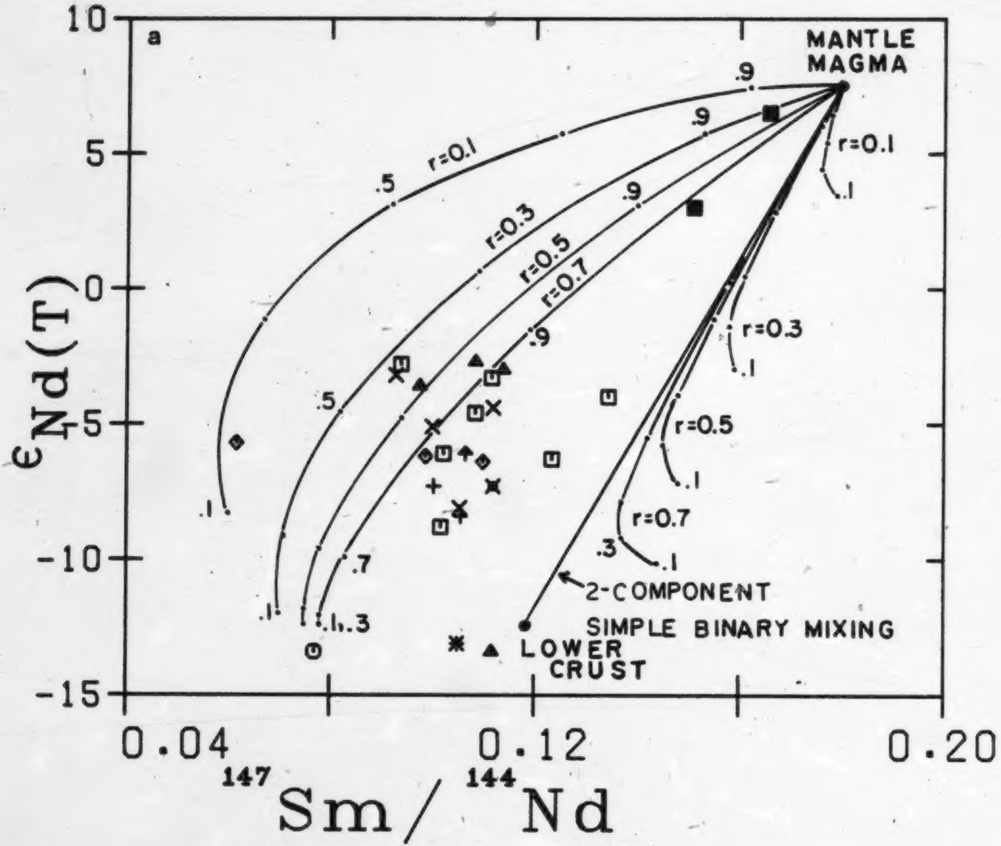

Fig. 7.16a-b. Various model mixing curves showing changes in ^{147}Sm/^{144}Nd for a mantle magma undergoing AFC with a lower crust. For endmember compositions see Fig. 7.11. Simple binary mixing line is shown by the straight line joining the two endmembers. For different r values (0.1 t0 0.7), AFC curves due to plagioclase fractionation only fall to the right of the simple binary line. While curves due to either a. cpx+hb or b. cpx only fractionation fall to the left, where all the samples plot. F values shown by dots. $D^{Sm,Nd}$ taken from Hanson (1980). M_a/M_m^o isopleths are for constant $D^{Sm,Nd}$, but for variable r. For the model crust used, samples from all the batholiths are consistent with a mantle fractionating either cpx+hb(a) or cpx(b).

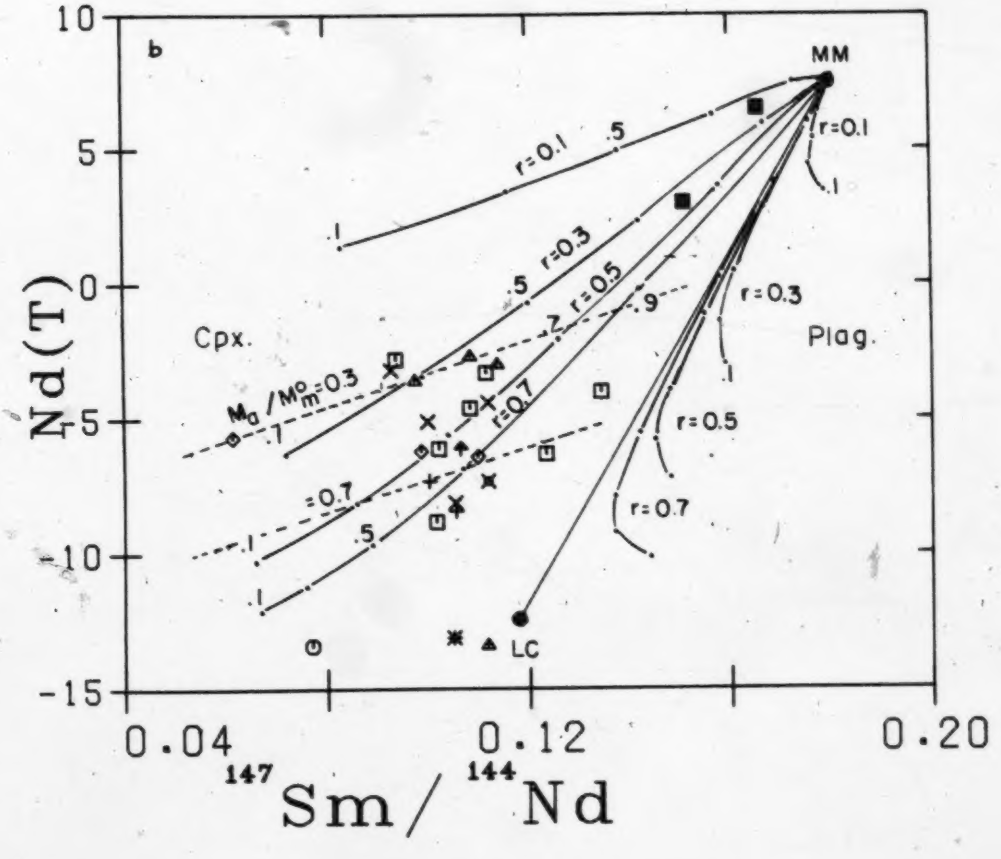
b
MM
LC
r=0.1
r=0.3
r=0.5
r=0.7
.5
.1
.9
Cpx.
Plag.
M_a/M_m^o=0.3
Nd(T)
10
5
0
-5
-10
-15
0.04
0.12
0.20
^{147}Sm/^{144}Nd

(Table. 7.1). They have wide range in both Sm ppm (2.75 to 8.26) and Nd ppm (14.72 to 67.17). Therefore even if they were derived from a homogeneous lower crustal source, their trace element abundances suggest considerable chemical fractionation. If the model lower crust had Sm and Nd concentrations of 5 ppm and 26 ppm respectively (like average lower crust), the sample 8064E has undergone elemental fractionation opposite to the other samples. Also relative Sm/Nd fractionation is different for 8064E (UNIT A) compared to 8021D and 8088C. Average atomic Sm/Nd ratios of 8021D and 8088C are however similar to that assumed for the lower crust (0.115).

DePaolo (1981a) discussed in detail the variation in Sm/Nd ratios for the Peninsular Ranges and Sierra Nevada Batholiths. Samples with $\epsilon_{Nd}(T) > 0$, have higher Sm/Nd ratios than those with $\epsilon_{Nd} < 0$. He expressed the degree of fractionation in Sm/Nd by a 'fractionation factor' g (or α according to Farmer and DePaolo, 1983) where g or α is defined as

$$\alpha = (Sm/Nd)_{rock}/(Sm/Nd)_{source} \quad \text{.........} \quad (7.21)$$

For the granitic samples in the Nelson-Rossland Arc, all the samples have α values between 0.7 and 0.98 (Fig. 7.17). These α values have been calculated relative to the two component 'mixture'. Unlike the Peninsular Ranges and Sierran Batholiths, granitic batholiths in this Arc have $\epsilon_{Nd}(T)$ invariably less than 0. However, $^{147}Sm/^{144}Nd$ ratios of the batholiths in the Nelson-Rossland Arc are similar to those in California with $\epsilon_{Nd}(T)$ less than 0. This general constancy in Sm/Nd ratios in the Phanerozoic granitic rocks all along the western Cordillera is significant in modelling the evolution of the continental crust. (Allègre and Ben Othman, 1980; DePaolo, 1981a).

From Fig. 7.17. it is seen that invariably all the samples fall to the left of the two-component mixing line. Therefore a simple mixing of mantle magma with an 1.8 Ga old lower crust is incapable of explaining the data. Igneous differentiation processes which decrease $^{147}Sm/^{144}Nd$ must be responsible along with the crustal mixing.

Figs. 7.16a-b show the mixing curves due to AFC taking cpx-plag and cpx+hb-plag as the fractionating phases respectively. These mixing curves have been superimposed on the data

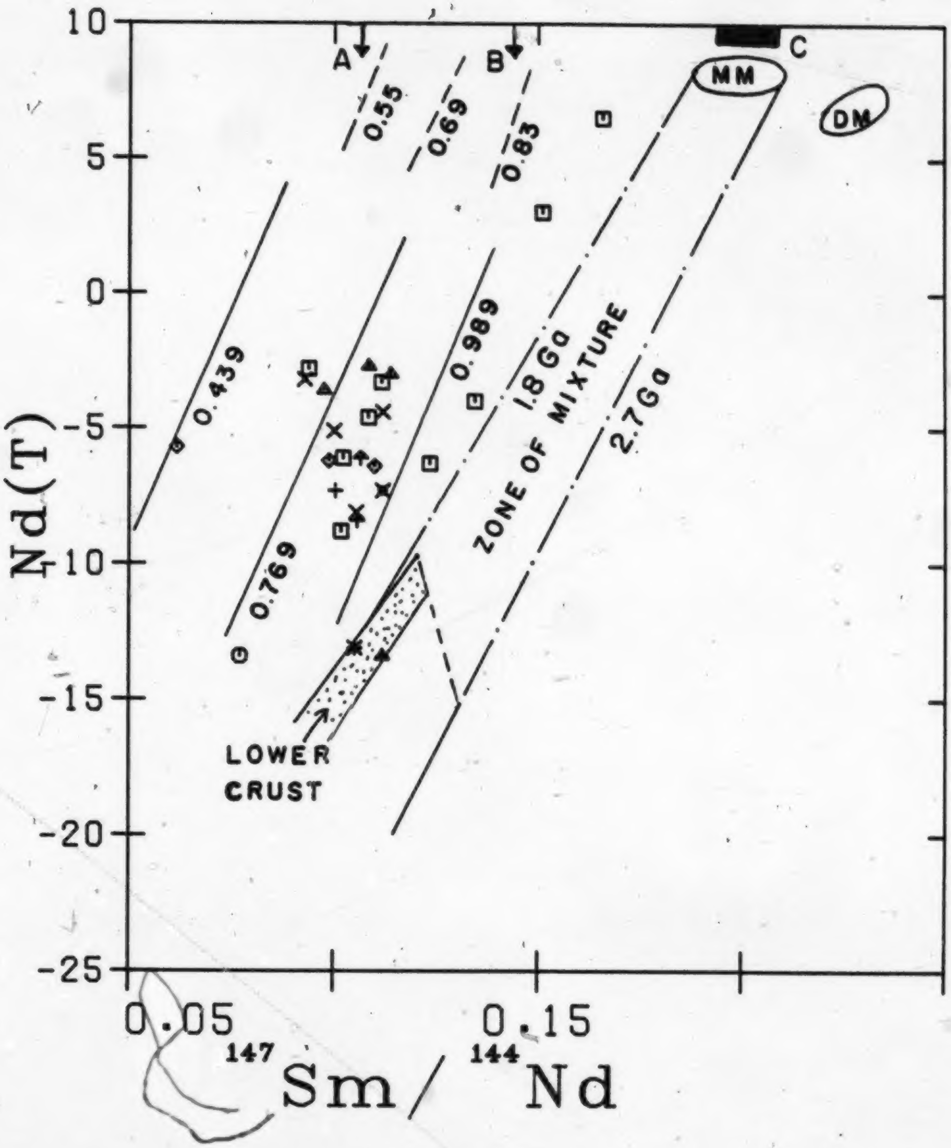

Fig. 7.17. ϵ_{Nd} vs Sm/Nd, showing the relative positions of the samples to those of mantle-derived magmas(MM), model depleted mantle(DM), island-arc tholeiites(C), average island arc(B), average Canadian Shield(A). All the samples plot to the left of the mixing zone of mantle magma and 1.8 to 2.7 Ga old crusts. As igneous differentiation decreases $^{147}Sm/^{144}Nd$ in the derivative magmas, extent of this decrease is expressed by the factor g or α (see text), which is contoured for the area where all the samples plot. These g values are either with respect to 'mixtures' (solid) or mantle (dashed lines). Most samples with $\epsilon_{Nd}<0$, have Sm/Nd less than average island arc.

array. Different curves represent different r values (0.1 to 0.7). Curves due to cpx (or cpx+hb) and plag fractionation fall on either side of the two-component mixing line. D^{Sm} and D^{Nd} for plag are similar (0.11 and 0.14 respectively, Hanson, 1980). Therefore plag is not very effective in fractionating Sm/Nd ratio. Curves drawn for plagioclase fractionation show that with increasing r, Sm/Nd ratios are pulled towards the crustal value as long as F is large. However at very low F values (less than 0.3) the decreasing trend is reversed and a slight increase in Sm/Nd ratio takes place.

On the other hand, fractionation of either cpx or hb (separately or in combination) is very effective in causing large Sm/Nd fractionation. Both the phases (either fractionating or acting as residual) will reduce Sm/Nd ratio as both have $D^{Sm} > D^{Nd}$ (see Table 7.7). Sm/Nd fractionation is an indicator of the degree of fractionation within the REE group. (DePaolo, 1981a).

For each batholith/pluton, it is seen that for a given $\epsilon_{Nd}(T)$ value, there is considerable variation in Sm/Nd (Tables 7.1, 7.2 and Figs.7.16a-b). For example, NB samples have $^{147}Sm/^{144}Nd$ ratios ranging from 0.0938 to 0.1344. Sm/Nd ratios for other batholiths or plutons are 0.0975 to 0.1138 for BP, 0.1003 to 0.1056 for KB, 0.0616 to 0.1099 for TP and TN and 0.0928 to 0.1119 for BB. This intra-batholith/pluton variation in Sm/Nd at a given $\epsilon_{Nd}(T)$ value could be due to different degrees of fractionation of cpx or hb or to differential diffusion of Sm and Nd in chemically stratified magma chamber in the upper crust (Hildreth, 1979, 1981). However, Michael (1983) and Miller and Mittlefehldt (1982) suggested that such fractionation is a normal consequence of fractional crystallization. The AFC model gives credence to the idea that Sm/Nd fractionation is due to separation of phases with unequal distribution coefficients for Sm and Nd, while magma was assimilating the crust. If both cpx and hb are taken as the fractionating phases, then most of the samples fall in an area bounded by curves with r values between 0.5 and 0.9 (Fig. 7.16a). As discussed before, (see Fig.7.11), combined Sr and Nd modelling distinguished two groups of samples: (1) one group affected by cpx+hb fractionation only and (2) the other group by plag fractionation only. The AFC picture is not all that simple. Figs. 7.16a and 7.16b show that both the groups are characterised by Sm/Nd ratios which vary within a very narrow range between 0.09 and 0.12. Only two samples have Sm/Nd ratios higher than the model crustal value of 0.115 (see table 7.1 and Fig. 7.16a). Juxtaposition of the two groups on these Figs. suggests cpx and hb fractionation for the Group 2 as well at some point of magma evolution. To reconcile these two contradictory observations, it is necessary to explore other alternative steps in the chemical evolution of the magma.

If it is true that Group 2 did not undergo cpx + hb separation, then to produce Sm/Nd ratios and $\epsilon_{Nd}(T)$ values found in them, a lower crust with Sm/Nd=0.07 (similar to 8064E) but $\epsilon_{Nd}(T) = -10.0$ is required to mix with the mantle magma. Then only plag separation at r values between 0.5 to 0.9 could account for the variations in Sm/Nd ratios of Group 2. This low Sm/Nd is exactly opposite to what is expected for 1.8 Ga old crust with $\epsilon_{Nd}(0) = -10.0$ derived from the depleted mantle similar to that of DePaolo (1981b). For a crust with ϵ_{Nd} = -10.0. instead of -14, Sm/Nd ratio should be at least 0.136. On the other hand, for an 1.8 Ga old crust derived from a depleted mantle will have Sm/Nd = 0.118 if $\epsilon_{Nd} = -14$. This value is very similar to the value assumed for the model lower crust used in the present study. The other alternative is that the melt was produced by partial melting of a lower crust above amphibolite stability field or an amphibole free lower crust (leaving cpx and plag as residue) will have very low Sm/Nd ratio. If this magma is mixed with the mantle magma, then a two component magma mixing will produce granitic samples with appropriate Sm/Nd ratios. But this simple two component mixing is not supported by AFC models discussed earlier with respect to Sr and Nd isotopes and their abundances.

Fig. 7.16b shows the mixing curves due to only cpx separation. In this case a slightly lower r values (0.3 to 0.7) are required to explain the data. All or some of the samples that need r values greater than 0.9 in $\epsilon_{Nd}(T)$ vs. $\epsilon_{Sr}(T)$ diagram also plot below the trajectory r=0.7 in Figs. 7.16a-b. Therefore AFC modelling on the basis of both these diagrams give consistent results. If an appropriate $D^{Sm,Nd}$ values are chosen for a combination of all three phases i.e., by reducing D values, these samples could be accomodated for an r value close to 0.7.

7.10 Nd-Sr isotopic relationships of Phanerozoic granitoids and crustal growth

In Table 7.3 are shown the T^{Nd}_{DM} ages of the granitic rocks in southeastern British Columbia. Though the model age range is relatively large (0.8 to 1.58 Ga), most of the samples have model age falling in the range, 1.0 to 1.3 Ga, which is much younger than the proven ≅1.8 Ga old lower crust in the study area and much older than the ages of crystallization (0.051 to 0.173 Ga). This intermediate T^{Nd}_{DM} model-age range is a strong evidence for crust-mantle mixing origin for the granitic rocks in southeastern B. C. and points to the fact that crustal recycling is important in the generation of young granites(s.l.). Very low T^{Nd}_{DM} model age (0.39 Ga) obtained for the least contaminated RV sample (74/054) shows clearly the effect of crustal contamination in altering the model age. Therefore degree of departure of the model age from the crystallization age is directly proportional to the degree of mixing (Farmer and DePaolo, 1983).

Zircon inheritance age (1.9 Ga) obtained for two samples (8021D and 8064E) is slightly older than their T^{Nd}_{DM} (i.e., 1.58 and 1.27 Ga) unlike the general agreement between the two ages found for the Peninsular Malaysian Batholiths (Liew and McCulloch, 1985). This significant difference between two types of ages for these two samples probably reflects the effects of small fractionation in Sm/Nd (lower than the source) during melting or a small mantle input. Former explanation is more reasonable as these two samples have $\epsilon_{Nd}(0)$ values similar to a model 1.8 Ga old continental crust.

Zircons from different parts of the Nelson Batholith have not yielded reliable inheritance ages because of their near concordance. Similar observations have been made for the Sierra Neveda and Peninsular Ranges Batholith (Chen and Moore, 1982) in southwestern U.S.A.

In a review of Sr and Nd isotopic compositions of old and young granitoid rocks, Allègre and Ben Othman (1980) have shown that old granitoids (>2 Ga) have $\epsilon_{Nd}(T)$ and $\epsilon_{Sr}(T)$ values close to CHUR evolution curve, while the young granitoids diverge significantly from the above curve or the evolution curve for the model depleted mantle, indicating large amount of recycled older continental crust. They interpreted such observations as evidence of quasi-continuous continental growth through geological time. Invariably higher $\epsilon_{Nd}(T)$ values (-8 to -2) from granites in southeastern B. C. than that for the lower crust ($\simeq$-13) strongly suggests variable amounts of mantle input in the Cordilleran granitic batholiths. This is even more pronounced in the case of Sierra Nevada and Peninsular Ranges Batholiths, significant parts of which show positive $\epsilon_{Nd}(T)$ values as high as +8.0 (DePaolo, 1981a).

Fig. 7.18 shows the initial $\epsilon_{Sr}(T)$ and $\epsilon_{Nd}(T)$ fields of Phanerozoic continental margin plutonic and volcanic belts. These belts define a relatively narrow curving band. The granites plotted could be divided into two types: I- and S-types. Nd and Sr isotopic compositions of I-type volcano-plutonic magmatic belts (e.g., southeastern B. C., southwestern U.S.A., Andean, eastern margin of the Lachlan Fold Belt of southern Australia, British Caledonian Newer Granites) plot in the upper region of the band with a large range in $\epsilon_{Nd}(T)$ (-8 to +8), but a smaller range in $\epsilon_{Sr}(T)$ (0 to +100). The reverse is true for the S-type magmatic belts (e.g., British Caledonian 'Older Granites', West Coast Province of Peninsular Malaysia), i.e., these belts have very large $\epsilon_{Sr}(T)$ (>100), but very narrow range in ϵ_{Nd} (-10 to -16). ϵ_{Nd} values lower than -16 are not generally found in Phanerozoic granitoids, indicating non-involvement of Archean crust in their genesis. Therefore only Proterozoic and younger crusts are being recycled along the continental margin young granites. However it is important to note that both the mantle material and heat flux from the mantle magma related to subduction processes are the main causes of incorporating large but variable degrees of older crust and therefore the net mantle input is significant in the generation of the Phanerozoic I-type granites.

In Fig. 7.19 are shown the ranges of $\epsilon_{Nd}(T)$ for the Phanerozoic magmatic belts in relation to the evolutionary curves for a model depleted mantle (DePaolo, 1981b), CHUR, and model crusts of 1.8 and 2.5 Ga age. It is clearly seen that most I-type granitoids have significant proportions of mantle derived materials, if the age of the crustal contaminant is as old as 1.8 Ga. If the general hypothesis for continental margin I-type magma genesis (e.g., magma originated in the mantle rose to the crustal level and interacted with the local old crust with concomitant fractional crystallization), is correct, it is evident that mantle derived magmas

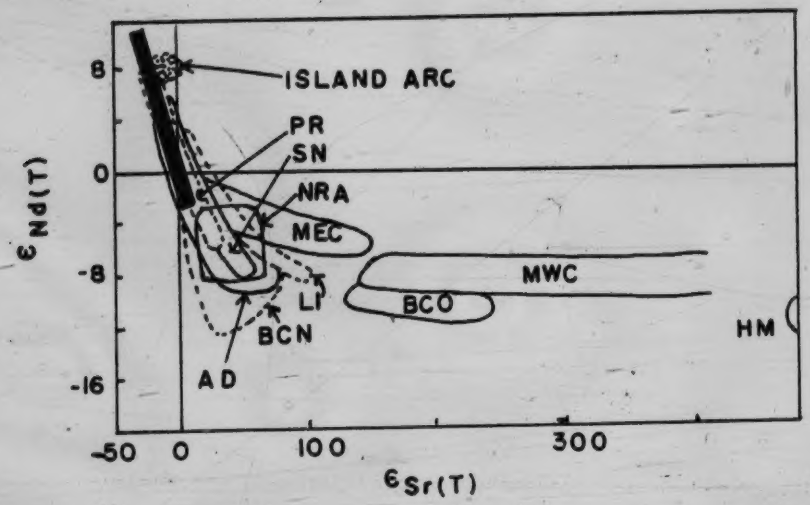

Fig. 7.18 Initial $\epsilon_{Sr}(T)$ and $\epsilon_{Nd}(T)$ fields for the Phanerozoic continental margin magmatic belts (both I-type and S-type). I-types display a large range in ϵ_{Nd} while S-types show a very large range in ϵ_{Sr}. I-types: NRA, Nelson-Rossland Arc; PR, Peninsular Ranges; SN, Sierra Nevada; LI, Laclan Fold Belt I-type; AD, Central Andean; BCN, British Caledonian Newer Granites; S-types: MEC, MWC, Malaysian East and West Coast; BCO, British Caledonian Older Granites; HM, Himalaya. Data from Allègre and Ben Othman (1980); Hamilton et al. (1980); Hawkesworth et al. (1982); McCulloch and Chappell (1982); McCulloch et al. (1982); Halliday (1984) and Liew and McCulloch (1985).

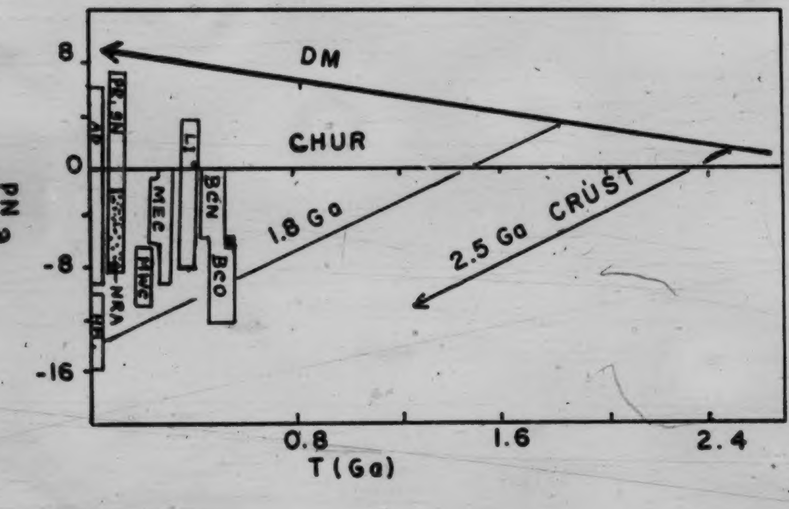

Fig. 7.19 Nd evolution diagram for the Phanerozoic granites. Vertical open bars show the range in $\epsilon_{Nd}(T)$ for the magmatic belts mentioned in Fig, 7.18. Also shown are the evolution curves for a model depleted mantle (DePaolo, 1981b), CHUR and model crusts of ages 1.8 and 2.5 Ga.

played a dominant role in the genesis of the Phanerozoic volcano-plutonic belts.

8. PB ISOTOPE GEOCHEMISTRY OF GRANITIC ROCKS

8.1 Introduction

In recent years lead isotopes have been increasingly used in studies of provenance of Phanerozoic igneous rocks (Cooper and Richards, 1966; Doe, 1967, 1973; Tatsumoto, 1969; Oversby and Ewart, 1972; Zartman, 1974; Armstrong and Cooper, 1971; Stacey and Kramer, 1975; Cumming and Richards, 1975; Tatsumoto, 1978; Sun, 1980; Chase, 1981; Vitrac et al., 1981). Most models can be grouped into two categories: (1) evolution of Pb isotopes due to decay of U and Th either in single stage or in multiple stages and (2) "Mixing models":- mixing of different distinct reservoirs which developed with their unique μ ($^{238}U/^{204}Pb$) values.

Pb isotopic characteristics of arc volcanics compared with those of MORB, oceanic islands and continental basalts have been used to argue variously for massive sediment subduction along subduction zones (Armstrong, 1968, 1981), small amount of recycling of continent-derived sediments (Kay et al, 1978), and no recycling (Oversby and Ewart, 1972; Meijer, 1976, 1985).

The arc magmas have similar Pb isotopic compositions to the range displayed by MORB, OIB or subcontinental sources. Subcontinental sources are reflected in a variety of kimberlite matrices (host magmas) and nucleated autoliths from pipes in South Africa and Lesotho (Kramers, 1977). Sun (1980) argued that the confinement of Pb isotopic ratios for some arcs (Aleutian, Tonga-Kermadec, Taiwan) between the array defined by MORB and sediments in the appropriate trenches strongly suggests contamination of primary mantle sources by the sediments in the neighbourhood of arc magma genesis. If this is true only a small fraction of sedimentary Pb component is necessary to alter the mantle source Pb composition as the Pb contents of the oceanic sediments (on the order of 30-40 ppm, Armstrong and Cooper, 1971) is large compared to the lead in the upper mantle (0.3 ppm). Kay et al. (1978) calculated only 1-2% of sediment is required to produce a shift in Pb isotopic composition of an MORB type source to that reflected in arc volcanics.

This sediment contamination concept becomes even more complex with respect to the continental margin arc magmas where a third component (crystalline basement and the overlying miogeoclinal and eugeoclinal sediments) plays an important role (Zartman and Doe, 1981; James, 1982; Farmer and DePaolo, 1983). In addition, if the magma is produced from or interacted with subcontinental mantle, a fourth component is introduced in the overall picture. Nature of subcontinental mantle may be different from that of suboceanic mantle (Allègre et al., 1981, 1982; Leeman, 1977; Menzies, 1983a, 1983b; Carlson, 1984). It is becoming exceedingly clear that granitoid rocks in the continental margin arc regimes contain significant amount of old crustal material (Ben Othman et al., 1984a; Allègre and Ben Othman, 1980; DePaolo, 1981a; Farmar and DePaolo, 1983, 1984; James, 1982). Possibility of interaction with the cratonic crust or local geoclinal sediments (Briqueu and Lancelot, 1979; Francis et al., 1980) derived from the old crust reduces the importance of or mask the effects of sediment contamination in the source regions of the mantle magma.

Continental crust has been shown to be chemically stratified with respect to LILE (Heier, 1973). For Rb-Sr and U-Th-Pb systematics, the parents (Rb and U) are lithophile elements while for Sm-Nd, the daughter (Nd) is more lithophile in character than Sm. Therefore during intra-crustal differentiation Rb/Sr and U/Pb decrease to a large extent and Sm/Nd may increase to a small extent for the lower crust. Depending on the timing and the degree of differentiation, the two crustal layers will follow different isotopic evolutionary paths. However, because of the limited degree of fractionation in Sm/Nd which is possible as both are REEs, differences in isotopic characters between the lower and upper crust will be less pronounced or minimal in case of Nd isotopes than for Sr and Pb.

The isotopic composition of most of the continental crust could not possibly result from a closed system evolution over the whole geologic time. (Patterson and Tatsumoto, 1964; Doe, 1967; Russell 1972; Zartman, 1974; Stacey and Kramer, 1975; and Cumming and Richards, 1975). Therefore such sources must have experienced multiple changes in μ in the past. The lower portion of the continental crust generally consists of very high grade metamorphic rocks e.g., pyroxene granulite or garnet granulite. These rock-types whether studied as surface outcrops or as xenoliths in volcanics, have very low U contents (0.1-1.0 ppm) and therefore low $^{238}U/^{204}Pb$ (0.5-5.0) (Moorbath and Gale, 1969; Heier, 1973). Th and Pb contents are generally in the range 1-10 ppm and 2-20 ppm respectively and are similar to the upper crustal values (Doe and Zartman, 1979). Therefore there will be a greater difference between the two segments of the crust with respect to $^{206}Pb/^{204}Pb$ than to $^{208}Pb/^{204}Pb$.

Mantle Pb is tapped by MORB and Oceanic Island Basalts(OIB). Sun (1980) reviewed their Pb isotopic composition on a global scale and found considerable mantle heterogeneity. Generally the major difference found between the arc batholiths and the MORB or OIB is that the former have higher $^{207}Pb/^{204}Pb$ for a given $^{206}Pb/^{204}Pb$ ratio. This fact requires a component enriched in $^{207}Pb/^{204}Pb$. Local miogeoclinal sediments are excellent candidates for such a component.

As shown previously in the discussion using Nd and Sr isotopes, granitic rocks of the batholiths in the study area are best explained by mixing mantle magma with bulk lower crust. This general lower crustal contamination model is not overwhemingly supported by Pb isotopes, however. The object of this chapter is to evaluate the degree of contributions of lower and upper crustal Pb components to the granitic samples and the paleogeographic controls of crustal contamination.

8.2 Analytical Data or Results

The measured Pb isotopic compositions have been decay corrected back to the known or accepted time of crystallization using μ and $\kappa(=^{232}Th/^{204}Pb)$ values calculated from measured U, Th and Pb concentrations. Table 8.1 and 8.2 show the U, Th and Pb concentrations and initial Pb isotopic compositions of the granitic batholiths/plutons. Table 8.3 shows the same parameters for the sedimentary rocks. Sedimentary Pb isotopic compositions have been corrected to only 164 Ma when most of the granitic bodies were emplaced, so that a direct comparison could be made. Some batholiths/stocks are Cretaceous in age, but corrected (at 164 Ma) sedimentary Pb values will not be much different from those at 100 Ma. Considerable variation in Pb isotopic composition is found among the granitic batholiths and many have negative

Table 8.1 Initial Pb Isotopic Ratios of granitic rocks.

SAMPLE	T(Ga)	U	Th	Pb	238U/204Pb	232Th/204Pb	Th/U	Pb-6/4	Pb-7/4	Pb8/4
NB										
8011A	0.164	9.96	23.00	33.00	19.51	46.56	2.39	18.475	15.611	38.810
8012B	0.164	3.27	12.00	36.60	5.82	22.07	3.79	19.258	15.704	39.099
SB29.7	0.168	2.59	10.00	35.00	4.83	19.27	3.99	19.414	15.684	39.121
8049A	0.063	8.00	9.00	26.00	19.78	22.99	1.16	18.822	15.620	38.657
8049C	0.063	7.00	15.00	28.00	16.08	35.60	2.21	18.934	15.630	38.579
8049D	0.063	5.00	7.00	15.00	21.45	31.03	1.45	18.896	15.622	38.618
8049E	0.063	11.00	8.00	25.00	28.28	21.25	0.75	18.726	15.610	38.685
8052A	0.164	1.51	3.00	11.70	8.29	17.01	2.05	18.888	15.615	38.447
8052B	0.164	2.00	7.00	9.00	14.36	51.94	3.62	19.016	15.635	38.319
8052C	0.164	2.00	2.00	12.00	10.72	11.08	1.03	18.869	15.627	38.561
8052D	0.164	2.00	3.00	12.00	10.70	16.58	1.55	18.821	15.609	38.431
8053A	0.164	2.24	5.00	26.90	5.38	12.42	2.31	18.978	15.644	38.962
8053B	0.164	3.00	5.00	27.00	7.22	12.43	1.72	19.111	15.679	39.099
8053D	0.164	4.00	4.00	31.00	8.51	8.79	1.03	20.247	15.750	38.995
8053E	0.164	7.00	5.00	28.00	16.24	11.99	0.74	18.931	15.682	39.028
8057A	0.164	1.00	8.00	15.00	4.35	35.98	8.27	19.333	15.663	39.146
8057B	0.164	2.22	8.00	15.20	9.53	35.49	3.72	19.170	15.676	39.122
8057C	0.164	6.00	20.00	24.00	16.42	56.55	3.44	19.020	15.672	39.398
8057E	0.164	5.00	12.00	13.00	25.16	62.39	2.48	18.712	15.654	39.131
8059A	0.164	1.95	8.00	14.60	8.73	37.00	4.24	19.201	15.674	39.202
8059B	0.164	3.00	10.00	21.00	9.35	32.21	3.44	19.247	15.675	39.316
8059D	0.164	5.00	9.00	23.00	14.21	26.42	1.86	19.087	15.667	39.271
8059E	0.164	5.00	9.00	12.00	27.13	50.46	1.86	18.838	15.604	38.759
BP										
8021A	0.164	1.00	2.00	14.00	4.58	9.46	2.07	18.741	15.631	38.618
8021B	0.164	1.32	2.00	14.00	6.03	9.44	1.57	18.663	15.612	38.487
8021D	0.054	8.97	13.00	39.00	14.48	21.69	1.50	17.692	15.504	38.487
8022A	0.164	3.14	8.00	17.00	11.81	31.09	2.63	18.198	15.559	38.661
8022B	0.164	3.00	6.00	20.00	9.53	19.70	2.07	18.048	15.522	38.552
8022C	0.164	2.84	11.00	18.00	10.08	40.35	4.00	18.194	15.557	38.588
8067A	0.164	1.84	5.00	10.90	10.77	30.25	2.81	18.130	15.548	38.624
8067B	0.164	2.40	2.00	19.00	8.09	6.97	0.86	18.758	15.620	38.471
8067G	0.164	2.00	6.00	11.00	11.65	36.10	3.10	18.598	15.593	38.322
8067H	0.164	2.00	6.00	11.00	11.67	36.18	3.10	18.669	15.611	38.384
8068A	0.164	4.54	34.00	17.80	15.99	123.76	7.74	17.125	15.459	37.527
8068B	0.164	5.00	67.00	36.00	8.83	122.24	13.85	17.813	15.504	37.998
8075A	0.164	2.75	10.00	11.00	16.26	61.09	3.76	19.060	15.660	38.598
8075B	0.164	2.00	9.00	11.00	11.75	54.62	4.65	18.876	15.664	38.454
8075C	0.164	2.00	10.00	12.00	10.81	55.85	5.17	19.074	15.677	38.554
8075F	0.164	1.76	13.00	10.00	11.45	87.43	7.63	19.166	15.669	38.459
8075G	0.164	4.35	8.00	12.00	23.78	45.20	1.90	19.312	15.672	38.934
8075J	0.164	4.00	12.00	12.00	21.57	66.88	3.10	18.758	15.633	38.375
8075K	0.164	4.00	12.00	12.00	21.69	67.22	3.10	18.857	15.672	38.620
RV										
74/054	0.164	0.50	2.00	3.00	10.71	44.25	4.13	19.030	15.619	38.030
75/116	0.164	0.50	2.00	3.00	10.75	44.42	4.13	18.995	15.631	38.342

Table 8.2. Initial Pb Isotopic compositions for Granitic samples.

SAMPLE	T(Ga)	U	Th	Pb	238U/204Pb	232Th/204Pb	Th/U	Pb-6/4	Pb-7/4	Pb8/4
TP										
8072A	0.164	3.32	15.00	19.00	11.16	52.09	4.67	17.998	15.547	38.618
8072B	0.164	5.00	15.00	24.00	13.25	41.08	3.10	18.275	15.615	38.030
8072C	0.164	3.00	10.00	22.00	8.57	29.52	3.44	17.222	15.463	38.556
8073A	0.164	2.20	10.00	16.00	8.81	41.39	4.70	18.656	15.653	38.285
8073C	0.164	2.00	10.00	15.00	8.51	43.95	5.17	18.684	15.625	37.939
8073D	0.164	4.00	11.00	22.00	11.41	32.42	2.84	17.115	15.445	38.460
TGN										
8070B	0.164	1.00	1.00	17.00	3.79	3.91	1.03	18.944	15.655	38.746
8070C	0.164	1.08	1.00	16.00	4.34	4.15	0.96	18.852	15.662	38.678
8070E	0.164	1.00	4.00	14.00	4.51	18.66	4.13	18.281	15.477	38.096
8070F	0.164	1.00	1.00	6.00	10.67	11.03	1.03	18.625	15.604	38.473
8070H	0.164	4.00	10.00	14.00	18.36	47.44	2.58	18.501	15.629	38.363
8071A	0.164	6.63	10.00	15.00	28.59	44.55	1.56	18.437	15.618	38.650
UA										
8064E	0.054	2.03	12.00	32.00	4.05	24.73	6.11	18.245	15.549	38.956
BB										
8038A	0.090	6.72	16.00	24.00	18.25	44.91	2.46	19.106	15.642	39.216
8038B	0.090	8.81	26.00	20.00	28.66	87.38	3.05	18.991	15.622	38.852
8038C	0.090	8.47	16.00	21.00	26.23	51.21	1.95	19.044	15.621	38.987
8038D	0.090	6.83	13.00	25.00	17.72	50.94	2.87	18.939	15.623	39.014
8096E	0.090	4.47	10.00	20.00	14.40	33.29	2.31	18.849	15.626	38.732
8096G	0.090	4.00	10.00	20.00	12.99	33.55	2.58	18.988	15.633	39.189
8096I	0.090	4.00	12.00	21.00	12.31	38.17	3.10	18.989	15.621	38.842
8096J	0.090	2.98	14.00	19.00	10.14	49.24	4.85	19.037	15.616	38.814
8038E	0.090	2.00	12.00	20.00	6.47	40.11	6.20	19.098	15.625	38.872
SLCS										
8088A	0.051	18.46	20.00	38.00	31.55	35.32	1.12	18.991	15.670	39.135
8088B	0.051	19.00	23.00	37.00	33.46	41.85	1.25	19.098	15.690	39.221
8089D	0.051	17.00	4.00	46.00	24.21	5.89	0.24	19.325	15.706	39.564
8089F	0.051	13.00	4.00	52.00	16.00	5.09	0.32	18.396	15.586	38.918
SS										
8007A	0.102	1.65	5.00	19.00	5.64	17.65	3.13	19.095	15.666	39.162
8007B	0.102	2.31	5.00	20.00	7.49	16.76	2.24	19.059	15.668	39.144
KB										
8033A	0.173	0.63	2.00	15.00	2.72	8.92	3.28	19.199	15.651	38.955
8033C	0.173	0.70	2.00	13.00	3.50	10.33	2.95	19.219	15.761	39.005
8033D	0.173	0.60	2.00	14.00	2.78	9.58	3.44	19.219	15.677	39.057
8033G	0.173	0.66	2.00	18.00	2.38	7.44	3.13	19.232	15.660	39.006
8033M	0.173	1.05	2.00	14.00	4.87	9.58	1.97	19.209	15.665	39.035
8033H	0.173	0.70	2.00	18.00	2.52	7.44	2.95	19.200	15.663	38.999
8033P	0.173	0.94	2.00	13.70	4.46	9.80	2.20	19.210	15.666	39.063

Table 8.3 Initial Pb Isotopic composition for Sedimentary rocks.

SAMPLE	T(Ga)	U	Th	Pb	238U/204Pb	232Th/204Pb	Th/U	Pb-6/4	Pb-7/4	Pb8/4
ALDR										
8002A	0.164	2.95	8.00	20.00	9.59	26.88	2.80	18.709	15.632	39.421
8002B	0.164	2.58	7.00	38.00	4.33	12.14	2.80	17.382	15.584	39.625
8002C	0.164	3.00	12.00	46.00	4.06	16.80	4.13	17.739	15.550	37.586
8002D	0.164	3.00	26.00	19.00	10.33	92.55	8.96	18.606	15.620	39.472
8002E	0.164	3.00	8.00	32.00	5.88	16.19	2.76	17.922	15.568	37.743
8002F	0.164	3.00	10.00	33.00	5.69	19.59	3.44	17.881	15.543	37.649
8001C	0.164	2.50	12.00	21.00	7.49	37.13	4.96	17.733	15.560	37.966
8001D	0.164	3.24	34.00	16.00	14.18	153.76	10.84	20.574	15.779	42.036
8001E	0.164	4.33	13.00	25.00	10.99	34.09	3.10	17.827	15.573	38.431
8001F	0.164	3.00	15.00	13.00	15.53	80.22	5.17	19.406	15.692	40.677
8001H	0.164	3.00	6.00	22.00	8.66	17.90	2.07	17.973	15.565	38.559
8001I	0.164	3.00	11.00	14.00	13.93	52.77	3.79	18.753	15.622	39.033
IV										
IRV1A	0.164	0.55	6.00	3.08	11.60	130.71	11.27	19.139	15.637	37.990
IVR1B	0.164	0.62	6.00	3.00	13.50	134.95	10.00	19.238	15.663	38.201
IRV-3	0.164	0.60	3.00	3.00	13.07	67.54	5.17	19.333	15.629	38.770
HORS										
8094A	0.164	3.06	18.00	4.00	56.07	340.82	6.08	21.797	15.924	41.807
8094B	0.164	3.00	18.00	4.00	55.73	345.52	6.20	22.607	15.995	42.070
8094D	0.164	3.00	18.00	4.00	57.48	356.38	6.20	23.518	16.058	43.662
HAM										
8090A	0.164	5.66	13.00	13.50	29.13	69.13	2.37	21.105	15.799	41.144
8090C	0.164	5.00	13.00	13.00	26.71	71.76	2.69	21.168	15.791	41.099
LARD										
8037B	0.164	0.40	6.00	16.00	1.63	25.28	15.50	19.263	15.724	39.256
8037C	0.164	0.48	2.00	13.00	2.41	10.36	4.31	19.255	15.709	39.321
8037D	0.164	3.30	9.00	17.00	12.85	36.23	2.82	19.618	15.719	39.652
8037M	0.164	0.27	2.00	13.00	1.33	10.19	7.65	18.628	15.615	38.783
LAIB										
8084A	0.164	2.74	21.00	5.73	32.03	253.66	7.92	19.359	15.732	38.487
8084B	0.164	3.00	20.00	6.00	33.08	227.87	6.89	18.882	15.705	38.216
NEL										
8010Q	0.164	2.00	7.00	11.00	11.98	43.32	3.62	19.104	15.822	39.631
8010R	0.164	2.00	1.00	7.00	18.67	9.65	0.52	18.615	15.791	39.639
8010S	0.164	2.52	11.00	22.00	7.50	33.81	4.51	18.914	15.829	39.512
8010T	0.164	2.00	2.00	7.00	18.62	19.24	1.03	18.864	15.790	39.083
8010U	0.164	2.00	10.00	10.00	13.07	67.50	5.17	18.711	15.804	39.175
8010V	0.164	2.00	10.00	10.00	12.81	66.17	5.17	18.492	15.617	38.103
ACT										
8009D	0.164	12.36	1.00	18.00	47.61	3.98	0.08	22.925	15.893	39.123
8009R	0.164	6.96	2.00	10.00	47.25	14.03	0.30	21.144	15.851	39.186
8009T	0.164	6.56	6.00	17.00	26.48	25.02	0.95	22.726	15.918	38.856
8009U	0.164	7.00	2.00	9.00	52.70	15.56	0.30	21.209	15.829	38.832

```
MIL
 8003B  0.164   3.00   6.00  17.00  11.36   23.48   2.07  18.696  15.645  38.657
 8003C  0.164   3.45  13.00  19.00  11.70   45.54   3.89  18.599  15.654  38.604
 8003D  0.164   3.00  13.00  16.00  12.13   54.34   4.48  18.849  15.650  38.621
 8003E  0.164   2.38   2.00   9.00  16.90   14.67   0.87  18.287  15.609  38.474
 8003F  0.164   0.36   2.00   6.00   3.84   22.06   5.74  18.686  15.640  38.512
 8027B  0.164   2.21   2.00  14.00  10.25    9.59   0.94  19.234  15.709  38.874
 8027C  0.164   2.00  10.00  11.00  11.94   61.70   5.17  19.348  15.717  39.115
 8027D  0.164   2.00  16.00  11.00  12.02   99.40   8.27  19.404  15.705  39.284
 8027I  0.164   4.71  12.00  24.00  12.81   33.73   2.63  19.267  15.740  38.911
 8027P  0.164   2.00   2.00   8.00  16.29   16.83   1.03  19.064  15.699  39.051
 8027S  0.164   1.69   2.00   8.00  13.94   17.05   1.22  19.433  15.710  39.728
 8058A  0.164   3.52  10.00   5.89  38.94  114.31   2.94  18.107  15.659  38.649
 8098A  0.164   3.53  10.00  21.00  10.83   31.69   2.93  18.617  15.645  38.708
 8098B  0.164   3.00  10.00  20.00   9.67   33.30   3.44  18.683  15.644  38.734
 8098D  0.164   3.00  10.00  20.00   9.83   33.86   3.44  19.264  15.702  39.321
 8102A  0.164   4.70  10.00  10.00  32.83   72.18   2.20  23.820  15.893  38.680
 8105B  0.164   2.14  10.00  15.50   8.90   42.99   4.83  18.756  15.624  38.644
 8105C  0.164   2.00  10.00  15.00   8.67   44.79   5.17  19.133  15.607  38.893
 8105D  0.164   2.00  10.00  15.00   8.53   44.05   5.17  18.493  15.587  38.323
YMR
 8006D  0.164   0.24   2.00  16.00   0.94    8.13   8.61  17.936  15.522  38.246
 8006G  0.164   3.08   6.00   5.00  40.06   80.64   2.01  18.316  15.608  38.590
 8006H  0.164   3.00   4.00  10.00  19.34   26.64   1.38  18.548  15.631  38.673
 8006K  0.164   3.00   6.00   7.00  28.01   57.89   2.07  18.556  15.667  39.186
 8006L  0.164   3.39   9.00   9.00  24.39   66.90   2.74  18.495  15.632  38.592
 8062I  0.164   2.54   9.00   1.98  82.88  303.44   3.66  16.874  15.550  36.621
 8080A  0.164   3.03   9.00  10.20  19.16   58.80   3.07  18.727  15.639  38.272
SLCN
 8035A  0.164   2.29   2.00  10.00  14.77   13.33   0.90  18.699  15.642  38.808
 8035C  0.164   3.00   6.00  12.00  16.16   33.41   2.07  18.744  15.653  38.716
 8035D  0.164   3.00  13.00  19.00  10.21   45.71   4.48  18.732  15.652  38.784
 8035F  0.164   3.17  19.00  20.00  10.25   63.50   6.19  18.734  15.665  38.656
 8035G  0.164   3.00  20.00  20.00   9.66   66.56   6.89  18.785  15.678  38.275
 8106B  0.164   0.20   2.00   5.50   2.33   24.05  10.33  18.778  15.630  38.384
 ------------------------------------------------------------------------------
```

(future) model ages with respect to an U-Th-Pb system with single stage growth histories.

8.2.1 Bonnington Pluton(BP)

Samples collected from five different localities have Pb isotopic compositions falling into five different groups (Figs. 8.1 and 8.2). The least radiogenic Pb comes from two samples 8068A and 8068B with $^{206}Pb/^{204}Pb$=17.125-17.813, $^{207}Pb/^{204}Pb$=15.459-15.504, $^{208}Pb/^{204}Pb$=37.527-37.998 followed by three alkaline granites samples (8022-group, 18.048-18.198, 15.552-15.661, 38.555-38.665). Slightly more radiogenic Pb is found in two groups of samples (8067-group and 8021-group) with $^{206}Pb/^{204}Pb$=18.130-18.741, $^{207}Pb/^{204}Pb$=15.548-15.631, $^{208}Pb/^{204}Pb$=38.322-38.624). Most radiogenic samples come from the centre of the pluton (8075-group) with $^{206}Pb/^{204}Pb$=18.758-19.312, $^{207}Pb/^{204}Pb$=15.634-15.677, $^{208}Pb/^{204}Pb$=38.375-38.934). Therefore it is seen that samples collected even from a small geographic area have considerable range in Pb isotopic compositions compared to either Nd and Sr. This must be related to either extreme heterogenous nature of the lower crust or variable degree of mixing. Except for 8075-group of samples most samples have such unradiogenic Pb as to mirror that of the lower crust which is probably the dominant source of this Pb. This variability in Pb isotopic composition is not related to the chemistry of the rocks but varies in an E-W direction (Fig. 7.3a). This in turn reflects the importance of paleogeography in granite genesis in the Nelson-Rossland Arc.

8.2.2 Nelson Batholith(NB)

Like BP, different units of NB show similar variability in Pb isotopic composition. The main difference is, on an average, NB samples are more radiogenic than BP. The most basic alkaline unit (8052-group) has least radiogenic Pb (18.821-19.016, 15.610-15.635, 38.319-38.561). The other three groups (8053, 8057, and 8059) have similar isotopic compositions but are more radiogenic (18.978-20.247, 15.664-15.750, 38.962-39.995) than the 8052-group (Fig. 8.1 and 8.2). Like BP, for this batholith also, more eastern samples have more radigenic Pb. The sample with highest Pb isotopic composition comes from the northern part of the batholith (SB29.7, 19.414, 15.684, 39.121). A single sample (1012B) coming from very close to Nelson town has also very radiogenic isotopic composition (19.258, 15.704, 39.099)

8.2.3 Bayonne Batholith(BB)

Two groups of samples collected from this batholith (8038-group and 8096-group) have virtually same Pb-isotopic composition and fall in a tight group (18.939-19.106, 15.616-15.642, 38.814-39.216). It is interesting to note that the Bayonne Batholith Pb is confined within that of NB, but is closer to the lower end of the range (like 8052-group). This breaks the general pattern of increasing radiogenic Pb towards east and therefore suggests a fundamental change in character in granitic source material for this batholith (Fig. 7.3a, Chapter 7).

8.2.4 Summit Stock(SS)

Two samples collected from SS have similar $^{206}Pb/^{204}Pb$ and $^{208}Pb/^{204}Pb$ to BB (19.059-19.095 and 39.144-39.162) and $^{207}Pb/^{204}Pb$ (15.666-15.668) similar to that of 8075-group.

8.2.5 Kuskanax Batholitth(KB)

Except one sample, KB has the smallest range in Pb isotopic composition (19.199-19.232,15.651-15.677, 38.955-39.005) and occupies the upper part of the NB range.

8.2.6 Shore Line Creek Stock(SLCS)

A small stock on the east shore of the Kootenay Lake has considerable range in Pb-isotopic composition (18.325-19.396, 15.586-15.706, 38.918-39.564). One sample (8088C) analysed for Nd suggests this stock was derived from partial melting of 1.8 Ga old lower crust.

8.2.7 Trail Pluton(TP) and Gneiss(TN)

As expected, two groups of samples collected from the Trail Pluton have less radiogenic Pb isotopic composition than NB as this pluton is situated SW of the Bonnington Pluton and

Fig. 8.1 ^{206}Pb/^{204}Pb vs. ^{207}Pb/^{204}Pb. Shows plot of time-corrected Pb-isotopic ratios for all the granitic and selected sedimentary units (average values, Table 7.5) from southeastern British Columbia. Sedimentary samples have higher ^{207}Pb/^{204}Pb than the granites for a given ^{206}Pb/^{204}Pb.

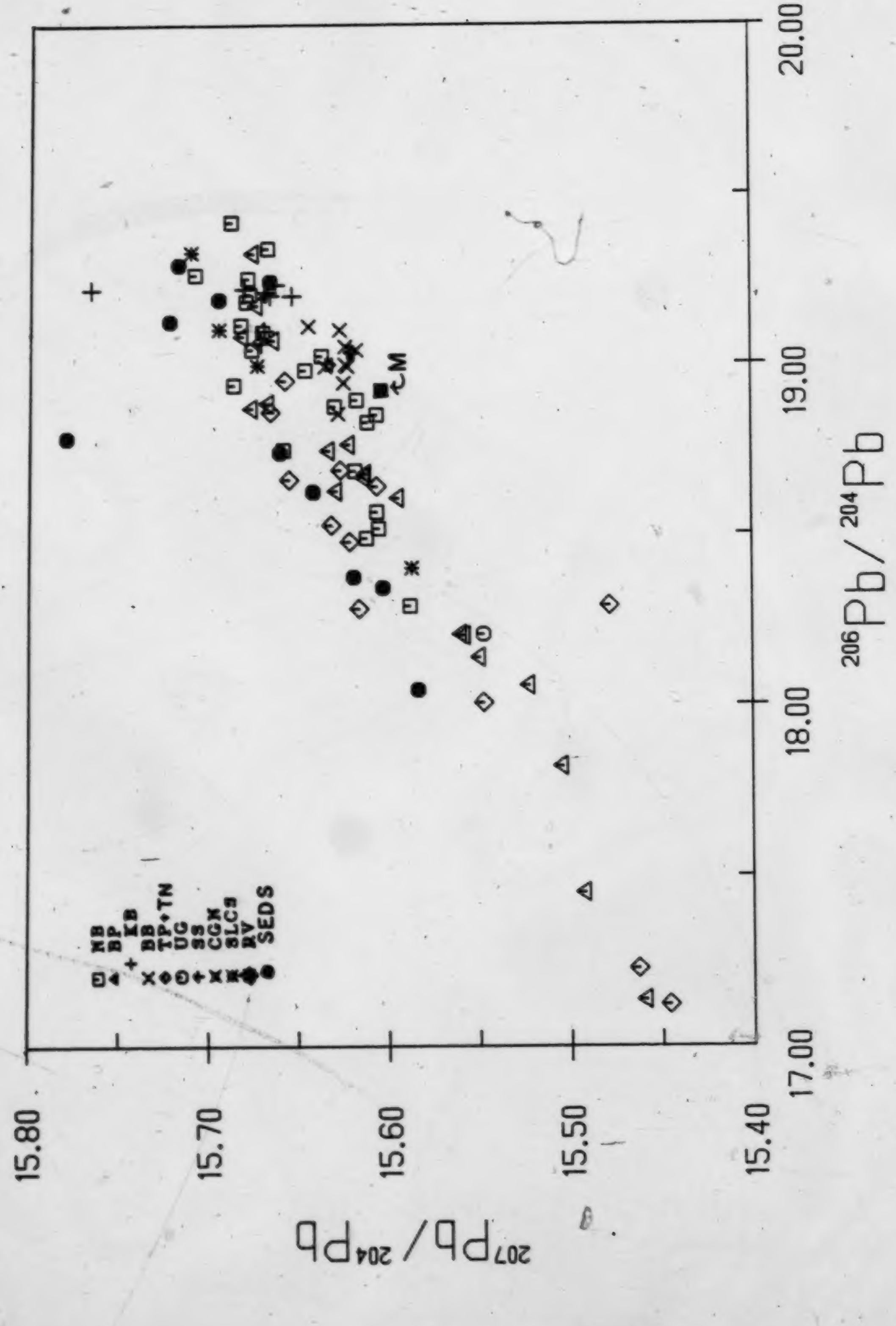
NB
BP
KB
BB
TP+TN
UG
SS
CGM
SLCS
RV
SEDS
CM
15.80
15.70
15.60
15.50
15.40
^{207}Pb/^{204}Pb
17.00
18.00
19.00
20.00
^{206}Pb/^{204}Pb

Fig. 8.2. ^{206}Pb/^{204}Pb vs. ^{208}Pb/^{204}Pb. Shows that range in ^{208}Pb/^{204}Pb is similar for both the granites and sediments.

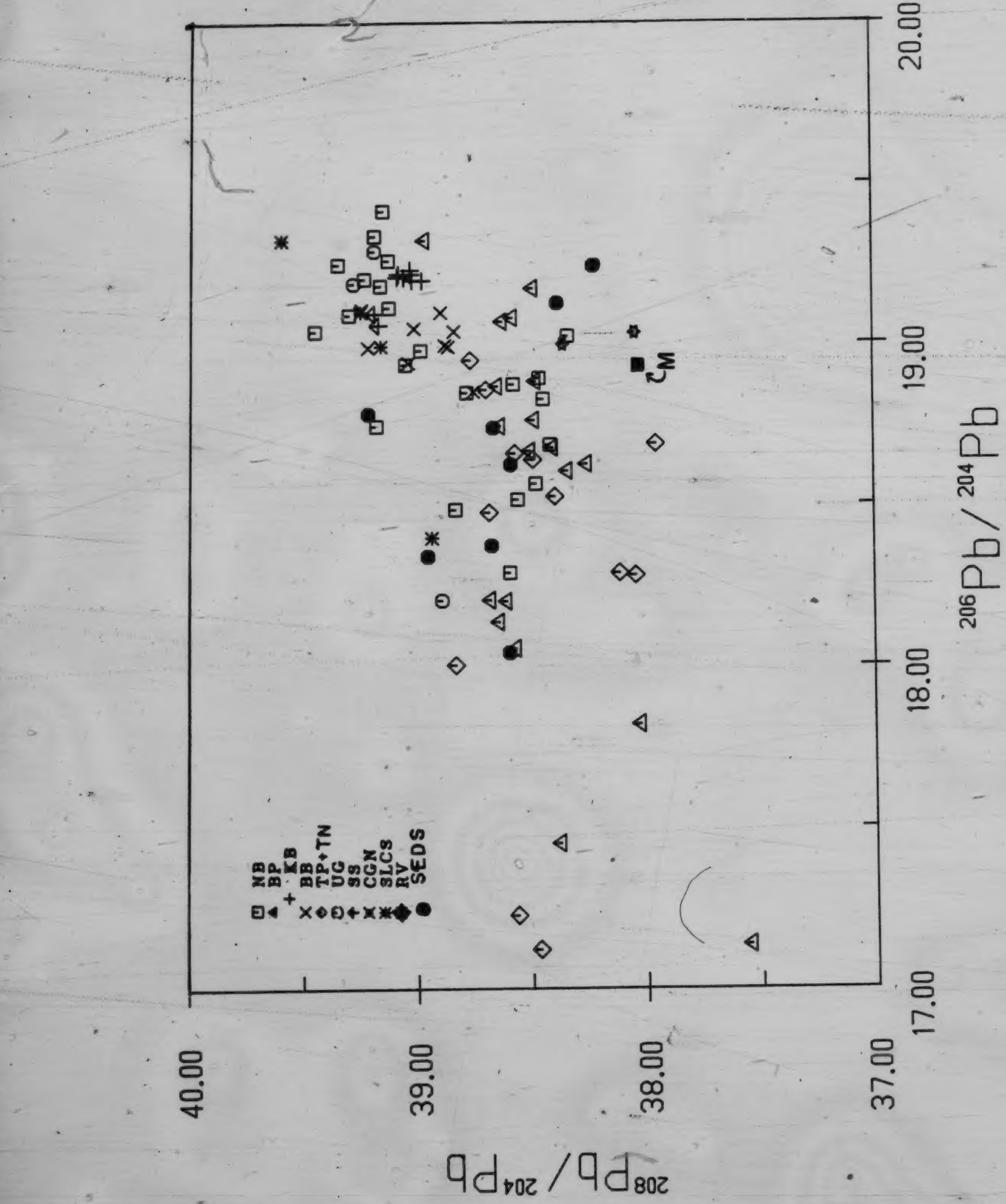
NB
BP
KB
BB
TP+TN
UG
SS
CGN
SLCS
RV
SEDS
M
17.00
18.00
19.00
20.00
^{206}Pb/^{204}Pb
37.00
38.00
39.00
40.00
^{208}Pb/^{204}Pb

west of the Pb line. The isotopic range is similar to that found in BP (without 8075-group). The range for both the groups(8072- and 8073-groups) taken together is 17.115-18.684, 15.446-15.653, 37.939-38.618). Six samples collected from the Trail Gneiss (Location # 30, 31), occupy the upper part of the range shown by TP and therefore are more homogeneous campared to the pluton.

8.2.8 Unclassified Granite UNIT A(8064E) and 8021D

These two samples also have very unradiogenic isotopic compositions. 8064E (18.245, 15.549, 38.956) is more radiogenic than 8021D (17.692, 15.504, 38.487) (Tables 8.1 and 8.2). As discussed before these two samples along with 8088C (SLCS) hold key to deciphering the nature of the lower crust in the study area.

8.2.9 Rossland Volcanics(RV)

Two samples analysed for Sr and Nd have also been analysed for Pb isotopic composition. Both Nd and Pb isotopic compositions are reported for the first time. Average Pb isotopic compositions for the two samples are: 19.012, 15.625, 38.186. (see Table 8.1 for individual values).

8.3 Mantle Pb

RV samples have been shown to be altered hydrothermally to some extent on the basis of oxygen isotopic study and petrography (Beddoe-Stephens, 1979). As Nd isotopic composition is not susceptible to hydrothermal alteration (Hawkesworth, 1979), ϵ_{Nd}(T) value of 6.7 for 74/054 (close to the average island arc volcanics of 8.0) is certainly due to small crustal contamination or the magma was derived directly from the subcontinental mantle which is slightly more LREE enriched compared to the source of average island arc. In fact in a recent paper on CRB, Carlson (1984) used a mantle component (C1) with $\epsilon_{Nd}=6.5$. It cannot be proved, as dicussed before, if such mantle existed underneath RV. It is assumed here that Rossland magma was derived from average island arc source and then was contaminated with the local crust. If this model is correct, mantle Pb should be lower than those preserved in the two samples. Therefore an uncontaminated mantle Pb compositions are taken to be $^{206}Pb/^{204}Pb = 18.88$, $^{207}Pb/^{204}Pb = 15.60$ and $^{208}Pb/^{204}Pb = 38.00$ (assuming a small (≃ 5% UC contamination). This is different from Cl of Carlson (1984) who took the following composition: 18.80, 15.51, 38.30 as the mantle value. In a recent study of Pb and Sr isotopic evidence for crustal interaction and compositional zonation in the source regions of Pleistocene basalts and rhyolitic magmas of the Coso volcanic field, California, Bacon et al. (1984) used a mantle Pb value of 19.05, 15.62 and 38.63 preserved in one basaltic flow. For the Nelson-Rossland Arc, even though slightly different mantle Pb value could be taken, but the value chosen is probably close to true composition. Moreover for other values, there will not be much qualitative difference in the interpretation of the results. More study on RV is, however, needed to firmly establish the nature of the mantle Pb in the area.

8.4 Discussion

Figs. 8.3 and 8.4 show the plot of all samples (granitic rocks and associated sediments). All the granitic samples are confined within a narrow band (Fig. 8.3) whose upper boundary is occupied by the sedimentary rocks. These sedimentary rocks have higher $^{207}Pb/^{204}Pb$ ratios for a given $^{206}Pb/^{204}Pb$ compared to the granitic samples. On the other hand, highly radiogenic sedimentary samples fall along the extension of the lower end of the band. A pooled slope of the granitic samples is ≃0.085 which is equivalent to a model age of ≃ 1.33 Ga. This model age is similar to average Nd model age of the granitic samples, supporting mixing of crust and mantle. Such linear relationships are not found on $^{208}Pb/^{204}Pb$ vs. $^{206}Pb/^{204}Pb$ plot (Fig. 8.4). There is considerable scatter both among the granitic and sedimentary rocks. However all the samples plot within the area bounded by two lines whose μk ($^{232}Th/^{238}U$) values are ≃1.0 and 2.3 respectively. It is interesting to note that mean Th/U ratio of the range shown by the granitic and sedimentary rocks from southeastern British Columbia is lower than that of average crust (3.5). Less radiogenic sedimentary samples overlap the granitic samples and do not form the upper boundary as in Fig. 8.3. The exact reasons for this sactter is not understood, but it is

Fig. 8.3. Same plot as Fig. 8.1, but it includes more radiogenic sedimentary samples. All the granitic samples are confined within a narrow band whose upper boundary is occupied by the relatively less radiogenic sedimentary samples. The highly radiogenic sedimentary samples plot along the extension of the lower boundary. The average slope of all the granitic samples is about 0.085 which is equivalent to a model age of about 1.33 Ga. The letter M represents the average mantle Pb isotopic composition in the study area.

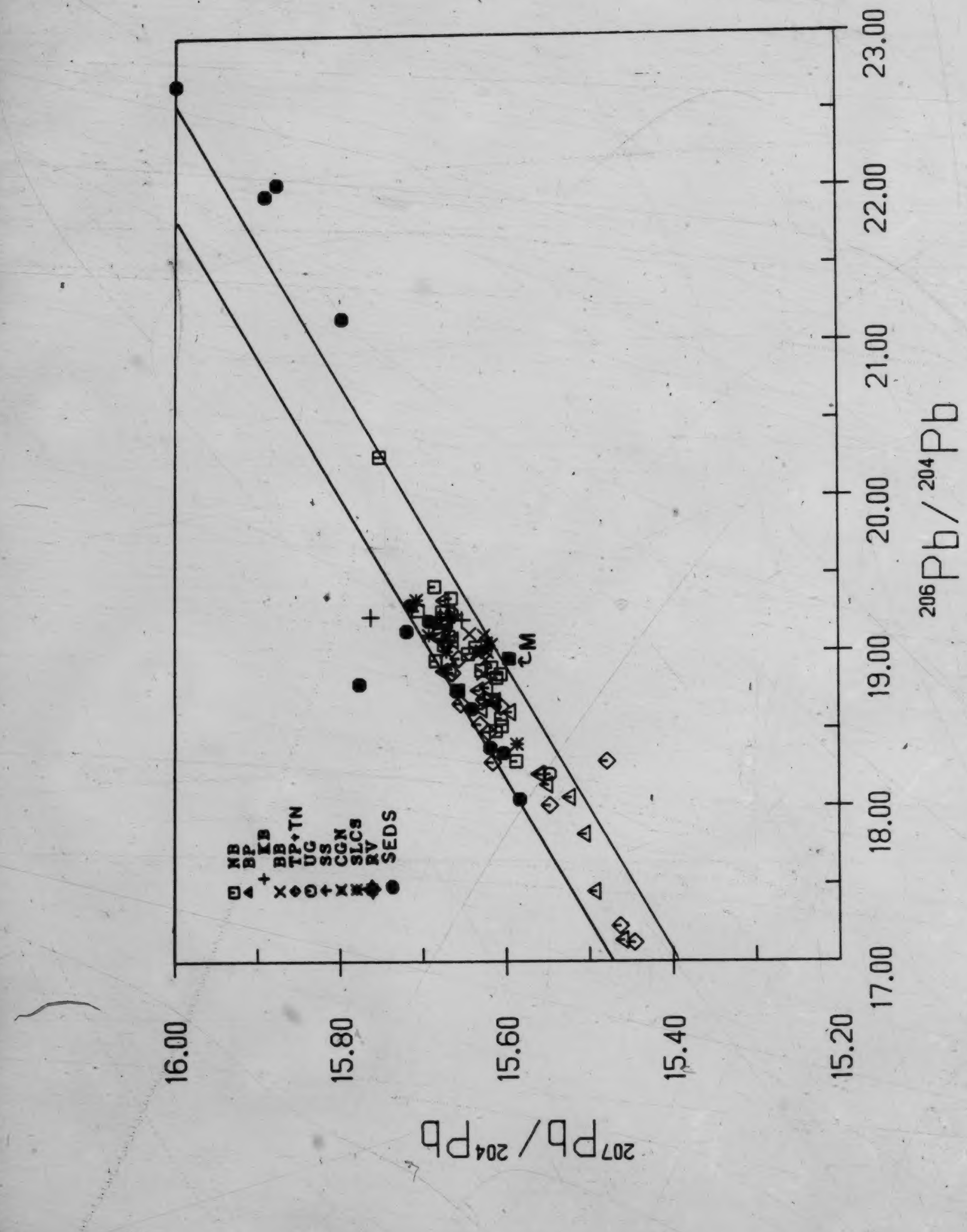

XB
BP
KB
BB
TP+TN
UG
SS
CGN
SLCS
RV
SEDS
M
16.00
15.80
15.60
15.40
15.20
17.00
18.00
19.00
20.00
21.00
22.00
23.00
$^{207}Pb/^{204}Pb$
$^{206}Pb/^{204}Pb$

Fig. 8.4. Same plot as Fig. 8.2, but it includes more radiogenic sedimentary samples. Unlike Pb6/4-Pb7/4 diagram, there is greater scatter of data points. The letter M represents average Pb isotopic composition of the mantle in the study area.

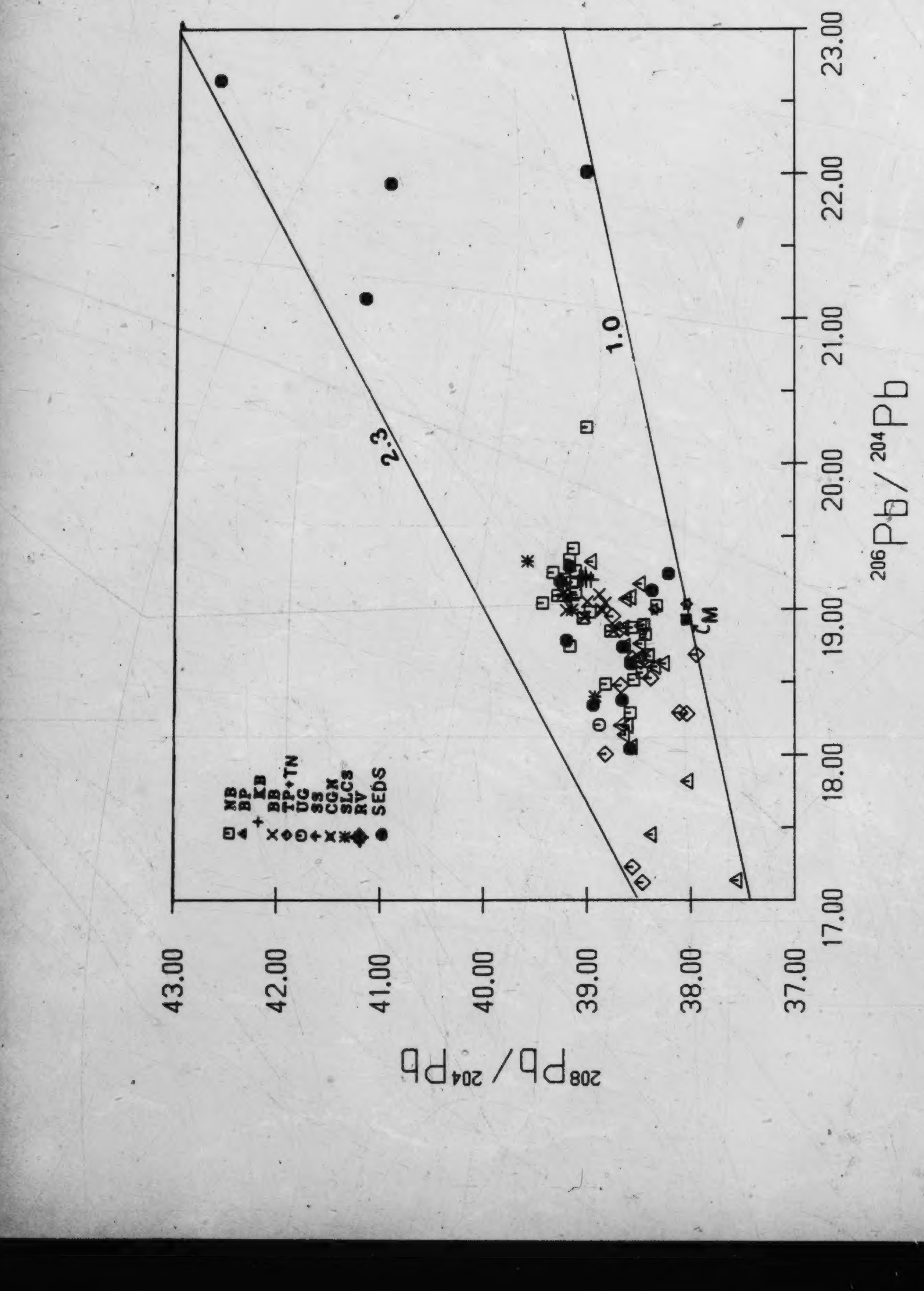
NB
BP
KB
BB
TP+TN
UG
SS
CGM
SLCS
RV
SEDS
2.3
1.0
M
43.00
42.00
41.00
40.00
39.00
38.00
37.00
17.00
18.00
19.00
20.00
21.00
22.00
23.00
$^{206}Pb/^{204}Pb$
$^{208}Pb/^{204}Pb$

probably due to: (1) large scale variations in Th/U ratios in the sedimentary provenances, and effects of erosion and deposition or (2) some artifacts of mixing.

Figs. 8.5 and 8.6 show a similar plot excluding the highly radiogenic sedimentary samples. On these diagrams are shown three Pb isotope provinces as defined by Zartman (1974). Area I-type Pb derived from very old Precambrian basement. This area is divided into two small parts: 1a and 1b. Area 1a Pb is associated with 2.7 Ga old crystalline basement while area 1b with 1.8 Ga old basement. Igneous rocks plotting in area 1b have comparatively unradiogenic Pb but with considerable range (16.2-18.8, 15.30-15.75, 36.5-39.9). Area II-type lead represents a more restricted range in isotopic composition with $^{206}Pb/^{204}Pb=19.1-19.7$, $^{207}Pb/^{204}Pb=15.65-15.85$, $^{208}Pb/^{204}Pb=38.90-40.30$. It contains isotopically homogeneous lead derived from a sedimentary pile eroded dominantly from adjacent Precambrian rocks. Such lead is generally found in great thicknesses of the Cordilleran miogeoclinal rocks. While area III-type lead has intermediate isotopic composition and such lead is found in association with young eugeoclinal plutonic and volcanic arc derived sedimentary rocks.

This general 3-fold classification has been found to be very useful in understanding the source provenance of igneous rocks and ore deposits in the Cordillera of the western USA.

As seen in Figs. 8.5 and 8.6 invariably all the less radiogenic (with respect to manlte) samples plot in area Ib type lead. This strongly suggests that these samples plotting in this area have significant Pb component derived from 1.8 Ga old crystalline basement. It is extremely interesting to note that samples 8064E and 8021D plot in this area also. Therefore this fact combined with their Nd isotopic compositions proves beyond doubt that a lower crust existed below the western part of the Pb line. Thus this lower crust played a key role as a density filter for the mantle derived magmas and thereby as a potential crustal contaminant. This geological evidence therefore supports the AFC model discussed in Chapter 7.

The wide variability in Pb composition of samples with less radiogenic Pb than the assumed mantle value is difficult to explain if a lower crust of fixed Pb isotopic composition is assumed to exist. Both Nd and Sr data suggest that it is quite uniform. A possible explanation is variable degree of contamination with the mantle magma as strongly suggested by Nd isotope.

Alternatively the hidden crust is extremely heterogeneous with respect to Pb isotopes. It is possible both are valid. For the mixing calculations (in Chapter 7) Pb isotopic composition similar to 8064E was taken to be representative of the average lower crust (18.200, 15.550, 38.880). Other compositions could also be taken, but this sample plots in the center of the field Ib and therefore is thought to represent the average Pb composition of the 1.8 Ga old crust. Compared to the deduced mantle value, this lower crustal Pb is more radiogenic in $^{208}Pb/^{204}Pb$ but less radiogenic in $^{206}Pb/^{204}Pb$ and $^{207}Pb/^{204}Pb$ (similar to the Pb isotopic compositions of mantle and lower crust of Doe and Zartman, 1976).

Fig 8.6. shows a $^{208}Pb/^{204}Pb$ vs. $^{206}Pb/^{204}Pb$ with the Zartman's Pb provinces superimposed. Between Fig. 8.5 and Fig. 8.6, there are important differences for the samples with the least radiogenic Pb isotopic compositions. Some samples (8068A, 8073D, 8072C, 8021D and 8072A) plot in 1a-type Pb area which suggests they were derived from 2.7 Ga old crystalline crust. This discrepancy can not be solved at this time as there is no evidence of a 2.7 Ga old crust in the area.

In Fig. 8.5, area III (Pb source material "eugeoclinal plutonic, volcanic and sedimentary rocks, possibly associated with subduction processes", Zartman, 1974, Table 1) contains Pb data of those samples belonging to NB, BB, SS, SLCS and 8075-series of BP. Most radiogenic samples of these granitic batholiths/plutons/stocks also plot in the area II (Pb source material "isotopically homogenised miogeoclinal sedimentary rocks eroded from adjacent Precambrian sialic upper crust"). These samples include SB29.7, 8012B, 8057A, 8059A, 8059B of NB and 8088C of SLCS. In Fig. 8.5. KB samples also plot in the overlapping area of type II and III Pb. Overall agreement between the two diagrams is significant considering the complex and variable nature of mixing processes responsible for generating the present distributions of the initial isotopic compositions.

The observed distribution of Pb isotopic data for the NB batholith suggests they contain Pb of both mantle and crustal sources (most likely of upper crustal as against the lower crustal).

Fig. 8.5. Three Pb isotope provinces (Zartman, 1974) are superimposed on the data set. Area I-type Pb is thought to have derived from very old Precambrian basement. This area is divided into two parts: Ia (province is older, i.e., 2.7 Ga) and Ib (province is younger, i.e., 1.8 Ga). Area II-type Pb represents more isotopically homogeneous Pb derived from a sedimentary pile, e.g., cordilleran miogeocline, while III-type Pb has intermediate isotopic composition and represents Pb found in young eugeoclinal plutonic and volcanic arcs.

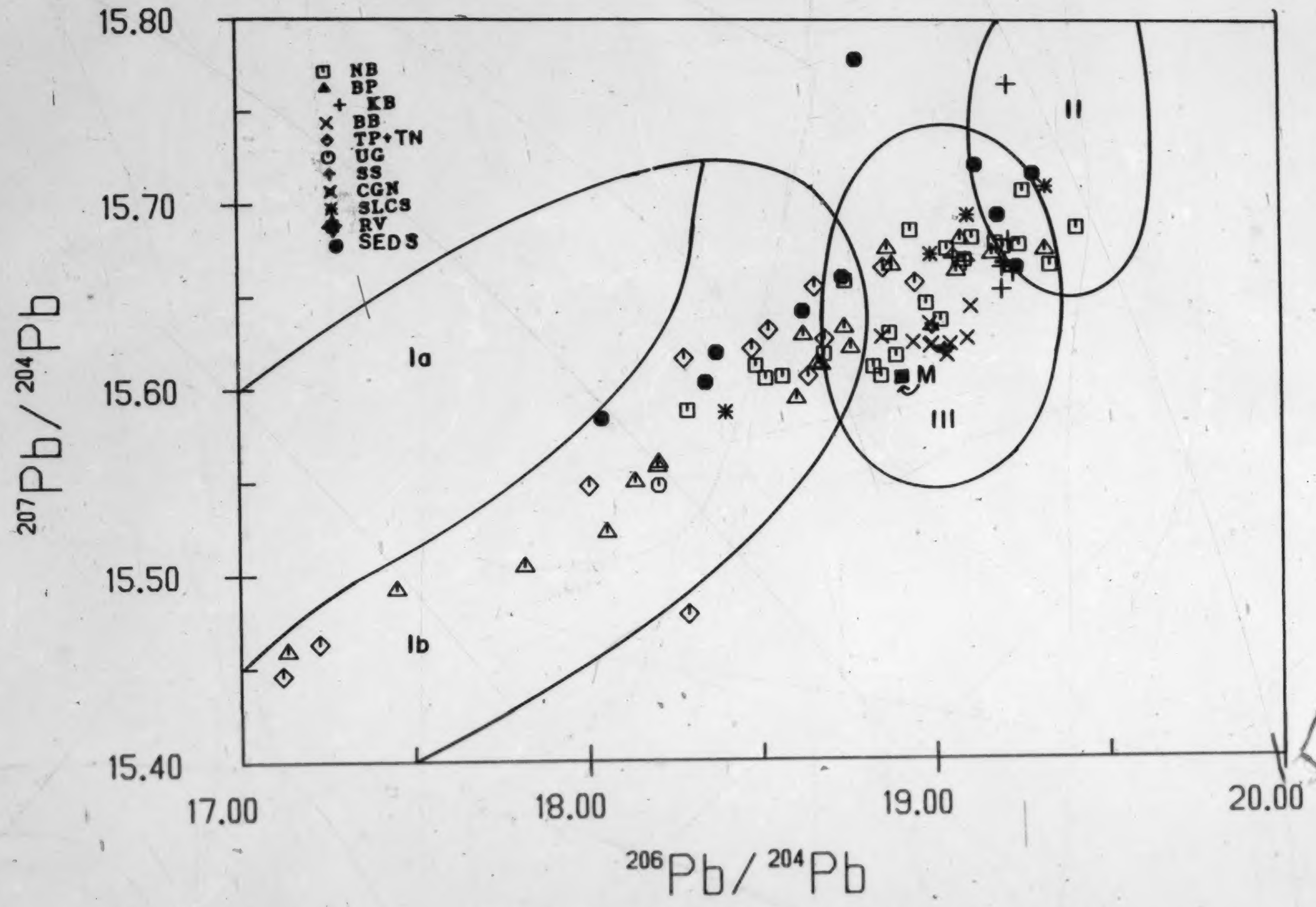
NB
BP
KB
BB
TP+TN
UG
SS
CGN
SLCS
RV
SEDS
Ia
Ib
II
III
M
15.80
15.70
15.60
15.50
15.40
17.00
18.00
19.00
20.00
$^{207}Pb/^{204}Pb$
$^{206}Pb/^{204}Pb$

Fig. 8.6. Also shows three Pb isotope provinces as defined in figure caption of Fig. 8.5.

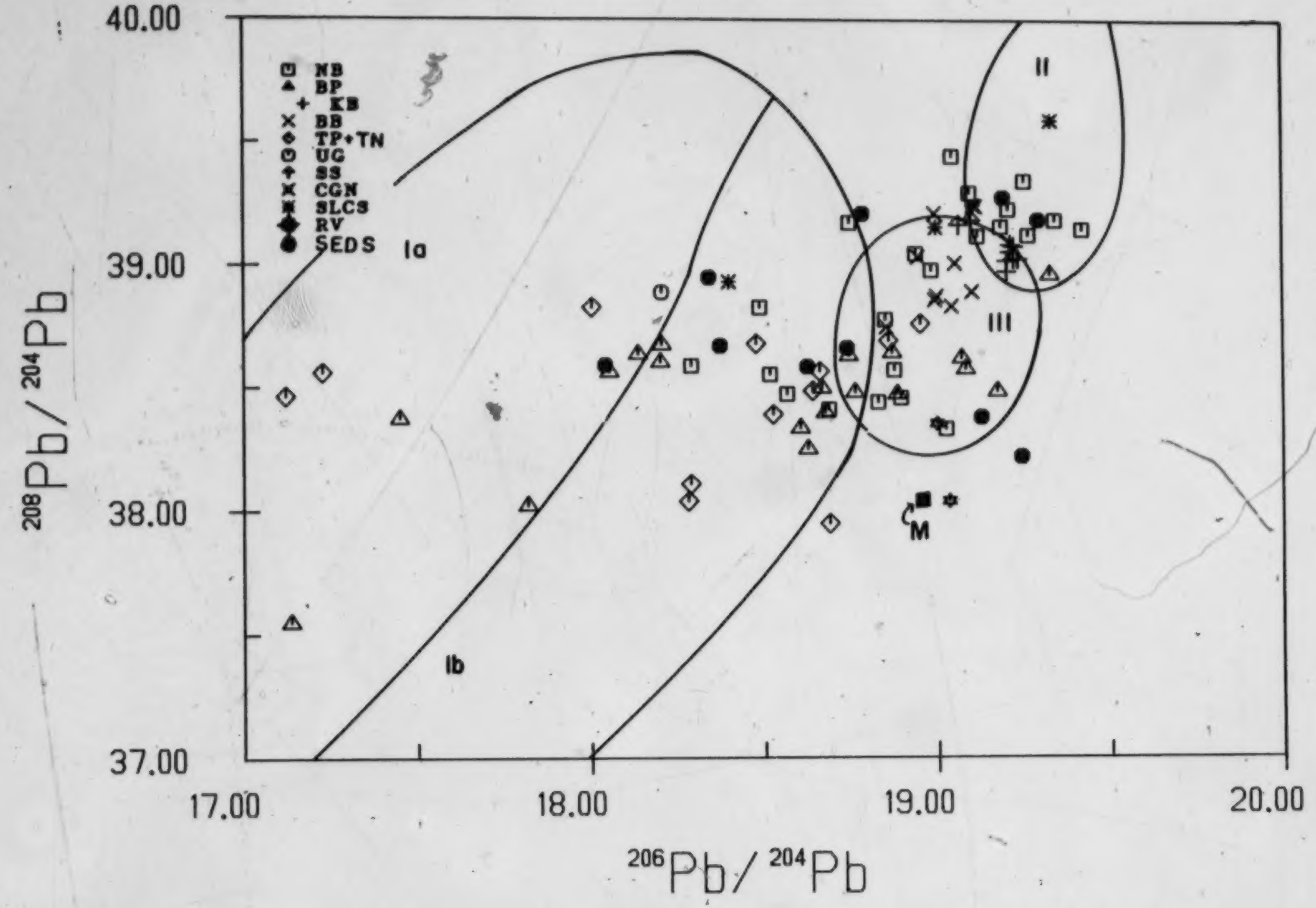
NB
BP
KB
BB
TP+TN
UG
SS
CGN
SLCS
RV
SEDS
Ia
Ib
II
III
M
40.00
39.00
38.00
37.00
17.00
18.00
19.00
20.00
$^{208}Pb/^{204}Pb$
$^{206}Pb/^{204}Pb$

Lack of any linear trends among the samples from any particular batholith indicates simple mixing was not the mechanism for producing the data array as such two-component mixing will always define a straight line on Pb-Pb diagrams. Because of this fact, Pb-Pb data can shed no further light on other mixing processes (e.g., AFC) (James, 1982).

Position of individual sedimentary units on Figs. 8.1 and 8.3. is helpful in identifying which sedimentary units are most likely contaminants. Aldridge Formation, Horsethief and Hamill Group have been rejected as likely contaminants on the basis of either Sr or Nd isotopes. This is also supported from their Pb isotopic compositions. Aldridge sediments have most unradiogenic Pb (average of two groups of samples is: 18.191, 15.592 and 38.761, see Table 8.3 for individual analysis) of all the sedimentary units analysed so far and very unradiogenic with respect to the mantle Pb. Therefore mixing of any type will not produce large range of the batholithic Pb. Some samples of BP (west of the Pb line) might contain Aldridge sediment Pb, but this is very unlikely as these sediments have high Sr-initial ratios and existence of Aldridge sediments west of the Pb line is not supported geologically. Evidence from all three isotopes therefore strongly suggests Aldridge sediments did not participate in the magma genesis of the batholithic rocks. Sedimentary samples belonging to the Horsethief, Active and the Hamill Groups are very radiogenic and all plot below the lower limit of the band containing bulk of the granitic samples (Fig. 8.3). Mixing mantle magma with any of these sediments will produce Pb isotopic compositions very different from batholith-type Pb. Even Ymir, Slocan and Milford (series 8003) are unlikely contaminants because of their less radiogenic nature of Pb than the mantle-value, and the rocks with Pb isotopic compositions less than that of mantle magma are shown to be the products of mixing mantle magma with the lower crust rather that the upper crust. Also the above sedimentary Groups outcrop to the east of the Pb line. If the above conclusions are true, the remaining sedimentary units likely to be contaminants, for the granitic batholiths with Pb isotopic composition greater than that of mantle magma are the Lardeau, Laib, Nelway and Milford-27. Because of very high ^{207}Pb/^{204}Pb ratios of the Nelway Formation, percent of this Formation in the bulk sedimentary composite, likely to be contaminant, will be very small.

9. TECTONICS OF SOUTHEASTERN BRITISH COLUMBIA

9.1 Introduction

The understanding of the tectonic evolution of southeastern B. C. is crucial to that of the whole Cordillera, as this area provides an unique opportunity to decipher the sequence of tectonic episodes that took place between the two terranes: the western allochthonous terranes Quesnellia(Q) and Eastern Assemblage(E) (parts of larger terrane I of Monger et al., 1982) and the thick eastern sedimentary sequences presently thought to be overlying the craton. The autochthonous nature of this eastern sedimentary sequence has been brought into question recently by Chamberlain and Lambert (1985). It has been traditionally thought that this Proterozoic to Ordovician (Belt-Purcell to Active Formation) sedimentary mass constitutes a classical terrace wedge formed outboard on the attenuated cratonic crust and adjacent oceanic crust (Price, 1981). This attenuation was due to rifting associated with the development of the western margin of North America in Proterozoic and early Paleozoic times. Firm evidence of allochthoneity or autochthoneity of this terrace wedge is therefore needed. The present study focuses on this problem on the basis of isotopic geochemistry of this sedimentary package.

Different lines of geophysical evidence established that the western edge of the Canadian Craton lies along the Kootenay Arc. The importance of this knowledge has been repeatedly shown by Monger et al. (1982) and Price (1981) as the juxtaposition of the two terranes along this boundary controlled the development of the complex structural and metamorphic and igneous intrusive episodes of the Kootenay Arc, the Purcell Anticlinorium and the fold and thrust belt of the Rocky Mountains. Besides establishing this western boundary of this craton through the use of isotopic data, it is also equally important to obtain knowledge of the basement of Quesnellia on which the rocks (such as Triassic sediments, Lower Jurassic volcanic rocks and mid-Jurassic granitic batholiths) have developed. The isotopic study brought out definite information on this problem and established the basis of a framework to understand the petrogenesis of the granitic batholiths. Also, the present isotopic study offers an unique opportunity to compare geochemically the nature of Quesnellia basement with that of the miogeocline to the east.

Timing of accretion of terrane I with terrane III (of Chamberlain and Lambert, 1985) is to be firmly established on the basis of accurate age determination of the granitic batholiths that straddle the boundary of the two. As the Nelson Batholith shows intrusive relationships to both the volcanic rocks of Quesnellia (Rossland Volcanic Group) and the Paleozoic sedimentary units (Hamill, Lardeau, Laib, Active and Nelway Formations) of terrane III, it is probably the best candidate to determine the upper time limit of accretion of the two terranes. U-Pb dating of zircons from the Nelson Batholith, puts constraints on the above problem. Geochemical studies of this batholith also determined the degree and nature of the crustal involvement in its genesis.

Simony (1979) regarded the Trail Gneiss as a partially reworked and possibly allochthonous piece of the Precambrian North American craton based only on field evidence. Such a hypothesis must be proved by isotopic dating. Nd isotopic signatures rule out the possibility of its being directly correlatable to the basement of Hudsonian age. Nd isotopic compositions and presence of old inherited Pb in Castlegar Gneiss have proved the existence of a lower crust under the study area, but its relationship with the exposed granitic and gneissic rocks of the Okanagan Complex (Okulitch, 1984) is not known and it is assumed here that they are probably parts of the same crust.

Detailed isotopic and geochemical study have been therefore applied to critically evaluate the existing tectonic models.

9.2 Lower Crust

One of the most significant discoveries made during the present work is the concrete evidence of the presence and nature of a lower crust underlying the study area. It was shown in Chapters 7 and 8 that the three samples collected from three small granitic stocks (from east to west, 8088C (Shoreline Stock), 8021D (east side of the Bonnington Pluton) and 8064E (Unit A)) have $\epsilon_{Nd}(0) \simeq -14.0$, the lowest of all granitic batholiths/plutons in the area. A model crust with average $f_{Sm/Nd} = -0.40$ if extracted from the model depleted mantle of DePaolo (1981a) will have $\epsilon_{Nd}(0) = -14.0$, if the crust formation age is 1.8 Ga. However T^{Nd}_{DM} model ages calculated for these three samples are slightly less (by 0.2 to 0.3 Ga) than expected (i.e., 1.8 Ga), implying a small fractionation in Sm/Nd during the melting events. Parrish and Wheeler (1983) dated the Kuskanax Batholith by U-Pb zircon method and found the upper and lower intercepts with the concordia at ≈ 2060 Ma and 173 Ma respectively. The component of inherited Pb must have come from a Precambrian basement similar to that in the Monashee Complex (Parrish and Armstrong, 1983). This basement underlying the Kuskanax Batholith might be the northern extension of the lower crust established in the south under the Nelson Batholith from the Nd results.

All geophysical evidence (Monger and Price, 1979) suggest that the cratonic crust extends as far as west of the Kootenay Lake. As geophysical properties change drastically for the crust west of the Kootenay Lake, the lower crustal material being sampled by the two samples (8021D and 8064E) is certainly different from that being sampled by 8088C from the Shoreline Stock along the east shore of the Kootenay lake. Its location and timing of intrusion at about 51 Ma suggest its derivation from the melting of the lower cratonic crust confirming the existence of such a crust based on geophysical data. The unlikelihood of its derivation by melting the lower part of the miogeoclinal sediments has been discussed in Chapter 7 (Section 7.6)

In Chapter 4, it has been shown that the sedimentary rocks belonging to the miogeocline of the western Cordillera were derived from a source provenance not older than 1.8 Ga. Frost and O'Nions (1984) have shown that the crustal residence ages of the gneissic drilled-core samples from the Canadian craton east of the Southern Rocky Mountain Trench (SRMT) range in between 2.6 to 3.2 Ga. Therefore their work and the present study strongly suggest that the Canadian craton east of the SRMT did not act as a source for the miogeoclinal sediments.

Tectonic and structural evidence (Price, 1981) suggested about 200 kms northeastward displacement of the miogeoclinal rocks over to the craton. Therefore it is very well possible that these miogeoclinal sediments were derived from the part of the craton presently underlying it, but not from the part of the craton east of the SRMT. $\epsilon_{Nd}(0)$ values for the craton east of the SRMT are around -20, much lower than those west of the trench (inferred to be -14.0). This geochemical difference between the craton east and west of the SRMT is also supported by the geophysical evidence to some extent (Chandra and Cumming, 1972). At the SRMT, a lower crustal layer to the east with seismic velocity of 7.15 km/s and density 3.03 g/cc and an upper mantle layer with velocity of 8.20 km/s and density of 3.43 g/cc disappear abruptly and both are replaced by an upper mantle layer with velocity and density equal to 8.0 km/s and 3.36 g/cc respectively. This coincidence of seismic velocity difference and also gravity anomalies across SRMT suggest that SRMT is a vertical fault at depth, separating lithospheres of contrasting geophysical and geochemical properties.

If the above argument for the derivation of miogeoclinal sediments from the part of the craton bounded by SRMT and the Kootenay Arc is accepted, then it is possible that the part of the miogeocline consisting of the north-tapering wedge of Proterozoic and Phanerozoic metasediments of the Purcell, Windermere, Hamill, Lardeau, Laib, Broadview, Active, Nelway Formations and the underlying craton were together since the beginning of sedimentation. This part of the craton bounded by SRMT and the Kootenay Arc will be called craton(A) onward. This portion of the miogeocline is a part of the recently defined terrane III (Chamberlain and Lambert, 1985).

9.3 Times of Collision

Monger et al. (1982) defined two super-terranes, I and II comprising the western Cordillera, allochthonous with respect to the North American craton. The Terrane I, consisting of four smaller terrranes (St, Cc, Q and E), amalgamated together by latest Triassic-earliest Jurassic time. The present study involves rocks belonging to terranes Q, E and III. Terranes E and Q have been shown to be stratigraphically overlapped by Middle or Upper Triassic strata in south-central British Columbia (Read and Okulitch, 1977). In the Lardeau map area, the Milford Group (belonging to E) rests unconformably on deformed basement of the Lardeau Group (Klepacki, 1983). Andesitic volcanics of the Kaslo Group initiated in late Mississippian time deposited partly on lower carbonate and clastic sequences of the Milford Group (apparently derived from the east) and partly on the oceanic crust. This marginal oceanic basin was the site of deposition of the Slocan Group clastics, some of which were derived from the west (Cairnes, 1934). Such a continental margin-oceanic crust deposional environment of sediments from the Lardeau to Slocan Groups requires Eastern assemblage and the Slocan Group (part of Q) to be attached to terrane III, as the Lardeau Group was also attached to craton (A) (Klepacki, 1983). In the central Kootenay Arc, Leclair (1983) observed small angular difference in trend between the strata of the Milford Group and older rocks (e.g. Lardeau Group), suggesting presence of a strike fault, though its magnitude and direction are not known. But throughout the Kootenay Arc, an unconformity separates the Milford Group from the underlying Lardeau Group. The stratigraphic and structural evidence across which indicate a difference in one phase of folding (Brown et al., 1981).

In the southern part of the Kootenay Arc, the Lower Paleozoic sediments (Laib, Nelway and Active Formations) constitute a series of thrust sheets or structural belts (Eastern, Argillite and Mine Belts). Thrusting took place from the east to the west along the Black Bluff, Argillite and Waneta Faults and brought miogeoclinal rocks of these belts along the westernmost Waneta fault over the Lower Jurassic volcanic rocks of the Rossland Group (part of terrane Q). These thrusts are therefore post Lower Jurassic. Intrusive relationships in the southern part of the Nelson Batholith to the miogeoclinal sediments and the westerly verging thrust faults are clearly shown by the southern tail of this mid-Jurassic Batholith, which cuts across the Lower Paleozoic Laib and its equivalent Lardeau Groups. Smaller plutons in the Salmo map area also show clear intrusive relationship with both Q and the miogeocline. For example, the Bunker Hill Stock (BH, mid-Jurassic) intrudes both the Rossland Group and the Laib Formation and cuts across the Waneta Fault. Such structural evidence suggests that terrane Q was accreted to the miogeocline or terrane III by mid-Jurassic time.

Besides voluminous mid-Jurassic plutonism in the southern Nelson-Rossland Arc, intense deformation and metamorphism, in the southern Kootenay Arc, also commenced in mid-Jurassic time due to accretion of the composite allochthonous terrane I to terrane III (Archibald et al., 1983; Monger et al., 1982; Chamberlain and Lambert, 1985)

9.4 Evidence of Allochthoneity

The above discussion strongly suggests that terrane I and terrane III were together since at least mid-Jurassic time. Palaeontological and palaeomagnetic and structural data are now available to show that most of the North American Cordillera is made up of "suspect terranes" or "allochthonous terranes".

Palaeontological evidence (Tozer, 1970; Monger and Ross, 1971; Yaney, 1975; Nichols and Silberling, 1979; Tipper, 1981) show that Permian, Triassic and Jurassic rocks in different terranes contain faunas which may be disjunctive with one another and also with those in rocks deposited on or near the North Amercan craton. Original biostratigraphic conditions of the disjunctive faunas suggest displacements of these terranes on the order of thousands of kilometers (Price et al., 1981). For example, Permian faunas of the Cache Creek Group closely resemble those in areas surrounding the western Pacific and ancient Tethys, but other faunas resemble to those in southeastern United States and Mexico.

Recently, Gabrielse (1985) estimated the cumulative dextral displacement along the major transcurrent faults in the western Cordillera based on offsets of shelf to off-shelf facies boundaries in Lower Paleozoic rocks and also among younger granitic plutons. It is probable that the total displacement of terranes west of the faults relative to the terrane east of NRMT was >1000 km. Transcurrent movements started from mid-Cretaceous or earlier and continued till late Eocene or Oligocene. Though SRMT is almost co-linear with the Tintina and NRMT faults, large transcurrent movement along it has not been documented from mid-Cretaceous time onwards. But the graben structure of SRMT may have been superimposed on cover rocks thrust over the locus of an earlier transcurrent fault continuous with NRMT. A Mesozoic or Paleozoic trasncurrent movement along it has been suggested by Leech (1966). Otherwise the southerly continuation of NRMT fault zone must lie in a structurally complex region or flanking the Shuswap Metamorphic Complex (Gabrielse, 1985).

In addition to the N-S transcurrent movements documented above, thrust faulting in the southern part of the Rocky Mountain Belt involves a net horizontal displacement of >200 km between the mid-Jurassic magmatic arc (Nelson-Rossland Arc) to the west and the North

American craton (Bally et al., 1966; Price, 1981).

Different terranes in the western Cordillera preserve paleomagnetic data that document latitudinal shifts relative to the cratonic North America ranging up to several thousand kilometers (Irving et al., 1980; Monger and Irving, 1980). Earlier palaeomagnetic data (Irving and Yole, 1972; Hillhouse, 1977; van der Voo et al., 1980) suggested that the Triassic, Jurassic and Lower Cretaceous rocks on Stikinia might have travelled northward relative to the cratonic North America by about 13°, whereas Triassic strata of Wrangellia by as much as 33°. The most recent palaeomagnetic study by Irving et al. (1985), concluded that a composite block made up of Wrangellia, the Coast Plutonic Complex, Cascade terrane, Stikinia and perhaps Quesnellia was situated in a latitude corresponding to what is today northern Mexico during mid-Cretaceous time and since then has undergone a common history of northerly transport and clockwise rotation. They calculated a total displacement of about 2400 km and a rotation in the range of 40-70° clockwise during a period starting after mid-Cretaceous (about 90 Ma) and before mid-Tertiary time.

Recently Armstrong et al. (1985) dated the Axelgold Gabbro emplaced in rocks of the Cache Creek Group and reviewed the previously determined K-Ar and Rb-Sr dates. They proposed a maximum age of emplacement of 125 Ma for this gabbro body. As the early to mid-Cretaceous batholiths like the Raft intrude both the Cache Creek Group and Quesnellia, and mid-Jurassic batholiths (e.g. Nelson Batholith, Salmo Stock, Bunker Hill Stock) intrude both Quesnellia and terrane III, and there is no evidence of large-scale post-Jurassic north-south movements between terrane I and III, the most recent conclusion of Irving et al. (1985), that the Quesnellia and other western terranes undergone northerly displacement of about 2400 km must also apply to the northeast tapering wedge of Proterozoic and Phanerozoic metasediments of the Purcell, Winderemere, Hamill, Lardeau, Laib, Active and Nelway Formations in southeastern B.C. As it was discussed before that these sediments were probably derived from the craton underlying them, the part of the craton in between SRMT and the Kootenay Lake) might also have the same degree of allochthoneity as that of Quesnellia.

9.5 Structural Setting of the Nelson-Rossland Arc

In southeastern B. C., an arcuate belt (approximately N-S) of volcanic rocks (Rossland Volcanic Group) and plutonic granitic batholiths (Kuskanax, Nelson, Bonnington and Trail) are closely associated. This close association of volcanic and plutonic rocks has been tentatively termed as "Nelson-Rossland Arc" (Chapter 2). Origin of this N-S trending Lower to mid-Jurassic Arc is not clearly understood in terms of complex Cordilleran tectonics.

In Chapters 5 and 6, it was shown that both the Nelson Batholith and Bonnington Pluton are typically calc-alkaline in nature, similar to other granitic batholiths in western U.S.A. (e.g., Sierra Nevada and Peninsular Ranges). The Lower Jurassic Rossland Volcanic Group consists of a succession of agglomerates, lavas, fine-grained volcaniclastics and pyroclastics intercalated with marine shales and siltstones (Beddoe-Stephens, 1982). The lava groups are dominantly basic and consists of basalt(58%), ankaramite(26%) and andesite(16%). The alkalic rather than a tholeiitic or high-alumina parent magma is suggested due to the presence of amphibole-bearing basalts and ankaramitic rocks. Detailed petrographic, mineralogic and geochemical study of the Rossland lavas (Beddoe-Stephens and Lambert, 1981, Beddoe-Stephens, 1982) suggests an island-arc tectonic environment. Immobile trace element data (Ti, Zr and Y), Sr-initial values (0.70328-0.70404) and δO^{18} of clinopyroxenes (4.8-6.5), all point to a mantle origin for the Rossland lava that developed on an oceanic crust or a thin lower crust without significant crustal contamination. The present Nd, Sr and Pb isotopic studies support the latter alternative. $\epsilon_{Nd}(T)$ value of one of the two samples from the Rossland Group is slightly lower (by 2ϵ -units) than the average island arc volcanic rocks (+8, DePaolo and Waserburg, 1976). Because of the alkalic nature of the Rossland Volcanic Group, it might have also developed in the latest phase of the arc-activity. Such alkalic and shoshonitic magmas have developed in the Tabir-Lihir-Tonga-Feni group of islands (Jhonson et al., 1976), the Papuan Highlands (McKenzie, 1976) and the New Hebrides (Colley and Warden, 1974).

Detailed trace element and isotopic modelling (Chapters 5, 6, 7, 8) showed that the granitic batholiths have undergone complex history of crystal fractionation and crustal contamination. The parental magmas originated in the mantle, in a similar way to average oceanic island arc magmas and rose through the local lower crust. Though the precise boundaries of this lower crust cannot be defined from the present study, it could be however concluded that the Nelson-Rossland Arc developed either totally on this local crust or along its eastern edge. The character of isotopic contamination of the igneous rocks sharply changes from the west to the east along a N-S line (called Pb-line) approximately coincident with the Slocan Lake and Champion Lake faults (see Chapters 7 and 8). Such a Pb-line is possibly coincident with the pre-Mesozoic western limit of the sedimentary appron that might have existed before the arc activity began. With reference to the chosen mantle Pb-composition, igneous samples west and east of this line have Pb-isotopic compositions that are invariably lower and higher than this mantle value respectively.

Structurally the southern part of the Arc is fault-bounded on both the east and west sides. On the west, the N-S trending Champion Lake Fault (Little, 1962; Simony, 1979; Corbett and Simony, 1984) juxtaposes the Trail Gneiss against the Bonnington Pluton and the Rossland Volcanics. This fault probably cuts through the Trail Pluton and an age of 163 Ma (Corbett and Simony, 1984) for the Trail Pluton gives the maximum age of faulting. Simony's (1979) argument of about 5 kms dip-slip is however disputed by Little (1982) who concluded that the fault is of hinge-type and the maximum displacement cannot be so great. In the north, the western boundary of the Nelson Batholith is in fault contact with the Valhalla Gneiss Complex along the Slocan Lake Fault (Parrish, 1981, 1984), possibly a listric normal fault with rocks to the east sliding downwards. This fault probably developed concurrently with the north-side trending anticlinal arching and doming of the Valhalla Gneiss Complex (Reesor, 1965), which probably occurred during late Cretaceous or early Tertiary (Eocene?) time (Parrish, 1981). On the east, along the Waneta fault, Cambro-Ordovician rocks were thrust over the Jurassic complex of the Rossland-Salmo area.

9.6 Relationship among Metamorphism, Deformation and Plutonism

The southeastern part of the Omineca Crystalline Belt consists of a high-grade metamorphic infrastructure (Shuswap Metamorphic Complex, Okulitch, 1984) and a lower grade suprastructure (mainly eugeoclinal Paleozoic to mid-Jurassic rocks belonging to terranes, Q and E, and miogeoclinal sedimentary sequences, Price et al., 1981). Oldest rocks in the infrastructure have been dated at 1.96 Ga (Thor-Odin Complex, Wanless and Reesor, 1975) and the youngest rocks at 63 Ma (Valhalla Dome, Parrish, 1983), and at 54 Ma (Castlegar Gneiss). Along the eastern boundary of the suprastructure lies a N-S trending belt of amphibolite facies regional metamorphism that transects major structures of the Kootenay Arc (Crosby, 1968). This belt plunges to the north under the Purcell Anticlinorium, but in the south it merges with a plutonic-metamorphic complex in northern Idaho (Miller and Engels, 1975). Archibald et al. (1983) compiled all the data on metamorphic mineral assemblages in pelitic rocks and have drawn the regional metamorphic isograds in the Kootenay Arc (Fig. 2 of Archibald et al., 1983).

The highest grade of metamorphic rocks is recorded by the presence of sillimanite-K-feldspar gneiss in the Riondel area (Hoy, 1976, 1980) and corresponds to a pressure between 0.5 to 0.6 GPa and a temperature close to 650°C (Archibald et al. 1983). Beside this arealy restricted zone, the innermost sillimanite zone (10-15 km across) forms the core of the metamorphic culmination recorded in rocks as old as the Aldridge Formation in the south and as young as the Triassic Slocan Group in the north (Parrish, 1981). Isograds of lesser metamorphic grade (St/St-Ky, Gt and Bi) form concentric zones in the area and therefore indicates metamorphic grade decreases both east- and westward. In the south, around the Mine and Wall Stocks a narrow zone of high-grade metamorphic rocks appears as local salient on the regional trend. In this area, Archibald et al. (1983) noted that "post-kinematic quenching of prograde metamorphic reactions occurred at a temperature of about 500°C and a depth of about 15 km (P=0.38 GPa) south of the Mine Stock, but a temperature of about 600°C and a depth of about 20 km (P=0.55GPa) on the north side". Due to lack of any structural evidence for a local differential uplift, they suggested that the difference in metamorphic pressure conditions was due to the progressive increase in depth of burial and diachronous quenching of metamorphic reactions.

Therefore both in the north, in the Riondel area rocks as young as the Lardeau Group and in the south, in the Summit Creek area rocks as young as the Windermere Supergroup are involved in the highest grade of metamorphism at pressures from 0.5 to 0.6 GPa, corresponding to a depth of burial of about 20 km. As there is no evidence of burial of these sedimentary Groups down to mid-crustal level to lower crustal levels due to normal sedimentary loading, burial due to tectonic overlapping is the best alternative (Price et al., 1981; Archibald et al. 1983).

Three periods of intrusive activities are defined by the available K-Ar and U-Pb zircon dates (Archibald et al., 1983; Parrish and Wheeler, 1983; Duncan and Parrish, 1979; Duncan et al., 1979; Nguyen et al., 1968; Wanless et al., 1968a; and the present study). Granitic Batholiths (Nelson, Bonnington, Mine, Wall, Shaw Creek, Porcupine Creek, Carlyle and Mount Toby) were emplaced during mid-Jurassic time (171-164 Ma) in the Nelson-Rossland Arc and western part of the Kootenay Arc. These are considered to be late-synkinematic to post-kinematic granitic(s.l.) bodies accompanying regional metamorphism and deformation (Reesor, 1973; Glover, 1978; Archibald et al., 1983).

The second phase of intrusive activity took place post-kinematically in mid-Cretaceous time (about 100 Ma) and saw emplacement of the Bayonne Batholith, Summit Stock, White Creek and Fry Creek Batholiths, Corn Creek and west Creston Gneisses. These batholiths or gneisses form a linear N-S trending belt east of the mid-Jurassic intrusives and either overlap or cross-cut the trend of high-grade metamorphic culmination. The youngest phase is defined by the Eocene (50 Ma) intrusives of small bodies of syenites, Shore Line Stock, Unit A and parts of Castlegar Gneiss.

Mid-Jurassic plutons also yield K-Ar mineral dates which are as young as mid-Cretaceous and are commonly highly discordant. For example, K-Ar biotite dates are younger than hornblende and this difference is due to slow cooling of a large magmatic body or thermal overprinting of younger phases of batholiths or unrelated mid-Cretaceous or younger intrusive or metamorphic events. Also younger dates could result from an uprising geotherm due to erosion of lithosphere, an end result of the subduction processes. Due to higher closure temperature for hornblende (about 500°C, Harrison, 1981), K-Ar hornblende dates are therefore better estimates of the time of emplacement than dates obtained from biotite and muscovites (with closure temperatures of about 280°C and 350°C respectively, Berger and York, 1979; Harrison and McDougall, 1980).

Like the mid-Jurassic plutons, mid-Cretaceous plutons also yield K-Ar dates which are younger than the emplacement age and range upto Eocene (100 to 40 Ma, Archibald et al., 1984). They have contoured the K-Ar dates (55 to 90 Ma) from igneous rocks and found that these contours are broadly conformable with the regional metamorphic isograds, i.e., young towards the metamorphic culmination. K-Ar muscovites and whole rock dates also appear to show similar trends.

Archibald et al. (1984) interpreted the mid-Cretaceous to Eocene isotopic dates as being due to diachronous cooling following differential post-emplacement uplift (0.1 to 0.4km/Ma from mid- to late-Cretaceous and higher upto 0.7 km/Ma during earliest Cretaceous time.

9.7 Tectonic Model

Fig. 9.1 is a schematic representation of a tectonic model that tries to incorporate the available structural, metamorphic and geochemical data. This tentative model is neither unique nor original but differs from the previous models in some details.

In the previous discussion, it was suggested that the cratonic crust (A) in between SRMT and the Kootenay Arc and the overlying miogeoclinal rocks are allochthonous like Quesnellia(Q) with respect to the craton east of SRMT. Therefore the agreement that the northwesterly tapering prism of miogeoclinal strata deposited along and outboard from the ancient rifted margin of a craton could be accommodated in the present model. This differs from Chamberlain and Lambert's model (1985) where only the miogeoclinal rocks are considered allochthonous. The lower crusts both east and west of the Kootenay Arc appear geochemically similar ($\epsilon_{Nd}(0) \cong -14.0$) and therefore may be considered to be rifted equivalents.

Fig. 9.1 Schematic representation of the tectonic evolution in the southeastern British Columbia. a. Early rifting created depositional environment for continent-derived sediments in a migeocline. Sediments from upper Proterozoic to Paleozoic age apparently derived from the Craton(A) to the east. A portion of the Mesozoic sediments is thought to have derived from the west. b. Due to accretion of the terranes St and Cc to the western margin of the terrane Q after 200 Ma, an eastward dipping subduction started leading to the extrusion of the Rossland Volcanics and overthrusting of western edge of the Paleozoic miogeosynclinal sediments above the volcanic piles along the Waneta, Argillite and Black Bluff Faults. With increasing arc maturity, thickenend crust led to the formation of the mid-Jurassic granitic (s.l.) batholiths (KB, NB, BP, TP) of which NB cuts the above the thrust faults. These lower Jurassic and mid-Jurassic volcanics and granitic batholiths constitute the "Nelson-Rossland Arc" c. Telescoping of the miogeoclinal sediments started with continued eastward movement of terrane I. Mine Stock (mid-Jurassic) probably formed due to crustal thickeneing of the western part of the Craton(A). Continued eastward movement caused impingement of Q onto the miogeoclinal rocks and resulted in the tectonic burial of such rocks (e.g., Widermere and Lardeau Groups, Archibald et al., 1983) to great depths (20-24 km) during a short time interval (165 to 155 Ma). d. Westward subduction ensued soon after or during the early Cretaceous when the oceanic crust flooring part of the migeocline started subducting below Q. Cretaceous batholiths west and east of the Nelson-Rossland Arc formed during this subduction episode (see text for further discussion). Abbreviations used: BP=Belt-Prucell, W=Windermere, Pal=Paleozoic, Meso=Mesozoic sediments, NRA=Nelson-Rossland Arc, MS=Mine Stock, BB=Bayonne Batholith, PA=Purcell Anticlinorium, KA=Kootenay Arc, St=Stikine, Cc=Cache Creek terranes, A=Craton(A), SS=Canadian Sheild, SRMT=Southern Rocky Mountain Trench.

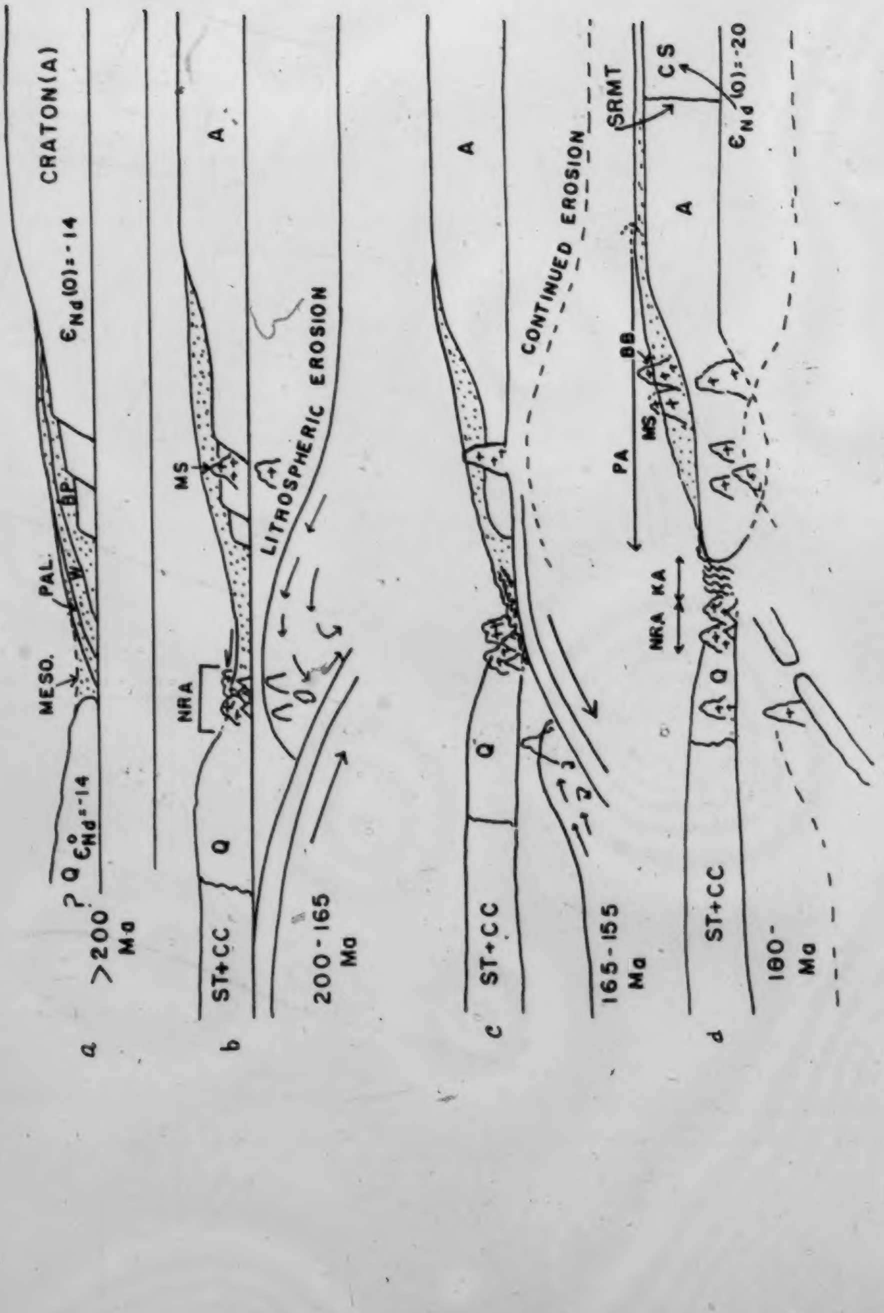
a
>200 Ma
?
Q
ε°Nd=-14
MESO.
PAL.
W
BP
εNd(0)=-14
CRATON(A)
b
ST+CC
Q
200-165 Ma
NRA
MS
LITROSPHERIC EROSION
A
c
ST+CC
Q
165-155 Ma
CONTINUED EROSION
A
d
ST+CC
Q
180- Ma
NRA
KA
PA
MS
BB
A
SRMT
CS
εNd(0)=-20

In such a case (Fig. 9.1a), thick sedimentary sequence of the Purcell, Windermere and Paleozoic sediments were derived from the craton (A) to the east and they could be considered to be always part of the craton. There were intermittent volcanic activities e.g., Irene Volcanic Formation, volcanic rocks at the base of Windermere and Hamill Groups, and Kaslo Group. Similar crustal residence ages of the craton(A) and the sediments (Chapter 4) overlying it suggest they were together since the time of deposition. Such a model supports the view of Monger and Price (1979) and Price (1981).

Klepacki (1983) proposed a model which requires that the Eastern Assemblage and Slocan Group sediments to be attached to the craton(A) to the east if the Lardeau Group was attached to the craton(A). The evidence that sparse paleocurrent data and facies changes (Cairnes, 1934) suggest that some of the Slocan sediments have a westerly source could be fit in the present model if it is thought that old rifted crust to the west acted partly as a source. This is supported by the old T_{CR} ages obtained for the Slocan (1.89 Ga) and the Ymir (1.71 Ga) Groups.

The above scenario however changed during latest Triassic and early Jurassic time when terranes like Stikinia and Cache Creek collided with Quesnellia (western part of the rifted craton probably acted as its basement) and a eastward subduction started (Fig. 9.1b). This led to the formation of the Rossland Volcanic Group probably along the eastern edge of the basement of Quesnellia and partly on the oceanic crust (Fig. 9.1b). Small amount of crustal involvement in the Rossland lava (see Chapters 7 and 8) supports such a view. Occurrence of the greater part of this volcanic group east of the Pb-line and the signature of the upper crustal Pb (i.e., sedimentary) suggest that magma interacted with oceanic sediments derived from the craton. During this time there was eastward movement of terrane I, resulting in westward overthrusting of the Lower Paleozoic miogeoclinal sediments above Quesnellia (along Waneta, Argillite and Black Bluff Fault). With arc maturity, thickened crust led to the formation of the mid-Jurassic granitic batholiths (e.g. KB, NB, BP, and TP) some of which cut the above thrust faults and therefore westward thrusting took place before mid-Jurassic time. These Lower and mid-Jurassic volcanics and plutonic rocks constitute the "Nelson-Rossland Arc".

Continued eastward movement of terrane I started with telescoping of the miogeoclinal sediments. The western part of the attenuated craton(A) underwent crustal thickening and partial melting ensued to produce the mid-Jurassic Mine Stock (171-162 Ma). Erosion of lithosphere and rising heat-flux might have accentuated such a melting event. Such a condition of melting might also be true for the mid-Jurassic Mount Toby Stock.

Available ϵ_{Nd} data from the batholiths show the importance of mantle-derived material in the generation of such batholiths. A restricted range in $\epsilon_{Nd}(T)$ (-2 to -8) lying in between the average island arc magma (+8) and the local lower crust(-13) supports the view that arc developed mostly on the old basement and interacted with it. This is possible as the mantle magma continues to rise into the overlying lower crust, the crust becomes a semi-molten mixture of mantle-magma, crustal-melts and crystal cumulates. Alternatively large magma fluxes might rise through the crust much faster without much crustal interaction. Absence of Nd data from the Mine Stock makes it impossible to assess the amount of mantle vs. crustal Nd in its genesis. Small increase in crustal thickness in the Mine Stock area, coupled with a low flux of magma from the mantle, probably caused pure crustal melts to rise to the higher levels of the crust.

If all or most of the Nelson Batholith and Bonnington Pluton were emplaced in mid-Jurassic time, younger K-Ar dates are probably related to a continued effect of thermal flux from below. During subduction, as downward flow of mantle (asthenosphere) occurs along the subducting plate causing an upward and westward flow of hot mantle replacing the sinking material (McKenzie, 1969, Marsh, 1979). This results in the erosion of relatively colder lithosphere and an eastward propagation of rising geotherms. Effect of such a heat flux will certainly cause resetting of K-Ar dates in biotites and muscovites as found in the granitic batholiths.

Continued eastward movement of terrane I caused impingement of Quesnellia into the miogeocline and resulted in the tectonic burial of the rocks (e.g., Windermere, Lardeau Groups) to depths of 20-24 km during a short time span of 10 Ma (165 to 155 Ma, Archibald et al., 1983).

Westward subduction ensued soon after, or during early Cretaceous, when the intervening oceanic crust upon which part of the miogeocline was deposited started disappearing along a westward dipping subduction zone (A-subduction zone cf Bally, 1975). Early and mid-Cretaceous granitic plutons both west and east of the Nelson-Rossland Arc formed as a result of this subduction. Cretaceous batholiths west of the arc were the direct results of the subduction process. However those (Bayonne, White Creek and Fry Creek Batholiths) to the east of the arc, which intruded the miogeocline, were due to the effect of crustal thickening that happened in the craton(A) and the raised geotherm (shown as dashed line in Fig. 9.1d). Nd isotopic data for the Bayonne Batholith and Summit Stock however show that (Chapter 7) there is considerable input of mantle material. This is possible due to high heat flow in the region and mantle magma, which while rising through the thickened crust caused extensive melting. Other Cretaceous batholiths (which are mostly of the two-mica variety) probably formed in a similar way, but the lack of Nd isotopic composition at the present time prohibits any inference regarding the amount of mantle input in their source.

Palinpastic reconstruction by Price (1981) requires that in late Cretaceous time the deformed and metamorphosed eugeoclinal and miogeoclinal strata of the Kootenay Arc and Purcell Anticlinorium and the associated granitoid plutons were situated at least 100 km west of their present position. As the Kootenay Arc and Purcell Anticlinorium formed during late Cretaceous (Campanian) to early Paleocene time, after the mid-Cretaceous granitic plutons were emplaced in the deformed miogeoclinal prism, they were displaced more than 100 km northeast across the continental margin on to the craton(A) and also on the North American Craton over a steplike ramp in the craton(A) corresponding to the ancient rifted margin of the continent.

REFERENCES:

Allègre, C. J. 1982. Chemical Geodynamics. Tectonophysics, 81, 109-132.

Allègre, C. J., Ben Othman, D. 1980a. Nd-Sr isotopic relationships in granitoid rocks and continental crust development: a chemical approach to Orogenesis. Nature, 226, 335-341.

Allègre, C. J., Ben Othman, D., Polve, M., Richard, P. 1979. The Nd-Sr isotopic correlation in mantle materials and geodynamic consequences. Phys. Earth Planet. Inter., 19, 293-306.

Allègre, C. J., Brevart, O., Dupre, B., Minster, J. F., 1980b. Isotopic and chemical effects produced in a continuously differentiating earth's mantle. Phil. Trans. R. Soc. Lond., Ser A, 297, 447-477.

Allègre, C. J., Dupre, B., Richard, P., Rousseau, D., Brooks, C., 1982. Subcontinental vs. suboceanic mantle II: Nd-Sr-Pb isotopic composition of continental tholeiites with mid-ocean ridge tholeiites, and the structure of the continental lithosphere. Earth and Planet. Sci. Lett., 57, 25-34.

Allègre, C. J., Dupre, B., Lambert, B., Richard, P. 1981. The subcontinental vs. suboceanic debate, I: Lead-neodymium-strontium isotopes in primary alkali basalts from a shield area: the Ahaggar volcanic suite, Earth and Planet. Sci. Lett., 52, 85-92.

Allègre, C. J., Hart, S. R., Minster, J. F., 1983. The chemical structure and evolution of the mantle and continents determined by inversion of Nd and Sr isotopic data II: Numerical experiment and discussion. Earth and Planet. Sci. Lett., 66, 191-213.

Allègre, C. J., Minster, J. F., 1978. Quantitative models of trace element behaviour in magmatic processes. Earth and Planet. Sci. Lett., 38, 1-25.

Allègre, C. J., and Rousseau, D., 1984. The growth of continents through geological time studied by Nd isotopic analysis of shales. Earth and Planet. Sci. Lett., 67, 19-34.

Andrew, A., Godwin, G. I., Sinclair, A. 1984. Mixing Line Isochrons: A New interpretations of Galena Lead Isotope Data from Southeastern British Columbia., Econ. Geol., 79, 919-932.

Archibald, D. A., Glover, J. K., Price, R. A., Farrer, E., Carmicheal, D. M. 1983. Geochronology and tectonic implications of magmatism and metamorphism, southern Kootenay Arc and neighbouring regions, southeastern British Columbia. Part I: Jurassic to mid-Cretaceous. Canadian Jour. Earth Sciences, 20, 1891-1913.

Archibald, D. A., Krogh, T. E., Armstrong, R. L., Farrer, E. 1984. Geochronology and tectonic implications of magmatism amd metamorphism, southern Kootenay Arc and neighbouring regions, southeastern British Columbia. Part II: mid-Cretaceous to Eocene. Canadian Jour. of Earth Sciences, 21, 567-583.

Armstrong, R. L., 1968. A model for the evolution of strontium and lead isotopes in a dynamic earth. Rev. Geophys. Space Phys., 6, 175-199.

Armstrong, R. L. 1981. Radiogenic isotopes: the case for crustal recycling on a near steady-state no continental-growth Earth. Phil. Trans. R. Soc. Lond., Ser A 301, 443-472.

Armstrong, R. L., Cooper, J. A, 1971. Lead isotopes in island arcs. Bull. Volcanology, 35, 27-63.

Armstrong, R. L., Hein, S. M. 1973. Computer simulation of Pb and Sr isotope evolution of the earth's crust and upper mantle. Geochim. Cosmochim. Acta., 37, 1-18.

Armstrong, R. L., Monger, J. W. H., Irving, E. 1985. Age of magnetisation of the Axelgold Gabbro, north-central British Columbia. Canadian Journal of Earth Sciences, 22, 1217-1222.

Armstrong, R. L., Taubeneck, W. H., Hales, P. Q., 1977. Rb/Sr and K-Ar geochronometry of Mesozoic granitic rocks and their Sr isotopic composition, Oregon, Washington, and Idaho: Geol. Soc. Am. Bull., 88, 397-411.

Arth, J. E. 1976. Behaviour of trace elements during magmatic processes: a summary of theoretical models and their applications. Jour. of Research, U. S. Geol. Surv., 4, 41-47.

Arth, J. G., Barker, F. 1976. Rare earth element partitioning between hornblende and dacitic liquid and implications for the genesis of trondhjemitic-tonalitic magma. Geology, 4, 534-536.

Atherton, M. P., McCourt, W. J., Sanderson, L. M., Taylor, N. P. 1979. The geochemical character of the segmented Peruvian coastal Batholith and associated volcanics; In Origin of granite batholiths: Geochemical evidence, eds., M. P. Atherton and J. Tarney, 45-64.

Baadsgaard, H., Folinsbee, R. E., Lipson, J. 1961. Potassium-Argon dates of Biotites from Cordilleran Granites. Geol. Soc. Amer. Bull., 72, 699-702.

Bacon, C. R., Kurasawa, H., Delevaux, M. H., Kistler, R. W., Doe, B. R. 1984. Lead and Strontium isotopic evidence for crustal interaction and compositional zonation in the source regions of Pleistocene basaltic and rhyolitic magmas of the Coso volcanic field, California. Contrib. Petrol. Mineral., 85, 366-375.

Bally, A. W. 1975. A geodynamic scenario for hydrocarbon occurrences. 9th. World Petroleum Congress(Tokyo), 2, 23-44.

Bally, A. W., Gordy, P. L., Stewart, G. A. 1966. Structure, seismic data and orogenic evolution of the southern Canadian Rockies. Canadian Petroleum Geologists Bull., 14, 337-381.

Barker, A. 1981. Introduction to special issue on Granites and Rhyolites: A special commentary for the non-specialist. Jour. Geophys. Res., 86, 10131-10135.

Batchelor, R. A., Bowden, P. 1985. Petrogenetic interpretation of granitoid rock series using multicationic parameters. Chem. Geol., 48, 43-55.

Bateman, P. C., Chappell, B. W. 1979. Crystallisation, fractionation and solidification of the Toulumne intrusive series, Yosemite National Park, California. Geol. Soc. Am. Bull., 90, 465-482.

Bateman P. C., Nokleberg, W. J. 1978. Solidification of Mt. Givens Granodiorite, Sierra

Nevada, California. Jour. Geol., 86, 563-579.

Beddoe-Stephens, B. 1977. The Petrology and Geochemistry of the Rossland volcanic rocks, southern British Columbia. Ph. D. thesis, Univ. of Durham.

Beddoe-Stephens, B., Lambert, R. St J. 1981. Geochemical, mineralogical, and isotopic data relating to the origin and tectonic setting of the Rossland volcanic rocks, sourthern British Columbia. Canadian Jour. of Earth Sciences, 18, 858-868.

Beddoe-Stephens, B. 1982. The petrology of the Rossland volcanic rocks, southern British Columbia. Geol. Soc. Am. Bull., 93, 585-594.

Benvenuto, G. L., Price. R. A. 1979. Structural evolution of the Hosmer thrust sheet, southeastern British Columbia. Bull. Canadian Petroleum Geology, 27, 360-394.

Ben Othman, D., Fourcade, S. and Allègre, C. J. 1984a. Recycling processes in granite-granodiorite complex genesis: the Querigut case studied by Nd-Sr isotopic systematics. Earth Planet. Sci. Lett., 69, 290-300.

Ben Othman, D., Polve, M., Allègre, C. J. 1984b. Nd-Sr isotopic composition of granulites and constraints on the evolution of the lower continental crust. Nature, 307, 510-515.

Berger, G. W., York, D. 1979. ^{40}Ar-^{39}Ar dating of multicomponent magnetisations in the Archean Shelley Lake granite, northwestern Ontario, Canadian Journal of Earth Sciences, 16, 1733-1941.

Biscaye, P. E., Dasch, E. J. 1971. The rubidium, strontium and strontium-isotopic system in deep sea sediments, Argentina Basin: Jour. Geophys. Res., 76, 5087-5096.

Bishop, D. T., Morris, H. C., Edmonds, F. R. 1970. Turbidites and depositional features in the Lower Belt-Purcell Supergroup(Abstr.), Geol. Soc. Am. Abstr., 2, No7, 497.

Blatt, H. Jones, R. L. 1975. Proportions of exposed igneous, metamorphic and sedimentary rocks. Geol. Soc. Amer. Bull., 86, 1895-1988.

Bofinger, V. M., Compston, W. 1967. A reassessment of the age of the Hamilton Group, New York and Pennsylvania, and the role of inherited radiogenic Sr^{87}. Geochim. Cosmochim. Acta, 31, 2353-2359.

Bofinger, V. M., Compston, R. L., Vernon, M. J. 1868. The application of acid leaching to the Rb-Sr dating of a Middle Ordovician shale, Geochim. Cosmochim. Acta, 32, 823-833.

Bielski-Zyskind, M., Wasserburg, G. J., Nixon, P. H. 1984. Sm-Nd and Rb-Sr systematics in volcanics and Ultramafic Xenoliths from Maliata, Solomon Islands, and the nature of the Ontong Jave Plateau. Jour. Geophys. Res., 89, 2415-2424.

Bond, G. C., Kominz, M. A. 1984, Construction of tectonic subsidence curves for the early Paleozoic migeocline, sourthern Canadian Rocky Mountains, age of breakup, and crustal thinning. Geol. Soc. Amer. Bull., 95, 155-173.

Bowden, P., Whitley, J. E., 1974. Rare earth pattern in peralkaline and associated granites. Lithos, 7, 15-26.

Bowen, N. L., 1928. Evolution of the Igneous Rocks. 322 , Princeton Univ. Press. Princeton, N. J.

Briqueu, L., Lancelot, J. R. 1979. Rb-Sr systematics and crustal contamination models for calc-alkaline ingeous rocks. Earth Planet. Sci. Lett., 43, 385-396.

Brown, R. L., Fyles, J. T., Glover, J. K., Høy, T., Okulitch, A. V., Petro, V. A., Read, P. B. 1981. Southern Cordilleran cross-section- Cranbrook to Kamloops. In Field guides to geology and mineral deposits. Calgary, Ann. Meeting, eds., R. I. Thompson and D. G. Cook. 335-372.

Brown, R. L., Tippet, C. R. 1978. The Selkirk fan structure of the southeastern Canadian Cordillera, Geol. Soc. Amer. Bull., 89, 548-558.

Burchfiel, B. C., Davies, G. A. 1975. Nature and controls of Cordilleran Orogenesis, Western United States: Extensions of an earlier synthesis, Amer. Jour. of Sci., 275A, 363-396.

Brame, S. 1979. Mineralisation, N. E. margin of Nelson Batholith, British Columbia. M. Sc. thesis, Univ. of Alberta.

Burke, W. H., Denison, R. E., Hetherningt0n, E. A., Koepnick, R. B., Nelson, H. F., Otto, J. B. 1982. Variation of seawater ^{87}Sr/^{86}Sr throughout Phanerozoic time. Geology, 10, 516-519.

Burwash, R. A., Baadsgaard H., Peterman, Z. E. 1962. Precambrian K/Ar dates from the Western Canada Sedimentary basin. Jour. Geophys. Res., 67, 1617-1625.

Cairnes, C. E. 1934. Slocan Mining Camp, British Columbia. Geol. Surv. Can. Mem., 173, 137p.

Carlson, R. W. 1984. Isotopic constraints on Columbia River flood Basalt genesis and the nature of the subcontinental mantle, Geochim. Cosmochim. Acta, 48, 2357-2372.

Carmaichael, I., DePaolo, D. J. 1980. Nd and Sr isotopes in the lavas of Colima, Mexico. Geol. Soc. Amer. Abstr. with Programs, 12, p398.

Carr, S. D. 1985. Ductile shearing and brittle faulting in Valhalla Gneiss Complex, southeastern British Columbia., In Current Res., pt. A, Geol. Surv. of Canada, Pap. 85-1A, 89-96.

Cawthorn, R. G., O'Hara, M. J. 1976. Amphibole fractionation in calc-alkalic magma genesis. Amer. Jour. of Sci., 276, 309-329.

Chamberlain, V. E., Lambert. R. St J. 1985, Cordilleria, a newly defined Canadian microcontinent. Nature, 314, 707-713.

Chappell, B. W., White, A. J. R. 1971. Two contrasting granite types, Pacific Geology, 8, 173-174.

Chase, C. G. 1981. Oceanic island Pb: Two stage histories and mantle evolution. Earth and Planet. Sci. Lett., 52, 277-284.

Chaudhuri, S., Brookins, D. G. 1967., Rb-Sr studies of Paleozoic sediments(abstr.). Trans. Amer. Geophys. Union, 48, p242.

Chen, J. 1977. Uranium-Lead isotopic ages from the southern Sierra Nevada Batholith and adjacent Areas, California. Ph. D. thesis, U. of Calif., santa Barbara, 183p.

Chen, J.H. and Moore, J. G. 1982. Uranium-Lead isotopic ages from the Sierra Nevada Batholith, california. Jr. Geophys. Res., 87, 4761-4784.

Clayton, R. N. and Mayeda, T. K. 1963. The use of bromine pentafluoride in the extraction of oxygen from oxides, silicates for isotopic analysis. Geochim. Cosmochim. Acta, 27, 43-52.

Cloud, P. 1973. Paleoecological significance of the banded-iron formation. Econ. Geol., 68, 1135-1143.

Cohen, R. S., O'Nions, R. K. 1982. Identification of the recycled material in the mantle from Sr, Nd and Pb isotope investigations. Earth and Planet. Sci. Lett., 61, 63-84.

Colley, H., Warden, A. J. 1974. Petrology of New Hebrides. Geol. Soc. Amer. Bull., 85, 1635-1646.

Compston, W., Pidgeon, R. T. 1962. Rb-Sr dating of shales by the total rock method. Jour. Geophys. Res., 67, 3493-3502.

Coney, P. J., Jones, D. L., Monger, J. W. H. 1980. Cordilleran suspect terranes. Nature, 288, 329-333.

Condie, K. C. 1978. Geochemistry of Proterozoic granitic plutons from New Mexico, USA. Chem. Geol., 21, 131-149.

Cooper, J. A., Richards, J. R. 1966, Lead isotopes and volcanic magmas. Earth and Planet. Sci. Lett., 1, 259-269.

Corbett C. R., Simony, P. S. 1984. The Champion Lake Fault in the Trail-Castlegar area of southestern British Columbia. In Current Res., Pt. A, Geol. Surv. of Canada, Pap. 84-1A, 103-104.

Cordani, U. G., Kawashita, K., Filho, A. T. 1978. Applicability of the Rubidium-Strontium Method to Shales and Related rocks, In: Contributions to the Geological Time Scale, eds., G. V. Cohee, M. F. Glassner and H. D. Hedberg. Am. Assoc. Petrol Geol. Studies, Geology, 6, 93-117.

Cox, J. 1979. The NW margin of the Nelson Batholith, British Columbia, M. Sc. Thesis, U. of Alberta.

Cox, K. G., Bell, J. D., Pankhurst, R. J. 1979. The interpretation of Igneous Rocks. George Allen and Unwin. London, p450.

Crosby, P. 1968. Tectonic, plutonic and metamorphic history of the central Kootenay Arc, British Columbia. Geol. Soc. of Amer. Sp. Pap., 99, 94p.

Cumming, G. L., Richards, J. R. 1975, Ore lead isotopic ratios in a continuously changing earth. Earth and Planet. Sci. Lett., 52, 277-284.

Daly, R. A. 1933. Igneous Rocks and the Depths of the Earth. 598 . McGraw-Hill, New York, N. Y.

Dasch, E. J. 1969. Strontium isotopes in weathering profiles, deep-sea sediments, and sedimentary rocks. Geochim. Cosmochim. Acta, 33, 1521-1552.

de la Roche, H., Laterrier, J., Grand Claude, P., Marchal, M. 1980. A classification of volcanic and plutonic rocks using R1-R2 diagrams and major element analysis- its relationships with current nomenclature. Chem. Geol., 29, 183-210.

DePaolo, D. J. 1979. Implications of correlated Nd and Sr isotopic variations for the chemical evolution of the crust and mantle, Earth and Planet. Sci. Lett., 43, 201-211.

DePaolo, D. J. 1980. Crustal growth and mantle evolution: inferences from models of element transport and Nd and Sr isotopes. Geochem. Cosmochim. Acta., 44, 1185-1196.

DePaolo, D. J. 1980a. Sources of continental crust: Neodymium isotope evidence from the Sierra Nevada and Peninsular Ranges. Science, 209, 648-687.

DePaolo, D. J. 1981a. A neodymium and strontium isotopic study of Mesozoic calc-alkaline granitic batholiths of the Sierra Nevada and Peninsular Ranges, California. Jour. Geophys. Res., 86, 10470-10488.

DePaolo, D. J. 1981b. Nd in the Colorado Front Range and implications for crust formation and mantle evolution in the Proterozoic. Nature, 291, 193-196.

DePaolo, D. J. 1981c. Trace element and isotopic effects of combined wallrock assimilation and fractional crystallization. Earth and Planet. Sci. Lett., 53, 189-202.

DePaolo, D. J. 1981d. Crustal growth and mantle evolution: inferences from models of element transport and Nd and Sr isotopes: (reply to a comment by R. L. Armstrong). Geochim. Cosmochim. Acta, 45, 1253-1354.

DePaolo, D. J. 1983. The mean life of continents: Estimates of continental recycling rates from Nd and Hf isotopic data and implications for mantle structure. Geophys. Res. Lett., 10, 705-708.

DePaolo, D. J. Johnson, R. W. 1979. Magma genesis in the New Britain island-arc and constraints from Nd and Sr isotopes and trace element patterns. Contrib. Mineral. Petrol., 70, 367-379.

DePaolo, D. J., Wasserburg, G. J. 1976. Nd isotopic variations and petrogenetic models. Geophys. Res. Lett., 3, 249-252.

DePaolo, D. J., Wasserburg, G. J. 1977. The sources of island arcs indicated by Nd and Sr isotopic studies. Geophys. Res. Lett., 4, 465-468.

DePaolo, D. J., Wasserburg, G. J. 1979. Petrogenetic mixing models and Nd-Sr isotopic patterns. Geochim. Cosmochim. Acta, 43, 615-627.

Dewey, J. F., Windley, B. F., 1981. Growth and differentiation of the continental crust. Phil. Trans. R. Soc. Lond., A301, 188-206.

Dickinson, W. R. 1970. Relation of andesites, granites and derivative sandstones to arc-trench tectonics. Rev. Geophys. Space Phys., 8, 813-860.

Didier, J., Duthou, J. L., Lameyre, J. 1982. Mantle and crustal granites, genetic classification of orogenic granites and the nature of their enclaves. Jour. Volcanol. Geotherm. Res., 14, 169-186.

Dodge, F. C. W. 1979. The Wyaijah ring structure, Kingdom of Saudi Arabia. U. S. Geol. Surv. Prof. Pap., 774-E, 17p.

Doe, B. R. 1967. The bearing of lead isotopes on the source of granitic magma. Jour. Petrol. 8, 51-83.

Doe, B. R. 1973. Variations in lead isotopic compositions in Mesozoic granitic rocks of California: A preliminary investigation. Geol. Assoc. Amer. Bull., 84, 3513-3526.

Doe, B. R., Zartman, E. 1979. Plumbotectonics, the Phanerozoic. In: Geochemistry of Hydrothermal Ore Deposits, H. Barnes, ed., 22-70, New York, John Wiley and Sons.

Douglas, R. J. W., Gabrielse, H., Wheeler, J. O., Scott, D. F. and Belych, H. R. 1970. Geology of Western Canada; Chapter 7 in Geology and Economic Minerals of Canada. GSC., Econ. Geol. Rept. 1., 367-488.

Drake, M. J., Weill, D. F. 1975. Partition of Sr, Ba, Ca, Y, Eu^{+2}, Eu^{+3} and other REE between plagioclase feldspar and magmatic liquid: an experimental study. Geochim. Cosmochim. Acta, 39, 689-712.

Duncan, I. J., Parrish, R. R. 1979. Geochronology and Sr-isotope geochemistry of the Nelson Batholith: A post-tectonic intrusive complex in southsstern British Columbia: Geol. Soc. Am. Abs. with Programs, 11, 76.

Duncan, I. J., Parrish, R. R., Armstrong, R. L. 1979. Rb/Sr geochronology of the post-tectonic intrusive events in the Omineca Crystalline Belt, southeastern British Columbia(Abstr.). Cordilleran Section of the Geol. Assoc. of Canada, Vancouver, B. C., Program and Abstracts, p15.

Eichelberger, J. C. 1978. Andesitic volcanism and crustal evolution. Nature, 275, 21-27.

Elston, D. P., Bressler, S. L. 1980. Paleomagnetic poles and polarity zonation from the middle Proterozoic Belt Supergroup, Montana and Idaho. Jour. Geophys. Res., 85, 339-359.

Emeleus, C. H. 1963. Structural and petrographic observations on layered granites from southern Greenland. Mineral. Soc. Amer. Spec. Pap. I, 22-29.

Engel, A. E. J., Itson, S. P., Engel, C. G., Stickeney, D. M., Cray, E. J. Jr. 1974, Crustal evolution and global tectonics: a petrogenetic view. Geol. Soc. Amer. Bull., 85, 843-858.

Evans, M. E., Bingham D. K., McMurray E. W., 1975. New Paleomagnetic results from the Upper Belt-Purcell Supergroup of Alberta. Canadian Jour. Earth Sciences, 12, 52-61.

Farmer, G. L. and DePaolo, D. J. 1983. Origin of Mesozoic and Tertiary granite in the Western United States and Implications for Pre-Mesozoic crustal structure. I. Nd and Sr isotopic studies in the geocline of the northern Great Basin, Jour. Geophys. Res., 88, 1179-3401.

Farmer, G. L. and DePaolo, D. J. 1984. Origin of Mesozoic and Tertiary granite in the Western United States and Implications for Pre-Mesozoic crustal structure. II. Nd and Sr isotopic studies of Unmineralised and Cu- and Mo-Mineralised granite in the Precambrian craton. Jour. Geophys. Res. 89, 10141-10160.

Faure, G., Murtaugh, J. G., Montigny, R. J. E. 1968. The geology and geochronology of the basement complex of the central Transantartic Mountains. Canadian Jour. of Earth Sciences, 4, no3, ptII, 555-560.

Flynn, R. T., Burnham, C. W. 1978. An experimental determination of rare earth partition coefficients between a chloride-containing vapour phase and silicate melts. Geochim. Cosmochim. Acta., 42, 685-701.

Francis, P. W., Thorpe, R. S., Moorbath, S., Kretzschmar, G. A., Hamill, M. 1980. Strontium isotope evidence for crustal contamination of calc-alkaline volcanic rocks from Cerro Galan, northwest Argentina. Earth Planet. Sci. Lett., 48, 257-267.

Frebold, H. 1959. Marine Jurassic rocks in Nelson and Salmo areas, southern British Columbia. Geol. Soc. Canada Bull., 49.

Frey, M. 1970. The step from diagenesis to metamorphism in pelitic rocks during Alpine Orogenesis. Sedimentology. 15, 261-279.

Frey, F. A., Chappell, B. W., Roy, S. D. 1978. Fractionation of rare-earth elements in the Toulumne Intrusive series, Sierra Nevada batholith, California. Geology, 6, 239-242.

Frost, C. D., O'Nions. R. K. 1984. Nd evidence for Proterozoic crustal development in the Belt-Purcell Supergroup. Nature, 312, 53-65.

Fyles, J. T. 1964. Geology of the Duncan Lake area, Lardeau district, British Columbia. B. C. dept. of Mines and Petroleum Resources Bull., 49.

Fyles, J. T. 1967. Geology of the Ainsworth-Kaslo area, British Columbia. B. C. department of Mines and Petroleum Resources Bull., 53, 125p.

Fyles, J. T. 1970. Geological setting of the lead-zinc deposits of the Kootenay Arc and Salmo areas of British Columbia. In: Lead-zinc Deposits in the Kootenay Arc, northwestern Washington and adjacent British Columbia. Bull #61. Washington State Division of Mines and Geology, ed. A. E. Weissenbom.

Fyles, J. T., Hewlett, C. G. 1959. Stratigraphy and structure of the Salmo Lead-Zinc area. British Columbia department of Mines, Bull. #41.

Gabrielse, H. 1972. Younger Precambrian of the Canadian Cordillera. Amer. Jour. of Sci., 272, 521-536.

Gabrielse, H. 1985. Major dextral transcurrent displacements along the Northern Rocky Mountain Trench and related lineaments in north-central British Columbia. Geol. Soc. Amer. Bull., 96, 1-14.

Gabrielse, H., Reesor, J. E. 1974. The nature and setting granitic plutons in the central and eastern parts of the Canadian Cordillera, Pacific Geology, 8, 189-196.

Garrels, R. M., McKenzie, F. T. 1971. Evolution of sedimentary Rocks. W. W. Norton Company Inc. New York.

Gebauer, D., Grunenfelder, M. 1976. U-Pb Zircon and Rb-Sr whole rock dating of low-grade sediments, Example: Montagne Noire (Southern France). Contrib. Mineral. Petrol., 59, 13-32.

Ghosh, D. K., Lambert R. st J. 1982. Isotopic and geochemical studies of Upper Paleozoic and lower Mesozoic sediments in SE B. C. (Abstr.). Geol. Assoc. Canada, Mineralog. Assoc. Canada, Canadaian Geophys. Union Ann. Mtg., 7, 52.

Ghosh, D., Lambert. R. St J. 1983. Pb isotopes in sediments and batholiths from the Nelson-Salmo area SE B. C. (Abstr.). Geol. Assoc. Canada, Mineralog. Assoc. Canada, Canadian Geophys. Union Ann. Mtg., Victoria, 8, A26.

Gill, J. 1981. Orogenic Andesites and Plate Tectonics. 390 , Springer, New York, N.Y..

Glover, J. K. 1978. Geology of the Summit Creek map-area, southern Kootenay Arc, British Columbia. Ph. D. thesis. Queen's University, Kinston, Ontario, 143p.

Glover, J. K., Price, R. A. 1976. Stratigraphy and structure of the Windermere Supergroup, southern Kootenay Arc, British Columbia. In Report of Activities, pt. B, Geol. Surv. Canada Paper 76-1B, 21-23.

Goldstein, S. L., O'Nions, R. K. 1981. Nd and Sr isotopic relationships in pelagic clays and ferromanganese deposits. Nature, 292, 324-327.

Goldstein, S. L., O'Nions, R. K., Hamilton, P. J. 1984. A Sm-Nd isotopic study of atmospheric dusts and particulates from major river systems. Earth and Planet. Sci. Lett., 70, 221-236.

Greenland, L. P. 1970. An equation for trace element distribution during magmatic crystallization. Amer. Mineral., 55, 455-465.

Gromet, L. P., Silver, L. T. 1983. Rare earth element distributions among minerals in a granodiorite and their petrogenetic implications. Geochim. Cosmochim. Acta, 47, 925-940.

Grove T. L., Gerlach, D. C., Sando, T. 1982. Origin of calc-alkaline series lavas at Medicine Lake volcano by fractionation, assimilation and mixing. Contrib. Mineral. Petrol., 80, 160-182.

Gulson, B. L., Krogh, T. E. 1973. Old lead components in the young Bergell Massif, southeast Swiss Alps. Contrib. Mineral. Petrol., 40, 239-252.

Halliday, A. N. 1983. Crustal melting and the genesis of isotopically and chemically zoned plutons in the Southern Uplands of Scotland. 54-61, In Migmatites, Melting and Metamorphism. eds., M. P. Atherton and C. D. Gamble. Shiva Geology Series.

Halliday, A. N. 1984. Coupled Sm-Nd and U-Pb systematics in late Caledonian granites and the basement under northern Britain. Nature, 301, 229-233.

Hamilton, J. M., Delany, G. D., Hauser, R. L., Ransom, P. W. 1983. Geology of the Sullivan Deposit, Kimberley, B. C., Canada. In Short Course in sediment-hosted stratiform lead-zinc deposits, ed., D. F. Sangster, Mineral. Assoc. Canada.

Hamilton, P. J., O'Nions, R. K., Bridgewater, D., Nutman, A. 1983. Sm-Nd studies of Archean metasediments and metavolcanics from West Greenland and their implications for the Earth's early history. Earth and Planet. Sc. Lett., 62, 263-272.

Hamilton, P. J., O'Nions, R. K. and Pankhurst, R. J. 1980. Isotopic evidence for the provenance of some Caledonian granites. Nature, 287, 297-284.

Hanson, G. N. 1978. The application of trace elements to the petrogenesis of igneous rocks of granitic composition. Earth and Planet. Sci. Lett., 38, 26-43.

Hanson, G. N. 1980. Rare earth elements in petrogenetic studies of igneous systems. Ann. Rev. Earth Planet. Sci., 8, 371-406.

Harker, A. 1904. The Tertiary igneous rocks of Skye. Mem. Geol. Surv. Scot., 481p.

Harland, W. B., Cox, A. V., Llewellyn, P. G., Pincton, C. A. G., Walters, R. 1982. A geological time scale. Cambridge, England, Cambridge University Press. 131p.

Harrison, J. E. 1972. Precambrian Belt basin of northwestern United States: Its geometry, sedimentation and copper occurrences. Geol. Soc. Amer. Bull., 83, 1215-1240.

Harrison, T. M. 1981. Diffusion of ^{40}Ar in hornblende. Contrib. Mineral. Petrol., 78, 324-331.

Harrison, T. M., McDougall, I. 1980. Investigations of an intrusive contact, northwest Nelson, New Zealand- I. Thermal, chronological and isotopic constraints. Geochim. Cosmochim. Acta., 44, 1985-2003.

Harrison, J. E., Kleinkopf, M. D., Wells, J. D. 1980. Phanerozoic thrusting in Proterozoic Belt-rocks, northwestern United States. Geology, 8, 407-411.

Hartogen, J., Gijbels, R. 1976. Calculation of trace element fractionation during partial melting. Geochim. Cosmochim. Acta., 40, 179-195.

Hart, S. R. 1969. A test for excess Ar^{*} in micas, Jour. Geophys. Res., 71, 1769

Hart, S. R., Tilton, G. R. 1966. The isotopic geochemistry of strontium and lead in Lake Superior sediments and water: Geophy. Monograph., 10, The Earth Beneath the Continents, 127-137.

Haskin, L. A., Wildeman, T. R., Frey, F. A., Collins, K. A., Keedy, C. R., Haskin, M. A. 1966. Rare earths in sediments. Jour. Geophys. Res., 71, 6091-6105.

Hawkesworth, C. J. 1979. $^{143}Nd/^{144}Nd$, $^{87}Sr/^{86}Sr$ and trace element characteristics of magma along destructive plate margins. In M. P. Atherton and J. Tarney(eds.). Origin of Granite Batholiths: Geochemical evidence. Shiva , 76-89.

Hawkesworth, C. J. 1982. Isotopic characteristics of magmas erupted along destructive plate margins. In: R. S. Thorpe (ed), Orogenic Andesites. J. Wiley and Sons, New York. N.Y., 549-571.

Hawkesworth, C. J., Hammill, M., Gledhin, A. R., van Calsteren, P. and Rogers, G. 1982. Isotope and trace element evidence for late-stage intra-crustal melting in the Andes. Earth Planet. Sci. Lett., 58, 240-254.

Hawlas, D. B., Simony, P. S. 1986. The Castlegar Gneiss Complex, southern British Columbia., In Current Res., Pt. A, Geol. Surv. of Canada, Pap. 86-1A, 583-587.

Heier, K. S. 1973. Geochemistry of granulite facies and problems of their origin. Phil. Trans. Roy. Soc. Lond., Ser A, 273, 429-442.

Herzberg, C. T., Fyfe, W. S., Carr, M. J. 1983. Density contrasts on the formation of the Continental Moho and Crust. Contrib. Mineral. Petrol., 84, 1-5.

Higuchi, H., Nagasawa, H. 1969. Partition of trace elements between rock forming minerals and their host volcanic rocks. Earth and Planet. Sci. Lett., 7, 281-287.

Hildreth, W. 1979. The Bishop Tuff: Evidence for the origin of compositional zonation in silicic magma chambers. Geol. Soc. Amer. Spec. Paper, 180, 43-75.

Hildreth, W. 1981. Gradients in silicic magma chambers: Implications for lithospheric magmatism, Jour. Geophys. Res., 86, 10153-10192.

Hillhouse, J. 1977. Paleomagnetism of the Trissic Nikolai Greenstones, McCarthy Quadrangle, Alaska. Canadian Jour. Earth Sciences, 14, 2578-2592.

Høy, T. 1976. Calc-silicate isograds in the Riondel area, southeastern British Columbia. Canadaian Jour. of Earth Sciences, 13, 1093-1104.

Høy, T. 1977. Stratigraphy and structure of the Kootenay Arc in the Riondel area, southeastern British Columbia. Canadian Jour. of Earth Sciences, 14, 2301-2315.

Høy, T. 1980. Geology of the Riondel area, central Kootenay Arc, southeastern British Columbia. B. C. Ministry of Energy, Mines, and Petroleum Resources Bull., 73, 89p.

Høy, T., Diakow, L. 1981. Geology of the Proterozoic Purcell Supergroup, Moyie Lake area; in Geological Fieldwork, 1980, B. C. Ministry of Energy, Mines and Petroleum Resources, Geol. Div. paper 81-1.

Høy, T., Edmonds, F. R., Hamilton, J. M., Hauser, R. L., Muraro, T. W. and Ransom, P. W. 1981. Lead-zinc and copper-zinc deposits in southeastern British Columbia. In Field Guides to Geology and Mineral Deposits, Calgary, '81 GAC, MAC, CGU, 41-67.

Høgdohl, O. T., Melson, S., Bowen, V. 1968, Neutron activation analysis of lanthanide elements in sea-water. Adv. Chem. Ser., 73, 308-325.

Hurley, P. M. 1968. Absolute abundance and distribution of Rb, K and Sr in the earth. Geochim. Cosmochim. Acta., 32, 273-283.

Hurley, P. M., Rand, R. Jr., 1969. Pre-drift continental neuclei. Science, 164, 1229-1242.

Hurley, P. M., Hughes, H., Faure, G., Fairbairn, H. W., Pinson, W. H. 1962. Radiogenic strontium-87 model of continent formation. Jour. Geophys. Res., 67, 5315-5334.

Irving, E., Monger, J. W. H., Yole, R. W. 1980. New paleomagnetic evidence for displaced terranes in British Columbia. In: Strangeway, D. W. ed., The continental crust and its mineral deposits. Geol. Assoc. of Canada Spec pap., 20, 441-456.

Irving, E., Woodsworth, G. J., Wynne, P., J., Morrison, A. 1985. Paleomagnetic evidence for displacement from the south of the Coast Plutonic Complex, British Columbia. Canadian Jour. of Earth Sciences, 22, 584-598.

Irving, E., Yole, R. L. 1972. Paleomagnetism and the Kinematic history of mafic and ultramafic rocks in the fold mountain belt, In: Irving, E., ed., The ancient oceanic lithosphere: Canada Dept. of Energy, Mines and Resources, Earth Physics Branch, 42, 87-95.

Irving, T. N., Baragar, W. R. A. 1971. A guide to the chemical classification of the common volcanic rocks. Canadian Jour. of Earth Sciences, 8, 523-548.

Jacobsen S. B., Wasserburg, G. J. 1979. The mean age of mantle and crustal Reservoirs, Jour. Geophys. Res., 84, 7411-7427.

Jacobsen, S. B., Wasserburg, G. J. 1980. Sm-Nd isotopic evolution of Chondrites. Earth and Planet. Sci. Lett., 50, 139-155.

Jaffey, A. H., Flynn, K. F., Glendenin, L. E., Bentley, W. C., Essling, A. M. 1971. Precision measurement of the half-lives and specific activities of ^{235}U and ^{238}U, Phys. Rev., C, 4, 1889-1906.

James, D. E., 1982. A combined O, Sr, Nd, and Pb isotopic and trace element study of crustal contamination in central Andean lavas, I. Local geochemical variations, Earth Planet.

Sci. Lett., 57, 47-62.

Johnson, R. W., Wallace, D. A., Ellis, D. J. 1976. Feldspathoid-bearing potassic rocks and associated types from volcanic islands of the coast of New Ireland, Papua, New Guinea. A preliminary account of the geology and petrology. In Volcanism in Australia, ed., R. W. Johnson, Elsevier, Armsterdam.

Kay, R. W., 1980. Volcanic arc magmas: implications of a melting-mixing model for element recycling in the crust upper-mantle system. Jour. Geol., 88, 497-522.

Kay, R. W., Kay, S. M. 1980. Chemistry of the lower crust: Inferences from magmas and xenolith. In Continental tectonics, 139-150, Washington National Academy of Science.

Kay, R. W., Sun, S. S., Lee-Hu, C. N. 1978. Pb and Sr isotopes in volcanic rocks from the Aleutian islands and Pribilot Islands, Alaska. Geochim. Cosmochim. Acta, 42, 263-273.

Kistler, R. W., Peterman, Z. E. 1973. Variations in Sr, Rb, K, N, and $^{87}Sr/^{86}Sr$ in Mesozoic granitic rocks and intruded wall rocks in central California. Geol. Soc. Amer. Bull., 84, 3489-3512.

Kistler, R. W., Peterman, Z. E. 1978. Reconstruction of crustal blocks of California on the basis of initial strontium isotopic compositions of Mesozoic granitic rocks. U. S. Geol. Surv. Prof. pap., 1071p.

Klepacki, D. 1983. Stratigraphic and structural relations of the Milford, Kaslo and Slocan Groups, Roseberry Qudrangle, Lardeau map-area, British Columbia. In Current research, part A, Geol. Surv. of Canada paper, 83-1A, 229-233.

Klepacki, D. W., Wheeler, J. O. 1985. Stratigraphic structural ralationships of the Milford, Kaslo and Slocan Groups, Goat Range, Lardeau and Nelson map areas, British Columbia: In Current Res., Pt. A, Geol. Surv. of Canada, Pap. 85-1A, 277-286.

Klepacki, D. W., Read, P. B., Wheeler, J. O. 1985. Geology of the headwaters of Wilson creek, Lardeau map area, southeastern British Columbia. In Current Res. Pt. A, Geol. Surv. of Canada, Pap. 85-1A, 273-276.

Kraig, D., Kay, R. W. 1981. Fate of sediments on the descending plate at convergent margins, Phil. Trans. Roy. Soc. Lond., A, 301, 233-251.

Kramers, J. D. 1977. Lead and strontium isotopes in Cretaceous kimberlites and mantle-derived xenoliths from southern Africa. Earth and Planet. Sci. Lett., 34, 419-431.

Kuno, H., 1950. Petrology of Hakone volcano and adjacent areas, Japan. Geol. Soc. Amer. Bull., 61, 239-256.

Leclair, A. D. 1982. Preliminary results on the stratigraphy, structure and metamorphism of central Kootenay Arc rocks, southeastern British Columbia. In Current Research, part A, Geol. Surv. Canada pap., 82-1A, 45-49.

Leclair, A. D. 1983., Stratigraphy and structural implications of central Kootenay Arc rocks, southeastern British Columbia. In Current Research, part A, Geol. Surv. Canada pap., 83-1A, 235-240.

Le Couteur P. C., Templeman-Kluit, D. J. 1976. Rb/Sr ages and a profile of initial $^{87}Sr/^{86}Sr$ ratios for plutonic rocks across the Yukon Crystalline Terrane. Canadian Jour. Earth Sciences, 13, 319-330.

Lee D. E., Van Loenen, R. E., 1971. Hybrid granitoid rocks of the southern Snake Range, Nevada, U. S. Geol. Surv. Prof. pap., 668, 48p.

Leech, G. B. 1962. Metamorphism and granitic intrusions of Precambrian age in southeastern British Columbia. Geol. Surv. Canada pap., 62-13.

Leech G. B. 1966. The Rocky Mountain Trench. In The World rift system. ed., T. N. Irving, Geol. Surv. Canada pap., 66-14, 307-329.

Leech, G. B., Lowden, J. A., Stockwell, C. H., Wanless R. K. 1963. Age determinations and geological studies. Geol. Surv. Canada paper, 63-17, 140p.

Leeman, W. P., 1972. Composition of Rb/Sr, U/Pb and rare earth characteristics of subcontinental and suboceanic mantle regions. Oreg. Dept. Geol. Mineral. Bull., 96, 149-168.

Leeman, W. P., Phelps, D. W., 1981. Partitioning of rare earths and other trace elements between sanidine and coexisting volcanic glass. Jour. Geophys. Res., 86, 10193-10199.

Le Roux L. J., Glendenin, L. E., 1963. Half-life of ^{232}Th. Nat. Mtg. Nucl. Energy (Pretoria, South Africa) Proc., 83-94.

Li Y., 1972. Geochemical mass-balance among lithosphere. hydrosphere and atmosphere. Amer. Jour. Science, 272, 119-137.

Liew, T. C. and McCulloch, M. T. 1985. Genesis of granitoid batholiths of Peninsular Malaysia and implications for models of crustal evolution: Evidence from Nd-Sr isotopic and U-Pb zircon study. Geochim. Cosmochim. Acta, 49, 587-600.

Lis, M. G., Price, R. A., 1976. Large-scale block faulting during deposition of the Windermere Supergroup(Hadrynian) in southeastern British Columbia. Geol. Surv. Canada pap., 76-1A, 135-136.

Little, H. W., 1962, Trail map-area British Columbia. Geol. Surv. Canada paper 62-5.

Little, H. W. 1960. Nelson map-area, West half, British Columbia(82FW1/2). Geol Surv. Canada Memoir, 308.

Little, H. W. 1965. Geology, Salmo, British Columbia. Geol. Surv. Canada Map, 1145A.

Little, H. W. 1982. Geology of the Rossland-Trail map-area, British Columbia. Geol. Surv. Canada paper 79-26.

Lowden, J. A., Stockwell, C. H., Tipper, H. W., Wanless, R. K. 1963. Age determinations and geological studies. Geol. Surv. Canada paper 62-17, 140p.

Lowden J. A. 1961. Age determinations by the Geol. Surv. Canada. Geol. Surv. Canada paper 61-17, 127p.

Lowe, D. R. 1980. Archean sedimentation. Ann. Rev. Earth Planet Sci., 8, 145-167.

Lugmair, G. W., Marti, K., Krutz, J. P., Scheinin, N. B. 1976. History and genesis of Lunar troctolite 76535 or: How old is old? Proc. Lunar Sci. Conf., 7th, 2009-2033.

Lugmair, G. H., Volke, R. D. Jr., Hanson G. 1978. A general mixing equation with applications to Icelandic basalts. Earth and Planet. Sci. Lett., 37, 380-392.

Magaritz, M., Taylor, H. P. 1986. Oxygen 18/oxygen 16 and D/H Studies of Plutonic Granitic and Metamorphic Rocks Across the Cordilleran Batholiths of Southern British Columbia. Jour. Geophys. Res., 91, 2193-2217.

Mahood, G., Hildreth, W. 1983. Large partition coefficients for trace elements in high silica rhyolites. Geochim. Coschim. Acta, 47, 11-30.

Marsh, B. D. 1979. Island arc volcanism. Amer. Jour. of Sci., A271, 217-248.

Masuda, A. N., Nakamura, A., Tenaka, T. 1973. Fine structures of mutually normalised rare-earth patterns of Chondrites. Geochim. Cosmochim. Acta, 37, 239-248.

Mathews, W. H. 1983. Early Tertiary resetting of potassium-argon dates in the Kootenay Arc, southeastern British Columbia., Canadian Jour. Earth Sciences., 20, 867-872.

McCarthy, T. S., Grove, D. I. 1979. The Blue Tier Batholith, Northeastern Tasmania. A cumulate-like product of fractional crystallization. Contrib. Mineral. Petrol., 71, 193-209.

McCarthy, T. S., Hasty, R. A. 1976. Trace element distribution patterns and their relationship to the crystallization of granitic melts. Geochim. Cosmochim. Acta, 40, 1351-1358.

McCarthy, T. S., Robb, L. J. 1978. On the relationship between cumulate mineralogy and trace and alkali element chemistry in an Archean granite from the Barberton region, South Africa. Geochim. Cosmochim. Acta, 42, 21-26.

McCulloch, M. T. and Chappell, B. W. 1982. Nd isotopic characteristics of S- and I-type granites. Earth Planet. Sci. Lett., 58, 51-64.

McCulloch, M. T., Chappell, B. W. and Hensel, H. D. 1982. Nd and Sr isotopic relationships in granitic rocks of the Tasman Fold Belt, Eastern Australia, 5th, Int. Conf. Geochron. Cosmochron. Isotope Geol., Japan, 246-247.

McCulloch, M. T., Gregory, R. T., Wasserburg. G. J., Taylor, H. P. 1980. A neodymium, strontium and oxygen isotopic study of the Cretaceous ophiolite and implications for the petrogenesis and sea-water-hydrothermal alteration of ocean crust. Earth and Planet. Sci. Lett., 46, 201-211.

McCulloch, M. T., Perfit, M. R. 1981. ^{143}Nd/^{144}Nd, ^{87}Sr/^{86}Sr and trace element constraints on the petrogenesis of Aleutian island arc magmas. Earth and Planet. Sci. Lett., 56, 167-179.

McCulloch, M. T., Wasserburg, G. J. 1978. Sm-Nd and Rb-Sr chronology of continental crust formation. Science, 200, 1003-1011.

McDonald, G. A., 1968. Chemical composition of Hawaiian lavas. Jour. Petrol. 5, 82-133.

McKenzie, D. 1969. Speculations on the consequences and causes of plate motions. Geophys. Jour. Res. Astron. Soc., 18, 1-32.

McKenzie, D. E. 1976. The nature and origin of late Cenozoic volcanoes in Papua New Guinea. In Volcanism in Australia, ed., R. W. Johnson, Elsevier, Amsterdam.

McLennan, S. M., Fryer, B. J., Young, G. M. 1978. Rare earth elements in Hurorian (Lower Proterozoic) sedimentary rocks: composition and evolution of the post-Kenoran upper crust. Geochim. Cosmochim. Acta, 43, 375-388.

McLennan, S. M., Taylor, S. R. 1981. Role of subducted sediments in island arc magmatism: constraints from REE patterns. Earth Planet. Sci. Lett., 54, 423-430.

McLennan, S. R., Taylor, S. R. 1982, Geochemical constraints on the growth of the continental crust. Jour. of Geol., 90, 347-361.

McLennan, S. M., Taylor, S. R. 1983. Continental freeboard, sedimentation rates and growth of continental crust. Nature, 306, 169-172.

McMechan, M. E., Price, R. A. 1982. Superimposed low-grade metamorphism in the Mount Fisher area, southeastern British Columbia: Implications for the East Kootenay Orogeny, Canadian Jour. Earth Sciences, 19, 476-489.

Meijer, A. 1985. Pb isotope evolution in the Earth: a proposal, Geophys. Res. Lett., 12, 741-744.

Meizer, A. 1976. Pb and Sr isotopic data bearing on the origin of volcanic rocks from the Mariana island arc system, Geol. Soc. Amer. Bull., 87, 1358-1369.

Menzies, M. A., Leeman, W. P., Hawkesworth, C. J. 1983. Isotopic geochemistry of Cenozoic volcanic rocks reveals mantle heterogeneity below Western U.S.A., Nature, 303, 205-209.

Menzies, M. A., Wass, Y. 1983. CO_2- and LREE-rich mantle below eastern Australia: a REE and isotopic study of alkaline magmas and apatite-rich mantle xenoliths from the southern Highlands Province, Australia. Earth and Planet. Sci. Lett., 65, 287-302.

Michael, P. J. 1983. Chemical differentiation of the Bishop Tuff and other high silica magmas through crystallization processes, Geology, 11, 31-34.

Michael, P. J. 1984. Chemical differentiation of the Cordilleran Paine granite (southern Chile) by in situ fractional crystallization. Contrib. Mineral. Petrol., 87, 179-195.

Michard, A., Gurriet, P., Soudant, M., Alberede, F., 1985. Nd isotopes in French Phanerozoic shales: external vs. internal aspects of crustal evolution. Geochim. Cosmochim. Acta., 49, 601-610.

Miller, F. K., Engels, J. C. 1975. Distribution and trends of discordant ages of the plutonic rocks of northeastern Washington and northern Idaho. Geol. Soc. Amer. Bull., 86, 517-528.

Miller, C. F., Mittlefehldt, D. W. 1982. Light rare earth depletion in felsic magmas. Geology, 10, 129-133.

Miller, C. F., Mittlefehldt, D. W. 1984. Extreme fractionation in felsic magma chambers: a product of liquid-state diffusion or fractional crystallization? Earth and Planet. Sci. Lett., 68, 151-158.

Mittlefehldt, D. W., Miller, C. F. 1983. Geochemistry of the Sweetwater Wash pluton, California: implications for "anomalous" trace element behaviour during differentiation of felsic magmas. Geochim. Cosmochim. Acta, 47, 109-124.

Monger, J. W. H., Irving, E. 1980. Northward displacement of north-central British Columbia. Nature, 285, 289-293.

Monger, J. W. H., Price, R. A. 1979. Geodynamic evolution of the Canadian Cordilleraprogress and problems. Canadian Jour. Earth Sciences, 16, 770-791.

Monger, J. W. H., Price, R. A., Templeman-Kluit D. J. 1982. Tectonic accretion and the origin of the two major matemorphic and plutonic welts in the Canadian Cordillera. Geology, 10, 70-75.

Monger, J. W. H., Ross, C. A. 1971. Distribution of fusulinaceans in the Canadian Cordillera. Canadian Jour. Earth Sciences, 8, 259-278.

Monger, J. W. H., Souther, J. G., Gabrielse, H. 1972. Evolution of the Canadian Cordillera: a plate tectonic model, Amer. Jour. Sci., 272, 577-602.

Moorbath, S. 1977. Ages, isotopes and evolution of Precambrian continental crust, Chem. Geol., 20, 151-187.

Moorbath, S. 1978. Age and isotopic evidence for the evolution of the continental crust. Phil. Trans. Roy. Soc. Lond., A288, 401-413.

Morton, J. P., Long, L. E. 1980. Rb-Sr dating of Paleozoic glauconite from the Liano region, central Texas. Geochim. Cosmochim. Acta, 44, 663-672.

Muehlenbachs, K., Clayton, R. N. 1971. Oxygen isotope ratios of submarine diorites and their constituent minerals. Canadian Jour. of Earth Sci., 8, 1591-1595.

Muehlenbachs, K., Clayton, R. N. 1976. Oxygen Isotopic composition of the Oceanic Crust and Its bearing on Seawater. Jour. Geophys. Res., 81, 4365-4369.

Mysen B. O. 1979. Trace element partitioning between garnet peridotite minerals and a water-rich vapour: Experimental data from 5 to 20 kbars. Amer. Mineral., 64, 274-287.

Nakamura, N. 1974. Determination of REE, Ba, Fe, Mg, Na and K in Carbonaceous Ordinary Chondrites. Geochim. Cosmochim. Acta, 38, 757-775.

Nance, W. B., Taylor, S. R. 1976. Rare earth element patterns and crustal evolution, I. Australian post-Archean sedimentary rocks. Geochim. Cosmochim. Acta, 40, 1539-1551.

Neuman, H., Mead, J., Vitailiano, C. J. 1954. Trace element variation during fractional crystallization as calculated from the distribution law. Geochim. Cosmochim. Acta, 6, 90-100.

Nguyen, K. K., Sincliar, A. J., Libby, W. G. 1968. Age of the northern part of the Nelson Batholith. Canadian Jour. of Earth Sciences, 5, 955-957.

Nichols, K. M., Silbreling, N. J. 1979. Early Triassic(Smithian) ammonites of paleoequatorial affinity from the Chulitna terrane, south-central Alaska. U. S. Geol. Surv. Prof. Pap., 1121-B, 5p.

Nodha, S., Wasserburg, C. J. 1981. Nd and Sr isotopic study of volcanic rocks from Japan. Earth and Planet. Sci. Lett., 52, 264-276. Obradovich J. D., Peterman, Z. E. 1968. Geochronology of the Belt series, Montana, Canadian Jour. of Earth Sciences, 5, 737-747.

Okulitch, A. V., 1984. The role of the Shuswap Metamorphic Complex in Cordilleran tectonism: a review. Canadian Jour. of Earth Sciences, 21, 1171-1193.

O'Nions, R. K. 1979. Geochemical and Cosmochemical applications of Nd isotopic analysis. Ann. Rev. Earth Planet Sci., 7, 11-38.

O'Nions, R. K., Evensen, N. M., hamilton, P. J. 1979. Geochemical Modelling of Mantle Differentiation and Crustal Growth. Jour. Geophys. Res., 84, 6091-6101.

O'Nions, R. K., Hamilton, P. J., Evensen, N. M. 1977, Variations in ^{143}Nd/^{144}Nd and ^{87}Sr/^{86}Sr ratios in oceanic basalts. Earth and Planet. Sci. Lett., 34, 13-22.

O'Nions, R. K., Hamilton, P. J., Hooker, P. J. 1983. A Nd-isotopic investigation of sediments related to crustal developments in the British Isles. Earth and Planet. Sci. Lett., 63, 229-240.

Oversby, V. M., Ewart, A. 1972. Lead isotopic compositions of Tonga-Kermadec volcanics and their petrogenetic significance. Contrib. Mineral. Petrol., 37, 181-210.

Parrish, R. R. 1981. Geology of the Nemo Lakes belt, norhtern Valhalla Range, southeastern British Columbia. Canadian Jour. of Earth Sciences, 18, 944-958.

Parrish, R. R. 1984. Slocan Lake Fault: a low angle fault zone bounding the Valhalla Gneiss Complex, Nelson map area, southern B. C., 1984 field works; in Current Res. Pt. A, Geol. Surv. of Canada, Pap. 84-1A, 323-330.

Parrish, R. R., Carr, S. D., Brown, R. L. 1985. Valhalla Gneiss Complex, southeast British Columbia., 1984 field work; in Current Res., Pt. A, Geol. Surv. of Canada, Pap. 85-1A, 81-87.

Parrish, R. R. and Ryan, B. 1983. Zircon dates reflecting Late Cretaceous Early Tertiary plutonism, deformation and isotopic resetting, Valhalla Complex, southeastern British Columbia. GAC., Prog. and Abstr., 8, pA-53.

Parrish, R. R., Armstrong, R. L. 1983. U-Pb zircon age and tectonic significance of gneisses in structural culminations of the Omineca Crystalline Belt, British Columbia. GSA., Abstr. and Progs., 15, p324.

Parrish, R. R., Wheeler, J. O. 1983. A U-Pb zircon age from the Kuskanax Batholith, southeastern British Columbia. Canadian Jour. Earth Sciences, 20, 1751-1756.

Patterson, C., Tatsumoto, M. 1964. The significance of lead-isotopes in detrital feldspar with respect to chemical differentiation within the earth's mantle. Geochim. Cosmochim. Acta, 28, 1-22.

Perry, E. A., Turekian, K. K. 1974. The effects of diagenesis on the redistribution of strontium isotopes in shales. Geochim. Cosmochim. Acta, 38, 929-935.

Peterman, Z. E. 1966. Rb-Sr dating of middle Precambrian metasedimentary rocks of Minnesota. Geol. Soc. Amer. Bull., 77, 1031-1044.

Peterman, Z. E., Hedge, C. E., Tourtelot, H. A. 1970. Isotopic composition of Sr in sea water throughout Phanerozoic time. Geochim. Cosmochim. Acta, 34, 105-120.

Petro, W. L., Thomas, A. V., Wilband, J. J. 1979. Major-element chemistry of plutonic rock series from compressional and extensional plate boundaries. Chem. Geol., 26, 217-235.

Powell, J. L., Skinner, W. R. and Walker, D. 1969. Whole-Rock Rb-Sr age of metasedimentary rocks below the Stillwater Complex, Montana. Geol. Soc. Amer. Bull., 80, 1605-1612.

Price, R. A. 1964. The Precambrian Purcell system in the Rocky Mountains of southern Alberta and British Columbia. Canadian Petroleum Geologists Bull., 12, 399-426.

Price, R. A. 1972. Rocky Mountain Trench- Golden to Cranbrook. In: Price, R. A., Balkwill, H., R., Charlesworth, H. A. K., Cook, D. G., Simony, P. S. The Canadian Rockies and Tectonic Evolution of the Southeastern Cordillera, Guidebook, field excursion AC15, XXIV Inter. Geol. Cong., Montreal, 77-85.

Price, R. A. 1981. The Cordilleran foreland thrust and fold belt in the southern Canadian Rocky Mountains, In Thrust and Nappe tectonics, eds., K. R. McClay and N. J. Price, Geol. Soc. Lond. Spec. Publ., 9, 427-488.

Price, R. A., Monger, J. W. H., Muller, J. E. 1981. Cordilleran cross-section- Calgary to Victoria. In Field guides to Geology and mineral deposits, Calgary, Ann. Meeting, Geol. Assoc. Canada.

Read, P. B. 1973. Petrology and structure of Poplar Creek map-area, British Columbia. Geol Soc. Canada Bull., 193, 144p.

Read, P. B. 1975. Lardeau Group, Lardeau map-area, West half (82K West half) British Columbia. In Report of Activities, pt. A, Geol. Soc. Canada paper, 75-1A, 29-30.

Read, P. B. 1976. Lardeau map area (82K West half), British Columbia. In Report of Activities, pt. A, Geol. Soc. Canada paper 76-1A, 95-96.

Read, P. B., Okulitch, A. V. 1977. The Triassic Unconformity of south-central British Columbia. Canadaian Jour. of Earth Sciences, 14, 606-638.

Read, P. B., Wheeler, J. L. 1976. Lardeau West half, Geol. Serv. Canada Open File Map 432.

Reesor, J. E. 1965. Valhalla gneiss complex, British Columbia. Geol. Surv. Canada Bull., 129.

Reesor, J. E. 1973. Geology of the Lardeau map-area, east half, British Columbia. Geol. Surv. Canada Memoir, 369, 129p.

Reynolds, P. H., Sinclair, A. J. 1971. Rock and ore-lead issotopes from the Nelson-batholith and the Kootenay Arc, British Columbia, Canada: Econ. Geol., 66, 259-266.

Rice, A., 1981. Convective fractionation: A mechanism to provide cryptic zoning (micro segregation), layering, cres-cumulates, banded tuffs and explosive volcanism in igneous processes. Jour. Geophys. Res., 86, 405-417.

Rice R. A. 1941. Nelson map-area, East half, British Columbia. Geol. Surv. Canada Mem., 228.

Ringwood, A. E. 1975. Composition and petrology of the Earth's Mantle. McGraw-Hill, New York.

Ringwood, A. E. 1982. Phase transformations and differentiation in subducted lithosphere: Implications for mantle dynamics, basalt petrogenesis, and crustal evolution. Jour. of Geol., 90, 611-643.

Ronov, A. B., Yroshevsky, A. A. 1969. Chemical composition of the earth's crust. Amer.

Geophys. Union Geophys. Mon., 13, 37-57.

Russell, R. D. 1972. Evolutionary model for lead isotopes in conformable ores and in ocean volcanics. Rev. Geophys. Space Phys., 10, 529-549.

Ryan, B., Blenkinsop, J. 1971. Geology and Geochronology of the Hellroaring creek stock, British Columbia. Canadain Jour. of Earth Sciences, 8, 85-95.

Schidlowski, M., 1978. Evolution of the Earth's atmosphere: Current state and exploratory concepts. In Origin of Life (ed. Nodha N.) 3-20. Tokyo, Center. Acad. Publ. Japan.

Schwarcz, H. P., Clayton, R. N., Mayeda, T. 1970. Oxygen isotopic studies of calcareous and pelitic metamorphic rocks, New England. Geol. Soc. Amer. Bull., 81, 2299-2316.

Schwartzman, D. H., Gilletti, B. J. 1968. 'Excess Argon' in Minerals from the Stillwater Complex, Montana. Trans. Am. Geophys. Union, 49, 359p.

Sears, J. W., Price, R. A. 1978. The Siberian connection a case for Precambrian separation of the North American and Siberian cratons. Geology, 6, 267-270.

Shand, S. J. 1951. Eruptive Rocks. John Wiley, New York.

Shaw, H. F., Wasserburg, G. J. 1985. Sm-Nd in marine carbonates and phosphates: Implications for Nd isotopes in seawater and crustal ages. Geochim. Cosmochim. Acta, 49, 503-518.

Shibata, K. Mizutani, S. 1982. Isotopic ages of Jurassic siliceous shale and Triassic bedded chert in Unuma, Central Japan. Geochem. Jour., 16, 213-223.

Siddans, A. W. B. 1977. The development of slaty cleavage in a part of the French Alps. Tectonophysics, 39, 533-557.

Simony, P. S. 1979. Pre-Carboneferous basement near Trail, British Columbia. Canadian Jour. of Earth Sciences, 16, 1-11.

Simony, P., S., Wind, G. 1970. Structure of the Dogtooth Range and adjacent portions of the Rocky Mountain Trench, In Wheeler J. O., ed., Structure of the southern Canadian Cordillera. Geol. Assoc. Canada Spec. paper No. 6, 41-51.

Southam, J. R., Hay, W. W. 1981. Global sedimentary mass balance and sea level changes, In: The Sea, 7, The Oceanic Lithosphere, C. Emeliani, ed., 1617-1684. Wiley-Interscience, New York. N.Y.

Smith, T. E. 1975. Layered Granitic rocks at Chebucto Head, Halifax County, Nova Scotia. Canadain Jour. of Earth Sciences, 12, 456-463.

Sleep, N. 1984. Tapping of magmas from ubiquitous mantle heterogeneities: an alternative to mantle plumes? Jour. Geophys. Res., 89, 10029-10041.

Stacey, J. S., Kramers, J. D. 1975. Approximation of terrestrial lead isotope evolution by a two-stage model. Earth and Planet. Sci. Lett., 26, 207-221.

Steiger, R. H. and Jager, E. 1977. Subcommission on Geochronology: Convention on the use of Decay Constants in Geochronology and Cosmochronology, Earth Planet. Sci. Lett., 36, 359-362.

Steiger, R. H. and Wasserburg, G. J. 1969. Comparative U-Th-Pb systematics in $2.7.10^9$ yr. pluton of different geological histories. Geochim. Cosmochim. Acta, 33, 1213-1232.

Stephens, W. E., Whitley, J. E., Thirlwell, M. F., Halliday, A. N. 1985, The Criffel zoned pluton: correlated behaviour of rare earth element abundances with isotopic systems. Contrib. Mineral. Petrol., 89, 226-238.

Stewart, J. H. 1972. Initial deposits in the Cordilleran geosyncline. Evidence of a late Precambrian(<850Ma) continental separation. Geol. Soc. Amer. Bull., 83, 1345-1360.

Stewart, J. H. 1976. Late Precambrian evolution of North America: plate tectonics implication, Geology, 4, 11-15.

Stormer J. C. and Nicholls, J. 1978. XFRAC Aprogram for the interactive testing of magmatic differentiation models. Computers and Geosciences, 4, 143-159.

Streckeisen, A. 1976. To each plutonic rock its proper name. Earth Sci. Rev., 12, 1-33.

Sun, S. S. 1980. Lead isotopic study of young volcanic rocks from mid-ocean ridges, ocean islands, and island arcs. Phil. Trans. Roy. Soc. Lond., Ser A, 297, 409-445.

Sun, C. O., Williams, R. J., Sun, S. S. 1974. Distribution coefficients of Eu and Sr for plagioclase-liquid equilibria in oceanic ridge basalts: an experimental study. Geochim. Cosmochim. Acta, 38, 1415-1433.

Tarney, J., Saunders, A. D. 1979. Trace element constraints on the origin of Cordilleran Batholiths, In Origin of granitic Batholiths: Geochemical evidence, eds., M. P. Atherton and J. Tarney, 90-105.

Tarney, J., Windley, B. F., 1979. Continental growth, island arc accretion and the nature of the lower crust- a reply to S. R. Taylor and S. M. McLennan. Jour. Geol. Soc. Lond., 136, 501-504.

Tatsumoto, M. 1969. Lead isotopes in volcanic rocks and possible ocean-floor thrusting beneath island arcs. Earth and Planet. Sci. Lett., 6, 369-376.

Tatsumoto, M., 1978. Isotopic composition of lead in oceanic basalt and its implication to mantle evolution. Earth and Planetary evolution. Earth and Planet. Sci. Lett., 38, 63-87.

Taylor, H. P. 1980. The effects of assimilation of country rocks by magmas on $^{18}O/^{16}O$ and $^{87}Sr/^{86}Sr$ systematics in igneous rocks. Earth and Planet. Sci. Lett., 47, 243-254.

Taylor, S. R. 1977. Island arc models and the composition of the continental crust. Amer. Geophys. Union, Maurice Ewing Series, 1, 325-335.

Taylor, S. R. 1979. Chemical composition and evolution of the continental crust: The rare earth element evidence. In McElhinny, M. W., ed., The Earth: Its origin, structure and evolution. London Academic Press, 353-376.

Taylor, S. R., McLennan, S. M. 1979. Discussion on chemistry, thermal gradients and evolution of the lower continental crust, by J. Tarney and B. F. Windley.

Taylor, S. R., McLennan, S. M. 1981a.The rare earth element evidence in Precambrian sedimentary rocks: implications for crustal evolution, In Kroner. A., ed., Precambrian Plate tectonics. Armsterdam, Elsevier, 527-548.

Taylor, S. R., McLennan, S. M. 1981b. The composition and evolution of the continental crust: rare earth element evidence from sedimentary rocks. Phil. Trans. Roy. Soc. Lond., Ser A, 301, 381-399.

Taylor, S. R., McLennan, S. M. 1883. Geochemistry of Early Proterozoic sedimentary rocks and the Archean/Proterozoic boundary. Geol. Soc. Amer. Mem., 161, 119-131.

Taylor, S. R., White, A. J. R. 1965. Geochemistry of andesites and the growth of continents. Nature, 205, 276-273.

Tindle, A. G., Pearce, J. A. 1981. Petrogenetic Modelling of in situ fractional crystallization in the zoned Loch Doon Pluton, Scotland. Contrib. Moneral. Prteol., 78, 198-207.

Tipper, H. W. 1981. Offset of an Upper Pliensbachian geographic zonation in the North American Cordillera by transcurrent faulting. Canadian Jour. of Earth Sciences, 18, 1788-1792.

Tipper, H. W. 1984. The age of the Jurassic Rossland Group. In Current Research, pt. A, Geol. Surv. Canada paper 84-1A.

Tipper, H. W., Woodsworth, G. J. 1981. Tectonic assemblge map of the Canadian Cordillera: GSC., Map, 1515A, Scale 1:2000000.

Turcotte, D. L. 1982. Magma migration, Ann. Rev. Earth Planet. Sci., 10, 397-408.

Turner, F. J., 1968. Metamorphic petrology, Mineralogical and field aspects. McGraw-Hill, New York, N.Y.

van der Voo, R., Jones, M., Gromme, C. S., Eberlin, G. D., Churkin, M. 1980. Paleozoic paleomagnetism and northward drift of the Alexander terrane, southeastern Alaska. Jour. Geophys. Res., 85, 5281-5296.

Veizer, J., Compston, W. 1974. $^{87}Sr/^{86}Sr$ composition of seawater during the Phanerozoic. Geochim. Cosmochim. Acta, 38, 1461-1484.

Veizer, J., Compston, W. 1976. $^{87}Sr/^{86}Sr$ in Phanerozoic carbonates as an index of crustal evolution. Geochim. Cosmochim. Acta, 40, 905-914.

Veizer, J., Jensen, S. L. 1979. Basemant and sedimentary recycling and continental evolution. Jour. Geol. 87, 341-370.

Veizer, J., Compston, W., Clauer, N., Schidlowski, M. 1983. $^{87}Sr/^{86}Sr$ in Late Proterozoic carbonates: evidence for a "mantle" event at about 900 Ma ago. Geochim. Cosmochim. Acta, 47, 295-302.

Vidal, Ph., Peucat, J. J., Larnier, B. 1980. Dating of granulites involved in the Hercynian fold-belt of Europe: an example taken from the granulite facies orthogneisses at La Picherais, Southern Armorican Massif, France. Contrib. Mineral. Petrol., 72, 283-289.

Vitorello, I., van der Voo, R. 1977. Late Hadrynian and Helikian pole position from the Spake Formation, Montana. Canadian Jour. Earth Sciences, 14, 67-73.

Vitrac, A. M., Albarede, F., Allègre, C. J. 1981. Lead isotopic composition of Hercynian granitic K-Feldspars: constraints on the continental genesis. Nature, 291, 460-464.

Walker, J. C. G. 1977. Evolution of the Atmosphere. MacMillan Publishing Co., Inc., New

York.

Wanless, R. K., Reesor, J. E., 1975. Precambrian zircon age of orthogneises in the Shuswap Metamorphic Complex, British Columbia, 12, 326-331.

Wanless, R. K., Loveridge, W. D., Mursky, G. 1968a. A geochronologocal study of the White Creek Batholith, southeastern British Columbia. Canadian Jour. Earth Sciences, 5, 375-386.

Wanless, R. K., Stevens, R. D., Lachance, G. R., Edmonds, C. M. 1968b. Age determinations and geological studies, K-Ar isotopic ages, Report, 8, GSC., paper 67-2A, 1-53.

Watson, B. 1976. Two-liquid partition coefficients: Experimental data and geochemical implications. Contrib. Mineral. Petrol., 56, 119-134.

Wetherill, G. W. 1956. Discordant uranium-lead ages. Trans. Amer. Geophys. Union, 37, 320-326.

Whalen, J. B. 1983. The Ackley City Batholith, southeastern Newfoundland, evidence for crystal vs. liquid-state fractionation. Geochim. Cosmochim. Acta, 47, 1443-1457.

Wheeler, J. O., Charlesworth, H. A. K., Monger, J. W. H., Muller, J. G., Price, R. A., Reesor, J. E., Roddick, J. A., Simony, P. S. 1974. Western Canada, In Mesozoic-Cenozoic Orogenic belts. ed., A. M. Spencer, Geol. Soc. Lond. Spec. Publ., 4.

White, A. J. R., Chappell, B. W. 1977. Ultrametamorphism and granitoid genesis. Tectonophysics, 43, 7-22.

White, W. M., Patchett, J. 1984. Hf-Nd-Sr isotopes and incompatible-element abundances in island arcs and implications for magma origins and crust-mantle evolution. Earth Planet. Sci. Lett., 67, 167-185.

Wilkinson, J. F. G., Vernon, R. H., Shaw, S. E. 1964. Petrology of an adamellite-porphyrite from the New England batholith (New South wales). Jour. Petrol. 5, 461-488.

Wilcox, R. E. 1944. Rhyolite-basalt complex on Gardiner River, Yellowstone Park, Wyoming, Geol. Soc. Amer. Bull., 55, 1047-1080.

Winkler, H. G. G. 1976. Petrogenesis of metamorphic rocks. Springer-Verlag, New York, N.Y.

Wise, D. U. 1974. Continental margins, freeboard and the volumes of continents and oceans through times, In C. A. Burke and C. L. Drake, eds., The Geology of Continenatal Margins, Springer-Verlag, 45-58.

Wright, T. L., Doherty, P. C. 1970. A linear programming and least squares computer method for solving petrologic mixing problems. Geol. Soc. Amer. Bull., 81, 1995-2008.

Yanacey, T. E. 1975. Permian marine biotic provinces in North America. Jour. Paleotology, 40, 758-766.

Yoder, H. S., Eugster, H. P. 1955. Synthetic and natural muscovites. Geochim. Cosmochim. Acta, 8, 225-280.

Yoder, H. S., Tilley, C. E. 1962. Origin of basaltic magmas: An experimental study of natural and synthetic rock systems. Jour. Petrol., 3, 342-532.

Young, F. G., Campbell, R. B., Poulton, T. P. 1973. The Windermere Supergroup of the southeastern Canadian Rockies. Belt Symposium, 1, 181-203.

Zartman, R. E. 1974. Lead isotopic provinces in the Cordillera of the Western United States and their geologic significance. Econ. Geol., 69, 792-805.

Zartman, R. E., Doe, B. R. 1981. Plumbotectonics- The model. Tectonophysics, 75, 135-162.

Zartman, R. E., Peterman, Z. E., Obradovich, J. D., Gallego, M. D., Bishop, D. T. 1982. Age of the Crossport C sill near Eastport, Idaho. In: S. E. G. Coeur d'Alene field conference Idaho, 1977 (R. R. Reid and G. A. Williams eds.). Idaho Bur. Min. and Geol. Bull., 24, 61-69.

Zen, E., Thompson, A. B., 1974. Low grade regional metamorphism: mineral equilibrium relations. Ann. Rev. of Earth Planet. Sci., 2, 179-212.

APPENDIX 1

SAMPLE LOCATION AND DESCRIPTION

Sample numbers from 8001 to 8039 were collected in 1980 summer, from 8040 to 8097 in 1981 summer and those from 8098 to 8106 in 1982 summer.

Brief description of the samples are given in Tables A1.2 and A1.3. Table A1.2 tabulates Sample Locations, Batholith/Pluton types, Rock types, Chemical types, Modal Mineralogies for the granitic(s.l.) rocks. Table A1.3 tabulates Sample locations, Formations/Groups, Rock types, Mineralogies and Grades of Metamorphism for the Sedimentary rocks.

Table A1.2 Sample Locations and Descriptions of Granitic Rocks

No	Sample	Location	Bath/Pluton	Rock-type	Chem-type	Mineralogy
1	8012A	16	NB	Bi-Gndi	Met, CA	Plag, Kf, Qz, Bi, Zr, Ap, Cpx.
2	8012B	16	..	..	..	..
3	8013A	17	..	..	..	Plag,Mic,Qz, Bi, Ep, Sph, All.
4	8013B	17	..	..	..	..
5	8013C	17	..	..	Per	Qz,Kf,Plag,Bi, Musc, Ep, Sph.
6	8052A	19	..	Cpx-Hb-Dior	Met, CA	Plag, Hb, Bi Cpx, Kf, Mic, Qz, Ep, Ap, Mt.
7	8052B	..	..	..	..	..
8	8052C	..	..	..	..	..
9	8052D	..	..	..	..	..
10	8053A	18	..	Bi-Hb-Gndi	..	Plag, Qz, Kf, Bi, Ep,Sph.
11	8053C	..	..	..	..	..
12	8053D	..	..	..	..	..
13	8053E	..	..	..	..	..
14	8057A	13	..	..	..	Plag, Qz, Kf, Bi, Hb, Ep, Ap, Sph, Mt.
15	8057B	..	..	..	..	..
16	8057C	..	..	..	..	..
17	8057E	..	..	..	..	..
18	8057G	..	..	..	..	..
19	8004	15	..	Bi-Hb-Monzo	..	Plag, Mcln, Qz, Bi, Hb, Ep, Sph.
20	8059A	..	..	..	..	..
21	8059B	..	..	..	..	..
22	8059D	..	..	..	..	..
23	8059E	..	..	..	..	..
24	8061A	20	..	NA	NA	NA
25	8061B	..	..	..	..	..
26	SB29.7	14	..	Hb-Bi-Gndi	..	Plag, Kf, Qz, Bi, Hb
27	8021A	33	BP	Monzo	..	Plag, Kf, Qz, Hb, Bi, Cpx, Ap.
28	8021B	..	..	..	..	..
29	8022A	..	..	Cpx-hb Syen	Alk	Kf(Perth), Cpx, Bi, Hb, Ap, Zr, Mt.

30	8022B	34	,,	,,	,,	Cpx, Bi, Kf(Perth), Qz, Ep, Ap, Mt.
31	8022C	,,	,,	,,	,,	Plag, Kf, Qz, Bi, Cpx, Hb, Sph.
32	8067A	35	,,	Bi-Hb-Gndi	Met, CA,	Plag, Qz, Kf, Bi, Hb, Cpx, Ap, Zr, Mt.
33	8067B	,,	,,	,,	,,	,,
34	8067C	,,	,,	,,	,,	,,
35	8067D	,,	,,	,,	,,	,,
36	8067E	,,	,,	,,	,,	,,
37	8067F	,,	,,	,,	,,	,,
38	8067G	,,	,,	,,	,,	,,
39	8068A	36	,,	Hb-Gr Gn	,,	Kf, Qz, Hb, Ap, Mt.
40	8068B	,,	,,	,,	,,	,,
41	8068C	,,	,,	,,	,,	,,
42	8068D	,,	,,	,,	,,	,,
43	8068E	,,	,,	,,	,,	,,
44	8075F	24	,,	Bi-Hb-Gndr	,,	Perth, Plag, Kf, Qz, Bi, Hb.
45	8075G	,,	,,	Cpx-Bi-Dior	,,	Perth, Bi, Cpx, Ap, Zr.
46	8075H	,,	,,	,,	,,	,,
47	8075J	,,	,,	,,	,,	,,
48	8075K	,,	,,	,,	,,	,,
49	8075K	,,	,,	Bi-Hb-Gndr	,,	Plag, Mcln, Bi, Hb, Mt.
50	8038A	3	BB	Two-mica Gr	Per	Kf, Plag, Qz, Bi, Musc.
51	8038B	,,	,,	Bi-Gr	,,	Kf, Plag, Qz, Bi.
52	8038C	,,	,,	,,	,,	,,
53	8038D	,,	,,	,,	,,	,,
54	8038E	4	,,	NA	NA	NA
55	8096E	5	,,	Two-mica Gr	Per	Qz Plag, Kf, Bi, Musc, Zr, Ap.
56	8096G	,,	,,	,,	,,	,,
57	8096I	,,	,,	,,	,,	,,
58	8096J	,,	,,	,,	,,	,,
59	8072A	29	TP	Gr Gn	Met, CA	Qz, Plag, Kf, Bi, Zr.
59	8072B	,,	,,	,,	,,	,,
60	8072C	,,	,,	,,	,,	,,
61	8073A	28	,,	,,	,,	,,
62	8073C	,,	,,	,,	,,	,,
63	8073D	,,	,,	,,	,,	,,
64	8070C	30	TN	Hb-Gn	,,	Hb, Bi, Fels, Qz.

65	8070E	..	..	..	..	..
66	8070F	..	..	..	..	..
67	8070H	31	..	..	..	..
68	8063A	39	CGN	Gn	..	Perth, Hb, Cpx, Bi, Ap, Zr.
69	8069B	32	..	Grdi	..	NA
70	8065A	37	..	Grdi	..	Kf, Qz, Plag, Hb
71	8064E	38	UA	Bi-Gr	..	Qz, Kf, Plag, Bi, Zr.
72	8021D	34		Gr	Per	Qz, Fels, Bi, Hb
73	8049A	40	VG	Bi-gr	..	Qz, Kf, Plag, Bi.
74	8049C	..	..	..	..	..
75	8049D					
		..		..	..	..
76	8049E	..	..	..	..	..
77	8088A	9	SLCS	Musc-Gr	..	qz, Kf, Plag, Musc
78	8088B	..	..	..	..	..
79	8088D	..	..	..	..	..
80	8089C	..	..	Two-mica Gr	..	Qz, Kf, Plag, Bi, Musc, Gt.
81	8089F	..	..	..	..	..
82	8007A	23	SS	Two-mica Gr	Per	Qz, Kf, Plag, Bi, Musc, Zr
83	8007B	..	..	..	..	..
84	8033A	42	KB	Syen	Met, CA	Kf, Plag, Qz, Bi, Hb, Sph, Ap, Mt
85	8033C	..	..	..	..	..
86	8033D	..	..	..	..	..
87	8033G	..	..	..	..	..
88	8033H	..	..	..	..	..
88	8033M	..	..	..	..	..
89	8033P	..	..	..	..	..
90	74/054	24a	RV	Ands		Plag, Cpx, opaque, Ground mass.
91	75/116	..	..	Hb-Ands	CA	Ground mass, Plag, Cpx, Hb, Opaque.

Table A1.3 Sample Locations and Descriptions of Sedimentary Rocks

No	Sample	Location	Formation	Rock-Type	Mineralogy	Metamorphism
1	8001B	1	Mid Aldridge	Turbidite	Qz, Bi, Musc	Greenschist
2	8001C	,,	,,	,,	,, +pl	,,
3	8001D	,,	,,	,,	,,	,,
4	8001E	,,	,,	,,	,,	,,
5	8001F	,,	,,	,,	,,	,,
6	8001G	,,	,,	,,	,, +pl	
7	8001H	,,	,,	,,	,, +pl	,,
8	8001I	,,	,,	,,	,, +pl	,,
9	8002A	2	,,	,,	Qz, Bi, Musc, Plag.	,,
10	8002B	,,	,,	,,	,,	,,
11	8002C	,,	,,	,,	,,	,,
12	8002D	,,	,,	,,	Qz, Bi, Musc	,,
13	8002E	,,	,,	,,	,,	,,
14	8002F	,,	,,	,,	,,	,,
15	8002G	,,	,,	,,	,,	,,
16	8002H	,,	,,	,,	,,	,,
17	8002I	,,	,,	,,	,, +Plag.	,,
18	8094A	6	Horsethief	Qz-Bi-Schist	Qz, Bi, Musc, Kf, Plag, Sph	Greenschist
19	8094B	,,	,,	,,	,,	,,
20	8094D	,,	,,	,,	,,	,,
21	8090A	7	Hamill	,,	,,	,,
22	8090C		,,	,,	,,	,,
23	8037B	8	Lardeau	Gneiss	Qz, Plag, Bi, Musc	
24	8037C	,,	,,	,,		
25	8037D	,,	,,	,,		
26	8037M	,,	,,	Amphibolite		
27	8084A	27	Laib	Phyllites		
28	8084B	,,	,,	,,		

29	8010Q	26	Nelway	Schist	Cc, Qz, Musc	Sub-greenschist
30	8010R	,,	,,	,,	,,	,,
31	8010S	,,	,,	,,	,,	,,
32	8010t	,,	,,	,,	,,	,,
33	8010U	,,	,,	,,	,,	,,
34	8010V	,,	,,	,,	,,	,,
35	8010W	,,	,,	,,	,,	,,
36	8009A	25	Active	Phyllite	Qz, Bi, Musc, Cc, Mt	Greenschist, Bi-grade
37	8009D	,,	,,	,,	,,	,,
38	8009J	,,	,,	,,	,,	,,
39	8009L	,,	,,	,,	,,	,,
40	8009R	,,	,,	,,	,,	,,
41	8009T	,,	,,	,,	,,	,,
42	8009U	,,	,,	,,	,,	,,
43	8003A	12	Milford	Schist	Qz, Bi, Musc, Gt, Stur	Greenschist, gt-grade
44	8003B	,,	,,	,,	,,	,,
45	8003C	,,	,,	,,	,,	,,
46	8003D	,,	,,	Amphibolite	Cc, Qz, Bi, Trem, Ilm Plag,	
47	8003E	,,	,,	,,	,,	
48	8003F	,,	,,	,,	,,	
49	8027B	11	,,	Schist	Cc, Qz, Bi, Musc	Greenschist'
50	8027C	,,	,,	,,	Qz, Bi, Musc	
51	8027D	,,	,,	,,	,,	,,
52	8027F	,,	,,	,,	,,	,,
53	8027H	,,	,,	,,	,, +iron oxide	,,
54	8027I	,,	,,	,,	,,	,,
55	8027P	,,	,,	,,	,,	,,
56	8027S	,,	,,	,,	,,	,,
57	8006D	21	Ymir	Slates	Cc, Qz, Musc	Greenschist
58	8006G	,,	,,	,,	,,	,,
59	8006H	,,	,,	,,	,,	,,
60	8006K	,,	,,	,,	,,	,,
61	8006I	,,	,,	,,	Qz, Bi, Musc	,,
62	8006L	,,	,,	,,	Cc, Qz, Musc	,,
63	8006M	22	,,	,,	,,	,,

64	8006N	,,	,,	,,	,,	,,
65	8006P	,,	,,	,,	,,	,,
66	8035A	41	Slocan	Phyllite	Cc, Qz, Bi, Musc, Mcln, Iron oxide	Greenschist
67	8035B	,,	,,	,,	,,	,,
68	8035C	,,	,,	,,	,,	,,
69	8035D	,,	,,	,,	,,	,,
70	8035E	,,	,,	,,	,,	,,
71	8035F	,,	,,	,,	,,	,,
72	8035G	,,	,,	,,	,, Cc-rich, Musc	,,
73	8035H	,,	,,	,,	,,	,,

APPENDIX 2

WHOLE ROCK CHEMICAL DATA AND METHODS OF ANALYSIS.

A2.1-Crushing.

Most of the samples collected were fresh, free from alteration marks. Those with visible alteration marks were cleaned using a chisel. Granitic samples, because of their coarse-grained nature weighed in the range 10-15 kg but the sediments weighed in the range 2-5 kg.

Large sample blocks were first broken by sledge hammer into smaller pieces which were fed into a jaw-crusher to reduce the size to smaller than 1cm in average diameter. A representative portion of this sample (≃50 gms) was then taken after repeated coning and quartering and ground to final powder (≃200 mesh) by crushing in a tungsten carbide swing mill. This powder was then stored in plastic vials both for XRF whole rock chemical and isotopic analyses.

For mineral separation, the sample after the jaw-crushing step was ground to ≃200 mesh using the grinding machine. The wilfley table was then used to separate the sample into two fractions: light fraction containing qartz, feldspar, biotite and muscovite(if any), and a heavy fraction containing zircon, sphene, apatite, epidote, hornblende etc. The heavy fraction was then dried out and cleaned with acetone. The magnetic tramps (iron flakes from the grinder) were removed with a help of a magnet. The different minerals from this heavy fraction were then separated using the Frantz Isodynamic Magnetic Separator and heavy liquids. The clean Zircon fraction was finally collected for further purification.

A2.2 XRF analysis.

Major and trace elements (whole rock) analyses were carried out by Dr. J. G. Holland at the University of Durham, England (for technical details see Beddoe-Stephens, 1977). Tables A2.2.1 and A2.2.2 contain the major elements(wt%), norms, trace elements(ppm) and trace element ratios for the Nelson Batholith and Bonnington Pluton respectively.

Table A2.2.1 Major and Trace element data for the Nelson Batholith.

Sample	8013A	8013B	8013C	8052B	8052A	8052D	8052C	8053E
SiO2	67.43	67.07	67.53	50.80	51.72	52.28	52.60	65.87
TiO2	0.47	0.45	0.48	0.73	0.72	0.05	0.62	0.58
Al2O3	15.69	16.08	16.04	15.00	15.52	14.37	14.97	15.55
Cr2O3	0.0	0.00	0.0	0.00	0.00	0.00	0.00	0.00
Fe2O3	0.87	0.84	0.88	2.18	2.24	2.25	2.10	1.13
FeO	2.70	2.65	2.70	6.31	6.61	6.63	6.22	3.46
MnO	0.08	0.08	0.09	0.23	0.22	0.16	0.17	0.09
MgO	1.34	1.25	1.38	5.41	4.98	5.86	5.32	1.73
CaO	3.69	3.68	3.21	10.27	9.93	9.69	9.14	4.40
Na2O	3.43	3.47	3.47	3.81	4.20	3.39	3.98	3.17
K2O	4.12	4.24	4.01	4.62	3.25	4.04	4.29	3.78
P2O5	0.18	0.17	0.19	0.62	0.61	0.69	0.60	0.24
NiO	0.0	0.0	0.00	0.00	0.00	0.00	0.01	0.00
S	0.01	0.03	0.01	0.03	0.01	0.0	0.0	0.02
Total	100.01	100.01	99.99	102.02	100.02	99.42	100.02	100.03
FeO*	(3.48)	(3.41)	(3.49)	(8.27)	(8.63)	(8.65)	(8.11)	(4.48)
FeO*/MgO	2.599	2.725	2.530	1.529	1.732	1.477	1.524	2.588
Mg/Mg+Fe	0.407	0.395	0.413	0.538	0.507	0.547	0.539	0.408
FeO/MgO	2.015	2.120	1.957	1.166	1.327	1.131	1.169	2.000
Mg/Mg+Fe	0.469	0.457	0.477	0.604	0.573	0.612	0.604	0.471
CIPW norm (wt)								
Q	21.08	20.06	21.96	0.0	0.0	0.0	0.0	20.23
or	24.34	25.05	23.69	22.17	19.20	23.87	25.34	22.33
ab	29.02	29.36	29.36	0.0	19.85	17.61	17.29	26.82
an	15.25	15.78	14.68	4.27	13.90	12.06	10.31	17.04
lc	0.0	0.0	0.0	13.29	0.0	0.0	0.0	0.0
ne	0.0	0.0	0.0	17.46	8.50	6.00	8.87	0.0
C	0.0	0.0	0.61	0.0	0.0	0.0	0.0	0.0
di-wo	0.79	0.57	0.0	17.80	13.10	13.15	12.99	1.35
di-en	0.37	0.26	0.0	10.19	7.15	7.34	7.41	0.64
di-fs	0.40	0.30	0.0	6.82	5.48	5.30	5.02	0.69
hy-en	2.96	2.85	3.44	0.0	0.0	0.0	0.0	3.67
hy-fs	3.21	3.27	3.61	0.0	0.0	0.0	0.0	3.94
fo	0.0	0.0	0.0	2.30	3.68	5.08	4.09	0.0
fa	0.0	0.0	0.0	1.69	3.11	4.04	3.06	0.0
mt	1.26	1.22	1.28	3.16	3.25	3.26	3.04	1.64
il	0.89	0.85	0.91	1.39	1.37	0.09	1.18	1.10
ap	0.42	0.39	0.44	1.44	1.41	1.60	1.39	0.56
hm	0.0	0.0	0.0	0.0	0.0	0.0	0.0	0.0
wo	0.0	0.0	0.0	0.0	0.0	0.0	0.0	0.0
cs	0.0	0.0	0.0	0.0	0.0	0.0	0.0	0.0
Total	99.99	99.97	99.97	101.98	100.00	99.41	100.01	99.99

Sample	8013A	8013B	8013C	8052B	8052A	8052D	8052C	8053E
Trace Elements (ppm)								
Ba	1470.0	1328.0	1340.0	1140.0	851.0	1156.0	1312.0	1095.0
Rb	139.0	138.0	136.0	113.0	67.0	94.0	99.0	110.0
Sr	665.0	627.0	678.0	1487.0	1123.0	1227.0	1220.0	558.0
Pb	23.0	25.0	22.0	9.0	8.0	2.0	12.0	28.0
Zr	153.0	144.0	159.0	48.0	41.0	12.0	18.0	111.0
Nb	16.0	16.0	11.0	6.0	6.0	5.0	5.0	14.0
Y	13.0	14.0	17.0	14.0	15.0	10.0	11.0	12.0
La	19.0	19.0	15.0	4.0	10.0	19.0	8.0	20.0
Ce	36.0	33.0	21.0	32.0	19.0	24.0	19.0	49.0
Nd	0.0	0.0	33.0	14.0	16.0	9.0	5.0	30.0
Cr	6.0	11.0	0.0	19.0	14.0	84.0	77.0	8.0
Co	0.0	0.0	8.0	42.0	37.0	42.0	58.0	38.0
Ni	3.0	6.0	6.0	10.0	7.0	34.0	34.0	7.0
Cu	1.0	1.0	1.0	110.0	139.0	151.0	154.0	10.0
Zn	76.0	79.0	86.0	102.0	93.0	75.0	74.0	95.0
Ratio (wt)								
K/Rb	246.059	255.061	244.772	486.335	402.685	356.788	359.731	285.270
Rb/Sr	0.209	0.220	0.201	0.076	0.060	0.077	0.081	0.197
Ce/Y	2.769	2.357	1.235	2.286	1.267	2.400	1.727	4.083
Zr/Nb	9.563	9.000	0.069	8.000	6.833	2.400	3.600	7.929
Ba/Sr	2.211	2.118	1.976	0.767	0.758	0.942	1.075	1.962
K/Ba	23.267	26.505	24.843	48.207	31.704	29.012	27.144	28.657
Na2O/K2O	1.201	1.222	1.156	1.738	0.774	1.192	1.078	1.192
Ca/Sr	39.648	41.937	33.829	49.348	63.181	56.428	53.530	56.342
A/C+N+K	0.934	0.947	1.010	0.467	0.545	0.521	0.538	0.899
LogK/Na	0.080	0.087	0.063	0.240	-0.111	0.076	0.033	0.076
Na2O+K2O	7.550	7.710	7.480	10.430	7.450	7.430	8.270	6.950
Ca/Na+K	0.489	0.477	0.429	0.985	1.333	1.304	1.105	0.633
LogC/N+K	-0.311	-0.321	-0.367	-0.007	0.125	0.115	0.043	-0.199

Sample	8053D	8053A	8053C	8057G	8057E	8057C	8057A	8057B
S102	66.10	66.86	67.59	60.03	63.34	65.29	66.34	66.51
T102	0.57	0.40	0.37	0.67	0.67	0.47	0.45	0.48
A1203	15.39	17.04	16.49	16.68	16.24	16.45	15.97	15.83
Cr203	0.00	0.0	0.00	0.00	0.00	0.00	0.00	0.00
Fe203	1.10	0.66	0.71	1.60	1.36	0.94	0.96	1.10
FeO	3.44	2.02	2.16	5.00	4.05	2.88	2.89	3.06
MnO	0.10	0.09	0.08	0.30	0.13	0.09	0.09	0.10
MgO	1.62	0.72	0.77	3.00	1.67	1.50	1.10	1.12
CaO	4.32	3.99	4.17	6.00	4.63	4.00	3.61	3.49
Na20	3.31	4.62	4.39	3.20	4.15	4.20	4.57	4.51
K20	3.85	3.40	3.08	3.00	3.44	6.02	3.78	3.65
P205	0.20	0.18	0.16	0.50	0.33	0.19	0.25	0.24
N10	0.01	0.00	0.01	0.00	0.00	0.00	0.00	0.00
S	0.01	0.05	0.02	0.02	0.0	0.0	0.0	0.0
Total	100.02	100.03	100.00	100.02	100.01	100.01	100.01	100.09
FeO*	(4.43)	(2.61)	(2.80)	(5.22)	(5.27)	(3.73)	(3.75)	(4.05)
FeO*/MgO	2.735	3.631	3.635	2.730	3.158	3.327	3.413	3.616
Mg/Mg+Fe	0.395	0.329	0.329	0.395	0.361	0.349	0.343	0.330
FeO/MgO	2.123	2.806	2.805	2.094	2.425	2.571	2.627	2.732
Mg/Mg+Fe	0.456	0.389	0.389	0.460	0.424	0.409	0.404	0.395
CIPW norm (wt)								
Q	19.83	17.27	20.06	3.41	11.56	11.66	15.78	16.74
or	22.74	20.09	18.20	25.34	14.41	35.56	22.33	21.56
ab	28.01	39.09	37.14	39.09	43.57	32.58	38.67	38.16
an	15.76	15.72	16.19	14.48	13.99	9.82	11.90	12.17
lc	0.0	0.0	0.0	0.0	0.0	0.0	0.0	0.0
ne	0.0	0.0	0.0	0.0	0.0	0.0	0.0	0.0
C	0.0	0.0	0.0	0.0	0.0	0.0	0.0	0.0
di-wo	1.82	1.21	1.44	3.47	2.85	0.99	1.83	1.49
di-en	0.84	0.49	0.58	1.62	1.23	0.42	0.75	0.61
di-fs	0.97	0.73	0.88	1.82	1.62	0.58	1.08	0.90
hy-en	3.20	1.30	1.34	3.14	2.93	2.37	1.98	2.18
hy-fs	3.69	1.94	2.04	3.53	3.83	3.32	2.85	3.21
fo	0.0	0.0	0.0	0.0	0.0	0.0	0.0	0.0
fa	0.0	0.0	0.0	0.0	0.0	0.0	0.0	0.0
mt	1.59	0.96	1.03	1.96	1.97	1.36	1.39	1.59
il	1.08	0.76	0.70	1.27	1.27	0.89	0.85	0.91
ap	0.46	0.42	0.37	0.86	0.76	0.44	0.58	0.56
hm	0.0	0.0	0.0	0.0	0.0	0.0	0.0	0.0
wo	0.0	0.0	0.0	0.0	0.0	0.0	0.0	0.0
cs	0.0	0.0	0.0	0.0	0.0	0.0	0.0	0.0
Total	99.99	99.98	99.97	99.98	100.01	100.00	100.00	100.08

Sample	8053D	8053A	8053C	8057G	8057E	8057C	8057A	8057B
Trace Elements (ppm)								
Ba	1097.0	1064.0	1184.0	1980.0	1198.0	1873.0	1278.0	1195.0
Rb	135.0	169.0	110.0	86.0	65.0	123.0	83.0	85.0
Sr	546.0	1099.0	1021.0	1309.0	1110.0	1031.0	1027.0	1066.0
Pb	31.0	23.0	22.0	15.0	15.0	13.0	12.0	24.0
Zr	131.0	152.0	150.0	205.0	197.0	195.0	173.0	164.0
Nb	14.0	21.0	18.0	48.0	26.0	25.0	31.0	34.0
Y	13.0	7.0	8.0	29.0	12.0	13.0	17.0	16.0
La	10.0	25.0	15.0	34.0	42.0	94.0	32.0	42.0
Ce	30.0	45.0	31.0	72.0	65.0	129.0	66.0	61.0
Nd	25.0	18.0	16.0	29.0	23.0	32.0	21.0	39.0
Cr	5.0	5.0	5.0	12.0	12.0	6.0	5.0	6.0
Co	54.0	25.0	48.0	34.0	23.0	35.0	31.0	25.0
Ni	4.0	2.0	4.0	11.0	10.0	4.0	6.0	6.0
Cu	11.0	12.0	9.0	6.0	5.0	9.0	7.0	7.0
Zn	87.0	97.0	80.0	126.0	102.0	87.0	85.0	93.0
Ga	0.0	0.0	0.0	0.0	0.0	0.0	0.0	0.0
Ratio (wt)								
K/Rb	236.746	167.012	232.442	414.110	311.625	406.301	378.068	356.476
Rb/Sr	0.247	0.154	0.108	0.066	0.059	0.119	0.081	0.080
Ce/Y	2.308	6.429	3.875	2.483	5.417	9.923	3.882	3.813
Zr/Nb	9.357	7.238	8.333	4.271	7.577	7.800	5.581	4.824
Ba/Sr	2.009	0.968	1.160	1.513	1.079	1.817	1.244	1.121
K/Ba	29.135	26.527	21.595	17.987	16.908	26.682	24.554	25.356
Na2O/K2O	1.163	0.736	0.702	0.929	0.474	1.564	0.827	0.809
Ca/Sr	56.533	25.941	29.183	27.729	29.804	18.781	25.116	23.393
A/C+N+K	0.881	0.920	0.909	0.817	0.832	0.926	0.879	0.894
LogK/Na	0.066	-0.133	-0.154	-0.032	-0.324	0.194	-0.082	-0.092
Na2O+K2O	7.160	8.020	7.470	8.910	7.590	9.870	8.350	8.160
Ca/Na+K	0.603	0.498	0.558	0.570	0.610	0.275	0.432	0.428
LogC/N+K	-0.219	-0.303	-0.253	-0.244	-0.215	-0.561	-0.364	-0.369

Sample	8059E	8059D	8004	8059B	8059A	8061B	8061A	SB29.7
S102	54.76	61.98	63.10	63.69	64.16	62.36	62.38	67.30
T102	1.26	0.66	0.63	0.63	0.57	0.80	0.78	0.38
A1203	16.54	15.77	16.34	15.24	15.53	17.14	16.48	16.27
Cr203	0.00	0.00	0.00	0.00	0.00	0.00	0.00	0.0
Fe203	2.04	1.42	1.21	1.40	1.24	3.01	4.09	3.03
FeO	6.03	4.35	3.74	4.18	3.81	1.76	1.81	0.00
MnO	0.15	0.14	0.13	0.14	0.11	0.11	0.12	0.01
MgO	5.10	2.34	2.09	2.29	1.97	2.57	2.66	0.68
CaO	7.63	4.85	4.31	4.24	4.01	5.11	4.52	3.08
Na20	2.89	3.70	4.03	3.76	3.69	2.98	3.07	4.60
K20	3.18	4.37	4.07	4.03	4.56	3.64	3.71	4.32
P205	0.38	0.41	0.34	0.40	0.33	0.41	0.34	0.10
N10	0.00	0.00	0.0	0.01	0.01	0.00	0.00	0.02
S	0.07	0.02	0.02	0.01	0.01	0.19	0.09	0.06
Total	100.04	100.02	100.11	100.02	100.00	100.08	100.05	99.85
FeO*	(7.87)	(5.63)	(4.83)	(5.44)	(4.93)	(4.47)	(5.49)	(2.73)
FeO*/MgO	1.542	2.405	2.416	2.376	2.501	1.739	2.064	4.010
Mg/Mg+Fe	0.536	0.426	0.066	0.429	0.416	0.506	0.463	0.308
FeO/MgO	1.182	1.859	19.684	1.825	1.934	0.685	0.680	0.000
Mg/Mg+Fe	0.601	0.489	0.083	0.494	0.480	0.722	0.724	1.000
CIPW norm (wt)								
Q	2.17	9.99	14.23	13.63	13.43	17.48	17.64	17.47
or	18.79	25.82	24.04	23.81	26.94	21.50	21.92	25.52
ab	24.45	31.31	34.10	31.81	31.22	25.21	25.98	38.92
an	22.77	13.51	14.47	12.80	12.34	22.64	20.20	10.99
lc	0.0	0.0	0.0	0.0	0.0	0.0	0.0	0.0
ne	0.0	0.0	0.0	0.0	0.0	0.0	0.0	0.0
C	0.0	0.0	0.0	0.0	0.0	0.0	0.01	0.0
di-wo	5.26	3.29	1.96	2.35	2.25	0.01	0.0	1.52
di-en	3.13	1.59	0.18	1.15	1.07	0.01	0.0	1.31
di-fs	1.87	1.64	1.98	1.16	1.15	0.0	0.0	0.0
hy-en	9.57	4.23	0.29	4.55	3.83	6.39	6.62	0.38
hy-fs	5.72	4.35	3.09	4.58	4.09	0.0	0.0	0.0
fo	0.0	0.0	0.0	0.0	0.0	0.0	0.0	0.0
fa	0.0	0.0	0.0	0.0	0.0	0.0	0.0	0.0
mt	2.96	2.06	1.75	2.03	1.80	3.71	3.96	-1.07
il	2.39	1.25	1.20	1.20	1.08	1.52	1.48	0.72
ap	0.88	0.95	0.79	0.93	0.76	0.95	0.79	0.23
hm	0.0	0.0	0.0	0.0	0.0	0.45	1.36	3.77
wo	0.0	0.0	0.0	0.0	0.0	0.0	0.0	0.0
cs	0.0	0.0	0.0	0.0	0.0	0.0	0.0	0.0
Total	99.96	99.98	98.08	99.99	99.97	99.89	99.96	99.76

Sample	8059E	8059D	8004	8059B	8059A	8061B	8061A	SB29.7
Trace Elements (ppm)								
Ba	956.0	1514.0	1412.0	1134.0	1352.0	1127.0	1049.0	1174.0
Rb	110.0	102.0	102.0	102.0	107.0	115.0	120.0	124.0
Sr	652.0	911.0	902.0	827.0	919.0	674.0	573.0	1186.0
Pb	12.0	23.0	16.0	21.0	22.0	35.0	36.0	35.0
Zr	58.0	170.0	187.0	167.0	141.0	185.0	180.0	197.0
Nb	11.0	35.0	38.0	40.0	34.0	24.0	23.0	22.0
Y	23.0	22.0	32.0	28.0	21.0	25.0	21.0	14.0
La	17.0	34.0	32.0	29.0	34.0	25.0	27.0	36.0
Ce	38.0	59.0	52.0	59.0	48.0	56.0	54.0	58.0
Nd	21.0	25.0	0.0	30.0	38.0	30.0	27.0	28.0
Cr	20.0	12.0	11.0	11.0	11.0	15.0	16.0	0.0
Co	43.0	49.0	0.0	50.0	53.0	29.0	31.0	129.0
Ni	10.0	6.0	5.0	5.0	8.0	6.0	4.0	0.0
Cu	27.0	8.0	2.0	7.0	7.0	10.0	8.0	11.0
Zn	115.0	110.0	106.0	113.0	101.0	117.0	179.0	71.0
Ga	0.0	0.0	21.0	0.0	0.0	0.0	0.0	0.0
Ratio (wt)								
K/Rb	239.989	355.662	331.246	327.990	353.783	262.760	256.655	289.213
Rb/Sr	0.169	0.112	0.113	0.123	0.116	0.171	0.209	0.105
Ce/Y	1.652	2.682	1.625	2.107	2.286	2.240	2.571	4.143
Zr/Nb	5.273	4.857	4.921	4.175	4.147	7.708	7.826	8.955
Ba/Sr	1.466	1.662	1.565	1.371	1.471	1.672	1.831	0.990
K/Ba	27.614	23.961	23.929	29.502	27.999	26.812	29.360	30.547
Na2O/K2O	1.100	1.181	1.010	1.072	1.236	1.221	1.208	0.939
Ca/Sr	83.616	38.040	34.142	36.633	31.178	54.172	56.364	18.556
A/C+N+K	0.750	0.803	0.866	0.835	0.849	0.945	0.954	0.912
LogK/Na	0.042	0.072	0.004	0.030	0.092	0.087	0.082	-0.027
Na2O+K2O	6.070	8.070	8.100	7.790	8.250	6.620	6.780	8.920
Ca/Na+K	1.257	0.601	0.532	0.544	0.486	0.772	0.667	0.345
LogC/N+K	0.099	-0.221	-0.274	-0.264	-0.313	-0.112	-0.176	-0.462

Table A2.2.2 Major and Trace element data for the Bonninton Pluton.

Sample	8022A	8022C	8022B	8021A	8021B	8067E	8067F	8067A
SiO_2	54.59	54.90	55.05	61.44	61.88	61.04	62.31	63.11
TiO_2	1.19	1.10	1.00	0.60	0.60	0.62	0.61	0.56
Al_2O_3	15.68	15.14	15.27	17.33	17.22	17.16	16.56	17.14
Cr_2O_3	0.01	0.01	0.01	0.0	0.0	0.00	0.00	0.00
Fe_2O_3	1.70	1.77	1.74	1.23	1.21	1.32	1.30	1.08
FeO	5.12	5.31	5.31	3.88	3.72	4.03	3.82	3.28
MnO	0.14	0.14	0.14	0.13	0.13	0.15	0.14	0.12
MgO	5.12	5.45	5.18	2.12	2.10	2.01	1.98	1.55
CaO	6.11	6.26	6.20	5.73	5.48	5.98	5.84	5.81
Na_2O	4.49	4.36	4.56	4.05	4.15	4.15	4.00	4.20
K_2O	4.48	4.66	4.65	3.18	3.23	3.22	3.13	3.00
P_2O_5	0.87	0.87	0.81	0.27	0.27	0.31	0.32	0.26
NiO	0.0	0.0	0.0	0.0	0.0	0.01	0.00	0.00
S	0.08	0.05	0.02	0.05	0.02	0.02	0.0	0.01
Total	99.58	100.02	99.94	100.01	100.01	100.02	100.01	100.13
FeO*	(6.65)	(6.90)	(6.88)	(4.99)	(4.81)	(5.22)	(4.99)	(4.25)
FeO*/MgO	1.299	1.267	1.327	2.352	2.290	2.596	2.520	2.743
Mg/Mg+Fe	0.578	0.585	0.573	0.431	0.438	0.407	0.414	0.394
FeO/MgO	1.000	0.974	1.025	1.830	1.771	2.005	1.929	2.116
Mg/Mg+Fe	0.641	0.647	0.635	0.493	0.502	0.471	0.480	0.457
CIPW norm (wt)								
Q	0.0	0.0	0.0	10.10	10.38	9.05	12.06	12.90
or	26.47	27.53	27.47	18.79	19.08	19.02	18.49	17.72
ab	31.64	30.42	30.38	34.27	35.11	35.11	33.84	35.54
an	9.40	7.98	7.46	19.71	18.82	18.68	17.99	19.05
lc	0.0	0.0	0.0	0.0	0.0	0.0	0.0	0.0
ne	3.44	3.51	4.44	0.0	0.0	0.0	0.0	0.0
C	0.0	0.0	0.0	0.0	0.0	0.0	0.0	0.0
di-wo	6.36	7.26	7.52	2.90	2.76	3.74	3.71	3.37
di-en	4.00	4.56	4.61	1.41	1.37	1.75	1.78	1.55
di-fs	1.97	2.26	2.48	1.44	1.33	1.95	1.88	1.78
hy-en	0.0	0.0	0.0	3.87	3.86	3.25	3.15	2.31
hy-fs	0.0	0.0	0.0	3.92	3.75	3.62	3.32	2.65
fo	6.14	6.32	5.81	0.0	0.0	0.0	0.0	0.0
fa	3.34	3.45	3.43	0.0	0.0	0.0	0.0	0.0
mt	2.46	2.57	2.52	1.78	1.75	1.91	1.88	1.57
il	2.26	2.09	1.90	1.14	1.14	1.18	1.16	1.06
ap	2.02	2.02	1.88	0.63	0.63	0.72	0.74	0.60
hm	0.0	0.0	0.0	0.0	0.0	0.0	0.0	0.0
wo	0.0	0.0	0.0	0.0	0.0	0.0	0.0	0.0
cs	0.0	0.0	0.0	0.0	0.0	0.0	0.0	0.0
Total	99.48	99.95	99.90	99.96	99.99	99.99	100.01	100.11

Sample	8022A	8022C	8022B	8021A	8021B	8067E	8067F	8067A
Trace Elements	(ppm)							
Ba	2527.0	2629.0	2514.0	1897.0	1866.0	1458.0	1398.0	1451.0
Rb	119.0	106.0	110.0	69.0	84.0	68.0	66.0	57.0
Sr	1780.0	1921.0	1834.0	1022.0	939.0	859.0	919.0	1005.0
Pb	17.0	18.0	20.0	14.0	14.0	18.0	14.0	8.0
Zr	183.0	165.0	167.0	130.0	130.0	142.0	129.0	99.0
Nb	37.0	30.0	32.0	13.0	11.0	13.0	15.0	11.0
Y	24.0	21.0	24.0	17.0	15.0	17.0	21.0	15.0
La	58.0	54.0	56.0	19.0	19.0	25.0	42.0	17.0
Ce	99.0	84.0	82.0	23.0	21.0	32.0	10.0	31.0
Nd	0.0	0.0	63.0	0.0	20.0	18.0	15.0	8.0
Cr	141.0	149.0	142.0	9.0	9.0	12.0	46.0	8.0
Co	0.0	0.0	0.0	0.0	0.0	48.0	6.0	41.0
Ni	54.0	60.0	59.0	3.0	3.0	6.0	9.0	10.0
Cu	48.0	45.0	55.0	10.0	4.0	11.0	94.0	8.0
Zn	83.0	86.0	92.0	85.0	85.0	105.0	0.0	89.0
Ga	0.0	0.0	0.0	0.0	0.0	0.0	0.0	0.0
Ratio	(wt)							
K/Rb	312.527	364.953	350.927	382.591	319.212	393.100	393.692	436.921
Rb/Sr	0.067	0.055	0.060	0.068	0.089	0.079	0.072	0.057
Ce/Y	4.125	4.000	3.417	1.353	1.400	1.882	0.476	2.067
Zr/Nb	4.946	5.500	5.219	10.000	11.818	10.923	0.933	9.000
Ba/Sr	1.420	1.369	1.371	1.856	1.987	1.697	1.521	1.444
K/Ba	14.717	14.715	15.355	13.916	14.370	18.334	18.586	17.164
Na2O/K2O	0.998	1.069	1.020	0.785	0.778	0.776	0.783	0.714
Ca/Sr	24.526	23.284	24.155	40.061	41.699	49.742	45.406	41.307
A/C+N+K	0.672	0.642	0.642	0.845	0.849	0.810	0.805	0.827
LogK/Na	-0.001	0.029	0.008	-0.105	-0.109	-0.110	-0.107	-0.146
Na2O+K2O	8.970	9.020	9.210	7.230	7.380	7.370	7.130	7.200
Ca/Na+K	0.681	0.694	0.673	0.793	0.743	0.811	0.819	0.807
LogC/N+K	-0.167	-0.159	-0.172	-0.101	-0.129	-0.091	-0.087	-0.093

Sample	8067G	8067D	8067B	8067C	8068C	8068C1	8068D1	8068F
SiO2	63.01	63.62	63.93	64.59	64.87	65.13	65.28	65.43
TiO2	0.48	0.57	0.58	0.49	0.64	0.29	0.30	0.26
Al2O3	16.64	16.84	16.62	16.69	15.21	18.57	18.25	18.59
Cr2O3	0.00	0.00	0.00	0.0	0.00	0.00	0.00	0.00
Fe2O3	1.14	1.08	1.12	1.02	1.08	0.67	0.66	0.59
FeO	3.43	3.26	3.19	3.09	3.23	1.99	2.00	1.77
MnO	0.15	0.13	0.13	0.11	0.08	0.14	0.13	0.11
MgO	1.61	1.49	1.58	1.32	1.70	0.18	0.33	0.50
CaO	5.74	5.34	5.21	4.99	3.52	4.99	4.79	4.88
Na2O	4.14	3.91	3.82	4.24	3.90	5.33	5.11	5.48
K2O	3.34	3.49	3.53	3.23	5.24	2.58	2.98	2.24
P2O5	0.30	0.28	0.29	0.23	0.53	0.14	0.15	0.14
NiO	0.00	0.00	0.00	0.01	0.00	0.00	0.00	0.00
S	0.01	0.01	0.01	0.0	0.02	0.0	0.04	0.03
Total	99.99	100.02	100.01	100.01	100.03	100.01	100.02	100.03
FeO*	(4.46)	(4.23)	(4.20)	(4.01)	(4.20)	(2.59)	(2.59)	(2.30)
FeO*/MgO	2.768	2.840	2.657	3.036	2.472	14.406	7.861	4.602
Mg/Mg+Fe	0.392	0.386	0.402	0.370	0.419	0.110	0.185	0.279
FeO/MgO	2.130	2.188	2.019	2.341	1.900	11.056	6.061	3.540
Mg/Mg+Fe	0.456	0.449	0.469	0.432	0.484	0.139	0.227	0.335
CIPW norm (wt)								
Q	12.16	14.07	14.92	14.99	12.86	13.40	13.54	13.84
or	19.73	20.62	20.85	19.08	30.96	15.24	17.60	13.23
ab	35.03	33.08	32.32	35.88	33.00	45.10	43.24	46.37
an	16.96	18.09	17.78	16.97	8.52	19.12	18.06	19.51
lc	0.0	0.0	0.0	0.0	0.0	0.0	0.0	0.0
ne	0.0	0.0	0.0	0.0	0.0	0.0	0.0	0.0
C	0.0	0.0	0.0	0.0	0.0	0.0	0.0	0.0
di-wo	3.99	2.74	2.58	2.62	2.29	1.97	1.97	1.58
di-en	1.80	1.25	1.23	1.15	1.14	0.29	0.47	0.54
di-fs	2.17	1.48	1.32	1.47	1.11	1.86	1.63	1.09
hy-en	2.21	2.46	2.71	2.14	3.10	0.16	0.36	0.71
hy-fs	2.67	2.92	2.90	2.75	3.02	1.03	1.24	1.45
fo	0.0	0.0	0.0	0.0	0.0	0.0	0.0	0.0
fa	0.0	0.0	0.0	0.0	0.0	0.0	0.0	0.0
mt	1.65	1.57	1.62	1.48	1.57	0.97	0.96	0.86
il	0.91	1.08	1.10	0.93	1.22	0.55	0.57	0.49
ap	0.70	0.65	0.67	0.53	1.23	0.32	0.35	0.32
hm	0.0	0.0	0.0	0.0	0.0	0.0	0.0	0.0
wo	0.0	0.0	0.0	0.0	0.0	0.0	0.0	0.0
cs	0.0	0.0	0.0	0.0	0.0	0.0	0.0	0.0
Total	99.98	100.01	100.00	100.00	99.99	100.01	99.98	99.99

Sample	8067G	8067D	8067B	8067C	8068C	8068C1	8068D1	8068F
Trace Elements (ppm)								
Ba	996.0	1869.0	1479.0	1366.0	1623.0	1601.0	1655.0	1476.0
Rb	72.0	60.0	73.0	79.0	159.0	54.0	71.0	54.0
Sr	794.0	959.0	892.0	836.0	1034.0	1377.0	1292.0	1316.0
Pb	11.0	14.0	19.0	18.0	14.0	20.0	19.0	19.0
Zr	146.0	81.0	95.0	110.0	250.0	101.0	123.0	99.0
Nb	10.0	10.0	12.0	16.0	71.0	19.0	19.0	24.0
Y	13.0	12.0	13.0	13.0	15.0	17.0	17.0	14.0
La	22.0	18.0	14.0	18.0	66.0	24.0	27.0	24.0
Ce	40.0	30.0	37.0	33.0	108.0	32.0	38.0	29.0
Nd	16.0	12.0	13.0	14.0	47.0	14.0	17.0	8.0
Cr	12.0	8.0	10.0	8.0	23.0	2.0	4.0	3.0
Co	32.0	31.0	18.0	47.0	28.0	23.0	31.0	38.0
Ni	5.0	5.0	7.0	3.0	15.0	8.0	6.0	4.0
Cu	8.0	8.0	7.0	8.0	8.0	16.0	11.0	23.0
Zn	93.0	87.0	93.0	77.0	59.0	68.0	56.0	55.0
Ga	0.0	0.0	0.0	0.0	0.0	0.0	0.0	0.0
Ratio (wt)								
K/Rb	385.097	482.870	401.428	339.416	273.584	396.627	348.429	344.358
Rb/Sr	0.091	0.063	0.082	0.094	0.154	0.039	0.055	0.041
Ce/Y	3.077	2.500	2.846	2.538	7.200	1.882	2.235	2.071
Zr/Nb	14.600	8.100	7.917	6.875	3.521	5.316	6.474	4.125
Ba/Sr	1.254	1.949	1.658	1.634	1.570	1.163	1.281	1.122
K/Ba	27.838	15.501	19.814	19.629	26.802	13.378	14.948	12.598
Na2O/K2O	0.807	0.893	0.924	0.762	1.344	0.484	0.583	0.409
Ca/Sr	51.654	39.787	41.734	42.649	24.324	25.893	26.490	26.496
A/C+N+K	0.798	0.846	0.849	0.854	0.823	0.900	0.897	0.915
LogK/Na	-0.093	-0.049	-0.034	-0.118	0.128	-0.315	-0.234	-0.389
Na2O+K2O	7.480	7.400	7.350	7.470	9.140	7.910	8.090	7.720
Ca/Na+K	0.767	0.722	0.709	0.668	0.385	0.631	0.592	0.632
LogC/N+K	-0.115	-0.142	-0.149	-0.175	-0.414	-0.200	-0.228	-0.199

Sample	8068E	8068A	8068B	8075H	8075G	8075F	8075K	8075J
SiO2	67.32	67.79	68.29	52.51	53.08	60.77	60.78	61.05
TiO2	0.16	0.68	0.36	1.35	1.20	0.71	0.79	0.86
Al2O3	17.84	15.11	16.09	15.27	15.85	16.19	16.05	15.84
Cr2O3	0.00	0.00	0.01	0.00	0.00	0.00	0.00	0.00
Fe2O3	0.41	0.93	0.67	2.44	2.28	1.51	1.46	1.47
FeO	1.23	2.79	2.07	7.19	6.78	4.42	4.52	4.29
MnO	0.06	0.06	0.06	0.21	0.21	0.14	0.13	0.13
MgO	0.33	0.82	0.50	6.61	6.02	2.66	3.26	3.17
CaO	3.69	2.45	1.82	8.70	8.82	4.90	5.81	5.87
Na2O	4.62	3.96	3.98	2.44	2.81	3.79	3.23	3.25
K2O	4.30	5.09	5.92	2.79	2.55	4.43	3.73	3.77
P2O5	0.05	0.33	0.21	0.44	0.35	0.40	0.23	0.27
NiO	0.00	0.00	0.00	0.01	0.01	0.00	0.00	0.00
S	0.0	0.0	0.03	0.10	0.09	0.02	0.03	0.04
Total	100.01	100.01	100.01	100.06	100.05	99.95	100.03	100.02
FeO*	(1.60)	(3.63)	(2.67)	(9.39)	(8.83)	(5.78)	(5.83)	(5.61)
FeO*/MgO	4.845	4.423	5.346	1.420	1.467	2.173	1.790	1.771
Mg/Mg+Fe	0.269	0.287	0.250	0.557	0.549	0.451	0.499	0.502
FeO/MgO	3.727	3.402	4.140	1.088	1.126	1.662	1.387	1.353
Mg/Mg+Fe	0.324	0.344	0.301	0.621	0.613	0.518	0.562	0.568
CIPW norm (wt)								
Q	15.52	18.56	17.17	0.0	0.0	7.37	10.27	10.81
or	25.40	30.07	34.97	16.48	15.06	26.17	22.04	22.27
ab	39.09	33.51	33.68	20.65	23.78	32.07	27.33	27.50
an	15.24	8.42	7.66	22.47	23.10	14.08	18.28	17.50
lc	0.0	0.0	0.0	0.0	0.0	0.0	0.0	0.0
ne	0.0	0.0	0.0	0.0	0.0	0.0	0.0	0.0
C	0.0	0.0	0.33	0.0	0.0	0.0	0.0	0.0
di-wo	1.14	0.66	0.0	7.44	7.67	3.18	3.78	4.12
di-en	0.37	0.25	0.0	4.49	4.55	1.63	2.08	2.33
di-fs	0.81	0.42	0.0	2.55	2.73	1.47	1.55	1.62
hy-en	0.45	1.79	1.25	11.93	10.38	4.99	6.03	5.57
hy-fs	0.96	2.93	2.76	6.77	6.21	4.49	4.48	3.87
fo	0.0	0.0	0.0	0.03	0.04	0.0	0.0	0.0
fa	0.0	0.0	0.0	0.02	0.03	0.0	0.0	0.0
mt	0.59	1.35	0.97	3.54	3.31	2.19	2.12	2.13
il	0.30	1.29	0.68	2.56	2.28	1.35	1.50	1.63
ap	0.12	0.76	0.49	1.02	0.81	0.93	0.53	0.63
hm	0.0	0.0	0.0	0.0	0.0	0.0	0.0	0.0
wo	0.0	0.0	0.0	0.0	0.0	0.0	0.0	0.0
cs	0.0	0.0	0.0	0.0	0.0	0.0	0.0	0.0
Total	100.00	100.00	99.96	99.95	99.95	99.91	99.99	99.97

Sample	8068E	8068A	8068B	8075H	8075G	8075F	8075K	8075J
Elements (ppm)								
Ba	2580.0	1782.0	1481.0	866.0	777.0	1545.0	973.0	660.0
Rb	106.0	162.0	147.0	81.0	77.0	96.0	107.0	45.0
Sr	1301.0	944.0	579.0	575.0	587.0	1064.0	516.0	618.0
Pb	18.0	16.0	36.0	11.0	12.0	21.0	12.0	10.0
Zr	91.0	313.0	262.0	57.0	40.0	155.0	96.0	59.0
Nb	13.0	71.0	105.0	7.0	8.0	36.0	13.0	8.0
Y	7.0	7.0	24.0	19.0	15.0	23.0	19.0	22.0
La	18.0	71.0	24.0	15.0	25.0	20.0	22.0	24.0
Ce	27.0	104.0	125.0	26.0	52.0	42.0	52.0	44.0
Nd	2.0	42.0	196.0	18.0	22.0	32.0	22.0	23.0
Cr	2.0	7.0	62.0	29.0	28.0	14.0	16.0	26.0
Co	26.0	24.0	7.0	50.0	44.0	37.0	35.0	39.0
Ni	5.0	4.0	40.0	11.0	13.0	5.0	12.0	17.0
Cu	13.0	5.0	5.0	36.0	28.0	5.0	28.0	35.0
Zn	23.0	58.0	11.0	127.0	117.0	119.0	76.0	117.0
Ga	0.0	0.0	51.0	0.0	0.0	0.0	0.0	0.0
Ratio (wt)								
K/Rb	336.759	260.831	334.319	285.940	274.920	383.080	289.389	695.481
Rb/Sr	0.081	0.172	0.254	0.141	0.131	0.090	0.207	0.073
Ce/Y	3.857	14.857	5.208	1.368	3.467	1.826	2.737	2.000
Zr/Nb	7.000	4.408	2.495	8.143	5.000	4.306	7.385	7.375
Ba/Sr	1.983	1.888	2.558	1.506	1.324	1.452	1.886	1.068
K/Ba	13.836	23.712	33.184	26.745	27.244	23.803	31.824	47.419
Na20/K20	0.931	1.285	1.487	1.143	0.907	1.169	1.155	1.160
Ca/Sr	20.266	18.544	22.460	108.110	107.361	32.906	80.453	67.868
A/C+N+K	0.941	0.917	0.990	0.668	0.677	0.812	0.806	0.788
LogK/Na	-0.031	0.109	0.172	0.058	-0.042	0.068	0.063	0.064
Na20+K20	8.920	9.050	9.900	5.230	5.360	8.220	6.960	7.020
Ca/Na+K	0.414	0.271	0.184	1.663	1.646	0.596	0.835	0.836
LogC/N+K	-0.383	-0.567	-0.736	0.221	0.216	-0.225	-0.078	-0.078

A2.3 ISOTOPIC ANALYSIS

A2.3.1 DISSOLUTION

A. Rb-Sr

Knowing Rb and Sr concentrations in the samples (through XRF analysis), samples of 50 to 100 mg are taken for chemical dissolution. Sample from the plastic vials was weighed out in clean Teflon beakers and spiked for both Rb and Sr using mixed spike 1A solution prepared by Dr. H. Baadsgaard. The spike has the following isotopic compositions:

^{84}Sr(total) spike= 2.00295 μg/g.

^{87}Rb(total) spike= 4.6628 μg/g.

^{84}Sr-spike (NBS-988) composition:

84 = 99.892 (at %)

86 = 0.059

87 =0.010

88 =0.039

^{87}Rb spike composition:

85 = 1.955 (wt %)

87 =98.045

0.5 ml of vapour-distilled water was then added to the sample and spike solution for a better mixing. To the above solution, a mixture of 10 ml of conc. HF and 5 ml of conc. HNO_3 was added and the beaker was shaken vigorously to prevent the sample from forming a cake. For sedimentary samples containing carbonates special care was taken while adding the above acid mixture. After an hour, the beaker (with the sample solution) and the lid were transferred to the hot plate and kept overnight at about for complete dissolution. Solution was evaporated to dryness and a mixture of 5 ml. of 50% HNO_3 and 10 ml of H_2O was then added and put back on the hot plate overnight with the lid on. This solution was then dried down to 5 ml and transferred to centrifuge tube. The clean solution was then treated with a few drops of $Ba(NO_2)_3$ solution. This results in the coprecipitation of Sr with Ba and Rb remains in the supernatant. The coprecipitation procedure is repeated for a purer Sr sample. This Sr from the precipitate is then separated using the cation exchange columns. The Rb from the supernatant is also separated by using similar ion exchange columns.

B. Pb IR and ID.

The dissolution procedure for Pb is same as that of Sr except the ion exchange columns. $Ba(NO_2)_3$ coprecipitation is also used for Pb. Chloride anion exchange resin is used for Pb separation. Samples for Pb-ID runs (i.e., for determination of Pb ppm) were spiked with a ^{206}Pb spike solution prepared by Dr. H. Baadsgaard.

C. U-Pb analysis for Zircon.

The zircon fraction for each sample was treated with a few ml of warm 7M HNO_3 for dissolving out the sulphides. The sample was then dried out with acetone and weighed out in the range of 30 to 70 mg in clean teflon beakers. Enough conc. HNO_3 was then added to cover the sample and then $\cong$10 ml of HF was added. The lid is put back on and the the closed beaker is inserted into a steel jacket(bomb) and heated in an oven at $\cong$ 170°C overnight. The bomb was the taken out and cooled to room temperature. The beaker is then opened to check if the dissolution is complete. If not more HF is added and the assembly is put back in the oven for overnight. The dissolution time varied from 1 to 4 days. After complete dissolution the beaker was taken out of the steel jacket and left for a few hours for equilibration with the room temperature.

The sample solution was then split into 3 parts for Pb-ID, Pb-IR and U-ID measurements. Pb-ID and U-ID parts are spiked separately with ^{208}Pb and ^{235}U spike solutions. Pb was purified from the Pb-IR and Pb-ID fractions in the same way as described before in section A2.3B. U fraction is dried out and then dissolved in 7N HNO_3 and then separation is done using a double nitrate anion-exchange columns.

Isotopic comopositions of U and Pb (Baadagaard, 1984, pers. comm.) of spike solutions are as follows:

^{235}U-spike,

$^{235}U = 99.872$ (at%)

$^{238}U = 0.128$

^{208}Pb-spike,

$^{208}Pb = 99.73$ (at%)

$^{207}Pb = 0.05$

$^{206}Pb = 0.22$

$^{204}Pb = <0.01$

D. Sm-Nd

About 100 to 300 mg (equivalent to 3 to 4 μg of Nd) of sample powder was weighed out in clean teflon beaker. For samples for which Sm and Nd concentrations are to be measured, at this point a solution of mixed ^{149}Sm-^{145}Nd spike is added to the sample. Spiking is done in a way so that $Nd^{145}_{Sample} \simeq Nd^{145}_{Spike}$ Following is the isotopic composition of the mixed Sm-Nd spike solution #1 (Baadsgaard, 1985, pers. comm.)

$^{144}Nd = 0.21081$ μg/g

$^{145}Nd = 5.25653$,,

$^{147}Sm = 0.020574$,,

$^{149}Sm = 5.54050$,,

About 0.5 ml of H_2O is added to the sample for better spike-sample mixing. A mixture of 2 ml HNO_3 and 8 ml of HF is added to the sample and the solution is swirled vigorously as many times as possible and kept in the acid-mixture at least for 24 hours. Then the covered beaker is put on the hot plate and heated at about overnight. If the dissolution is complete then the sample is dried out and baked. Then the sample is moistened with a few drops of water and is dissolved in 5 ml of 1.5N HCl. The beaker is then left on the hot plate for drying. The process is repeated twice and then the dried sample is taken up in 2 ml of 1.5N HCl for loading on to the first ion exchange column for REE separation.

A2.3.2 ION EXCHANGE CHROMATOGRAPHY:

The procedure followed here is similar to that of DePaolo (1978) for the first and second columns. This sample was further purified using a third cation-exchange column to remove Methylactic acid.

A2.4 STANDARDS AND BLANKS.

A. Rb-Sr:

Repeated analyses (10) (Table A2.4.1) of SRM 984 gave an average $^{85}Rb/^{87}Rb$ of $2.608 \pm 0.006 (2\sigma)$. From this value a Rb-fractionation factor (or correction for mass fractionation) is calculated to be 0.994. This value has been used to reduce the measured $^{85}Rb/^{87}Rb$ ratios of all the rock samples.

For Sr, SRM 987 was run 10 times (Table A2.4.1) which gave a mean value of $0.710213 \pm 35 (2\sigma)$. These ratios are fractionation corrected to $^{86}Sr/^{88}Sr = 0.1194$.

Table A2.4.1

SRM-984	SRM-987
2.60990±16	0.710231±16
2.59906±12	0.710194±26
2.60852±18	0.710216±25
2.60835±20	0.710270±24
2.61045±14	0.710191±28
2.60990±22	0.710283±17
2.60900±16	0.710198±22
2.61090±18	0.710200±18
2.61100±22	0.710180±20
2.60840±20	0.710190±17

Also SRM-607 K-feldspar was run 6 times (Table A2.4.2) to monitor the accuracy of both Rb ans Sr concentrations and $^{87}Sr/^{86}Sr$ and $^{87}Rb/^{86}Sr$ ratios. The average results are compared with NBS values in Table A2. 4.3. From the above results, 2σ errors of estimate are calculated to be :

0.01 % for $^{87}Sr/^{86}Sr$ and
0.98 % for $^{87}Rb/^{86}Sr$.

However for calculating isochron parameters, 2σ errors of estimate uesd are 0.05% and 1% for $^{87}Sr/^{86}Sr$ and $^{87}Rb/^{86}Rb$ respectively. The Rb and Sr blanks for the total procedure

Table A2.4.2

Rb ppm	Sr ppm	^{87}Rb/^{87}Sr	^{87}Sr/^{86}Sr
522.393	65.927	24.030	1.20056±75
523.638	65.942	24.096	1.20060±59
523.938	66.032	24.064	1.20075±41
524.834	66.055	24.096	1.20065±34
525.712	66.103	24.119	1.20050±50
523.602	65.813	23.990	1.20089±30

Table A2.4.3

	Present study	NBS values
^{87}Sr/^{86}Sr	1.20066±28	1.20039±20
^{87}Rb/^{86}Sr	24.0660±0.235	
Sr ppm	65.9630±0.015	65.4850±0.320
Rb ppm	523.6590±0.050	523.900±1.01

were determined to be less than 2 ng and 5 ng respectively, which are negligible compared to the amount of sample Rb and Sr analysed taken for analysis.

B. Pb and U.

For Pb, 10 duplicate analyses of SRM 981 were made to monitor the Pb-isotopic fractionation. The following ratios were obtained:

^{206}Pb/^{204}Pb=16.940±0.0025 (16.9371)

^{207}Pb/^{204}Pb=15.4953±0.0025 (15.4913)

^{208}Pb/^{204}Pb=36.7310±0.0170 (36.7213)

The numbers in bracket are NBS values.

Average within-run precision is about 0.02%.

2σ errors of estimate are:

0.03% for ^{206,207}Pb/^{204}Pb and

0.09% for ^{208}Pb/^{204}Pb

The measured total procedural Pb blank was kept less than 2 ng. For zircon analysis, U blanks were less than 1 ng which is negligible compared with the amount of sample U analysed.

C. Sm-Nd

Both the BCR and LaJolla standards were run for Nd isotopic compositions.

For BCR, the mean $^{143}Nd/^{144}Nd$ ratio obtained was 0.512620±30(2σ, n=4) and for LaJolla, 0.511840±12(2σ, n=4). The above ratios were normalised to $^{146}Nd/^{144}Nd=0.7219$.

Total procedural blanks for Sm and Nd were determined to be less than 1 ng and 3 ng respectively.

Within-run presicion for $^{143}Nd/^{144}Nd$ is better than 6 parts in 10^5.

For monitoring accuracy of measurements of Sm and Nd concentrations, the sample 8033G was run twice. The results obtained were for Sm, 3.93 ppm and 4.12 ppm and for Nd, 22.29 ppm and 22.51 ppm respectively.

A2.5 MASS SPECTROMETRY.

A. Loading:

Rb and Sr samples were loaded as chlorides using double Re-filament beads. Pb samples were loaded on a single Re filament using standard silica-gel phosphoric acid technique. U samples were loaded on a side filament of a double Re-filament bead as nitrates.

For Sm and Nd, a triple Re filament assembly was used. Sample dissolved in a drop of H_2O is split into two parts and each is loaded on two side filaments.

B. Analysis.

All the elements except Rb were measured on VG MM30 Mass Spectrometer equipped with on-line computer (HP9825A).

For Rb, Sr and U, data reduction was performed by using software written by Dr. G. L. Cumming. For Sr, ion beam intensities were measured at masses: 88, 87.5, 87, 86.5, 86, 85.5, 84, 83.5. Possible interferences caused by ^{87}Rb for ^{87}Sr was monitored at mass 85. ^{87}Sr/^{86}Sr ratios are normalised to ^{86}Sr/^{88}Sr=0.1194. For Pb, ion beam intensities were measured in the order 208, 207.5, 207, 206.5, 206, 205.5, 204, 203.5. Unlike Sr, due to absence of any internal control of isotopic fractionation, running conditions for Pb were carefully controlled with respect to temperature which is kept at about 1250°C to minimise the isotopic fractionation. Nd was analysed by measuring as Nd^+ species and using software developed by Dr. R. st J. Lambert. In each run, four isotopes (146, 143, 144 and 147) were measured with the ion beam intensities minitored in the sequence 146, 143.5, 143, 143.5, 144, 143, 144, 147, 146.5. Note that masses 143 and 144 were measured twice. The advantage of this method lies in the fact that similarity of the two ^{143}Nd/^{144}Nd ratios better indicates the precision of the run and the stability of base lines. Measured ^{143}Nd/^{144}Nd ratios were normalised to ^{146}Nd/^{144}Nd=0.7219. Possible interferences by ^{144}Sm was monitored by measuring ion beam intensity at mass 147.

A2.6 Oxygen Isotope

Oxygen was extracted from both quartz and feldspar by reaction with BrF_5 and then converted to CO_2 as described by Clayton and Mayeda (1963). ^{18}O/^{16}O ratios, determined on the CO_2 gas using Micromass 602D, are reported here in δ notation relative to the standard mean sea water (SMOW). Overall precision is ±0.1‰.